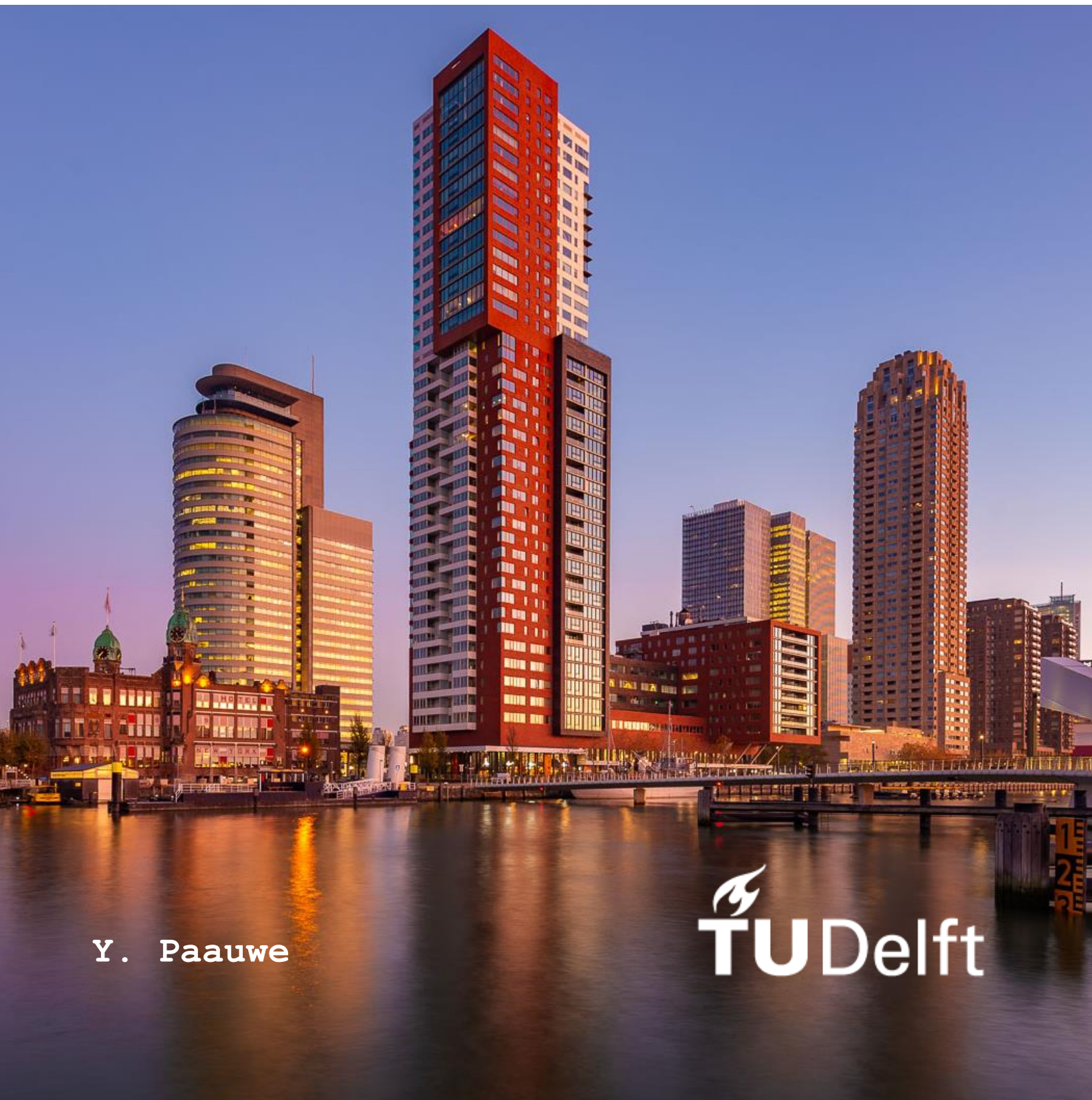Master Thesis Report   January 2020

Obtaining Insight into the Influence of the Main
Parameters in the Preliminary Structural Design
on the Wind-Induced Dynamic Response Including
Soil-Structure Interaction Effects of High-Rise
Buildings in the Netherlands

Y. Paauwe

TUDelft

Obtaining Insight into the Influence of the Main Parameters
in the Preliminary Structural Design on the Wind-Induced
Dynamic Response Including Soil-Structure Interaction
Effects of High-Rise Buildings in the Netherlands

in partial fulfilment of the requirements for the degree of

Master of Science
in Civil Engineering

at the Delft University of Technology,
to be defended publicly on Friday January 17, 2020 at 11:00 AM.

Faculty of Civil Engineering and Geosciences
Master: Building Engineering
Specialization: Structural Design

A research in collaboration with:

ABT Delft
Delftechpark 12, 2628 XH, Delft
Postbus 458, 2600 AL, Delft
T: +31 (0)15 270 36 11
E: info@abt.eu

Author:

Yaron Paauwe
Student ID nr.: 4625668

Graduation committee:

Chairman:	Prof. ir. R. Nijsse	TU Delft, CiTG, Building Engineering
Supervisor:	Dr. ir. K.C. Terwel	TU Delft, CiTG, Building Engineering
Supervisor:	Dr. ir. S.S. Gómez	TU Delft, CiTG, Hydraulic Engineering
Daily supervisor:	ir. J.C. (Chris) van der Ploeg	ABT

An electronic version of this thesis is available at: https://repository.tudelft.nl/

CONTACT INFORMATION

STUDENT

Name:	**BSc. Y. Paauwe**
Institution:	Delft University of Technology
Master track:	Building Engineering (Structural Design)
Address:	Rotterdamseweg 139 A125
	2628 AL Delft
Telephone:	06 55 13 66 47
E-mail:	yaronpaauwe@gmail.com
Student number:	4625668

GRADUATION COMMITTEE

Name:	**Prof. ir. R. Nijsse**
Organization:	Delft University of Technology
Faculty:	Civil Engineering and Geosciences
Chair:	Structural Design / Building Engineering
Address:	Stevinweg 1, S2 1.36
	2628 CN Delft
Telephone:	+31 15 278 54 88
E-mail:	R.Nijsse@tudelftt.nl

Name:	**Dr. ir. K.C. Terwel**
Organization:	Delft University of Technology
Faculty:	Civil Engineering and Geosciences
Chair:	Structural Design / Building Engineering
Address:	Stevinweg 1, 6.46
	2628 CN Delft
Telephone:	+31 15 278 15 12
E-mail:	K.C.Terwel@tudelft.nl

Name:	**Dr. ir. S.S. Gómez**
Organization:	Delft University of Technology
Faculty:	Civil Engineering and Geosciences
Chair:	Hydraulic Engineering
Address:	Stevinweg 1, 3.47
	2628 CN Delft
Telephone:	+31 15 278 14 98
E-mail:	S.SanchezGomez-1@tudelft.nl

Name:	**ir. J.C. (Chris) van der Ploeg**
Organization:	ABT
Address:	Delftechpark 12
	2628 XH Delft
Telephone:	+31 15 270 36 73
E-mail:	c.vd.ploeg@abt.eu

PREFACE

This thesis is my final piece to achieve my Master of Science degree in Building Engineering, specialization Structural Design, at the Faculty of Civil Engineering and Geosciences at Delft University of Technology. It has been performed in collaboration with the engineering company ABT in Delft, during the period from March 2019 till January 2020. The aim of this thesis report is to provide a description and overview of the research, the theoretical background and the resulting conclusions and recommendations.

It took a while before the precise topic of this research became clear. I was interested in the overall structural design of buildings and ABT had an interest in high-rise buildings in the Netherlands. I started with an investigation into the most important design decisions for the structural design of a high-rise building in the Netherlands. However, the topic was too broad and lacked theoretical profundity. This brought me back to one of my main interests during my study and an important aspect for the design of high and slender structures: the dynamic behaviour. I decided to let loose of the overall structural design and completely focus on the wind-induced dynamic behaviour of high-rise buildings in the Netherlands.

I would not have been able to bring this research to a successful end without the support of many people. I would like to express my gratitude for the shared knowledge, guidance and inspiration of the members of my graduation committee: Prof. ir. R. Nijsse (TU Delft), Dr. ir. K.C. Terwel (TU Delft), Dr. ir. S.S. Gómez (TU Delft) and ir. J.C. (Chris) van der Ploeg (ABT). Also, I would like to thank the company ABT and all colleagues for providing me with an inspiring working environment and their support during my research. A special thanks to Chris van der Ploeg, who not only helped me on the technical part of the research, but also guided me through the whole process of performing my graduation research. I also want to thank my friends for their support and advice. Last but not least, I would like to express my thankfulness and appreciation to my family for providing me the ability to study and support me in any possible way.

Delft, January 2020

Yaron Paauwe

ABSTRACT

The increasing rate of population and urbanization creates a scarcity of land in the densely urbanized parts in the Netherlands. This has initiated a trend for higher and more slender buildings. The design of a high-rise building is a complex task in which many different disciplines are incorporated. The structural design should provide sufficient strength and stiffness to withstand all types of loading on the structure. For high-rise buildings in the Netherlands, wind loading is the main horizontal load action. Especially for higher and more slender structures, the wind-induced dynamic behaviour of the building becomes more and more important. The comfort requirements, focussed on the maximum acceleration of the structure, are mend to secure a comfortable building and prevent the feeling of unsafety or even sickness by human beings. The increasing importance of the dynamic behaviour of high-rise buildings can result in a shift from a design approach focussed on statics, towards a design approach driven by dynamics.

The preliminary structural design is characterized by multiple design variants, changes in design and a limited amount of time. The structural engineer should be able to make informed and well-argued design decisions in a relatively short amount of time. Due to the complex nature of the dynamic behaviour of high-rise structures, the influence of design decisions on the maximum acceleration of the structure may not be considered in the preliminary design phase. This can be caused by the fast-changing design and limited amount of time, but also commonly used simplified methods do not provide insight into the consequences of design decisions. This may result in a lack of insight into the influence of design decisions on the dynamic behaviour of the structure.

This research investigates the influence of the main parameters in the structural design of a high-rise building in the Netherlands on the maximum acceleration at the top of the structure. This results in the main research question:

What are the influences of the parameters: geometrical dimensions, mass, stiffness, and damping ratio, of both the superstructure as the foundation, on the wind-induced dynamic response of high-rise buildings in the Netherlands?

With the generated data in this research, the consequences of design decisions can be determined for every possible combination of parameters within the domain of this research. Buildings between a 100 - and 300 meters high are investigated. However, the analysis procedure can also be used for cases outside the scope of this research. Using the knowledge from this research may lead to a more efficient design process and a better control of the maximum acceleration of the structure. It can provide inside into the influence of changes of the main parameters on the maximum acceleration of the structure, without performing a complete dynamic analysis. This saves time which is especially useful in the preliminary phase. Ultimately, it can result in an increased comfort level which adds to the quality of the design.

The parameters considered in this research are the geometrical dimensions of the superstructure (height h, width b and depth d), the structural parameters of the superstructure (stiffness EI, mass density ρ and damping ratio ξ) and the foundation parameters (mass density ρ_f, foundation depth D and the soil profile). The influence of the parameters is investigated in separate influence studies by varying the parameters within certain ranges. The parameter ranges are determined based on literature, existing measurements and hand calculations.

In practice, the dynamic behaviour of the structure is often considered separately in three uncoupled response directions: along-wind (in the wind direction), across-wind (perpendicular to the wind direction) and in torsion. In this research, the torsional response direction is not considered. To determine the maximum acceleration of the structure in one translational response direction, a spectral analysis is used. The spectral analysis describes the complete process from the wind velocity fluctuations to the dynamic response of the building. Within the analysis procedure, the mechanical admittance (also frequency

response function) of the structure is determined. In this research, a three-degree-of-freedom model is used to determine the mechanical admittance. The soil-structure interaction effects are taken into account by two degrees of freedom of the foundation. Analytical expressions are used to determine the frequency dependent values of the foundation variables.

The discrete three-degree-of-freedom model has the limitation that it cannot account directly for a different stiffness or mass over the height of the structure. The consequences of this limitation on the first two natural frequencies of a clamped beam system are investigated and presented with graphs. A calculation procedure is proposed to still be able to use the main analysis procedure to determine the maximum acceleration at the top of the structure in this research, in the case of unequal stiffness and/or mass over the height of the structure.

The main research question is answered with separate influence studies which determine the influence of the main parameters on the maximum acceleration at the top of the structure. The generated data can answers the main question for every possible combination of parameters within the domain of this research. However, due to the high dimensionality of the generated data, the influence of the main parameters can only be presented in a report by generating a large amount (hundreds) of different graphs. Because this is considered as unrealistic for working practice, only certain combinations of parameters are visualised in this report. A different medium is proposed to be able to extract and present the influence of all parameters in every possible combination considered in this research. By fixing multiple parameters, the dimensionality of the data can be reduced and clear graphs can be generated to show the influence of the different parameters on the maximum acceleration of the structure. The Montevideo tower is used as a case-study to show the application of the influence studies.
A digital platform/environment is proposed and considered as the most suitable medium for working practice to extract and present the knowledge from the generated data. Due to the limited amount of time, this digital platform/environment is not developed in this research.

Besides the influence of the main parameters on the maximum acceleration of the structure for each specific combination of parameters, general trends in the data are determined. From these trends, general conclusions and recommendations are provided. Regarding the influence of the main parameters, it is found that the foundation flexibility becomes more and more important for higher and more slender structures. The influence of the superstructure parameters (stiffness, mass density and damping ratio), is decreasing for increasing height and slenderness. The significance of a flexible foundation is shown and becomes larger for increasing slenderness. General trends are also found for the contribution of the second mode of vibration, the significance of a flexible foundation (SSI-effects) and the effective modal damping ratios. Further elaboration on these topics is provided in this report.

As extension of the research, the analysis procedure is applied in the two orthogonal translational response directions (along-wind and across-wind). A comparison is made between the maximum acceleration in both directions. This comparison showed that the across-wind response can be governing over the along-wind response for square cross-sections. Also, the phenomenon of vortex shedding can occur in the across-wind direction. An exploratory research into this phenomenon indicated that the contribution of the vortex shedding load may be neglected if the vortex shedding load and the natural frequencies of the building are well-separated (> 3 times larger).

All conclusions and recommendations provided in this research are based on the results of a simplified representation of a high-rise building in the Netherlands. Multiple assumptions and simplifications are made. The fact that this representation does not exactly reflect the reality, should always be kept in mind when using the results of this research.

Keywords: High-rise Buildings in the Netherlands, Wind-induced Dynamic Behaviour, Spectral Analysis, Soil-Structure Interaction Effects, Preliminary Structural Design, Data Generation, Influence stud, Flexible Foundation

CONTENT

LIST OF SYMBOLS

If a symbol is dimensionless or can have multiple units, this is indicated with a dash.

| Symbol	Description	Units
A	The cross-sectional area	m^2
A_b	The surface area	m^2
A_s	The force amplitude	—
A_w	The side wall solid contact area	m^2
B	The bandwidth of the vortex shedding load	—
B	The background factor	—
B	The half-width of the foundation	m
B_{EI}	The frequency factor for a difference in stiffness	—
B_ρ	The frequency factor for a difference in mass density	—
$C_{b,equi}$	The equivalent dashpot damping value of the superstructure	Ns/m
C_{emb}	The damping value for an embedded foundation	—
C_f	The shape factor	—
C_r	The rotational damping value of the foundation	Nms/rad
C_{sur}	The damping value for a surface foundation	—
C_x	The translational damping value of the foundation	Ns/m
D	The total depth of the foundation	m
D	The width of the frontal area of the cross-section	m
E_p	The modulus of elasticity for a foundation pile	N/m^2
E_s	The modulus of elasticity of the soil	N/m^2
EI	The overall bending stiffness of the superstructure	Nm^2
F	The force	N
$F_{e,i}$	The modal force (i = the mode of vibration)	N
$F_{u,dynamic}$	The dynamic wind load parallel to the wind direction	N
$F_{u,static}$	The constant (static) wind load parallel to the wind direction	N
$F_{v,dynamic}$	The dynamic wind load perpendicular to the wind direction	N
F_{vortex}	The force from vortex shedding	N
$G\ (G_0)$	The (small strain) shear modulus	N/m^2
H	The total depth of the homogeneous soil layer	m
H_i	The transfer function (i = the degree of freedom)	—
I_0	The mass moment of inertia of the foundation	kgm^2
I_b	The mass moment of inertia of the superstructure	kgm^2
I_u	The turbulence intensity of the u-component of the wind velocity	—
I_v	The turbulence intensity of the v-component of the wind velocity	—
I_x	The area moment of inertia in x-direction	m^4
I_y	The area moment of inertia in y-direction	m^4
I_z	The turbulence intensity at height z	—
K	The shape factor	—
$K_{b,equi}$	The equivalent spring stiffness of the superstructure	N/m
K_{emb}	The stiffness for an embedded foundation	—
K_r	The rotational stiffness of the foundation	Nm/rad
K_{sur}	The stiffness for a surface foundation	—
K_x	The translational stiffness of the foundation	N/m
L	The turbulence length scale	—
L	The half-depth of the foundation	m
M_0	The total mass of the foundation	kg
R	The resonance response factor	—

List of symbols

$S_{FF,u}$	The load spectrum parallel to the wind direction	$N^2 s/rad$
$S_{FF,v}$	The load spectrum perpendicular to the wind direction	$N^2 s/rad$
S_i	The response function (i = the degree of freedom)	–
S_{ii}	The spectral density functions (i = u, v)	–
Sc	The Scruton number	–
St	The Strouhal number	–
T_1	The fundamental period	s
U_i	The mode shape (i = the mode of vibration)	–
$\overline{V}$	The mean wind velocity	m/s
V_{La}	The Lysmer's analog wave velocity	m/s
V_s	The shear wave velocity	m/s
W_L / $S_{FF,vortex}$	The load spectrum of the vortex shedding load	$N^2 s$
W_L' / S_{vortex}	The normalized power spectrum of the vortex shedding load	–
a	The vibration acceleration	m/s^2
a_0	The dimensionless frequency	–
a_{max}	The maximum acceleration	m/s^2
b	The total width of the building	m
c	The damping value of the dashpot	Ns/m
$\tilde{c}$	The translational damping modifier	–
$\tilde{c}_r$	The rotational damping modifier	–
c_0	The orography factor	–
c_{cr}	The critical damping value	Ns/m
c_{dir}	The direction factor	–
$c_{e,i}$	The modal damping value (i = the mode of vibration)	Ns/m
c_{prob}	The probability factor	–
c_r	The roughness factor	–
$c_s c_d$	The structural amplification factor	–
c_{season}	The season factor	–
d	The total depth of the building	m
d	The diameter	mm
d_w	The height of the effective side wall contact	m
f	The frequency	Hz
f_1	The first natural frequency	Hz
f_L	The turbulence length scale	–
f_e	The fundamental frequency of the building	Hz
f_s	The vortex shedding frequency	Hz
h	The total height of the building from ground surface	m
h_0	The reference height	m
h_{sep}	The separation height	m
k	The stiffness of the spring	N/m
$k_{e,i}$	The modal stiffness (i = the mode of vibration)	N/m
k_i	The dynamic modifiers (i = x, y)	–
k_p	The peak factor	–
k_r	The terrain factor	–
m	The mass of the system	kg
$m_{b,equi}$	The equivalent mass of the superstructure	kg
$m_{e,i}$	The modal mass (i = the mode of vibration)	kg
p_u	The wind pressure	N/m^2
q	The distributed load	N/m
t	The variable time	s

t	The thickness	mm
u	The horizontal component of the wind velocity parallel to the wind direction	m/s
$\bar{u}$	The constant mean part of the u-component of the wind velocity	m/s
$\tilde{u}$	The fluctuating part of the u-component of the wind velocity	m/s
u_{max}	The maximum deflection at the top	m
v	The Poisson's ratio	—
v	The horizontal component of the wind velocity perpendicular to the wind direction	m/s
$\bar{v}$	The constant mean part of the v-component of the wind velocity	m/s
$\tilde{v}$	The fluctuating part of the v-component of the wind velocity	m/s
$v_{b,0}$	The fundamental wind velocity	—
v_b	The mean wind velocity at reference height of 10 meters	m/s
v_b	The standard wind velocity at a reference height of 10 meters	m/s
$v_{crit,i}$	The critical average wind velocity ($i = u, v$)	m/s
v_m	The average wind velocity	m/s
w	The vertical component of the wind velocity	m/s
$\bar{w}$	The constant mean part of the w-component of the wind velocity	m/s
$\tilde{w}$	The fluctuating part of the w-component of the wind velocity	m/s
x	The horizontal direction in the coordinate system	m
$\dot{x}$	The first time derivative of the displacement in x-direction	m/s
$\ddot{x}$	The second time derivative of the displacement in x-direction	m/s^2
y	The horizontal direction in the coordinate system	m
z	The vertical direction in the coordinate system	m
z	The height above the surface	m
z_0	The roughness length	m
z_w	The depth to the centroid of the effective side wall contact	m
α	The power-law exponent	—
α_{EI}	The stiffness ratio	—
α_i	The dynamic stiffness modifier ($i = x, y$)	—
α_ρ	The mass density ratio	—
β	The radiation damping ratio	%
γ	The pile factor	—
δ	The deflection due to the "momentane" load combination	m
δ_a	The contribution of the second run to the maximum acceleration	%
η_i	The embedment modifier ($i = x, y$)	—
λ_{min}	The minimum wave length	m
ξ	The percentage of critical damping (damping ratio) of the superstructure	%
π	The mathematical constant pi	—
ρ	The mass density (volumetric weight) of the superstructure	kg/m^3
ρ_{air}	The mass density (volumetric weight) of air	kg/m^3
ρ_{eq}	The equivalent mass density (volumetric weight) of the soil	kg/m^3
ρ_f	The mass density (volumetric weight) of the foundation	kg/m^3
ρ_s	The mass density (volumetric weight) of the soil	kg/m^3
σ	The standard deviation	—
σ^2	The total variance	—
$\sigma_{F,u}$	The standard deviation of the load parallel to the wind direction	N
$\sigma_{F,v}$	The standard deviation of the load perpendicular to the wind direction	N
σ_L	The standard deviation of the vortex shedding coefficient	—
σ_a	The standard deviation of acceleration	m/s^2
φ	The torsional direction in the coordinate system	—
χ_i	The aerodynamic admittance ($i = u, v$)	—

ψ_0	The load combination factor	—
ω	The angular frequency	rad/s
$\Delta v_{cr,i}$	The velocity interval for the lock-in effect	m/s
$\Im$	The imaginary part	—
$\Re$	The real part	—

CHAPTER 1
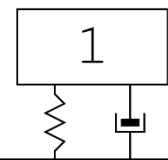
INTRODUCTION

This chapter introduces the motivation of this research, states the problem, discusses the objective, provides the research questions, outlines the focus of the research and shows the used methodology.

1.1   GENERAL

1.1.1   Increasing world population and urbanization

The need for high-rise buildings is mainly to be appointed to the increasing world population and rate of urbanization. The current world population is around 7.7 billion people (may, 2019) which is roughly double the world population in 1970 (United Nations, Department of Economic and Social Affairs, 2017). Also, the proportion of the total population living in urban areas is still increasing. A fundamental economic driver for the increase on the number of high-rise buildings is the scarcity of land in the densely urbanized parts of the world and the increasing population living in urban areas (Kayvani, 2014). A large increase in the amount of high-rise buildings worldwide, is shown in Figure 1.
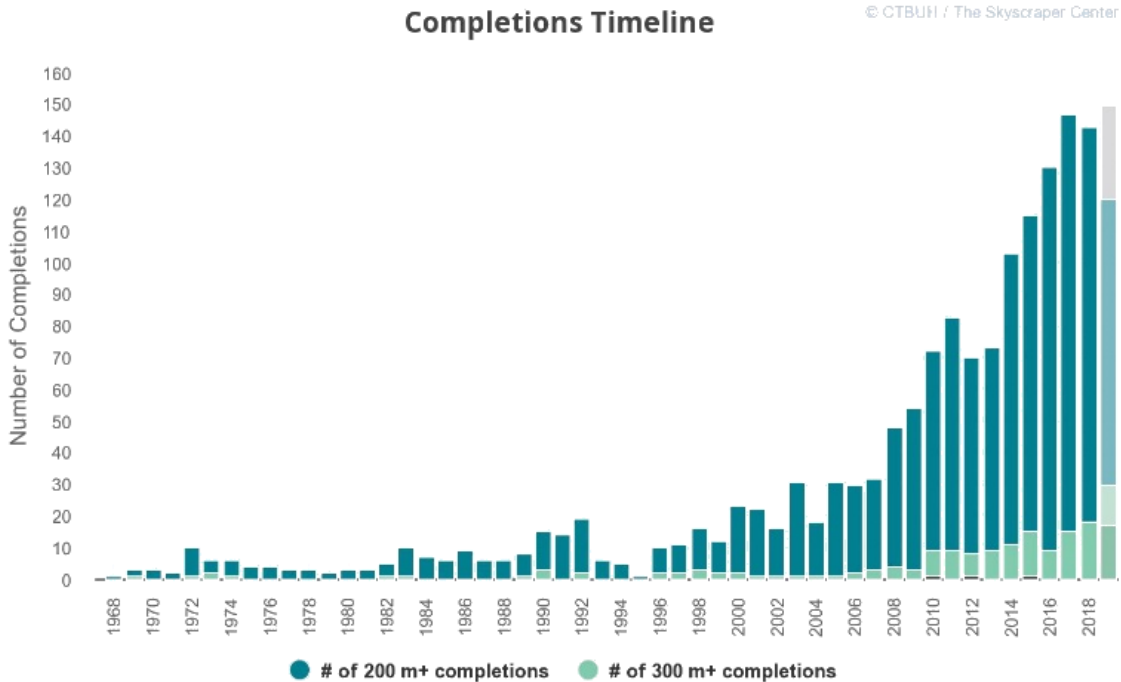

Figure 1: Number of completed high-rise buildings per year in the world (Council on Tall Buildings and Urban Habitat, 2018)

The increasing population and rate of urbanization is also present in the Netherlands and expected to keep growing according to (Kooiman, et al., 2016). To investigate whether this growth also results in an increasing number of high-rise buildings in the Netherlands, the database from The Skyscraper Center is used. This is the global tall building database of The Council on Tall Buildings and Urban Habitat (CTBUH).

From Figure 2, opposite to the global trend, it can be seen that there is no large increase in the number of completions in the Netherlands. On the contrarily, there has been a decrease in the total number of completions in the last five years. Yet, looking at the total number of proposed high-rise projects, there seems to be a large number of projects planned for the near future, although for most of these projects the year of completion is still undefined. The prediction of relatively many upcoming high-rise projects from the database, is confirmed by multiple people in practice.

As can be seen in Figure 3, there is no strong increase of average building height in the Netherlands. The average value (90 – 100 m) is much smaller than the world's average (247 meters for all completed 200-meter-plus buildings in 2018 (Council on Tall Buildings and Urban Habitat, 2018)). Extreme values exist in many years with the highest value in 2021, the Zalmhaven tower which is currently under construction. However, looking at the proposed projects, there is an increase in average building height for the coming years.
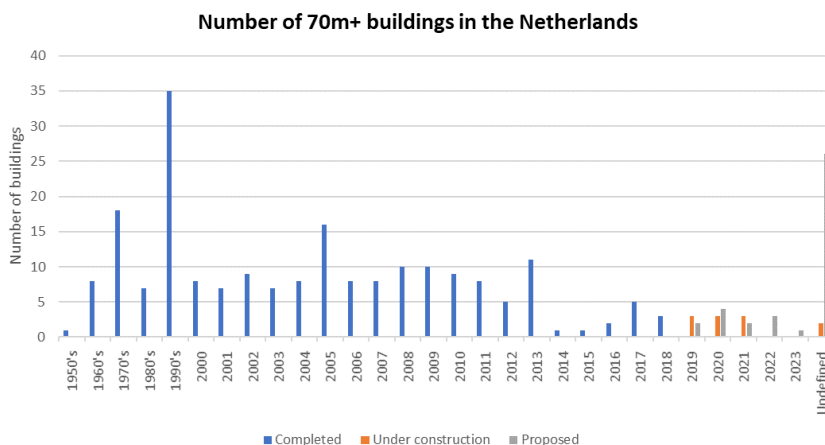
Number of 70m+ buildings in the Netherlands

Figure 2: Number of high-rise buildings (+70 m) per decade/year in the Netherlands (based on data from database of (Council on Tall Buildings and Urban Habitat, 2019))

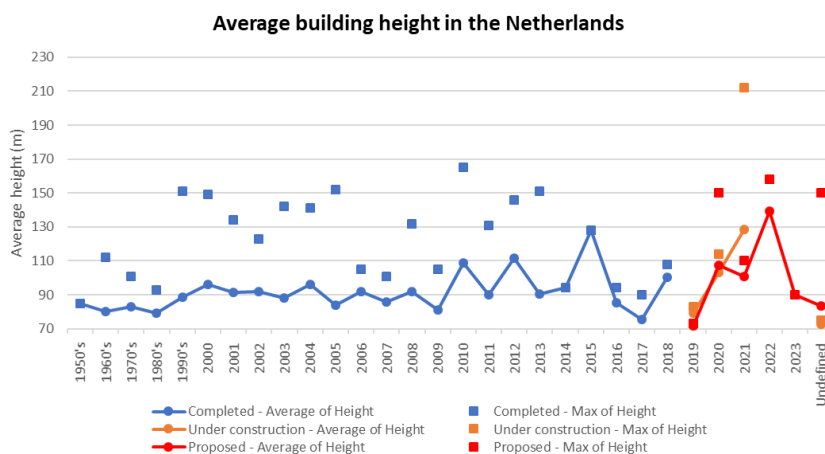**Average building height in the Netherlands**

Figure 3: Average building height (+70 m) in the Netherlands per decade/year (based on data from the database of (Council on Tall Buildings and Urban Habitat, 2019))

1.1.2   High-rise buildings in the Netherlands

Whether a building or structures can be called "tall" or a "high-rise" is a matter of a person's or community's perception. A suggested general definition by (Rana, 2014): "a high-rise building is a building whose height creates different conditions in the design, construction and use than those that exist in common buildings of a certain region and period". The geographical location of a building is of great importance whether a building is classified as high-rise or not. Worldwide, the general minimum height of 200 meters is often used in literature. In multiple regions in the world, a building of 200 meters high would easily blend in the urban landscape and would not stand out at all. Where as in the Netherlands, a building of 200 meters can be considered as exceptional at the moment. Therefore, the context is of great importance whether a building is classified as high-rise or not. This is visualized in Figure 4.
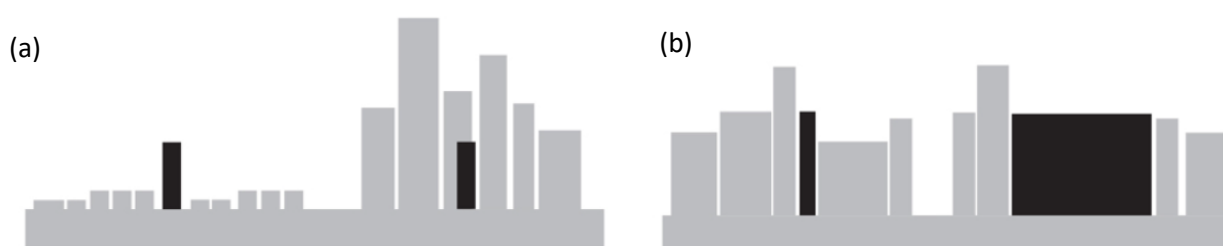
(a)   (b)

Figure 4: Height relative to context (a) and proportion (b) (Council on Tall Buildings and Urban Habitat, 2019)

The Dutch building code provides regulations for buildings not higher than 70 meters. When a building is higher than 70 meters, the design must be such that it meets the same requirements, for example on fire safety. Possibly additional measures should be taken to meet the requirements. This is in line with the earlier given general definition by (Rana, 2014). The height of the building creates different conditions than provided in codes and standards. Because multiple 100-meter-plus buildings are proposed for the near future in the Netherlands (database from CTBUH), this research will focus on buildings with a minimum height of 100 meters.

A maximum height is hard to identify. As already mentioned, the highest building, which is currently under construction, will be 215 meters tall. Multiple concept designs with heights up to 300 meters exist. These projects are just conceptual ideas and are far from realization. However, it shows that high-rise buildings up to 300 meters tall are considered in the Netherlands. Therefore, buildings up to 300 meters high are considered in this research.

1.1.3   Structural systems for high-rise buildings

The structural design is one of multiple design disciplines and numerous aspects should be taken into account. Because the stability system provides strength and stiffness against horizontal loads, the stability system is one of the most important parts in the structural design of high-rise structures.

Classification of multiple alternatives for structural stability systems for high-rise buildings started around the late 1960's with the classification of Fazlur Khan (Ali & Sun Moon, 2007). Multiple revisions were made and many other classification were opted after this. Most of these classifications are only based on height. A different classification is described in (Ali & Sun Moon, 2007) which makes the division between interior and exterior structures. The concept of the different systems is shown in Figure 5 and Figure 6.

Only a limited number of these systems is commonly used in the Netherlands. This is mainly because of the relatively limited height of high-rise buildings in the Netherlands. Looking at the current high-rise building stock in the Netherlands, the number of systems shown in Figure 5 and Figure 6 can be reduced. The research by (Zandbelt&vandenBerg, 2008), shows a good overview of the typical floor plans for Dutch high-rise buildings. It is observed that for residential buildings, often a system with shear walls is used. Either in the shape of a structural core or as individual walls. For office buildings, larger open spaces are preferred and therefore the use of individual walls is usually not chosen. The area for the vertical transportation is much larger for office buildings, and therefore the core is often used as structural element. For larger heights, the use of only a structural core may not be sufficient. In this case, outrigger structures can be utilized for extra strength and stiffness. The stability can also be provided by the façade. A framed tube structure, which is usually located in the façade, is the most common solution in the Netherlands.
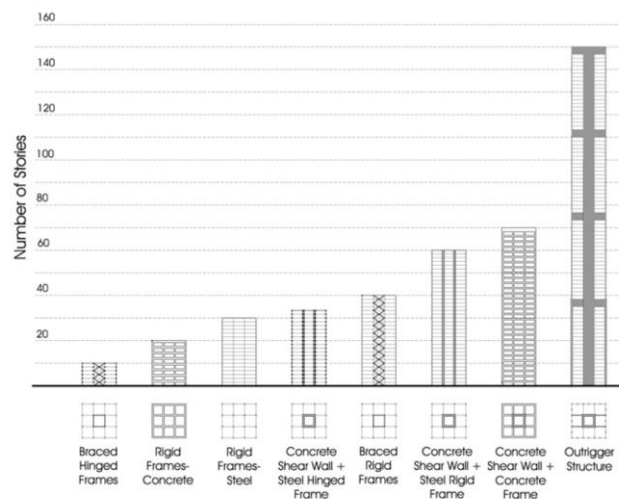

Figure 5: Interior structures (Ali & Sun Moon, 2007)
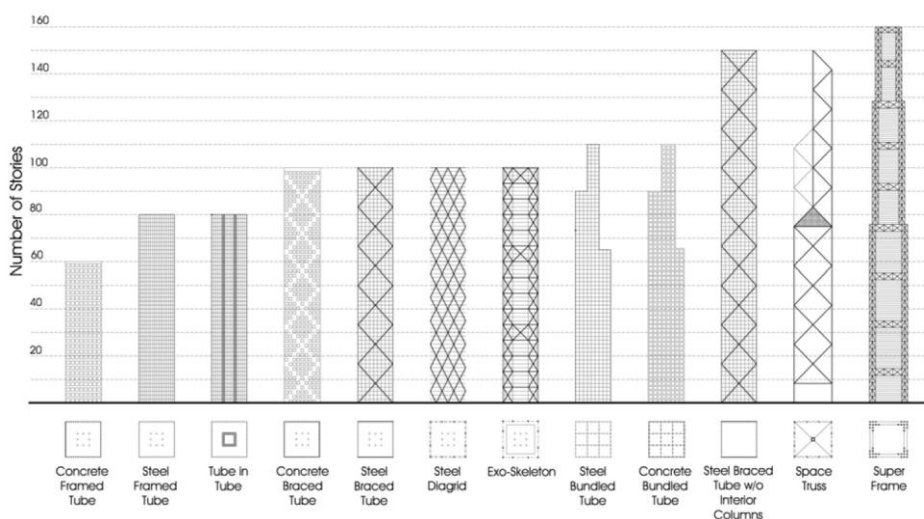
Figure 6: Exterior structures (Ali & Sun Moon, 2007)

The stability systems shown in Figure 5 and Figure 6, can be categorized as "traditional" stability systems. The design of these systems is often driven by statics. Generally speaking, this is currently also common practice in the Netherlands. However, there is a trend for higher and more slender structures, which may require a different design approach. These kind of structures form a new type of topology in high-rise design, and are dominated by dynamics instead of statics. Sometimes, advanced technologies are applied to control the dynamic behaviour, which reach further than just the structural system. Many of these technologies aim to increase damping, resulting in reduced motions. But also advanced wind engineering results in solutions that reduce the wind load on the structure.

1.1.4   Parameters in the structural design

As a rough separation, the structure of a high-rise building can be split up into two parts: the foundation and the superstructure. In terms of terminology, in this thesis the design of the superstructure is referred to as "superstructure design" and the design of the foundation is called the "foundation design", see Figure 7. The foundation design includes any possible basement levels.

Figure 7: Rough separation of a high-rise building in two parts

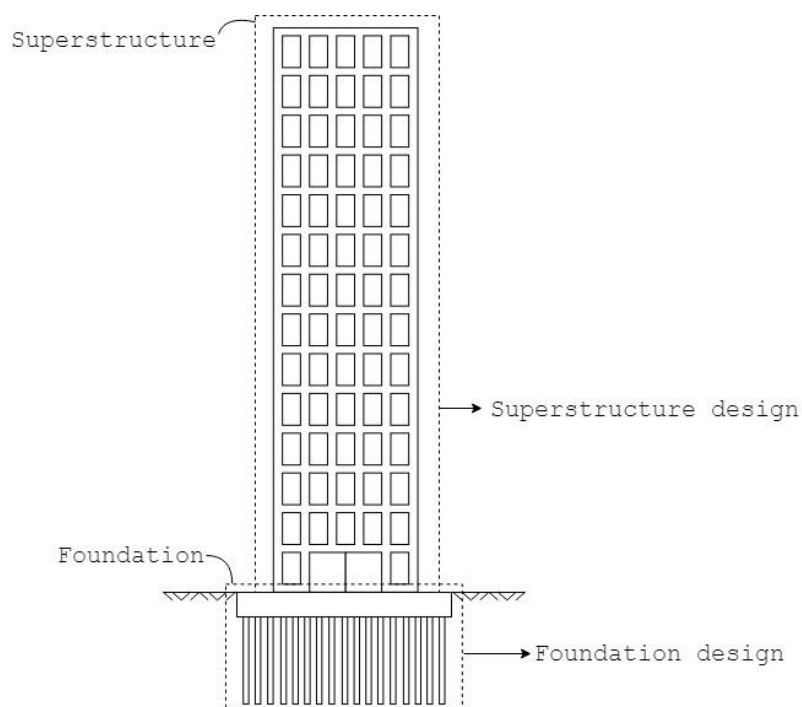Especially for tall and slender structures, both parts of the building have an influence on each other and therefore it is not advised to be considered completely separately. They both play an important role in terms of structural performance. In the dynamic analysis of structures, this dependency becomes even more significant, because the movement of the superstructure is influenced by the movement of the foundation. In preliminary design, a commonly applied rule of thumb is that 50% of the total deformation at the top is due to deformation of the superstructure and 50% of the total deformation at the top is due to deformations in the foundation. This emphasises the contribution of both parts in terms of deformations. The separation into a superstructure design and a foundation design is convenient for design purposes. However, the influence of both parts on each other is not taken into account. A better solution is to consider the structural design as a whole, instead of a separate superstructure design and a separate foundation design.
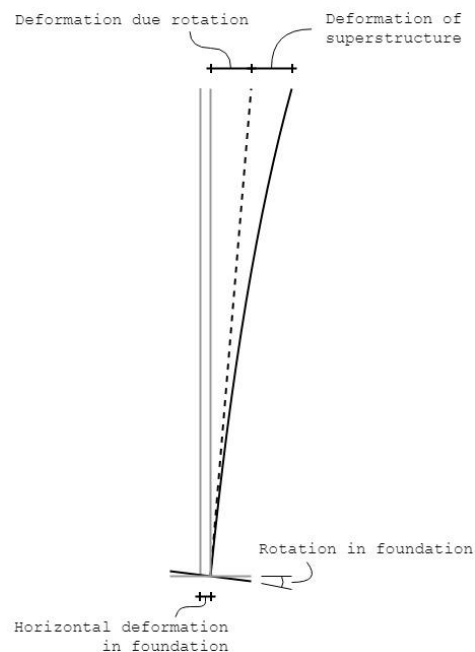

Figure 8: Total deformations of a simplified representation of a high-rise structure

The geometrical dimensions of the building are usually one of the first parameters which are set in the design. However, the choice for the geometrical dimensions has a large influences on many design decisions. Therefore, the geometrical dimensions of the building are considered as one of the main parameter in design.

Deformation requirements are often considered governing for design. The stability system should provide sufficient stiffness to keep deformations below certain limits. Therefore, the stiffness of the stability system is an important design parameter. The total displacements of the structure consist of the displacements of the superstructure plus the additional displacements due to deformation in the foundation. This can be a horizontal translation and/or a rotation, see Figure 8. Therefore, the horizontal and rotational stiffness of the foundation are important design parameters as well. Also from a dynamic point of view, the stiffness of both the superstructure as the foundation is an important design parameter. The stiffness plays an important role in the amplitude of vibration, but also determines the natural frequencies of the system.

The deformation of the superstructure can be divided in two parts: deformation due to bending and deformation due to shear. Theoretically, the total deformation can be: pure bending, combination of bending and shear and pure shear. Although in reality, the cases of pure shear and pure bending will never be the case. To reduce complexity and limit the amount of parameters in the model, only bending deformation is considered in this research. The stiffness of the superstructure is therefore given by the bending stiffness.

Another important design parameter is the mass of the building. The total mass of the building is of great importance for the foundation design. But also from a dynamic point of view, the mass has an influence on the amplitude of motions and the natural frequencies of the system.

Finally, from a dynamic point of view, the damping of the structure is important. Damping is a very complex phenomena and, due to its complexity, hard to predict for high-rise buildings (Geurts, et al., 2015). It is present in both the foundation as the superstructure. Although the damping is caused by different phenomena in both cases. Basically, damping is the dissipation of energy caused by the mechanical vibration of the structure (Berg, 2012). In following chapters, the damping in both the superstructure as the foundation is further discussed.

Concluding, the following parameters are distinguished for both the superstructure as the foundation:

- Geometrical dimensions;
- Mass;
- Stiffness;
- Damping.

## 1.1.5 Increasing significance of dynamic analysis

The design of a high-rise building is a very complex task and many different disciplines are incorporated into the design process. Because of its complexity, the design process itself is dynamic and therefore the structural design should be able to adapt to changes made by other disciplines and vice versa, throughout the entire design process. Especially in the preliminarily design, multiple variants of the design are investigated and changes in design are inevitable.

Especially for higher and more slender structures, the dynamic behaviour of the structure becomes more and more important. Generally speaking, the main reason for this is the increasing flexibility of the structure with increasing height/slenderness. The more flexible the structure is, the more vulnerable it will become for horizontal loads, regarding deflection and comfort requirements. The comfort requirements, focussed on maximum acceleration, are intended to secure a comfortable building and prevent the feeling of unsafety or even sickness by its inhabitants. The maximum acceleration can become dominant for design, and therefore result in a dynamic design approach instead of a static one. Because the comfort requirements can become governing for the design of high and slender structures, this research will focus on the serviceability limit state.

The horizontal loads acting on a structure can be due to, for example, wind or earthquakes. Because the most important horizontal loads, in the dense area where high-rise buildings are located in the Netherlands, are caused by wind, the focus of this research is on the wind-induced dynamic response.

The complete wind-induced response of high-rise buildings can be split up in three response components. One translational response in the wind direction, one translational response perpendicular to the wind direction, and one torsional response, see Figure 9. In reality, the three response directions are coupled and influence each other. To simplify the analysis procedure, the assumption of uncoupled response directions is often made in practice. This assumption is maintained in this research. Also, only the two orthogonal translational response directions are considered in this research, due to the limited available time. Besides the dynamic response due to the turbulent force of the wind, other phenomena can occur due to wind. For high-rise buildings, the phenomena of vortex shedding can become significant. Depending on the wind velocity and the cross-sectional dimensions of the building, the vortices tend to shed in a particular frequency. When this particular frequency is close to one of the natural frequencies of the system, an amplified response can occur perpendicular to the wind direction. The dynamic response of structures is more elaborated discussed in chapter 4.
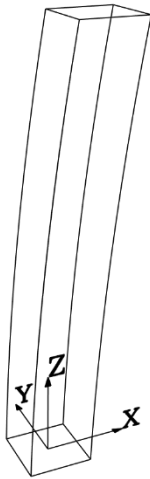
Response in the wind direction   Response perpendicular to the wind direction   Response in torsion
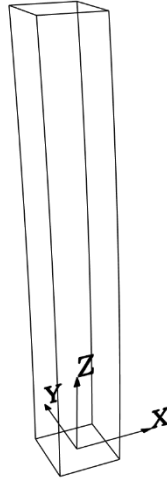
Figure 9: Simplification of three uncoupled response components (main wind direction in X-direction)

1.2   PROBLEM STATEMENT

In the dynamic process of the design of a high-rise building, the structural design should be able to adapt to changes in design and come up with the most optimal design in a relatively limited amount of time. The structural engineer should investigate multiple variants and make well-argued design decisions. The consequences of design decisions and changes should be determined and understood, to provide informed recommendations and come up with the best solution. This is true for all aspects related to the structural design. Focussing on the comfort requirements of high-rise buildings, the structural engineer should be able to assess the influence of design decisions and changes on the maximum acceleration of the structure, in a relatively short amount of time.

However, the consequences of design decisions or changes on the maximum acceleration of the structure are not always considered in the early stages of design. This can be caused by the fast changing design and/or the limited available time in the preliminary stage. Also, simplified methods of analysis may be used which do not provide insight into the influence or consequences of design decisions, and can be insufficient to capture the dynamic response of the structure. This can result in a lack of insight into the influence of design decisions and changes on the dynamic response of the structure.

To provide insight into the influence of design decisions or changes on the maximum acceleration of the structure, this research investigates the influence of the main parameters in the structural design of a high-rise building including soil-structure interaction effects, on the maximum acceleration of the structure. Using this insight, the structural engineer should be able to assess the influence of design decisions and changes on the maximum acceleration of the structure without performing a complete dynamic analysis. This will allow for well-argued recommendations and informed decisions, in a relatively short amount of time.

1.3   OBJECTIVE OF THE RESEARCH

The principal aim of the research is to provide more insight into the influence of the main parameters in the structural design of a high-rise building including soil-structure interaction effects, on the wind-induced dynamic behaviour of high-rise buildings in the Netherlands, focussing on the maximum acceleration of the structure.

A better understanding of the influence of the different parameters in the structural design, will allow for well-argued design decisions and a better control of the dynamic response already in the preliminary

structural design. Ultimately, this may lead to a more efficient design process and a better control of the maximum acceleration of the structure. An increased comfort level can add to the quality of the design.

The end product of the research are general recommendations and guidelines, where applicable, which provide insight into the influence of the main parameters on the maximum acceleration of the structure. In cases where general recommendations and guidelines are impossible to provide, case specific insight can be obtained. Case-specific insight is provided using a case-study in this report. A different medium, a digital environment/platform, is proposed to present case-specific insight for every possible case within the domain of this research. With this insight, informed decisions can be made in the preliminary design stage regarding the wind-induced dynamic response of a high-rise structure in the Netherlands.

The research is focused on the preliminary structural design. The scope is limited to high-rise buildings in the Netherlands which have a height between 100 and 300 meters. The research is focused on a general design space, resulting from the determined parameter ranges. As mentioned, the analysis procedure is also applied to a case-study.

1.4 RESEARCH QUESTIONS

The main research question is shown below, together with the sub-questions which serve to answer the main question.

Main research question

What are the influences of the parameters: geometrical dimensions, mass, stiffness, and damping ratio, of both the superstructure as the foundation, on the wind-induced dynamic response of high-rise buildings in the Netherlands?

Sub-questions

Model creation

- How is the wind load represented?
- What are the parameter ranges to use for the influence studies?
- Which model/expressions should be used for the soil-structure interaction parameters?

Parameter influence studies

- What is the influence of the distribution of mass and stiffness over the height of the structure on the first two natural frequencies of the system?
- What is the contribution of the second run of the analysis procedure to the maximum acceleration of the structure?
- What is the significance of the flexible foundation in terms of maximum acceleration?
- What is the influence of the different parameters, as given in the main question, on the maximum acceleration of the structure?

Application in two response directions

- What is the difference between the two perpendicular translational response directions, in terms of maximum acceleration of the structure?
- When does the phenomena of vortex shedding become dominant for design?
- How far should the vortex shedding frequency and the first fundamental frequency be apart to neglect the response due to the vortex shedding load?
- How significant is the response due to a vortex shedding load in the case that the frequencies are close together?

1.5 FOCUS OF THE RESEARCH AND REPORT OUTLINE

First, a literature study is performed into the current state of the art regarding design manuals of wind-induced dynamic behaviour of high-rise buildings often used in the Netherlands. A general overview is given in chapter 2.

Second, to analyse the influence of the main parameters, the focus of the research is determined. As discussed before, there are multiple parameters which influence the final response of a structure due to wind load. In general, all parameters can be categorized into three groups: "wind loading", "structural" and "criteria". In (Berg, 2012), a good overview of the parameters which mainly influence the dynamic response is given which is based on the wind loading chain by prof. A.G. Davenport (Berg, 2012) (Woudenberg & Vambersky, 2003). One important part is lacking in this overview, which are the parameters related to the foundation. A modified overview is given in Figure 10.
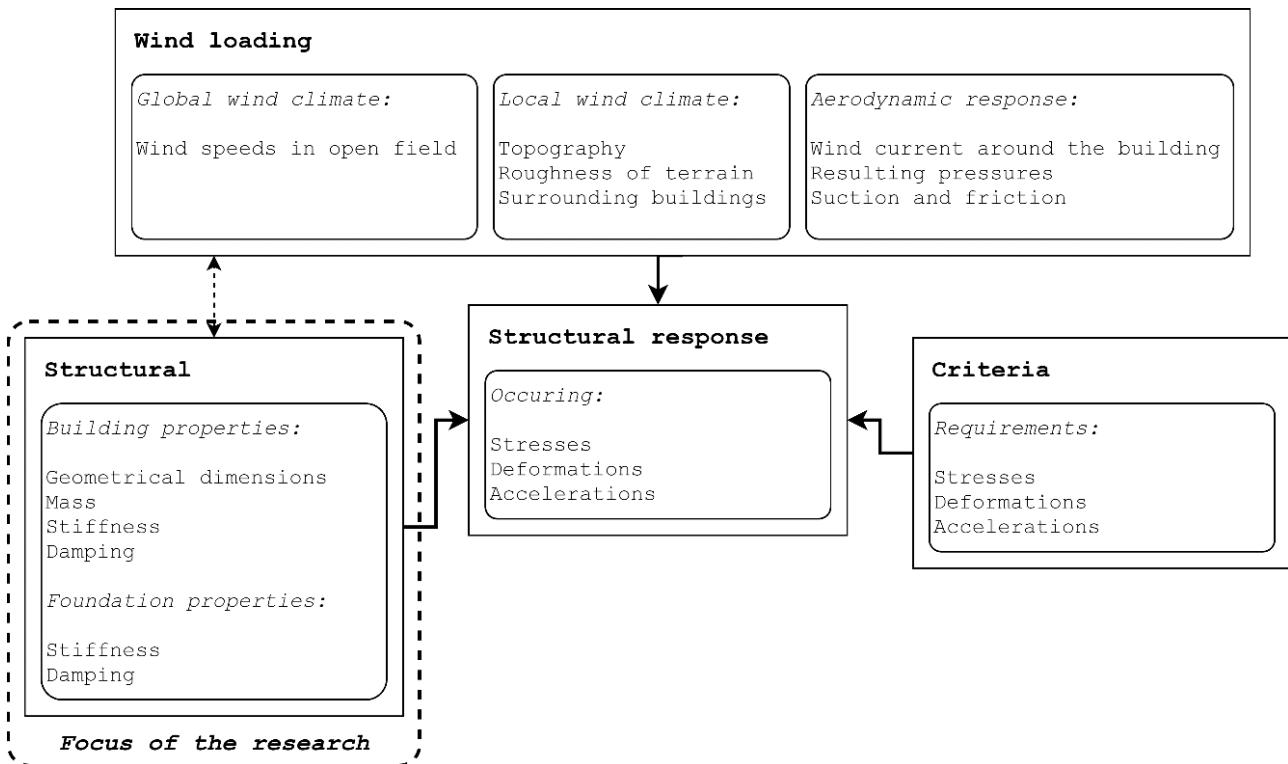
Wind loading

Global wind climate:

Wind speeds in open field

Local wind climate:

Topography
Roughness of terrain
Surrounding buildings

Aerodynamic response:

Wind current around the building
Resulting pressures
Suction and friction

Structural

Building properties:

Geometrical dimensions
Mass
Stiffness
Damping

Foundation properties:

Stiffness
Damping

Focus of the research

Structural response

Occuring:

Stresses
Deformations
Accelerations

Criteria

Requirements:

Stresses
Deformations
Accelerations

Figure 10: Overview of main parameters that influence the dynamic response (edited from (Berg, 2012))

As can be seen in Figure 10, there is an interdependency between the wind load and the structural parameters since the geometrical dimensions of the building influences the wind load. The wind load itself is a complex subject. There are advanced techniques available to limit the wind load on a structure, for example changing the shape of the building based on CFD[1]. But, these techniques require very specific information about the structure and surroundings. Therefore, recommendations from literature are used and assumptions are made for the wind load in this research. These will be explained in chapter 3.

Following, the determination of the dynamic response is discussed in chapter 4. The different response directions are explained and the chosen method is presented. Comfort requirements are set to limit the maximum occurring acceleration. A description of the comfort requirements from codes and literature is also provided in chapter 4.

---

[1] CFD: Computational Fluid Dynamics: a numerical analysis of the flow of fluids, in this case used for the flow of air.

As indicated in Figure 10, the focus of this research is on the 'structural' group. The influence of parameters in the design is investigated using multiple influence studies. Chapter 5 and 6 will describe the parameters and discuss realistic ranges which are used for the influence studies.

Chapter 7 aims to answer the question, how the distribution of mass and stiffness over the height of the structure influences the first two natural frequencies of a clamped beam system. The importance of a good estimate of the natural frequencies is shown. Finally, design formulas and graphs are provided to calculate the first two natural frequencies of a system with unequal stiffness and/or mass over the height. Also, a calculation procedure is proposed to be able to use the analysis procedure with the simplified model in this research, in the case of unequal stiffness and/or mass over the height of the structure.

Chapter 8 discusses the results of different analyses. First, the contribution of the second mode of vibration of the superstructure is discussed. After, three separate influence studies show the influence of different parameter groups on the maximum acceleration of the building. The first influence study shows the influence of the geometrical dimensions (height, width and depth). In this section, the effective modal damping ratios and the dimensionality of the presented graphs is also explained. The second influence study shows the influence of the foundation parameters (foundation depth and soil profile). The significance of a flexible foundation is shown in this section. The last study shows the influence of the superstructure parameters (mass density, stiffness and damping ratio).

In chapter 9, the previously discussed influence studies are performed for a case-study. The Montevideo tower in Rotterdam is chosen for this. The procedure for unequal parameters over the height of the structure is illustrated for the case study and the different influence lines for the different parameter groups are provided.

As extensions of the research, the analysis procedure is used in the two perpendicular translational response directions in chapter 10. In this way, both response directions are analysed without coupling between them. The comparison between the two perpendicular response directions is made for square cross-sections. Finally, the model is expanded with a vortex shedding load, perpendicular to the wind direction. From this, the significance of the phenomena of vortex shedding is discussed.

The last chapter, chapter 11, provides an overview of the most important conclusions and recommendations. Besides, a discussion is provided and further research is proposed.

1.6   METHODOLOGY

As introduced before, the principal aim of this research is to provide more insight into the influence of the main parameters in the structural design, on the wind-induced dynamic behaviour of high-rise buildings in the Netherlands including soil-structure interaction effects, focussing on the maximum acceleration of the structure. This aim originates from the hypotheses that, in practice, more insight into the influence of the main parameters can result in well-argued and informed decisions in the design process. This may lead to a more efficient design process, a better control of the maximum acceleration of the structure, an increased comfort level and ultimately an increased quality of the design.

This practical problem is investigated from a theorical basis. A quantitative research approach is applied in which the data collection is achieved with numerical simulation. An alternative to numerical data collation is experimental data collection. This type of data collection is not used because it requires experimental test setups which are not available for this research. However, existing data of measurements of high-rise buildings in the Netherlands (from (Geurts, et al., 2015)) is used for comparison. Numerical simulation has the advantage that the influence of parameters can be distinguished separately. Also, many different alternatives can be analysed. Disadvantages are limitations in computational demand and possibly large computation time. These disadvantages are handled by controlling to amount of variants analysed.

For the assessment of the dynamic behaviour of a structure, three general types of analysis procedures can be distinguished:

- Analysis with an equivalent static load;
- Analysis in the frequency domain (spectral analysis);
- Analysis in the time domain (time history analysis).

The advantages and disadvantages of the different approaches are summarized in Table 1. Which procedure is most suitable for the analysis is depending on the aim of the analysis.

Approach	Complexity	Time needed	Computational demand
Equivalent static load	Low	Low	Low
Spectral analysis	Medium	Medium	Medium
Time history analysis	High	High	High

Table 1: Advantages and disadvantages of three analysis approaches

The determination of the maximum acceleration of the structure is the main calculation procedure in this research. Each analysis procedure mentioned above, is capable of estimating the maximum acceleration of the structure. However, not all analysis procedures are suitable for the aim of this research. The equivalent static load approach provides very little insight into the dynamic behaviour of the structure and can be insufficient to capture the complete dynamic response. A time history analysis can have a relatively large computational demand and can require long computation time. The spectral analysis however, is considered suitable to capture the complete dynamic response and the computational demand and computation time can be limited. Therefore, the spectral analysis is chosen to be the most suitable for the determination of the maximum acceleration of the structure in this research. The complete analysis procedure of a spectral analysis is explained in section 4.3.

Besides the spectral analysis, other types of analysis procedures are used in this research. A modal analysis, the determination of the dynamic properties of a system in the frequency domain, is used for the verification of the natural frequencies of the system. For the verification of the expressions for the soil-structure interaction parameters, a time history analysis is used. The two verification parts are discussed in section 7.7 (modal analysis) and section 6.5 (time history analysis).

An overview of the entire analysis procedure performed in this research is shown in Figure 11. The program used for each step is also shown. The creation of the design alternatives, the determination of the model variables, the determination of the load spectrum and the calculation of the maximum acceleration of the structure is performed in separate Maple worksheets. The worksheets are linked together to be able to iterate over all design alternatives.

For the spectral analysis, a mechanical admittance function, also called a frequency response function, is determined. A linear discrete model, as shown in Figure 11, is used to determine the frequency response function. This discrete model is adopted from (Gómez, et al., 2018). This particular model is chosen because it is a discrete, three-degree-of-freedom (3DoF) model. This has the advantage that the model is governed by ordinary differential equations and has a finite number of mode shapes. This is convenient for the influence study of the main parameters in the design. The model variables are determined using a continuous Euler-Bernoulli beam model, for the superstructure variables, and analytical expressions from (Gazetas, 1991), for the foundation variables. In chapter 6, the analytical expressions from (Gazetas, 1991) are discussed, compared and verified. A more elaborate explanation of the model is provided in chapter 8.

The design alternatives are created using parameter ranges for all input parameters. The input parameters are shown in Table 2. For each parameter, a realistic range is determined based on literature and hand calculations. The parameter ranges are discussed in chapter 5 and chapter 6. As explained, all model variables are dependent on the input variables. All data from the analysis procedure is collected in Excel

sheets. Excel is chosen because of the export abilities from Maple to Excel. Also, the program is easy to use and can provide a quick overview of the data. For the post-processing of the data, the web-based interactive development environment, JupyterLab, is used. This environment is chosen because it offers a platform for data analysis and visualisation. Jupyter supports many different programming languages from which Python is used. A large amount of pre-programmed data analysis procedure is available, which enables for a relatively fast but detailed data exploration.
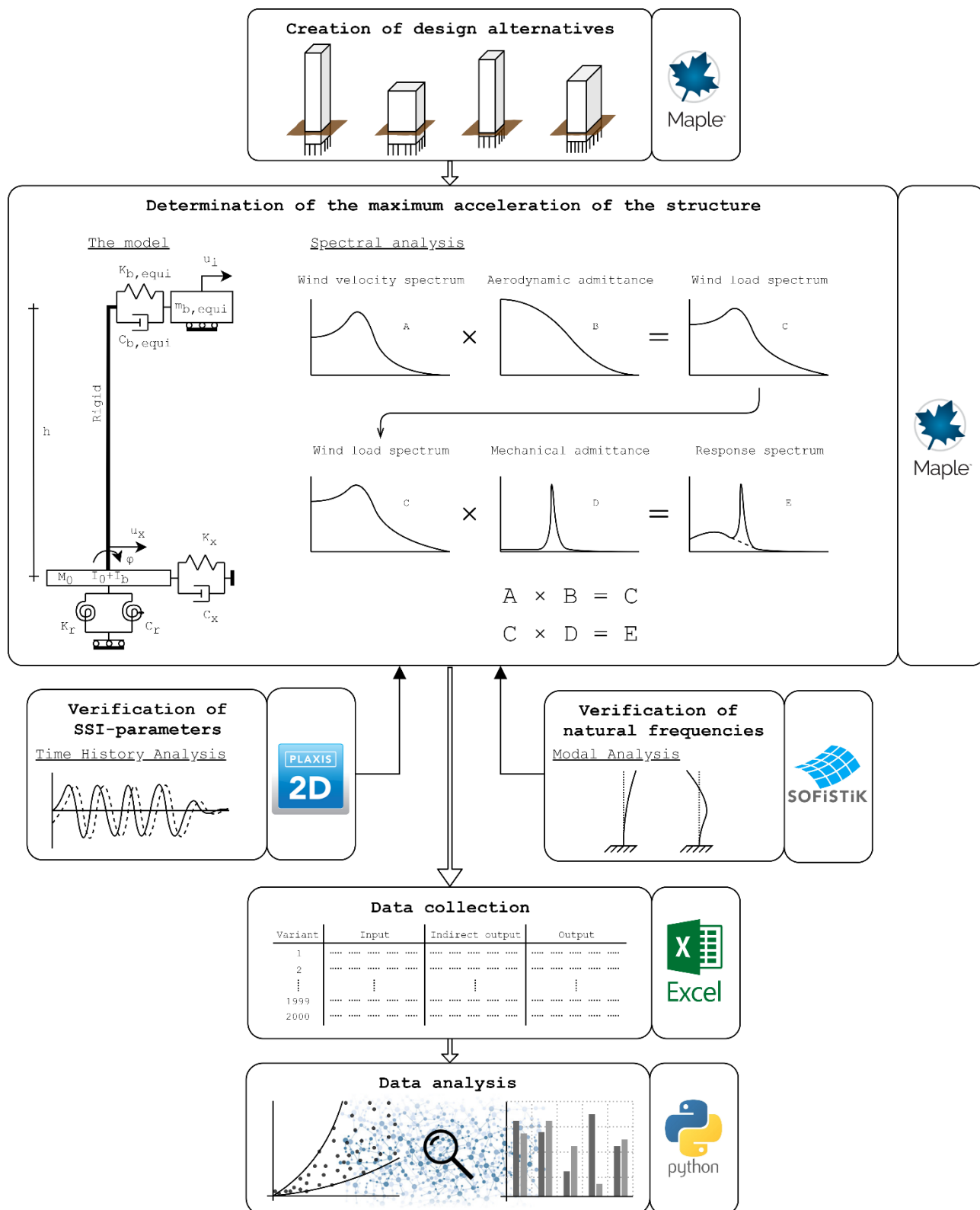

Figure 11: Overview of analysis procedure and used programs

	Parameter	Symbol	Units	Description
Superstructure				
Geometrical dimensions	Height	h	m	The total height of the building from ground surface.
	Width	b	m	The total width of the building. The width is always perpendicular to the wind direction.
	Depth	d	m	The total depth of the building. The depth is always parallel to the wind direction.
Superstructure parameters	Stiffness	EI	Nm^2	The overall bending stiffness of the superstructure, including all aspects for a dynamic analysis.
	Mass density	ρ	kg/m^3	The volumetric weight of the superstructure.
	Damping ratio	ξ	%	The percentage of critical damping in the superstructure.
Foundation				
Foundation parameters	Foundation depth	D	m	The total depth of the foundation.
	Mass density	ρ_f	kg/m^3	The volumetric weight of the foundation.
Soil profile	Small strain shear modulus	G_0	N/m^2	The shear modulus of the soil under small strain conditions.
	Volumetric weight	ρ_s	kg/m^3	The volumetric weight of the soil.
	Poisson's ratio	v	[$-$]	The Poisson's ratio of the soil (always equal to 0.45).
Wind load				
Wind load	Mean wind velocity	v_b	m/s	The mean wind velocity at reference height of 10 meters (always equal to 19.4 m/s, wind area II).
	Roughness length	z_0	m	The roughness length (always equal to 0.5 m, urban).

Table 2: Input parameters

In multivariate models, the dimensionality of the obtained data can become important. The dimensionality of data refers to the amount of attributes a dataset contains (StatisticsHowTo, 2016). One might think that the more attributes the better. However, the opposite is often true. The more attributes, the more difficult it becomes to isolate dependencies and visualize the data. This becomes even more difficult when attributes are correlated. The increasing difficulty to post-process data for increasing dimensionality, is often referred to as the curse of dimensionality (StatisticsHowTo, 2016). Dimensionality reduction is used to be able to understand data with a high dimensionality, either numerically or visually. Many different methods exist to perform dimensionality reduction. The visualization of high dimensional data becomes difficult as well. Different types of plots, ranging from 1-dimensional to 3-dimensional, and the use of line styles and colours enables for the visualization of higher-dimensional data, see Figure 12. However, the larger the dimensionality of the data to be visualized, the more complex the plot becomes.

From Table 2 it can be seen that the input domain has a dimensionality of 13. Since the parameters for the wind load are not varied in this research, this reduces to an input dimensionality of 11. Grouping the soil parameters together reduces to a total input dimensionality of 9. This only includes the direct input parameters. Using realistic parameter ranges (determined in chapter 5 and 6) and step sizes for each parameter, this results in a domain of approximately 25 million variants. With an average calculation time of 30 seconds this results in around 200.000 hours of computation time, which is not possible to perform. Therefore, the amount of variants is reduced. Each influence study is based on datasets up to 2000 variants. For each dataset, this results in a computation time of approximately 17 hours.
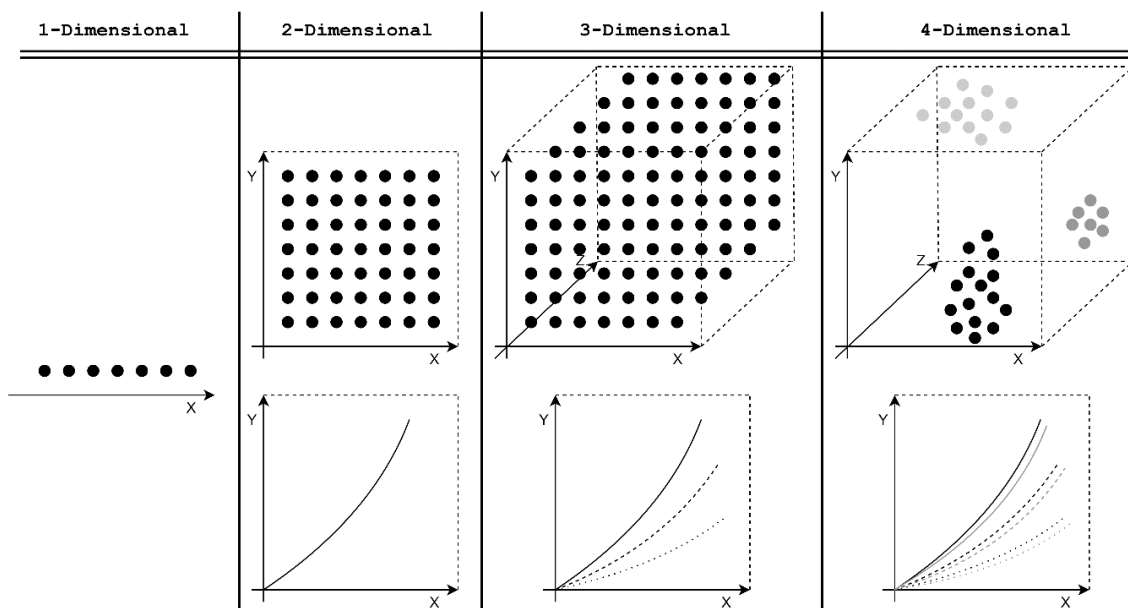
Figure 12: Visualization of dimensionality of data

Besides the direct input parameters, there are also indirect parameters which can be used to isolate dependencies. For example, the slenderness ($h/\sqrt{bd}$ or h/d). Besides the indirect input parameters, the model variables can also be used to describe dependencies. Altogether, the amount of direct or indirect attributes of the data in this research is around 20. This large amount of attributes and dependency of the attributes results in the general conclusion that the obtained data in this research is hard to be visualised in a generic manner. Therefore, it is chosen to, where possible, visualize the data for particular groups/clusters. This results in plots that are only applicable for certain situations or combinations of parameters. To be able to draw conclusions from the generated data, two approaches are applied, as shown in Figure 13. In the generic approach, all data is considered and general conclusions are drawn from overall trends in the data. The advantage is that those conclusions are generally applicable. The disadvantage is that the conclusions are conservative due to the possibly large spread in the data. The case-specific approach reduces the dimensionality of the data by fixing certain parameters. Possibly, also the bandwidth of the considered parameter is reduced. This can be done if there is only interest in a small deviation around a certain value. For example, not a height range from 100 meters till 300 meters, but around a height of 150 meters. Finally, case-specific conclusions can be drawn. The advantage is that the precise influence of a particular parameter can be obtained. Disadvantage is that this influence is only applicable to that certain case and not generally applicable.
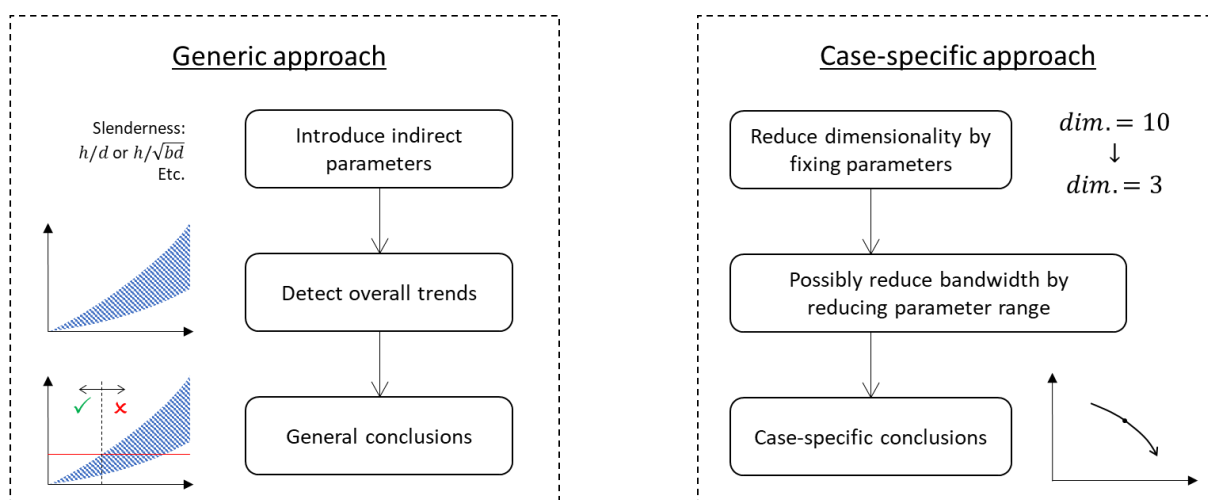

Figure 13: Two approaches to draw conclusions

The datasets obtained in this research contain much more information than can be presented in this report. For example, the influence of the different parameters within the model can be visualised for every particular case, using the case-specific approach. An example of the abilities to present the knowledge from this research with the medium of a paper report is provided in section 8.4. The required amount of plots, to present the knowledge from the data generated in this research, will be in hundreds. Therefore, a paper report is not considered as suitable medium to present the obtained data. As alternative, a digital environment in which all data can be visualised for every particular case would be the best option for practice. Considering the limited time for this research, this digital platform is not created within this research.
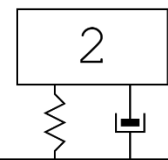
CHAPTER   2

CURRENT DESIGN MANUALS

In this chapter, the current state of the art regarding design manuals of wind-induced dynamic behaviour of high-rise buildings often used in the Netherlands is discussed. Also, an overview of existing influence studies is provided.

2.1   STATE OF THE ART

The current state of the art regarding design manuals of wind-induced dynamic behaviour of high-rise buildings often used in the Netherlands, can be split up in two reference groups: norms and codes, and books, papers and articles.

2.1.1   Norms and codes

The NEN-EN 1991-1-4 is the most commonly used code regarding wind actions in the Netherlands. It provides recommendations and methods for the analyses of wind-induced vibrations of buildings. Yet, the proposed methods do not provide much insight into the dynamic behavior of the structure, since only a estimation formula is given. Also, no elaboration is provided regarding the derivation of the formula and the influence of variables.

Besides the Eurocode, other norms and codes exist. Three of these are investigated by (Treels, 2019) and the capabilities of their proposed methods are summarised here. The focus lies with the capability to analyse the three response directions (alongwind response, acrosswind response and torsional response), separately or all together. The found capabilities are summarised in Table 3.

Norm or code	Alongwind response	Acrosswind response	Torsional response
NEN 6702	✓	✗	✗
NEN-EN 1991-1-4	✓	✗	✓
CNR-DT 207-2008	✓	✓	✓

Table 3: Summary of capabilities of proposed methods of multiple norms and codes

As can be seen in Table 3, only the CNR-DT 207-2008 provides a method to analyse the complete wind-induced dynamic response of a high-rise building. Yet, concluded by (Treels, 2019), there is insufficient empirical data (measurements of high-rise buildings) to validate the proposed methods.

The CNR-DT 207-2008 is a guide for the assessment of wind actions and effects on structures. It provides information about the fundamentals of the wind, possibly occurring phenomena and the dynamic analyses of structures. It also proposes different methods to analyse the wind-induced response for all three response directions. Yet, it does not provide insight into the influence of parameters and can therefore not directly be used to make informed decisions in a design process.

It can be concluded that the existing norms and codes do provide methods for a complete analysis of the wind-induced dynamic behaviour of high-rise buildings. Yet, these references are not providing insight into the influence of parameters and therefore cannot directly be used for informed decision making in a design process.

2.1.2   Books, papers and articles

Besides the norms and codes, many studies exist which investigate the wind-induced dynamic behaviour of structures. Many of these investigations focus on a specific part of the dynamic analysis. For example, the determination of damping. Other references provide recommendations about which methods to use, for example: (Gómez, 2019) (Steenbergen, et al., 2008) (Wisse & Staalduinen, 1992) (Fu, 2018) (Stathopoulos, 2007) (Strathopoulos & Baniotopoulos, 2007). Only a limited amount of references provide insight in the influence and consequences of parameters within a certain model. These are discussed in the following section. Generally, there are two drawbacks with the influence studies found in literature:

1. Simplified models are used which neglect certain aspects;
2. Results are presented in the form of graphs which are difficult to use for further research.

2.2 EXISTING INFLUENCE STUDIES

Research exist into the influence of the different parameters on the structural response due to wind load, e.g. (Berg, 2012), (Oosterhout, 1996) and (Oosterhout & Geurts, 2001). Different methods are used to identify the influence. For example, (Oosterhout, 1996) shows the influence of an increasing mass, stiffness or damping (in the direction of the arrows) for two types of buildings against the ISO criterion, see Figure 14. Building A: a slender tall building with first natural frequency around 0.2 Hz. Building B: a squat building with first natural frequency of 0.9 Hz. A spectral analysis is used for this research. A different influence of the parameters for the two different buildings can be observed. A conclusion from Figure 14 is for example, an increase of stiffness can be a solution for relatively squat buildings, but does not result in significantly lower accelerations for slender buildings. A simplification of the model used is, that the influence of the foundation is not taken into account. The structure is assumed to be clamped at foundation level. Also, the magnitude of the change of the parameters is not shown. (Oosterhout, 1996) (Oosterhout & Geurts, 2001)
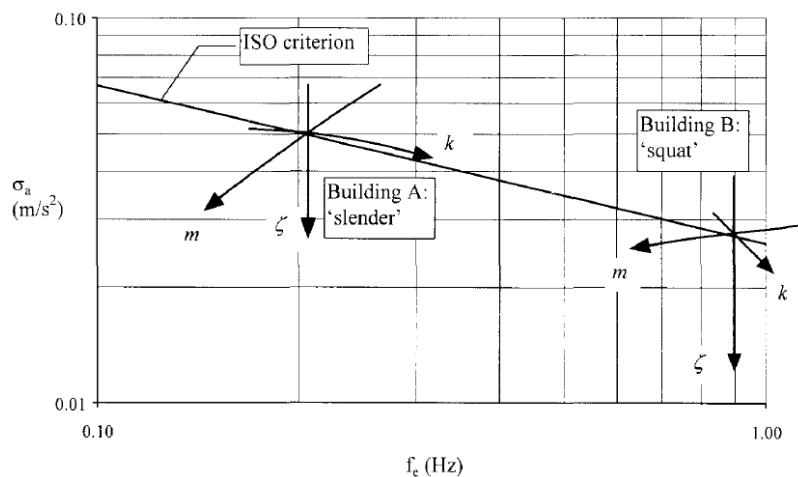
Explanation of graph:
On the x-axis, the fundamental frequency. On the y-axis, the standard deviation of the acceleration (see section 4.4.2). The arrows point in the direction of increasing parameter value.

Figure 14: ISO acceleration criterion and effects of effective mass, stiffness and damping (Oosterhout, 1996)

A different influence study is performed by (Berg, 2012). This research used the procedure described in the NEN-EN 1991-1-4 to obtain the structural amplification factor $c_s c_d$. Also in this research, only the parameters of the superstructure (stiffness, mass and damping) are investigated. The influence of the three parameters on the displacement and acceleration are shown in Figure 15.
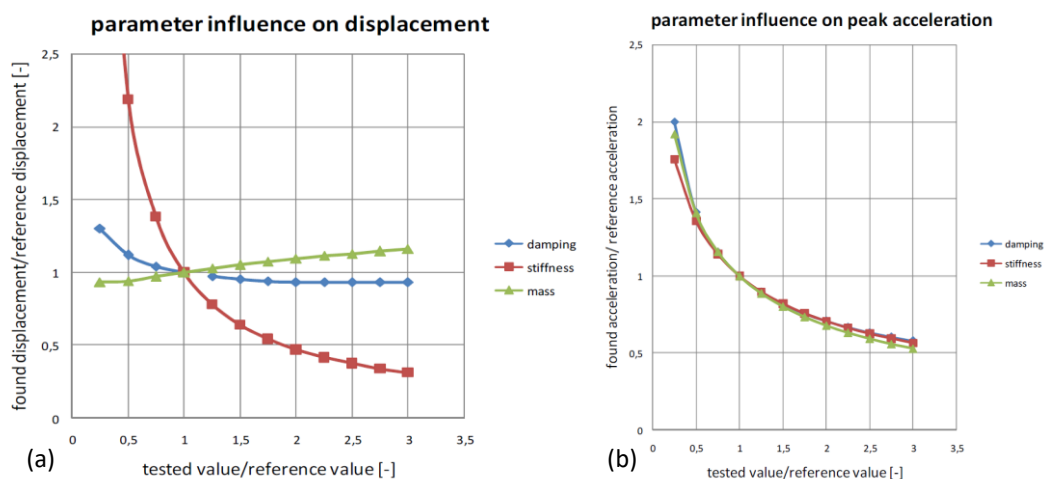

Figure 15: Influence study on displacements (a) and on accelerations (b) (Berg, 2012)

From Figure 15, it can be seen that the displacements are most strongly influenced by the stiffness. It also shows that the accelerations are more or less equally influenced by all three parameters. This result is explained using the derivation of the proposed procedure by NEN-EN 1991-1-4. This result deviates from the results of (Oosterhout, 1996), where a different influence of the three parameters on the accelerations is observed. This emphasises that the used analysis procedure also has influence on the results of the research.

Previous discussed studies can be very valuable in the preliminary design stage of a high-rise building. Yet, the existing influence studies are performed with simplified models which can be extended. For example by adding the influence of the foundation to the analysis. Also, results from existing research is only available in graphs which are hard to use for further research. Therefore, this research will improve/extend previous studies where possible.

CHAPTER 3
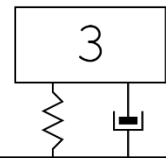
WIND

The dynamic wind load is the main loading mechanism used in this research. Multiple aspects are incorporated when defining the wind load on a structure. Based on literature, the way the fluctuating part of the wind is represented in the analysis procedure is discussed in this chapter.

3.1   GENERAL

The term wind, is used for the flow of air which is the result of horizontal pressure difference in the atmosphere. The pressure difference results in a flow of air from higher to lower pressure area with a certain strength and direction. When this flow is obstructed by an object, this results in an interaction between the airflow and the object.

For civil engineering practice, the wind-induced pressure on structures is of importance. The evaluation of these pressure loads on building surfaces, primary and secondary structural systems, and the consequent along wind, across wind and torsional response are the most important applications for structural engineering (Stathopoulos, 2007).

3.1.1 Notation

The three response directions are already mentioned: along wind, across wind and torsion. These three terms will often be used in this thesis and therefore deserve a clear description.

The used coordinate system is introduced as shown in Figure 16 (a). The system is such that the x-direction coincides with the main wind direction. Therefore, the width of the building is in y-direction and the depth in x-direction. The origin lies on ground level so the height of the building is given by the z-coordinate. The torsional direction would be given by φ.

The main response directions are related to the given coordinate system, see Figure 16 (b). Since the main wind direction is in x-direction, the alongwind response is parallel to the x-direction. Consequently, the acrosswind response is in the y-direction and the torsional response would be in the φ-direction.
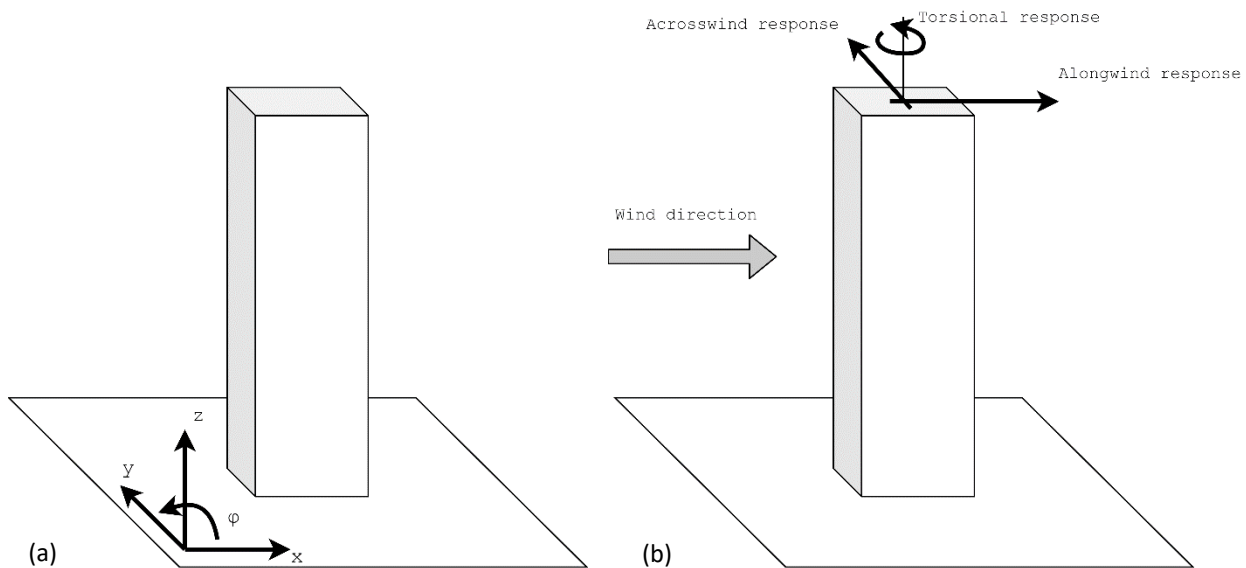

Figure 16: Coordinate system (a) and response components (b)

3.2   WIND VELOCITY

The wind is often represented by an average wind velocity depending on height z above the earth's surface. The wind velocity grows with altitude and decreases near the earth's surface due to obstacles. Near the earth, the wind velocity is lower due to friction but also creates turbulence in the wind flow. (Geurts, 1997)

The wind velocity in a specific point can be described in three orthogonal components: u in horizontal direction in the main wind direction, v in horizontal direction orthogonal to u, and w in vertical direction. The wind velocity consist of two parts, a constant mean part and a fluctuating part. By definition, the constant mean values of the v and w components are zero (Geurts, 1997).

This results in:

$$u = \bar{u} + \tilde{u}$$
$$v = \bar{v} + \tilde{v} = \tilde{v}$$
$$w = \bar{w} + \tilde{w} = \tilde{w}$$

(3.1)

$\bar{u}, \bar{v}, \bar{w}$ is the constant mean part [m/s]
$\tilde{u}, \tilde{v}, \tilde{w}$ is the fluctuating part [m/s]

The vertical component of the wind will not result in a dynamic response. On the other hand, the horizontal wind loads will result in horizontal motions. Therefore, only the horizontal components of the wind load are considered in this research.

3.2.1 Constant mean part of the wind velocity

The relation between the wind velocity, $\bar{u}(z)$, and the height above the earth surface, z, can be described by one of two formulas according to (Spijkers, et al., 2005) and (Gómez, 2019). The first is a theoretical derivation from fluid dynamics which results in a good approximation for heights under 200 meters, and results in the following function:

$$\bar{u}(z) = u(h_0) \frac{ln\left(\frac{z - h}{z_0}\right)}{ln\left(\frac{h_0 - h}{z_0}\right)}$$

(3.2)

$\bar{u}(z)$ is the wind velocity on height z above the earth surface [m/s]
h is the height of the building [m]
z_0 is a roughness length determined by the roughness of the terrain [m]
h_0 is the reference height [10 m]

The second formula uses the so-called power law:

$$\bar{u}(z) = u(h_0) \left(\frac{z - h}{h_0}\right)^\alpha$$

(3.3)

α is the power-law exponent

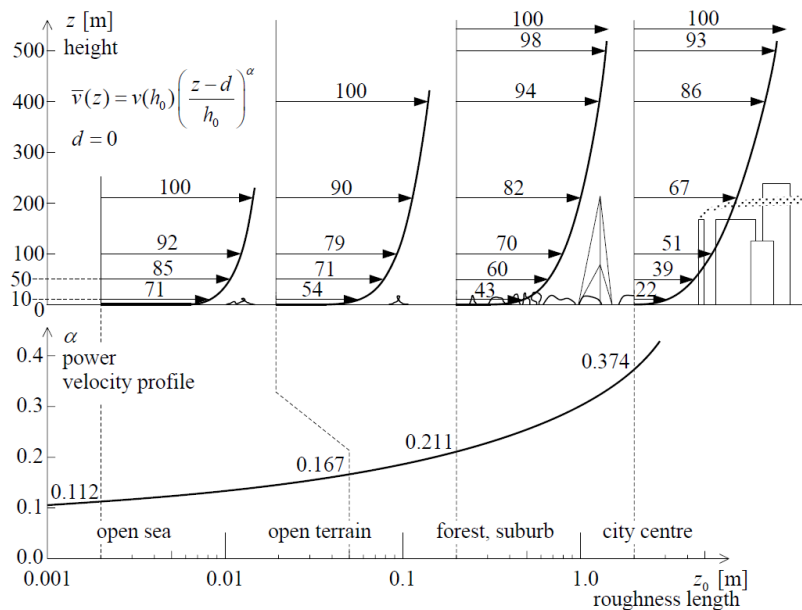Equation (3.3) is graphically illustrated in Figure 17.

Figure 17: Wind speed profiles according to the power-law model for different roughness values. (Spijkers, et al., 2005)

In NEN-EN 1991-1-4, the average wind speed on height z above the surface is given by ($\bar{u} = v_m$):

$$v_m(z) = c_r(z) \cdot c_0(z) \cdot v_b \tag{3.4}$$

c_r is the roughness factor
c_0 is the orography factor
v_b is the standard wind velocity at a reference height of 10 meters

The roughness factor is described by:

$$c_r(z) = k_r \cdot ln\left(\frac{z}{z_0}\right) \tag{3.5}$$

k_r is the terrain factor which is dependent on z_0
z_0 is the roughness length (coastal: 0.005 m   sub-urban: 0.2 m   urban: 0.5 m)

The terrain factor is given by:

$$k_r = 0.19 \cdot \left(\frac{z_0}{0.05}\right)^{0.07} \tag{3.6}$$

The orography factor takes into account the increase of wind velocity because of an inclined surface. This increase can be neglected if the average angle of the surface is less than 3°. For this research, this aspect will not be taken into account.

The standard wind velocity is given as:

$$v_b = c_{dir} \cdot c_{season} \cdot v_{b,0} \tag{3.7}$$

$v_{b,0}$ is the fundamental wind velocity (I: 29.5 m/s   II: 27.0 m/s   III: 24.5 m/s)
c_{dir} is the direction factor and should be equal to 1 according to NEN-EN 1991-1-4
c_{season} is the season factor and should be equal to 1 according to NEN-EN 1991-1-4

Considering the main wind direction(s) in the Netherlands, an example in Figure 18, the value for c_{dir} is questionable. It is a conservative assumption to consider the standard wind velocity equal in every direction. Since the wind load on high-rise buildings is governing for horizontal load cases, it could be very beneficial to take the wind direction into account. Yet, this requires specific information about the design and location. Since the aim of this research is to provide general applicable guidelines, these design and location specific aspects are not taken into account. Therefore, the assumption of the Eurocode ($c_{dir} = 1$) is used in this research.
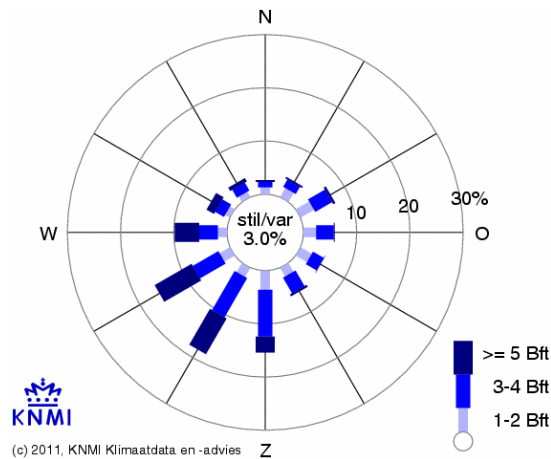

Figure 18: Multiple year (1981-2010) average wind direction in January in Rotterdam (Koninklijk Nederlands Meteorologisch Instituut, 2011)

The result of the Eurocode are the wind velocity profiles over the height for the different wind areas and roughness lengths as shown in Figure 19. The profiles show the same logarithmic relation as in Figure 17. The provided formulas in the Eurocode are only valid until a height of 200 meters. However, the NTA 4614-3 states that the formulas in the Eurocode are valid until a height of 300 meters in the Netherlands, with the addition that on large height there is no distinction between sub-urban and urban. The values for sub-urban can be used on large heights.

The wind velocity profiles of the three references are similar. Therefore, the choice which wind velocity profile to use will not influence the results significantly. Because the NTA 4614-3 states that the Eurocode formulas are valid until heights of 300 meters, the Eurocode formulas are used in this research.
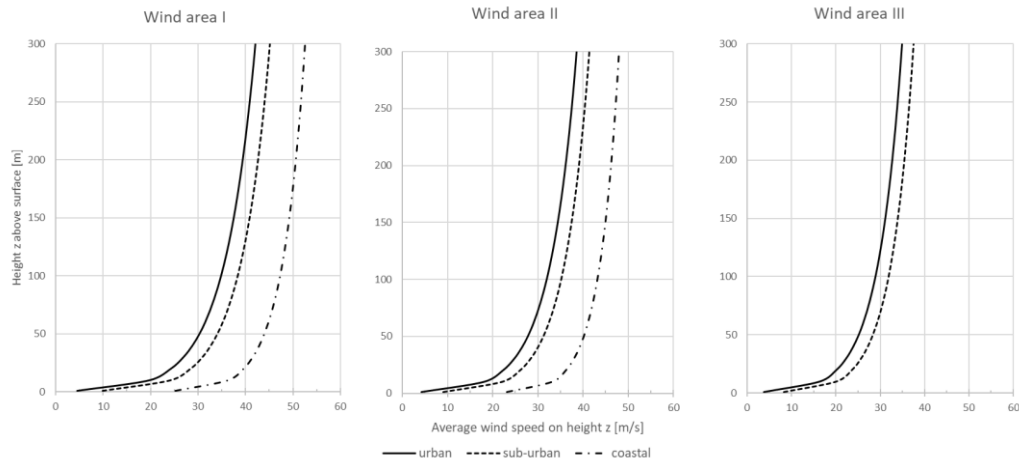

Figure 19: Average wind velocity on height z above the surface for $v_{b,0}(SLS) = 22.1\ (I), 19.4\ (II), 16.9\ (III)\ m/s\ and\ \rho_{air} = 1.25\ kg/m^3$ [NEN-EN 1991-1-4]

3.2.2   Fluctuating part of the wind velocity

Because the wind is obstructed by obstacles near the earth's surface, there is turbulence in the air flow. Also the interaction of the wind with the structure, creates turbulences in the wind velocity. This turbulence is the reason of the fluctuating part of the wind velocity (Geurts, 1997). This is visualized in Figure 20.
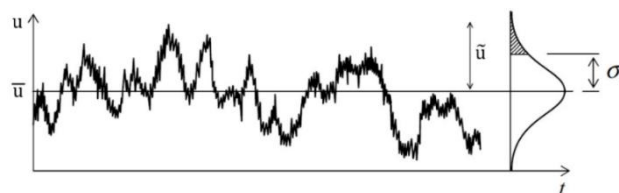
Figure 20: Fluctuating part of the wind velocity around the mean value (Berg, 2012)

The turbulence intensity is used for the fluctuating part of the wind velocity and is defined as the ratio of standard deviation σ of the representative component and the mean velocity at height z. In (Geurts, 1997), the following formulas are given for the turbulence intensities:

$$I_u(z) = \frac{\sigma_u(z)}{\bar{u}(z)} = \frac{1}{ln\left(\frac{z-d}{z_0}\right)} \qquad\qquad I_v(z) = \frac{\sigma_v(z)}{\bar{u}(z)} = \frac{0.8}{ln\left(\frac{z-d}{z_0}\right)} \tag{3.8}$$

The parameter d is used to take into account a corrected height of the surface level between densely built obstacles. Evaluating expression (3.8), the parameter d results in a shift to the right in Figure 19. Since this aspect is very location specific, this aspect is not taken into account in this research. By assuming this parameter equal to zero, the formulas of the turbulence intensity are the same as proposed in NEN-EN 1991-1-4.

3.3   WIND PRESSURE AND LOADING

3.3.1   Wind pressure

The wind velocity can be transformed into a wind pressure according to the following formula:

$$p_u = \frac{1}{2}\rho_{air}u^2 = \frac{1}{2}\rho_{air}(\bar{u}+\tilde{u})^2 \approx \frac{1}{2}\rho_{air}\bar{u}^2 + \rho_{air}\bar{u}\tilde{u} \tag{3.9}$$

ρ_{air} is the density of air (1.25 kg/m^3)

Here, the two different parts of the wind are observed: the constant mean part and the fluctuating part.

3.3.2   Shape factor

To be able to calculate the load on a structure, the shape factor, C_f, is used to take into account the influence of the dimensions of the structure. This factor takes into account the global effect of the wind on the structure, for example friction. For common shapes, most standards provide values which are determined experimentally. When the structure has a different shape, the shape factor should be determined with more advanced methods or wind tunnel tests. (Berg, 2012)

In NEN-EN 1991-1-4, an elaborated description of the C_f value is given. For rectangular sections with sharp angles, the value is between 0.9 and 2.4 depending on the ratio between the depth and width of the section, see Figure 21. In this research, only rectangular or square cross-sections of the building are considered. Therefore, the given values for the C_f-factor of the Eurocode are used.
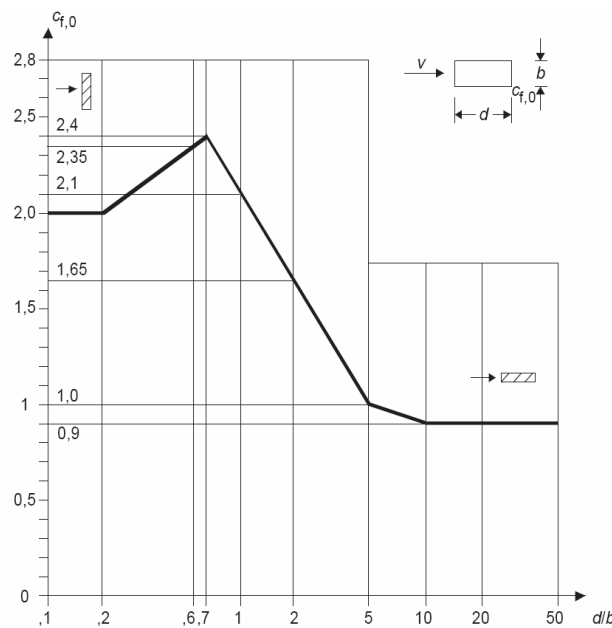
Figure 21: Shape factor for rectangular sections with sharp angles [NEN-EN 1991-1-4]

3.3.3   Wind load

The wind load can be obtained by multiplying the wind pressure, shape factor and the associated area on which the pressure is applied. This results in a constant (static) load and a dynamic load:

$$F_{u,static} = \frac{1}{2}\rho_{air}\,\bar{u}^2 A_u\,C_{f,u} \qquad\qquad F_{u,dynamic} = \rho_{air}\,\bar{u}\,\tilde{u}\,A_u\,C_{f,u} \tag{3.10}$$

For the orthogonal component, only a dynamic load is present:

$$F_{v,dynamic} = \rho_{air}\,\bar{u}\,\tilde{v}\,A_v\,C_{f,v} \tag{3.11}$$

The static and dynamic loads together, are visualized in Figure 22.

Figure 22: Combination of static and dynamic wind load over height

For the dynamic analysis of a structure, only the dynamic load is of importance. This load results in an extra response (deflection, velocity, acceleration) on top of the static deflection. This is visualized in Figure 23.
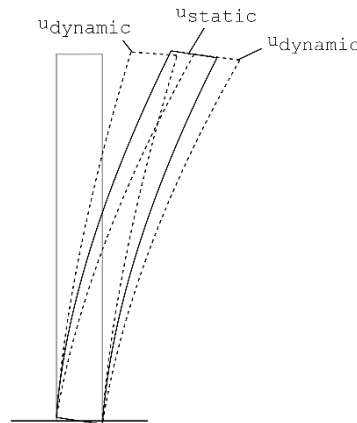
Figure 23: Dynamic response on top of the static deflection

3.4   SPECTRA OF WIND VELOCITY FLUCTUATIONS
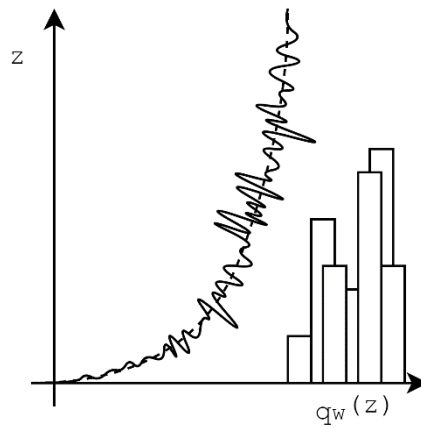
3.4.1   Spectral density functions

The fluctuating part of the wind contains a broad spectrum of frequencies. Much research is performed into the fluctuating part and multiple proposals are made for spectra to describe these fluctuations. These spectra describe the magnitude of the wind velocity fluctuations over the different frequencies. The spectral density functions are calculated from time series of fluctuating signals (Geurts, 1997).

An important property of these one-sided spectra is (Geurts, 1997):

$$\sigma_i^2 = \int_0^\infty S_{ii}(f)\, df \qquad\qquad i = u, v \qquad\qquad (3.12)$$

This means that the integral over the spectrum results in the total variance of the response. Taking the square root of the variance results in the standard deviation (σ_i).

The spectral density functions are usually represented as non-dimensional quantities. For this, the frequency is reduced by a length scale and the mean wind velocity. In (Geurts, 1997), the reference height z is proposed as length scale. Which results in:

$$f_L = \frac{f\, z}{\bar{u}(z)} \qquad\qquad (3.13)$$

In NEN-EN 1991-1-4, the turbulence length scale is proposed which results in:

$$f_L = \frac{f\,L(z)}{\bar{u}(z)} \tag{3.14}$$

Theoretically, the different spectra proposed in literature fit into a general expression (Geurts, 1997):

$$\frac{f\,S_{ii}}{\sigma_i^2} = \frac{A\,f_L^{\gamma}}{(C + B\,f_L^{\alpha})^{\beta}} \qquad\qquad i = u,v \tag{3.15}$$

The coefficients $\alpha, \beta, \gamma, A, B$ and C determine the shape and position of the spectrum. Multiple values are proposed in literature ((Wisse & Staalduinen, 1992), (Stathopoulos, 2007), (Oosterhout, 1996), (Geurts, 1997)) for the different coefficients from measurements, depending on geographical location and terrain type. Also NEN-EN 1991-1-4 provides a spectrum in appendix B of the NEN-EN 1991-1-4. The proposed values from the Eurocode and (Geurts, 1997) are assumed to be most representative for the Dutch situation and are shown in Table 4.

A direct comparison between the three spectra cannot be made since the frequency is scaled with a different length scale. In (Geurts, 1997) the reference height z is used and in NEN-EN 1991-1-4 the turbulence length $L(z)$ is used. The three spectra are scaled accordingly for $\bar{u}(z) = 26.9$ m/s, $z = 150$ m and $L(z) = 249{,}9$ m, which makes a comparison possible, which is shown in Figure 24. The spectrum from NEN-EN 1991-1-4 almost perfectly coincides with the spectrum for the v component of (Geurts, 1997). It is also observed that the u component of (Geurts, 1997) has lower density values for almost the complete frequency range. Because two spectra (u and v component) are needed for this research, the proposed spectra from (Geurts, 1997) will be used. Although measured in Eindhoven, the two spectra from (Geurts, 1997) are considered representative for the whole Netherlands.

		α	β	γ	A	B	C
NEN-EN 1991-1-4	—	1	5/3	1	6.80	10.20	1
(Geurts, 1997)	u	1	5/3	1	36.19	54.31	1
	v	1	5/3	1	11.71	17.56	1

Table 4: Values for $\alpha, \beta, \gamma, A, B$ and C according to the NEN-EN 1991-1-4 and (Geurts, 1997)
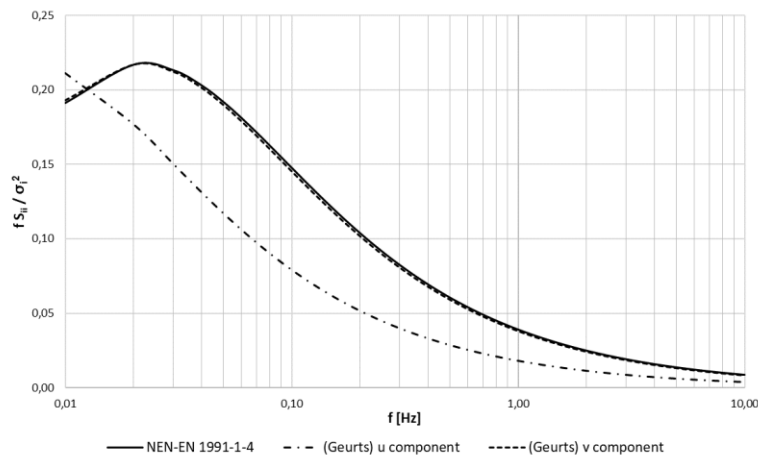

Figure 24: Spectral density functions of the NEN-EN 1991-1-4 and (Geurts, 1997)

The spectral density functions are (Geurts, 1997):

$$\frac{f\,S_{uu}}{\sigma_u^2} = \frac{36.19\,f_L}{(1 + 54.31\,f_L)^{5/3}} \qquad\qquad \frac{f\,S_{vv}}{\sigma_v^2} = \frac{11.71\,f_L}{(1 + 17.56\,f_L)^{5/3}} \tag{3.16}$$

f_L as given in equation (3.13)

3.4.2 Load spectrum

The fluctuating part of the load is given in equations (3.10) and (3.11). The standard deviation of the loading is then:

$$\sigma_{F,u}^2 = \left(\rho_{air}\,\bar{u}\,A_u\,C_{f,u}\right)^2 \sigma_u^2 \qquad\qquad \sigma_{F,v}^2 = \left(\rho_{air}\,\bar{u}\,A_v\,C_{f,v}\right)^2 \sigma_v^2 \qquad\qquad (3.17)$$

This yields for the loading spectra:

$$S_{FF,u}(\omega) = \left(\rho_{air}\,\bar{u}\,A_u\,C_{f,u}\right)^2 S_{uu}(\omega) \qquad\qquad S_{FF,v}(\omega) = \left(\rho_{air}\,\bar{u}\,A_v\,C_{f,v}\right)^2 S_{vv}(\omega) \qquad (3.18)$$

The two example loading spectra associated to the shown spectral density functions of Geurts in Figure 24, are shown in Figure 25. The spectra are plotted against the frequency f [Hz]. The difference between the two components is clearly visible.
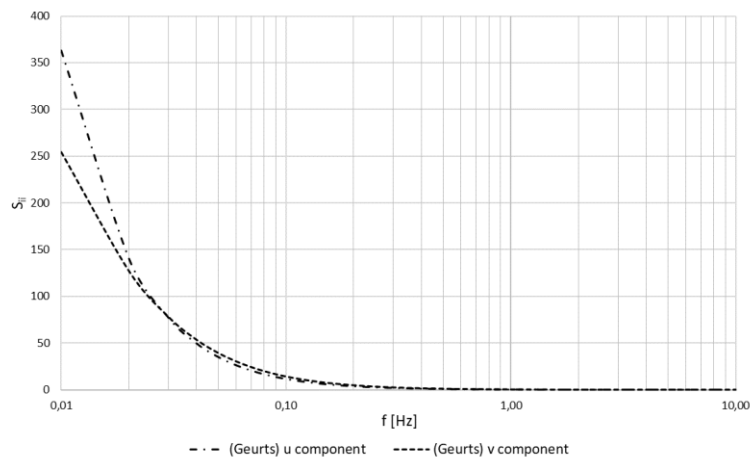

Figure 25: Loading spectra for the two wind components

In equation (3.18), the load spectrum is written in terms of ω [rad/s], which is the angular frequency instead of the frequency [Hz]. This is convenient for later calculations. For this, the spectral density function should be rewritten in terms of ω. This is performed in Appendix A. It is assumed that the spectral density function is constant over the height. The reference height z, is taken equal to the total height of the building. This is a conservative assumption since the load spectrum will take higher values for higher values of z. By doing so, the load spectrum is only depending on the angular frequency ω.

3.4.3 Aerodynamic admittance

In the spectral density functions, it is assumed that the fluctuations are perfectly correlated over the whole area. In reality, due to the gusts in the wind, this will not be the case, so a correction should be incorporated (Geurts, 1997). This correction should also be in the frequency domain and is called the aerodynamic admittance. It incorporates all aerodynamic phenomena and is measured from experiments and wind tunnel tests.

Vickery (1965) proposed the following empirical fit (Geurts, 1997):

$$|\chi_i(\omega)|^2 = \left(1 + \left(\frac{\frac{\omega}{\pi}\sqrt{A}}{\bar{u}}\right)^{4/3}\right)^{-2} \qquad\qquad i = u, v \qquad\qquad (3.19)$$

NEN-EN 1991-1-4 Annex B also provides formulas for the aerodynamic admittance:

$$\chi_i(\omega)^2 = R_h R_{b,i} \qquad\qquad i = u, v \qquad\qquad (3.20)$$

with:

$$R_h = \frac{1}{\eta_h} - \frac{1}{2\eta_h^2}\left(1 - e^{-2\eta_h^2}\right) \qquad\qquad R_{b,i} = \frac{1}{\eta_{b,i}} - \frac{1}{2\eta_{b,i}^2}\left(1 - e^{-2\eta_{b,i}^2}\right) \qquad (3.21)$$

with:

$$\eta_h = \frac{4.6\,h}{\bar{u}(z)} \cdot \frac{\omega}{2\pi} \qquad\qquad\qquad \eta_{b,i} = \frac{4.6\,b_i}{\bar{u}(z)} \cdot \frac{\omega}{2\pi} \qquad\qquad (3.22)$$

h is the height of the building
b_i is the width of the building in x- or y-direction

Both formulas are plotted in Figure 26. The empirical fit of Vickery is based on relatively small objects in test models (Geurts, 1997). Therefore, the aerodynamic admittance is relatively high for frequencies up to 0.1 Hz. Since the area of a building will be relatively large, the formula of NEN-EN 1991-1-4 will give a better correlation of wind fluctuations. Therefore, the aerodynamic admittance of NEN-EN 1991-1-4 is used in this research.
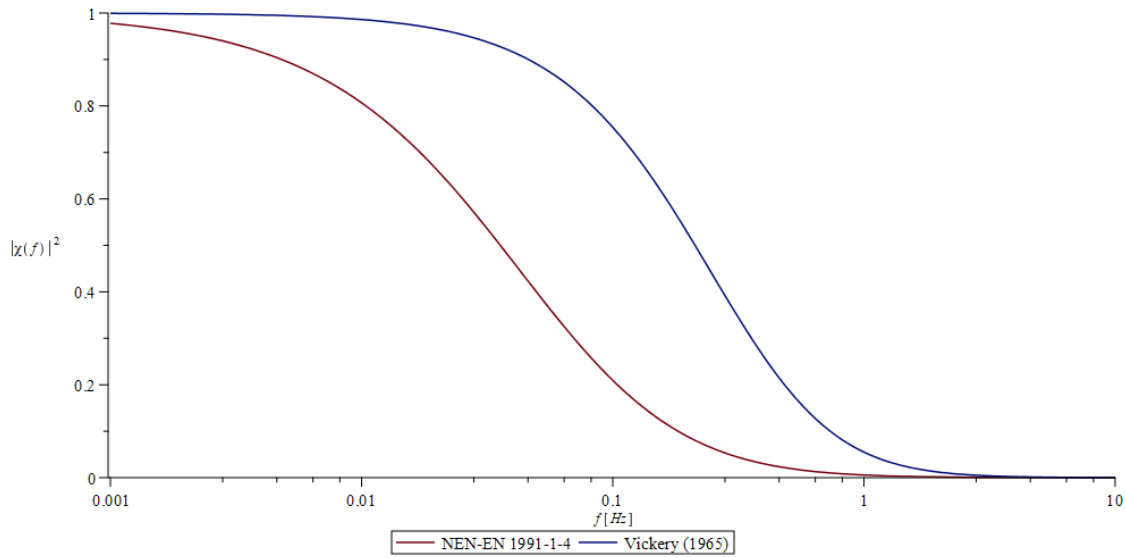
Figure 26: Aerodynamic admittance function of the NEN-EN 1991-1-4 and Vickery (1965) for h=150, b=30, $\bar{u}$=19.4 and z=h

3.4.4   Load spectrum including aerodynamic admittance

The load spectrum including the aerodynamic admittance is given by:

$$S_{FF,u}(\omega) = \left(\rho_{air}\,\bar{u}\,A_u\,C_{f,u}\right)^2 |\chi_u(\omega)|^2 S_{uu}(\omega) \qquad S_{FF,v}(\omega) = \left(\rho_{air}\,\bar{u}\,A_v\,C_{f,v}\right)^2 |\chi_v(\omega)|^2 S_{vv}(\omega) \qquad (3.23)$$

CHAPTER 4
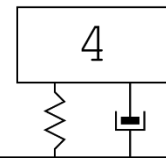
DYNAMIC RESPONSE OF STRUCTURES

For the dynamic analysis of high-rise buildings under wind load, two main parts can be distinguished. The first part is the determination of the load, which is described in chapter 3. The second part is the dynamic response of the structure, which will be discussed in this chapter.

First, the three response directions (along wind, across wind and torsion) are discussed. The along wind response is straight forward and does not require long elaboration. For the across wind response, the phenomena of vortex shedding can occur. How this is taken into account in this research is explained. The torsional response is not investigated in this research. To provide a complete overview, a short description is provided regarding the torsional response of the structure. When the three response directions are analysed separately, they have to be combined accordingly. This is also shortly described. It is good to keep in mind that the response directions are coupled in reality, which is also briefly discussed in this chapter. Second, the two types of commonly used systems, discrete and continuous system, are discussed. Then, the spectral analysis is explained, which is used to determine the maximum acceleration of the structure in this research. Finally, the most important aspects regarding the comfort criteria are provided. Different restrictions on the maximum acceleration of the building found in literature, are discussed.

4.1 RESPONSE DIRECTIONS

For high-rise buildings, the complete dynamic response can be described in three response directions as already introduced before: (see Figure 9 and Figure 16)

- Response parallel to the wind direction (along-wind response);
- Response perpendicular to the wind direction (across-wind response);
- Response in torsion.

For standard structures, the across-wind and torsional response are generally less significant than the along-wind response. However, for structures with significant height, the across-wind and torsional response can become more significant. (National Research Council of Italy, 2008)

A rule of thumb for the significance of the across-wind and torsional response is given by (National Research Council of Italy, 2008). The effects of the across-wind and torsional actions should be assessed if:

$$\frac{h}{\sqrt{b\,d}} \geq 3 \tag{4.1}$$

Equation (4.1) is evaluated in the considered geometrical domain of this research, namely: height $h = 100 - 300$ m, width $b = 30 - 90$ m, depth $d = 30 - 90$ m, and visualised in Figure 27. In the (A) area, equation (4.1) is always below 3.0 and therefore the across-wind and torsional actions are assumed to be small. In the (C) area, equation (4.1) is always above 3.0 and therefore the across-wind and torsional effects should be assessed. In the (B) area in between, the value of equation (4.1) is depending on the value of d.
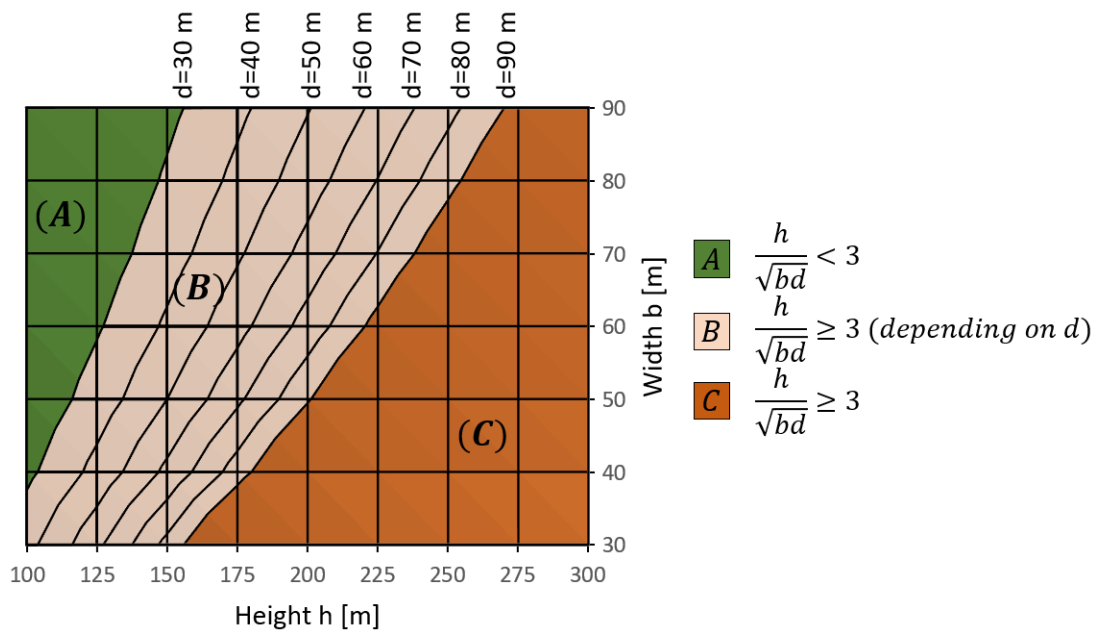
Figure 27: Visualisation of equation (4.1) in the geometrical domain of this research: h=100-300 m, b=30-90 m, d=30-90 m

4.1.1 Dynamic response in the wind direction (along wind)

With uncoupled modes, the along wind response has a linear relation with the along wind component u of the wind load. As shown in chapter 3, the along wind component u has a static and a dynamic part. Therefore, the along wind response will also have a static and dynamic response. This is visualised in Figure 23. In terms of deflection, the total deflection is the combination of the static deflection and the maximum of the dynamic deflection. In terms of acceleration, only the dynamic part of the wind results in accelerations. Therefore, the maximum acceleration is caused by only the dynamic part of the wind.

Under the assumption of uncoupled response directions, the along wind response can be analysed in a one directional model, either discrete or continuous, using the u component of the wind load.

4.1.2 Dynamic response perpendicular to the wind direction (across wind)

As also shown in chapter 3, the wind load has a fluctuating component v in the perpendicular direction. The same as with the along wind, the across wind response, in terms of acceleration, is only caused by this fluctuating part of the wind load perpendicular to the wind direction. Also for the across wind response, under the assumption of uncoupled response directions, the across wind response can be analysed with a one directional model, either discrete or continuous, using the v-component of the wind load.

Apart from this fluctuating component of the wind load, another phenomena, called vortex shedding, can cause a fluctuating load in the perpendicular direction. So, the total fluctuating load in the perpendicular direction can be the sum of:

- The fluctuating part of the v-component of the wind;
- The fluctuating load from vortex shedding.

However, the fluctuating load from vortex shedding is not always present. When air flows around a building, the flow separates at the corners of the building which can cause a periodic shedding of vortices. This periodic shedding of vortices creates fluctuating pressures and therefore forces on the building, see Figure 28 (Mooneghi & Kargarmoakhar, 2016). The occurrence of vortices is depending on the wind velocity and the shape of the cross-section of the building. It can occur with different frequencies and amplitude. Therefore, the load from vortex shedding is not always of importance for the design of high-rise structures.
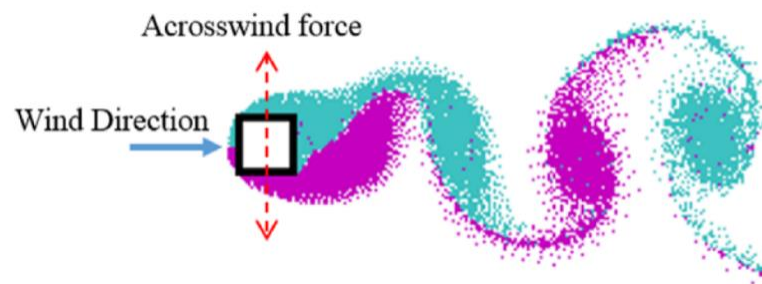
Figure 28: Vortex shedding (plan view) (Mooneghi & Kargarmoakhar, 2016)

In the case of vortex shedding, the distinction should be made between: (Wisse & Staalduinen, 1992)

- The response is such that no interaction between structure and wind flow occurs;
- The response is such that the movement of the structure influences the wind flow.

In the latter case, the so-called 'lock-in effect' can occur, when the movement of the building influences the flow around the building (Wisse & Staalduinen, 1992).

The vortexes tend to occur with a particular frequency. From wind tunnels tests, this frequency is dependent on the shape of the horizontal cross-section of the building. This particular frequency of vortex shedding can be determined with the Strouhal number:

$$f_s = \frac{St \, \bar{v}}{b} \tag{4.2}$$

> St is the Strouhal number
> b is the width of the building in y-direction

When the frequency of vortex shedding is close to one of the natural frequencies of the building, amplified acrosswind response can occur.

In NEN-EN 1991-1-4, it is stated that the effects of vortex shedding should be considered if the ratio between the largest and smallest dimension of the building, perpendicular to the wind direction, is larger

than 6. For high-rise buildings, this is also called the slenderness of the building. Also, a formula is given to check the significance of vortex shedding which is based on the average wind velocity. According to NEN-EN 1991-1-4, the effects of vortex shedding should be considered if:

$$v_{crit,i} > 1.25 \, \bar{v} \tag{4.3}$$

with:

$$v_{crit,i} = \frac{b \, f_{i,y}}{St} \tag{4.4}$$

$f_{i,y}$ is the natural frequency of the ith mode in y-direction

The Eurocode also provides values for the Strouhal number for simple shaped cross-sections, see Figure 29:

$$St = \begin{cases} 0.12 & 0 < d/b < 1 \\ 0.18 - 0.06 \, d/b & 1 \leq d/b < 2 \\ 0.06 & 2 \leq d/b < 3 \\ -0.48 + 0.18 \, d/b & 3 \leq d/b \leq 3.5 \\ 0.2433 - 0.02667 \, d/b & 3.5 < d/b < 5 \\ 0.13 - 0.004 \, d/b & 5 \leq d/b < 10 \\ 0.09 & d/b \geq 10 \end{cases} \tag{4.5}$$
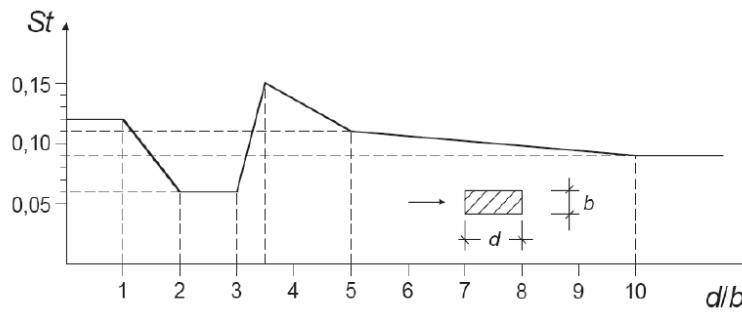

Figure 29: Strouhal number for rectangular shaped cross-sections with sharp angles

As a first approximation, the force from vortex shedding can be described by a harmonic function (National Research Council of Italy, 2008):

$$F_{vortex}(t) = A_s \, sin \, (2\pi f_s t) \tag{4.6}$$

A_s is the force amplitude
f_s *is the dominant vortex shedding frequency (equation* (4.2)*)*

When using this first approximation of the force, the following statements, given in (National Research Council of Italy, 2008), should be considered:

- With increasing turbulence in the air flow, the harmonic content of the force spreads over a broader range of frequencies, which mitigates the across-wind response;
- Since the mean wind velocity varies over height, the vortex shedding frequency does as well. A critical height can be determined to assess the response to vortex shedding. This critical point is located where the resonant vibration has a maximum, see Figure 30. Since the used model has only one degree of freedom related to the superstructure, the second mode shape of a continuous beam cannot be captures with the 3DoF model. Therefore, the assessment of vortex shedding is only investigated at the top of the building in this research, the critical point of the first mode of vibration of the continuous beam;
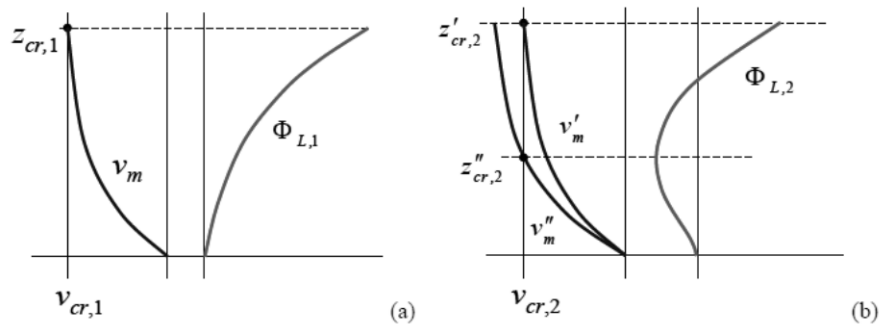
Figure 30: Critical positions for (a) the first mode and (b) the second mode of vibration (National Research Council of Italy, 2008)

- The already mentioned lock-in effect can occur. This has the consequence that the relation for the vortex shedding frequency, equation (4.2), is not linear anymore, see Figure 31. The width of the velocity interval $\Delta v_{cr,i}$ is broader, the smaller the Scruton number. This means that vibrations from vortex shedding can occur for mean wind velocities within the range shown in Figure 31 (b).
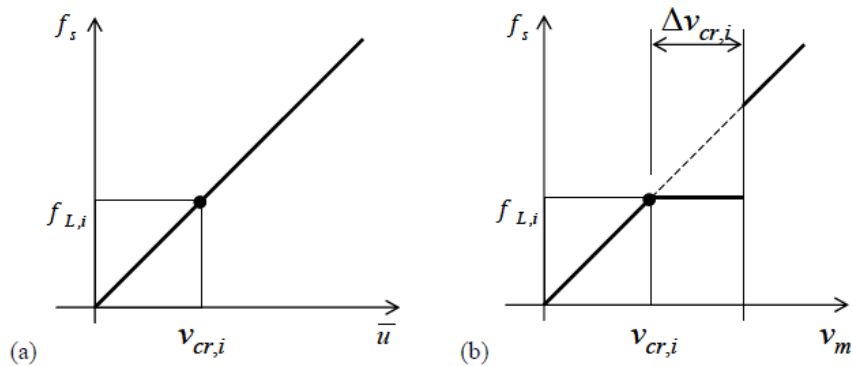
Figure 31: Strouhal law for (a) large and (b) small Scruton numbers (National Research Council of Italy, 2008)

Based on the Scruton number, three regimes can be identified, see Figure 32: "forced", "self-excited" and "transition". Indicatively, the transition from forced to self-excited response occurs for Scruton numbers of approximately 5 to 20. An usual design requirement is that the structure should remain in the field of forced vibrations (National Research Council of Italy, 2008). If the structure remains in the forced regime, the total across-wind load from vortex shedding can be taken as given in equation (4.6). If the structure enters the domain of the other regimes, an aeroelastic force, which depends on the motion of the structure, occurs. Reliable procedures of predicting the response in this latter case are still lacking.
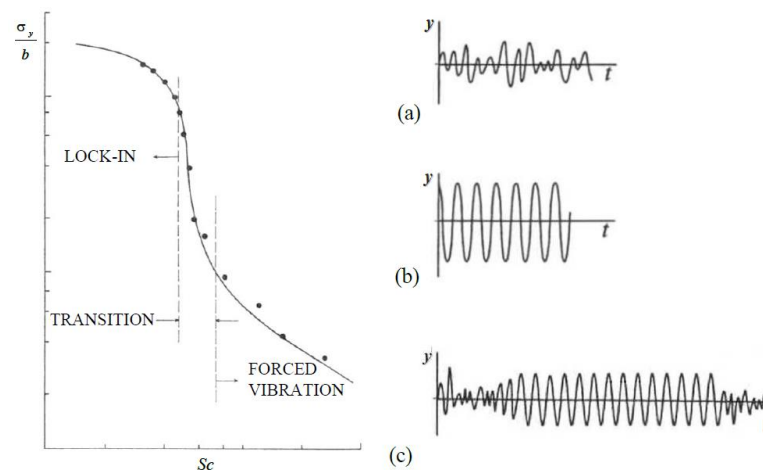
Figure 32: Domains of the across-wind response to vortex shedding and (a) forced, (b) self-excited and (c) transition response regimes (National Research Council of Italy, 2008)

The Scruton number is given by:

$$Sc = \frac{4 \pi \rho A \xi_{L,i}}{\rho_{air} b^2}$$ (4.7)

$\xi_{L,i}$ is the damping ratio in the ith across-wind vibration mode

Based on the indication from (National Research Council of Italy, 2008), a structure is assumed to be in the forced regime for Scruton numbers higher than 20 in this research. Within the influence study into vortex shedding, 96% of all cases have a Scruton number larger than 20. Therefore, only the forced regime is considered in this research. The remaining 4% could be in a transition - or self-excited regime. Yet, this is not considered within this research. The remaining 4% are buildings with a large width ($b = 90$ m), and have a minimum Scruton number of 17.2. For buildings which are not within the forced regime, the conclusions stated in this research may be invalid.

The force from vortex shedding is not strictly periodic, as given by equation (4.6), but has a spectral density. As already mentioned, this means that the harmonic content of the force spreads over a range of frequencies. The spectrum of the force from vortex shedding, per unit length, is given by: (Davenport & Novak, 2002)

$$W_L(f) = \left(\frac{1}{2}\rho_{air}D\bar{V}^2\sigma_L\right)^2 W_L'(f)$$ (4.8)

D is the width of the frontal area of the cross-section
$\bar{V}$ is the mean wind velocity
σ_L is the standard deviation of the vortex shedding coefficient
W_L' is the normalized power spectrum

Equation (4.8) is rewritten to have the same form as the spectrum formulas for the alongwind and acrosswind. These spectra are for a point force at a specific height. To rewrite equation (4.8) as a point load at a specific height, in this case the top of the building (h), the mean wind velocity is taken at height h. Also, a certain height over which the turbulent pressure from vortex shedding is working needs to be taken into account. This height is determined by the first mode shape of a clamped beam system. The integral over the height of the first mode shape is used as a reduced height over which the turbulent pressure from vortex shedding is working. This results in: $0.3915\ h$. The normalized power spectrum is written as $S_{vortex}(\omega)$. This yields for the loading spectrum for vortex shedding:

$$S_{FF,vortex}(\omega) = \left(0.3915 \cdot \frac{1}{2}\rho_{air}bh\bar{u}^2\sigma_L\right)^2 S_{vortex}(\omega)$$ (4.9)

The normalized power spectrum for vortex shedding is concentrated around the vortex shedding frequency f_s, and has a certain bandwidth that depends on the turbulence intensity. Such a spectrum can be described by a Gaussian-type curve: (Davenport & Novak, 2002)

$$W_L'(f) = \frac{1}{\sqrt{\pi}Bf_s} exp\left(-\left(\frac{1-f/f_s}{B}\right)^2\right)$$ (4.10)

B is the bandwidth
f_s is the vortex shedding frequency

Design values for the bandwidth B and standard deviation of the vortex shedding coefficient σ_L are obtained from literature. Three references ((Davenport & Novak, 2002), (Balendra, 1993), (Tsukagoshi, et al., 1993)) are found which propose relatively similar values for the bandwidth B. Because it is known that the bandwidth increases with increasing turbulence, the bandwidth B is linked to the turbulence intensity, as recommended by (Balendra, 1993): $B = \sqrt{2}I_v$. Using the Gaussian-type curve for the normalized power

spectrum, the σ_L determines only the height of the peak in the load spectrum. (Davenport & Novak, 2002) proposes a constant value for σ_L of 0.6 for square cross-sections. This value is also used for rectangular cross-sections. A higher or lower value for σ_L will result in a higher or lower acceleration response, since the load and the response have a linear relation.

Rewriting the normalized power spectrum in terms of angular frequency results in:

$$S_{vortex}(\omega) = \frac{1}{\sqrt{\pi}Bf_s} \, exp\left(-\left(\frac{1-\omega/2\pi f_s}{B}\right)^2\right) \tag{4.11}$$

An example of the load spectrum for vortex shedding is shown in Figure 33.
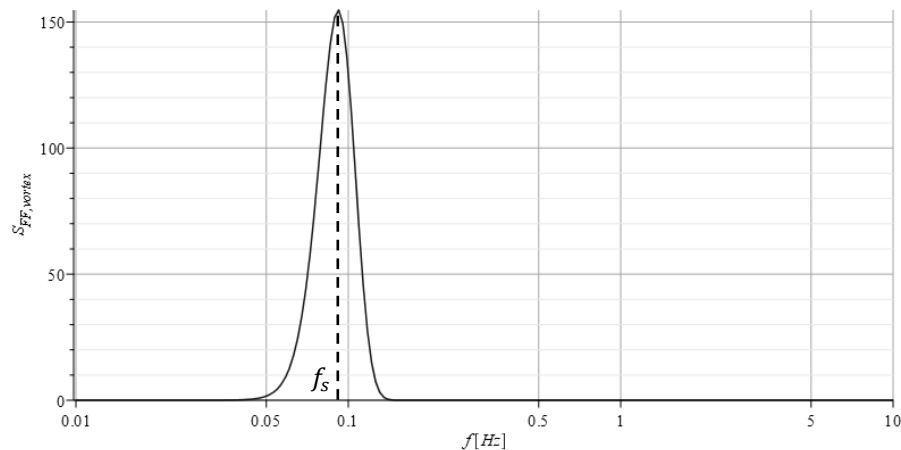
Figure 33: Example of the loading spectrum for vortex shedding with vortex shedding frequency of 0.09 Hz

4.1.3 Dynamic response due to a wind load in torsion

Because of the limited time for this research, the torsional response is not investigated. Also, the aim of the research is not necessarily to accurately predict the total response, but to provide insight into the influence of parameters. Still, a short description is provided in this section, because it is good to keep in mind that the torsional mode can have a contribution to the total response of the structure.

In determining the motion on the edges of a building, the torsional response of the building can have a contribution. If the building is vulnerable for torsional movement, meaning a relatively low torsional stiffness, the torsional response can become significant and should be considered in the analysis. In general it can be stated that, the lower the natural frequency in torsion, the higher the influence on the total response (Steenbergen & Geurts, 2011).

The mode shape in torsion is depending on the floor plan of the building. When the stabilizing elements are located at the sides of the building, a different torsional mode shape will occur than when the stabilizing elements are located in the centre of the building. An example of these two mode shapes is given in NEN-EN 1991-1-4 and (Steenbergen, et al., 2008), and shown in Figure 34.

Figure 34: Torsional mode shapes (Steenbergen, et al., 2008)

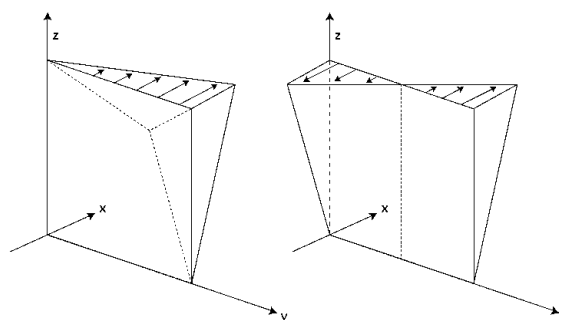A torsional response can also be caused by an asymmetrical load. Asymmetrical loading can occur due to a lag of correlation between the wind gusts on different locations on the building's facade. Also, if the wind load has a certain angle with respect to the façade, an asymmetrical loading can occur. This second cause of asymmetrical loading is shown in Figure 35. Both the NEN-EN 1991-1-4 and the CNR-DT 207-2008 propose the same pressure distribution to take asymmetrical loading into account. A triangular pressure distribution should be applied on the leeward face, and a uniform pressure distribution on the windward face, see Figure 35.
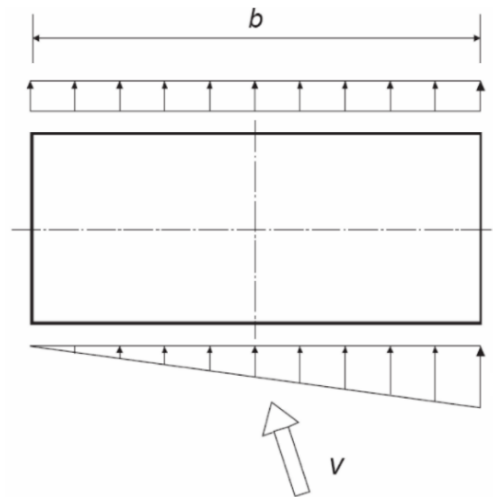

Figure 35: Pressure distribution for asymmetrical loading. Arrow indicates the direction of the wind [NEN-EN 1991-1-4]

4.1.4   Combination of response directions

Until now, all response directions are considered individually and separate analysis procedures can be performed. Yet, the different response directions can occur at the same time. This is especially true for the lateral (along- or across-wind response) and the torsional response. To take this into account, the results of the separate analysis procedures should be combined. For example, (Steenbergen, et al., 2008) states that the peak values of acceleration in the lateral and torsional mode shape should be combined as vectors. Alternatively, (National Research Council of Italy, 2008) proposes three different combination rules, including combination coefficients for the three response directions.

Because the aim of this research is not necessarily to accurately predict the maximum acceleration, the torsional response direction is not investigated in this research. Therefore, the combination of response directions is not of great importance for this research. Hence, further elaboration about the combination of response directions is not provided.

4.1.5   Coupling of response directions

As described, the different response directions can be considered separately and, if necessary, combined accordingly. Most common analysis procedures, including the one described in Eurocode, use this one-directional analysis procedure. This can give a good estimation of the response when a particular response direction is dominant. Yet, when the influence of the different response directions are close to each other, it is possible that the one-directional approach underestimates the response. Also, it will be the case that the different modes in the different directions have influence on each other. This influence is not considered in a one-directional approach. It is possible that certain dynamic behaviour is therefore overlooked. Yet, a model that can capture the coupled behaviour of the structure is complex and multiple extra parameters are introduced. The amount of parameters in a one-directional model is already large, let alone the amount in a three-directional model. Therefore, in this research, the one-directional model is used separately for the different response directions (along-wind and across-wind response).

4.2   ANALYTICAL SYSTEMS

Vibrating systems can move and rotate in three directions. Because the description of this movement in all directions is complicated for complex structures, many of these vibratory phenomena are understood by studying the behaviour of simpler systems. Two types of commonly used systems are:

- Discrete systems (single- or multi-degree-of-freedom);
- Continuous systems.

The main model used in this research is a discrete system. To illustrate the behaviour of a discrete system, the derivation of the response and frequency response function of the most simple one-degree-of-freedom system is explained using an example. An example of the derivation for a multi-degree-of-freedom system is provided in Appendix B. The case of a continuous system is also used in this research. The derivation of the response of a clamped beam system and modal properties are provided.

4.2.1   Discrete systems

In discrete systems, the mass of the structure is lumped into a single point or multiple points. These models are governed by ordinary differential equations. Every possible way the lumped mass can move is one degree of freedom. (Metrikine, n.d.)

Because only linear systems are considered, the stiffness of the system can be represented by a spring with a certain spring stiffness. When the system also includes damping, this can be represented by a dashpot with a certain value of viscous damping.

One-degree-of-freedom system

The most simple form of a one-degree-of-freedom system with damping is shown in Figure 36.
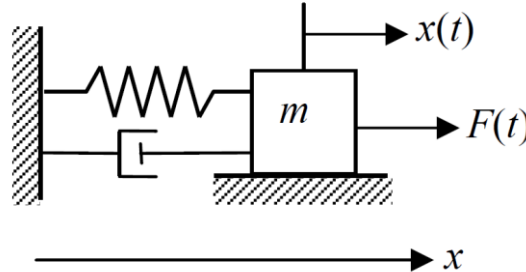
Figure 36: One-degree-of-freedom system with damping (Metrikine, n.d.)

The equation of motion of the system is:

$$m\ddot{x} + c\dot{x} + kx = F(t) \tag{4.12}$$

To find the natural frequencies of the system, the free vibration of the system should be analysed. For this, the general solution is substituted into the equation of motion. The general solution is:

$$x(t) = \sum_{n=1}^{2} C_n \, e^{s_n t} \tag{4.13}$$

From this, the characteristic equation is obtained from which the natural frequencies can be determined. In (Metrikine, n.d.), it is proven that the natural frequency of the damped system is almost equal to the natural frequency of the undamped system, for low damping ratio's (<10% critical damping).

The damping ratio is given by:

$$\xi = c/c_{cr} \tag{4.14}$$

with critical damping defined by:

$$c_{cr} = 2\sqrt{km} \qquad (4.15)$$

If the damping ratio is smaller than 10%, then:

$$\omega_1 = \sqrt{\omega_n^2 - n^2} \approx \omega_n = \sqrt{k/m} \qquad (4.16)$$

Rewriting the general solution results in the free vibration of the system, a damped harmonic function:

$$x(t) = A_0\, e^{-nt}\, cos\,(\omega_1 t - \varphi_0) \qquad (4.17)$$

A_0 is the amplitude depending on initial conditions $x(0) = x_0$ and $\dot{x}(0) = v_0$
φ_0 is the initial phase depending on initial conditions $x(0) = x_0$ and $\dot{x}(0) = v_0$
n is a measure for the viscous damping in the system: $2n = c/m$

The free vibration of the system is shown in Figure 37.
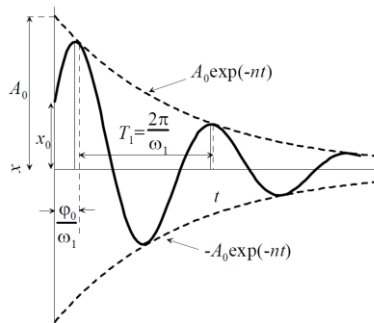
Figure 37: free vibration of the one-degree-of-freedom system with damping ($\zeta < \omega_n$) (Metrikine, n.d.)

For the forced vibrations, a harmonic force is introduced: $F(t) = F_0 cos\,(\omega t)$. This leads to the equation of motion:

$$m\ddot{x} + c\dot{x} + kx = F_0 cos\,(\omega t) \qquad (4.18)$$

The general solution is the sum of the homogeneous solution and a particular solution. The particular solution can be found in the form:

$$x_{part} = Re(\hat{X}\, e^{i\omega t}) \qquad (4.19)$$

Substitution of the particular solution into the equation of motion results in the complex amplitude:

$$\hat{X} = \frac{f_0}{-\omega^2 + 2in\omega + \omega_n^2} \qquad (4.20)$$

f_0 is a different notation of the force: $f_0 = F_0/m$

With this complex amplitude, the particular solution can be found:

$$x_{part} = \frac{f_0}{(\omega_n^2 - \omega^2)^2 + 4n^2\omega^2}\left((\omega_n^2 - \omega^2)\, cos(\omega t) + 2n\omega\, sin(\omega t)\right) \qquad (4.21)$$

Because the homogeneous solution gradually subsides in time (e^{-nt}), the steady state solution is given by the particular solution. The particular solution can be written as:

$$x_{part} = |X|cos\,(\omega t - \varphi) \qquad (4.22)$$

with:

$$|X| = \frac{f_0}{\sqrt{(\omega_n^2 - \omega^2)^2 + 4n^2\omega^2}} \qquad\qquad \varphi = arctan\left(\frac{2n\omega}{(\omega_n^2 - \omega^2)}\right) \qquad (4.23)$$

The term |X| is called the amplitude-frequency characteristic and is depending on the angular frequency. When substituting and dividing by the static deflection $x_{static} = F_0/k$, the so-called dynamic amplification factor, or frequency response function, is obtained:

$$\frac{|X|}{x_{static}} = \frac{1}{\sqrt{\left(1 - \frac{\omega^2}{\omega_n^2}\right)^2 + \gamma^2 \frac{\omega^2}{\omega_n^2}}} \qquad (4.24)$$

γ is a different notion for the damping: $\gamma = 2n/\omega_n$

In Figure 38, the amplification factor is plotted for various values of the amount of damping γ against the ratio ω/ω_n.
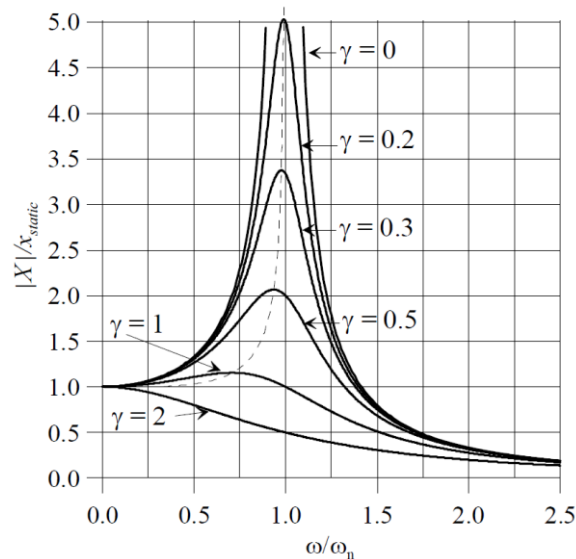
Figure 38: Magnification factor (Metrikine, sd)

Multi-degree-of-freedom systems

With multi-degree-of-freedom systems, the mass of the structure is lumped into multiple points which all have their own degrees of freedom and equation of motion. When the amount of degrees of freedom becomes large, the matrix notation is indispensable. (Spijkers, et al., 2005)

A good example of a multi-degree-of-freedom representation of a tall building is given in Figure 39.
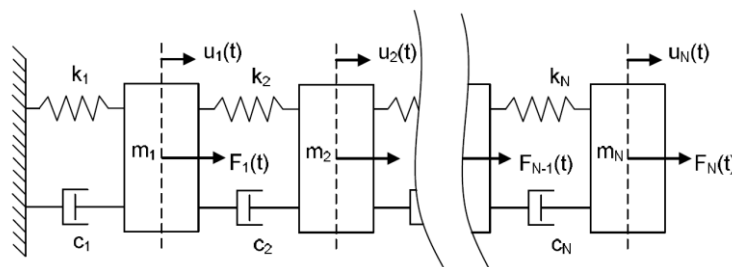
Figure 39: N-degree-of-freedom system (Berg, 2012)

The derivation of the response and frequency response function, together with the modal properties of a multi-degree-of-freedom-system, of the example of Figure 39 is given in Appendix B.

4.2.2   Continuous systems

Continuous systems have infinite degrees of freedom, infinite natural frequencies and infinite modes of vibration. The system's properties are distributed along a line, plane or volume. Their dynamic behaviour is described by means of partial differential equations. An example of a continuous system is the bending beam or shear beam. The bending beam, described by a fourth-order partial differential equation, is used in this research. (Spijkers, et al., 2005)

The equation of motion for a bending beam is obtained with Newton's seconds law and the kinematic and constitutive relations from the Euler-Bernoulli model. This results in the equation of motion:

$$EI\frac{\partial^4 u(z,t)}{\partial z^4} + \rho A\frac{\partial^2 u(z,t)}{\partial t^2} = f(z,t) \tag{4.25}$$

From the free vibration model, the eigenvalue problem is obtained:

$$\frac{d^4 u(z)}{dz^4} - \beta^4 u(z) = 0 \tag{4.26}$$

$$\beta^4 = \frac{\rho A\omega^2}{EI}$$

By assuming a solution for the eigenvalue problem ($u(z) = e^{\lambda z}$) and substitution in the characteristic equation, the solution is obtained. Rewriting the obtained solution results in:

$$u(z) = A\cosh(\beta z) + B\sinh(\beta z) + C\cos(\beta z) + D\sin(\beta z) \tag{4.27}$$

The four constants depend on the boundary conditions of the beam. In this research, cantilever beams are used. Therefore, the clamped cantilever beam is discussed here. The boundary conditions for a clamped cantilever beam are:

$$z = 0 \quad \rightarrow \quad \begin{cases} u = 0 \\ \dfrac{du}{dz} = 0 \end{cases} \tag{4.28}$$

$$z = L \quad \rightarrow \quad \begin{cases} -EI\dfrac{d^2 u}{dz^2} = 0 \\ -EI\dfrac{d^3 u}{dz^3} = 0 \end{cases} \tag{4.29}$$

Substitution of the boundary conditions in the homogeneous solution results in a system of algebraic equations. The non-trivial solution is found by setting the determinant of the system equal to zero. From this, the following equation is found:

$$\cos(\beta L) = \frac{-1}{\cosh(\beta L)} \tag{4.30}$$

Solving this equation results in infinitely many solutions. With the solutions for β, the eigen frequencies of the system can be found. Using one of the functions from the system, the associated eigenfunctions can be determined.

Modal properties of continuous systems

The mode shapes can be used to find uncoupled equations of motion for each mode. For continuous systems, the equation of motion in a particular mode can be written as (see Appendix C):

$$m_{e,i}\,\ddot{\Psi}_i + c_{e,i}\,\dot{\Psi}_i + k_{e,i}\,\Psi_i = \hat{F}_{e,i}\,cos(\Omega t) \tag{4.31}$$

$m_{e,i}$ is the modal mass
$c_{e,i}$ is the modal damping
$k_{e,i}$ is the modal stiffness
$\hat{F}_{e,i}$ is the modal force

The modal properties are given by:

$$m_{e,i} = \int_{z=0}^{h} \rho A\, U_i(z)^2\, dz \tag{4.32}$$

$$c_{e,i} = \int_{z=0}^{h} c_d\, U_i(z)^2\, dz \tag{4.33}$$

$$k_{e,i} = \int_{z=0}^{h} \beta_i^4 EI\, U_i(z)^2\, dz \tag{4.34}$$

$$\hat{F}_{e,i} = \int_{z=0}^{h} q(z)\, U_i(z)\, dz \tag{4.35}$$

The mode shapes for every mode of vibration are described by $U_i(z)$, which is a function of the height z.

4.3   SPECTRAL ANALYSIS

Since the wind flow is far from constant and contains many fluctuations, wind loading on buildings is a dynamic loading which varies in space and time. A commonly applied approach for a dynamic analysis is the spectral analysis. This approach is in the frequency domain and, applied for wind loading, describes the full process from the wind velocity fluctuations to the fluctuating response of the building. The procedure is shortly described supported by Figure 42 to Figure 46.

In section 4.2, the linear relation between the load and the response is derived with a transfer function. This linear relation, for the u-component of the wind load, is given by: (Vrouwenvelder & Geurts, 2006) (Berg, 2012)

$$S_u(\omega) = |H_u(\omega)|^2\, S_{FF,u}(\omega) \tag{4.36}$$

$S_u(\omega)$ *is the response spectrum*
$|H_u(\omega)|^2$ *is the transfer function*
$S_{FF,u}(\omega)$ *is the wind load spectrum including aerodynamic admittance (equation* (3.23)*)*

The total variance of the response is equal to the area under the response spectrum. As can be seen in Figure 46, the response consists of two parts, the quasi-static part and the dynamic part.

$$\sigma_u^2 = \int_0^{\infty} S_u(\omega)\, d\omega \tag{4.37}$$

$$\sigma_u^2 = \sigma_{u,QS}^2 + \sigma_{u,Dyn}^2 \tag{4.38}$$

From the total variance, the standard deviation is obtained by taking the square root.

In practice, the integral of equation (4.37) is often estimated using estimation formulas for both the quasi-static part as the dynamic part. The quasi-static part of the response is for a transfer function at $\omega = 0$ due to the peak in the wind spectrum, and is given by:

$$\sigma_{u,QS}^2 = |H_u(\omega = 0)|^2 \int_0^\infty S_{FF,u}(\omega)\, d\omega = \frac{1}{k_e^2} \int_0^\infty S_{FF,u}(\omega)\, d\omega = \frac{\sigma_{FF,u}^2}{k_{e,i}^2} \tag{4.39}$$

$k_{e,i}^2$ is the modal stiffness of the considered mode

The dynamic part of the response is the difference between the total and quasi-static response. This response is dominated by the peaks in the transfer function at the natural frequencies of the system. An approximation of the dynamic part can be obtained with the white noise approach (Vrouwenvelder & Geurts, 2006). The white noise approach assumes a constant spectral density S_0 equal to the spectral density at the considered natural frequency of the system, see Figure 40 (Berg, 2012).
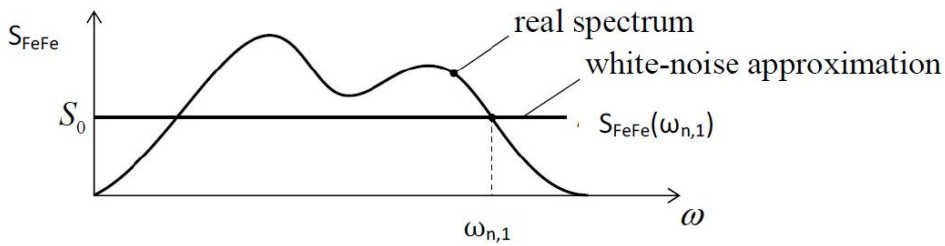

Figure 40: White noise approach (Berg, 2012)

The variance of the dynamic part is then:

$$\sigma_{u,Dyn}^2 = S_{FF,u}(\omega = \omega_i) \int_0^\infty |H_u(\omega)|^2\, d\omega$$

$$\sigma_{u,Dyn}^2 = S_{FF,u}(\omega = \omega_i) \frac{\pi \omega_i}{4 \xi_{e,i} k_{e,i}^2} \tag{4.40}$$

$\xi_{e,i}$ is the modal damping ratio of the considered mode

The total variance is now given as the summation of the quasi-static variance and the dynamic variance.

$$\sigma_u^2 = \frac{\sigma_{FF,u}^2}{k_{e,i}^2} + S_{FF,u}(\omega_i) \frac{\pi \omega_i}{4 \xi_{e,i} k_{e,i}^2} \tag{4.41}$$

Above formulas describe the response in terms of displacements [m]. To obtain the standard deviation in terms of acceleration [m/s²], the transfer function should be in terms of acceleration. This is reached by multiplying with ω^2.

The approximation procedure described above, results in an accurate estimation for single degree of freedom systems, since they have only one peak in their transfer function. In this research, a model with three degrees of freedom is used. Therefore, the integral approach, as given in equation (4.37), is used in this research.

The maximum acceleration of the structure can be determined from the standard deviation using the peak factor k_p. The NEN-EN 1991-1-4 provides the peak factor in Annex B.2, and is shown in Figure 41. The peak factor depends on the up-crossing frequency (gusts in the wind), the averaging time of the mean wind velocity ($T = 600\ s$), the background factor (B) and the resonance response factor (R). The background factor and the resonance response factor are two variables in the equivalent static load approach. To avoid mixing two analysis procedures and to reduce the complexity of the determination of the peak factor, a constant value of 3.5 is used. The value of 3.5 is chosen because it is consistent with the formulation of the

equivalent static load by NEN-EN 1991-1-4, also used later in equation (5.3). As rough estimate, the first natural frequency of a high-rise building in the Netherlands will be between the dashed lines as shown in Figure 41. This shows that the value of 3.5 can be considered as conservative.

The maximum acceleration of the structure is given by:

$$a_{max} = k_p \sigma_a \tag{4.42}$$
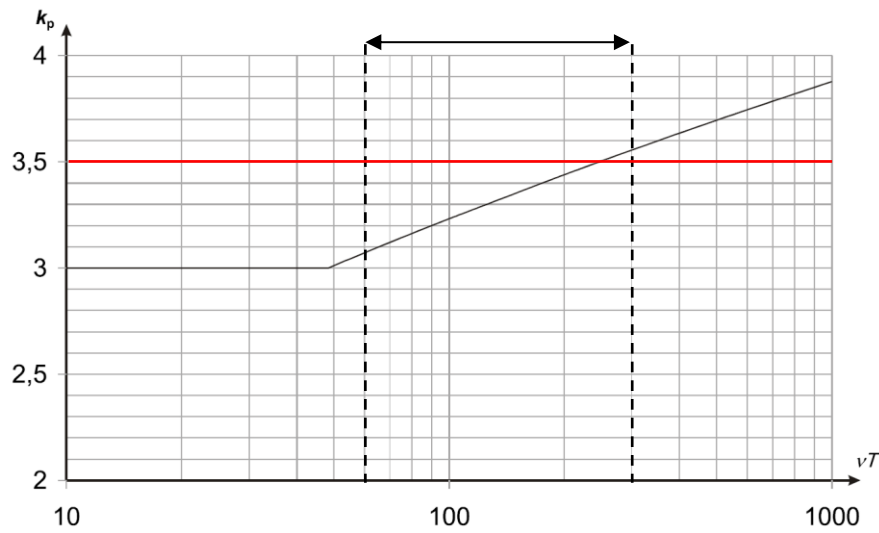
Figure 41: Peak factor [NEN-EN 1991-1-4]

Wind velocity spectrum

The power spectrum of the wind fluctuations gives the spectral density as a function of frequency. The wind velocity spectrum is dependent on terrain roughness, wind velocity, and height.

Figure 42: Wind velocity spectrum (Geurts, 1997)
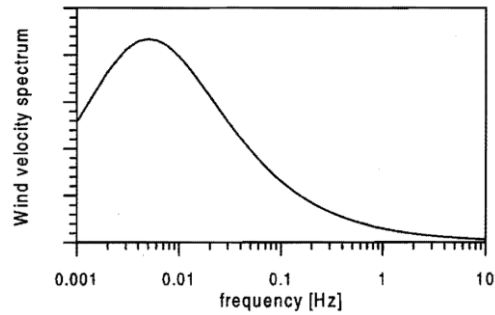
Aerodynamic admittance

The aerodynamic admittance takes into account that the pressures from the wind velocity are not fully correlated over the surface of the building.

Figure 43: Aerodynamic admittance (Geurts, 1997)
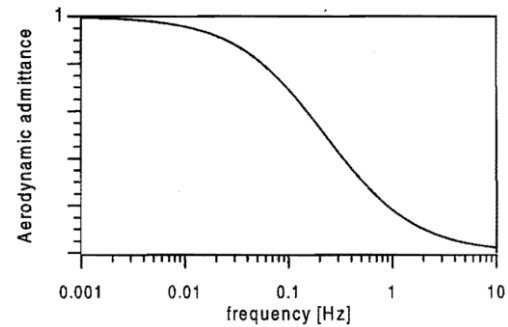
Wind load spectrum

The wind load spectrum is the transition from wind velocity into wind loading including the aerodynamic admittance.

Figure 44: Wind load spectrum (Geurts, 1997)
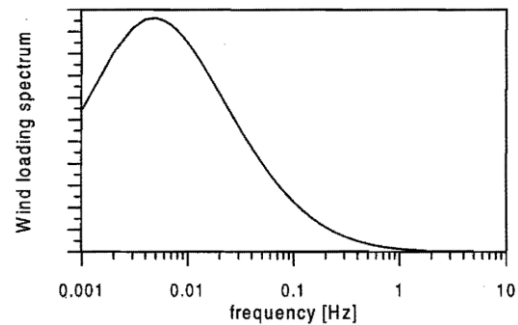
Mechanical admittance

The mechanical admittance, also frequency response function (FRF), describes the behaviour of a system and is dependent on structural properties, like dimensions, stiffness, mass, and damping. Here, the mechanical admittance of a single-degree-of-freedom system with natural frequency 0.2 Hz is given.

Figure 45: Mechanical admittance SDOF system (Geurts, 1997)
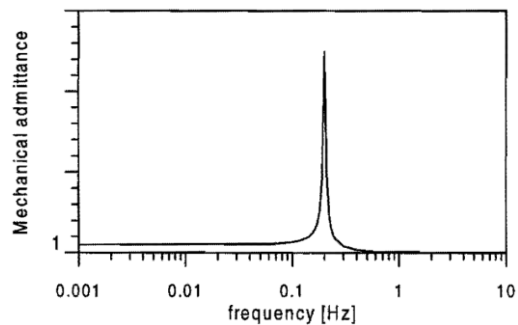
Response spectrum

The response spectrum (e.g. displacements or accelerations) is the multiplication of the wind load spectrum by the mechanical admittance. The response can be divided into two parts:

a) The quasi-static response;
b) The dynamic response.

Figure 46: Response spectrum (Geurts, 1997)
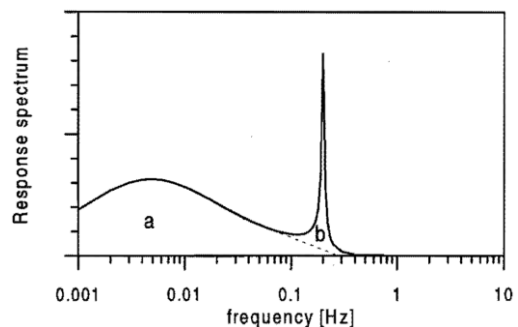
4.4 COMFORT CRITERIA

When designing a high-rise building, the structure should meet all requirements regarding strength and stiffness. These requirements consists of checks in the ultimate limit state, and checks in the serviceability limit state. Especially the comfort checks in the serviceability limit state can be governing for design of high-rise structures. Therefore, this research will focus on comfort checks.

Discomfort can be associated with large deformations or movements of the building which causes an unsafe experience for its inhabitants. The maximum deflection of a building is restricted to secure the serviceability of the building and to limit for example second order effects. Yet, the deflection of a building is not, or only marginally, experienced by the people inside the building. People are very sensitive to accelerations. Therefore, the accelerations are restricted to certain limits to secure a comfortable building and prevent the feeling of unsafety or even sickness by human beings.

4.4.1 Calculation of maximum accelerations

The calculation of the maximum accelerations is discussed in previous sections. Yet, no distinction was made between the ultimate limit state (ULS) and the serviceability limit state (SLS). This distinction is made in the fundamental average wind speed on a height of 10 meters. For the ULS, the values are as given in equation (3.7). For the SLS on the other hand, a reduction factor is applied. This reduction factor is a statistical value which taken into account the probability of exceeding for a particular return period. Practical meaning, for a return period of one year, the calculated maximum acceleration has a certain probability of exceeding this calculated value one time per year. The NEN-EN 1991-1-4 provides the factor c_{prob} which depends on the wind area:

$$c_{prob} = \left(\frac{1 - K \, ln(- \, ln(1 - p))}{1 - K \, ln(- \, ln(0.98))} \right)^n \tag{4.43}$$

K is the shape factor (I: 0.200   II: 0.234   III: 0.281)
n is the exponent (I: 0.5   II: 0.5   III:0.5)

The c_{prob} factor is plotted as function of the yearly probability of exceeding p in Figure 47.
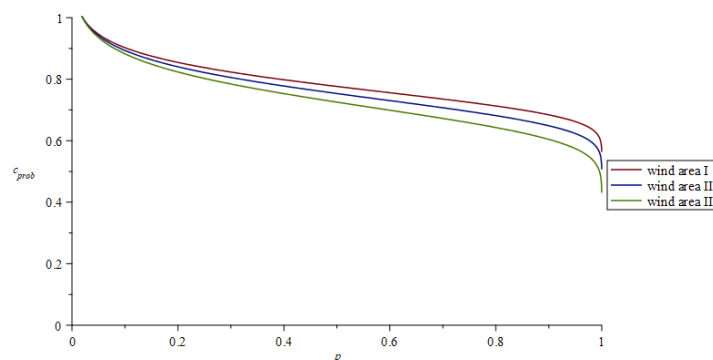
Figure 47: c_{prob} factor as function of the yearly probability of exceeding [NEN-EN 1991-1-4]

The NTA 4614-3 recommends values for the average wind speed for the SLS. The values are shown in Table 5, together with the values for the ULS. The recommendation from the NTA 4614-3 is also used in this research.

Wind area	ULS $v_{b,0}$ [m/s]	SLS $v_{b,0}$ [m/s]
I	29.5	22.1
II	27.0	19.4
III	24.5	16.9

Table 5: Values of the fundamental wind speed for ULS and SLS [NTA 4614-3]

4.4.2   Maximum allowable accelerations

In literature, many different restrictions are proposed. The maximum allowable acceleration restrictions are given depending on the first natural frequency of the structure. The most commonly used restriction in the Netherlands is given by the NTA 4614-3 / NEN 6702. The distinction is made between two groups of functions:

1. Office, education, industrial and others;
2. Public, residential, lodging, prison, healthcare, sports and retail.
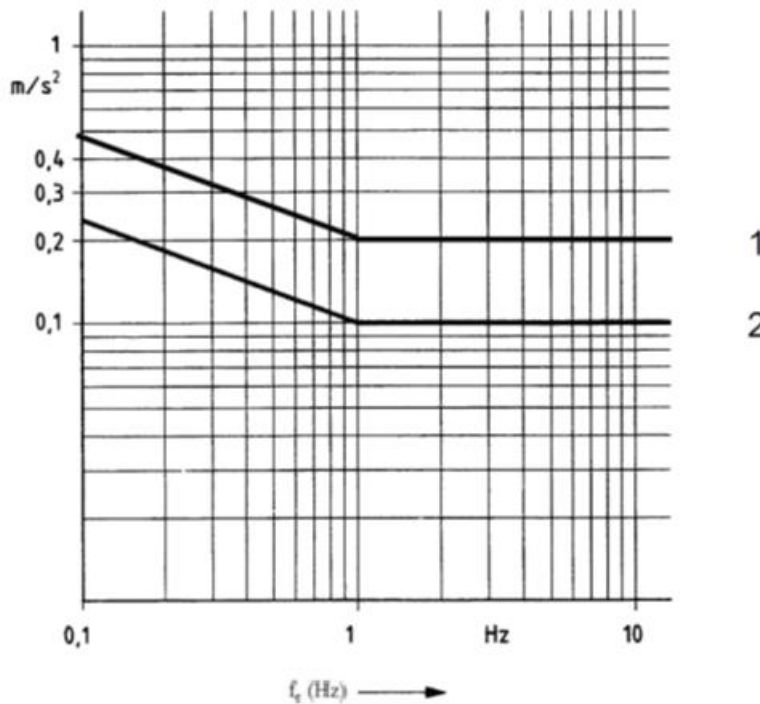
| Explanation of graph: |
| On the x-axis, the fundamental frequency. On the y-axis, the maximum allowable acceleration of the structure. |

Figure 48: Maximum allowable acceleration [NTA 4614-3]

Many more restrictions are proposed, see Figure 49. The values from the ISO 6897 are often used internationally. The values from NEN 6702 are based on the values of the ISO. Besides restrictions for the maximum allowable acceleration, also threshold values are provided. The threshold values should give a level of vibration in which the accelerations are not experienced by human beings. It can be observed that the maximum values are higher than the threshold values and no good agreement about the threshold values is present. It should be realized that, when a building is designed such that the expected maximum acceleration is close to the maximum value, the inhabitants will experience the accelerations (Oosterhout & Geurts, 2001).

The maximum acceleration of the structure will be different at each height. Therefore, a reasonable question to ask in the design process is whether it is economic to design the whole building for a maximum acceleration at the top. Various arguments can be put forward, but no strict requirements are set. The judgement is up to the engineer or client.

In this research, the maximum acceleration at the top is used as the main output variable, because this will result in the maximum values for the acceleration.
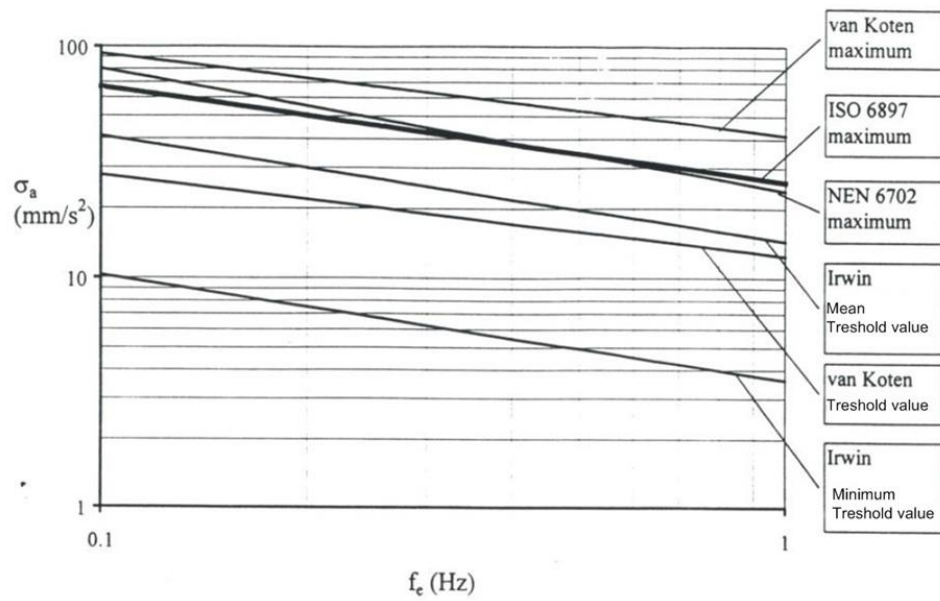
Figure 49: Maximum allowable standard deviation of the acceleration (Berg, 2012)

CHAPTER | 5 |
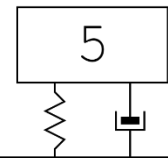
INPUT PARAMETERS SUPERSTRUCTURE

The three main parameters related to the superstructure design of a high-rise building considered in this research are the stiffness (EI), the mass density (ρ) and the damping ratio (ξ). In this chapter, realistic parameter range for these three parameters are determined and discussed.

5.1 STIFFNESS

From the current static design approach, a deformation requirement is used to come up with an initial stiffness value. In the preliminary design stage, it is common practice to assume that half of the total deflection at the top is caused by the rotation in the foundation. By using the commonly used total deflection criteria of $h/500$, and looking only at the superstructure, the applied requirement for the maximum deflection at the top of a building is:

$$u_{max} = \frac{h}{1000}$$

(5.1)

This rule of thumb is highly dependent on the soil conditions. Since a rough estimation is needed here, the given formula is assumed to be appropriate.

For the initial stiffness value, the structure is schematized as a clamped beam. From the well-known formula for the maximum deflection at the top, the formula for the stiffness value is obtained:

$$EI = \frac{qh^4}{8\,u_{max}} = \frac{qh^4}{\frac{8h}{1000}} = 125qh^3$$

(5.2)

For the distributed load, the static load from the NEN-EN 1991-1-4 is used. The extreme wind load is given as:

$$q(z) = \frac{1}{2}v_m^2\rho_{air}bC_f(1 + 7I_z)$$

(5.3)

This load has a logarithmic relation with height. However, an evenly distributed load is required. The evenly distributed load is found by forcing the top displacement of a clamped beam with the logarithmic load and a clamped beam with an evenly distributed load, to be equal, as shown in Figure 50. The top deflection in the case of the logarithmic load is found using the fourth order differential equation based on the Euler-Bernoulli beam theory. By forcing the top displacement of the clamped beam with the evenly distributed load to be equal to the top displacement of the clamped beam with the logarithmic load, the value of the evenly distributed load can be found. The obtained value of the distributed load can be described with equation (5.3) with a certain value for z. It turns out that the equivalent height is $0.7\,h$, see Figure 50.

The initial stiffness value, based on the deflection criteria, can be found by:

$$EI = 125q(z = 0.7h)h^3$$

(5.4)

Figure 50: Logarithmic wind load (a), evenly distributed wind load (b) and equivalent height (c)

The initial stiffness value found with equation (5.4), is an indication to meet the deformation requirements. This does not mean that the acceleration requirements are also met. In chapter 8, it is shown that the acceleration requirements are not always met with this stiffness of the superstructure. It is also shown what the influence of an increasing or decreasing stiffness value of the superstructure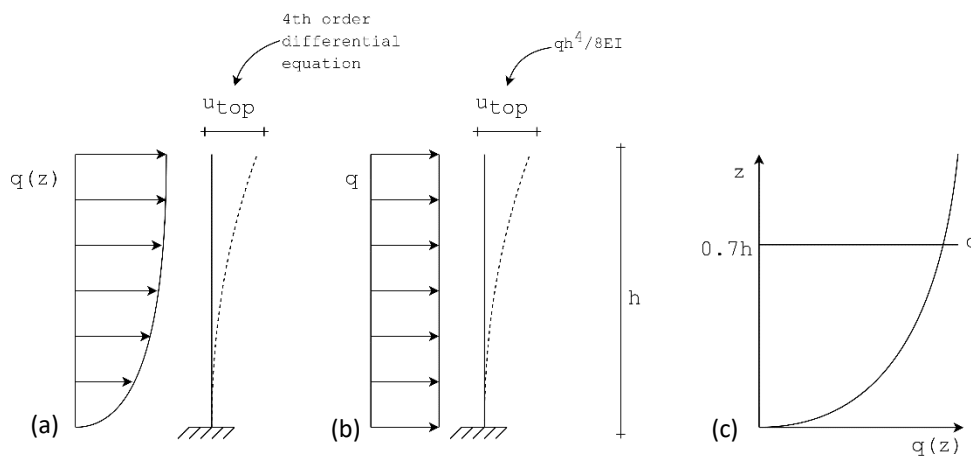 is on the acceleration. The range in which the stiffness is altered is between 0.2 and 5 times the initial stiffness. This rather broad range of stiffness is chosen because the stiffness of different structural stability systems can vary a lot.

To give an indication about the stability system required to reach a certain stiffness value, the following example is provided.

A building of 100 meters high with a concrete core as only stabilizing element. The concrete core has outer dimensions of 14 by 14 meters with a wall thickness of 400 mm. The moment of inertia of the core is calculated as if it would have no openings. Usually, the stiffness of the core is reduced by 20 to 30% due to openings. To compensate this reduction, extra internal walls can be added in the core. The core could look like the one used in the Rembrandt Tower, see Figure 52. A reduced elastic modulus E is assumed: $E_{red} = E/3 = 15000 \, \text{N/mm}^2 = 15 \cdot 10^9 \, \text{N/m}^2$.

$h = 100 \, \text{m}$
$b = 30 \, \text{m}$
$d = 30 \, \text{m}$
$A = 900 \, \text{m}^2$

$z_0 = 0.5 \, \text{m} \quad v_b = 27 \, \text{m/s} \quad \rho_{air} = 1.25 \, \text{kg/m}^3$
$b/d = 1 \rightarrow C_f = 2.1$
$q(z = 70) = 84.4 \, \text{kN/m}$

$EI_{required} = 125 \cdot 84.4 \cdot 10^3 \cdot 100^3 = 1.0 \cdot 10^{13} \, \text{Nm}^2$

$I_{required} = \dfrac{1.0 \cdot 10^{13}}{15 \cdot 10^9} = 666.67 \, \text{m}^4$

$b_{core,outer} = d_{core,outer} = 14.0 \, \text{m}$
$b_{core,inner} = d_{core,inner} = 13.2 \, \text{m}$

$I = \dfrac{1}{12} \cdot 14.0^3 \cdot 14.0 - \dfrac{1}{12} \cdot 13.2^3 \cdot 13.2 = 671.37 \, \text{m}^4$
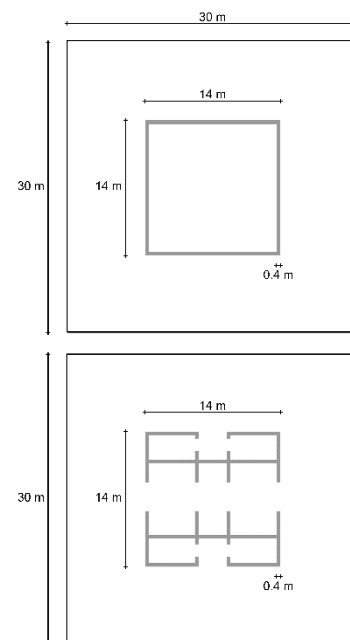
It should be emphasised that the stiffness value EI is an representative stiffness value that is used to determine the equivalent stiffness values $K_{b,i}$ in the model used in this research, see section 8.1. This EI-value should include all effects that influence the stiffness of the superstructure. For example, a reduced Youngs' modulus and the effects of partially cracked concrete. Also, the fact that the EI-value is used for a dynamic analysis should be considered. The dynamic stiffness can be different than the static stiffness, although the frequency dependency of the stiffness is not taken into account in this research.

As mentioned before, only the bending stiffness is considered in this research because bending deformations usually govern for high and slender structures. In the case that partial shearing behaviour should be taken into account, two reasonable ways are proposed. The first option is to take the extra stiffness due to shear into account by increasing the EI-value. This is theoretically not correct, since the EI-stiffness is considered to be purely bending. However, it will result in a higher equivalent stiffness $K_{b,i}$. The second option is to add the shearing stiffness GA to the determination of the equivalent stiffness value $K_{b,i}$.

5.2 MASS

The own weight of all elements in the building add to the total mass of the building. These are the structural elements like floors, beams, columns and structural walls, but also non-structural elements like

the façade, partition walls, ceilings, installations, etc. Beside the own weight of all elements in the building, there is also an imposed mass on the structure. This is the result of loads. The floor loads will contribute the most and depend on the function. Therefore, much of the mass is lumped at the location of the floors. For relatively low buildings, the effect of the lumped mass at floor height should be taken into account. In the case of high-rise buildings, the amount of floors is much larger and they are usually evenly distributed over the height. Therefore, the assumption is made that the mass can be considered as evenly distributed over the height of the structure.

The elements with the highest contribution to the mass can be roughly categorized in: load bearing structure, floor system, façade and live loads. All non-structural elements like ceilings, installations, partitioning walls, etc., that will add to the own weight, is accounted for in the floor system. For the live load, the characteristic value is multiplied by the ψ_0-factor.

With the assumption of evenly distributed mass, the mass should be given in $\mathrm{kg/m}$. To incorporate the cross-sectional dimensions of the structure, a volumetric mass density ($\mathrm{kg/m^3}$) is used. This mass density is depending on many different aspects. As explained, all elements of the building determine this mass density for a certain part, but also the dimensions of the building influence this mass density. The contribution of the floor system and the live load is influenced by the storey height. The higher the storey height, the lower the relative contribution to the total mass density. The contribution of the façade is influenced by the cross-sectional dimensions. Better said, the ratio between the circumference and the cross-sectional area of the building. The lower this ratio, the lower the relative contribution to the total mass density.

To have an indication of the mass density of high-rise buildings in the Netherlands, the mass density of two example buildings is roughly calculated, see Appendix . The relatively light Rembrandt Tower in Amsterdam and the relatively heavy Zalmhaven Tower in Rotterdam. The distribution of the mass density per category and total mass density of both buildings is shown in Figure 51.
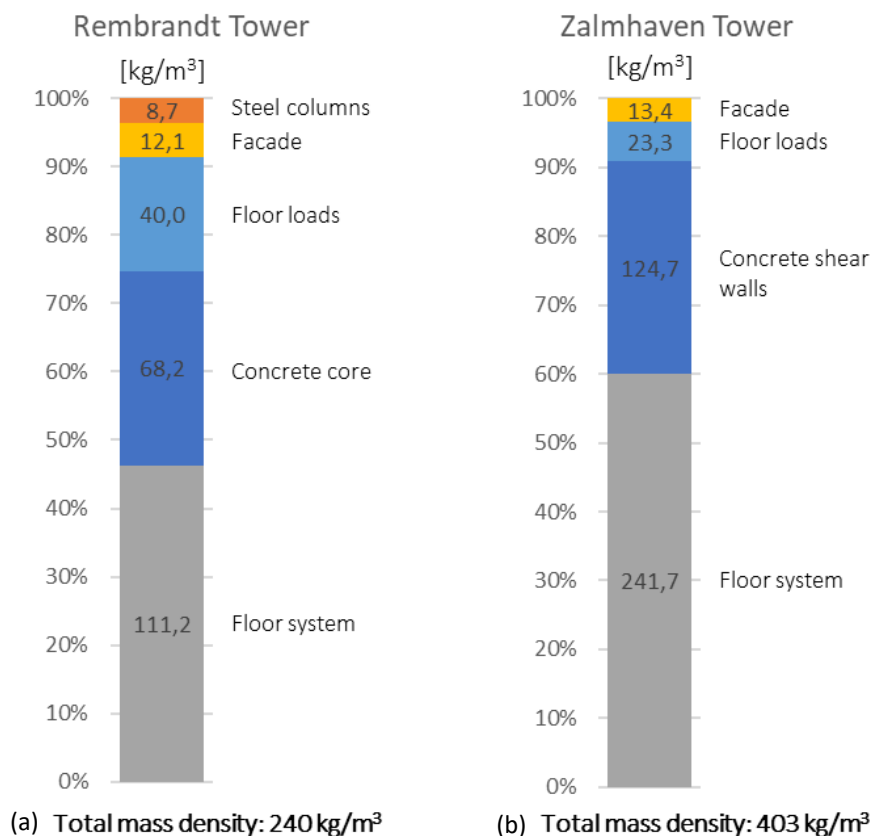
Figure 51: Distribution of mass density per category for the Rembrandt Tower (a) and Zalmhaven tower (b)

Rembrandt Tower

The Rembrandt Tower has a height of 135 meters and has 36 floor levels. The building consists of three parts with different cross-sectional dimensions. For this simplified mass calculation, an average cross-sectional area is used together with a square floorplan. The building has a concrete core which secures stability. Around the core, a steel column structure is used as main load bearing structure. A composite steel-concrete floor system is applied supported by steel beams. (Abspoel, 2013)
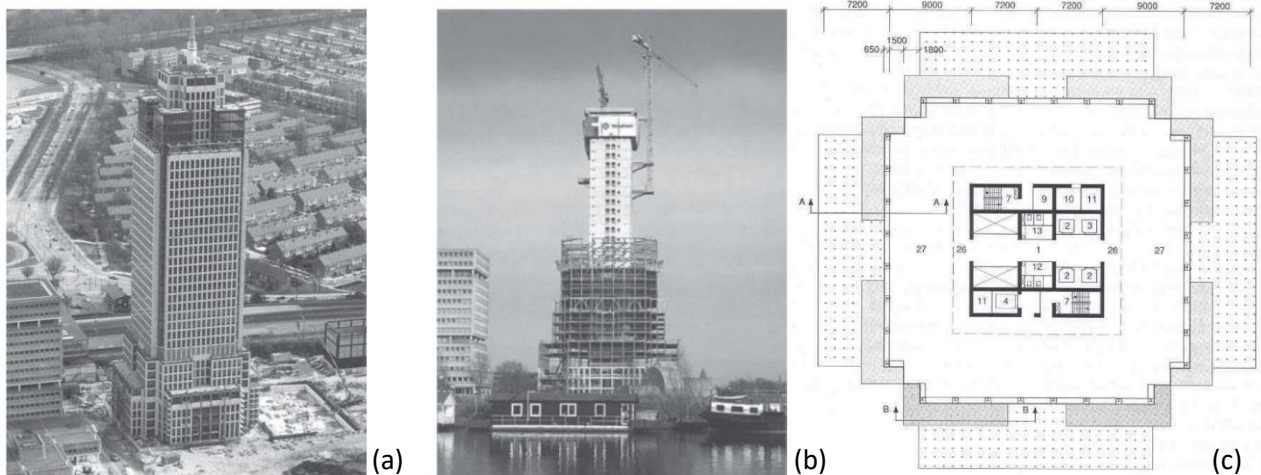
Figure 52: Complete building (a), during construction (b) and standard floorplan (c) (Abspoel, 2013)

Zalmhaven tower

The Zalmhaven Tower is currently under construction. The building will be 215 meters high with 66 floor levels. The design was initially made with an in-situ concrete shear wall structure. Later, an alternative with prefab-concrete was made. For the rough calculation Appendix , the initial design is used. Thus, the building has a concrete shear wall structure to secure stability. The floors are cast in-situ, together with the shear walls using the tunnel system.
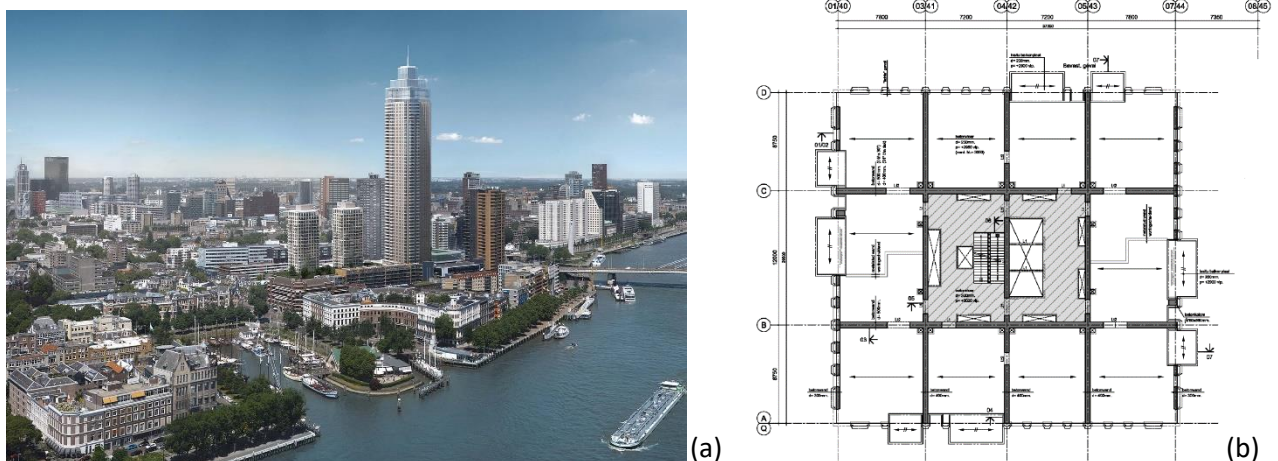
Figure 53: The Zalmhaven Tower (a) and standard floor plan (b)

For comparison, the calculated mass densities of seven different buildings by (Berg, 2012) are shown in Table 6. Because the values are just for indication, no further research is performed into the calculated values by (Berg, 2012). The calculated values for the Rembrandt Tower and Zalmhaven Tower are comparable to the values of (Berg, 2012), and therefore assumed to be reasonable estimations. Concluding, the mass density ρ ranges roughly between 200 kg/m^3 and 500 kg/m^3.

Building	Height [m]	$\rho A \cdot 10^3$ [kg/m]	A [m²]	ρ [kg/m³]	Load bearing structure	Floor type	Function
New EMC	120	430	880.0	488.6	Prefab concrete tube and core	Prefab slabs with compression layer	Hospital
Old EMC	112	795	2560.0	310.5	In-situ concrete core. In-situ and prefab concrete columns and facade	Prefab slabs with compression layer	Hospital
EWI	90	467	1462.0	319.4	Concrete shear walls and steel skeleton	Prefab concrete floors	Education
Kennedy	83	176	518.4	339.5	Steel braced frames	Composite floors	Office
Winston Churchill	80	250	1122.0	222.8	Concrete core with column structure	Concrete floors	Office
La Fenêtre	70	290	720.0	402.8	Steel braced frames on table structure	Infra+ floors	Residential

Table 6: Mass densities and structural description of six high-rise buildings in the Netherlands (Berg, 2012)

5.3   DAMPING

Damping is a determining parameter in the design of high-rise buildings. Unfortunately, damping is also the most difficult phenomena and currently it is still impossible to accurately predict the damping of high-rise buildings.

According to (Spijkers, et al., 2005), damping is best defined as the dissipation of mechanical vibration energy from the system. This definition is used because it makes no judgement concerning the cause of the energy dissipation. This cause is described by (Geurts, et al., 2015) with a focus on high-rise buildings as follows: damping is the transition from kinetic energy into heat, resulting in a lowering vibration amplitude. The heat is released by means of friction between structural materials or elements, or between the structure and its surroundings (wind, soil).

More in detail, the following mechanisms contribute to the total damping of structures: (Geurts, et al., 2015)

- Material damping;
  Development of heat within a material. A good example is the occurrence of cracks in concrete.
- Structure damping;
  Development of heat because of friction between elements. This can happen at the connection of structural elements but also at the interface with non-structural elements.
- Soil material damping;
  There is very little known about this kind of damping. It is assumed that for structures with a relatively large contact area with the soil, like buildings, this kind of damping can play an important role.
- Radiation damping;
  With relatively large deformations at the foundation, part of the energy will radiate into the soil.
- Aerodynamic damping;
  The surrounding air around a structure contributes to the total damping.
- Artificial damping:
  It is possible to provide more damping in a structure by adding damping devices.

It is still impossible to calculate the contribution of the different dissipation mechanism to the total damping of a structure (Geurts, et al., 2015). Therefore, mathematical modelling of damping is used for the complex reality.

For this research, the model with viscous damping is used. The reason for this, is that this model leads to linear differential equations with constant coefficients, which is required since linear systems are used. For low-damped structures with relatively low natural frequencies, like high-rise buildings, viscous damping models perform reasonably well (Spijkers, et al., 2005).

Viscous damping implies that the damping force is proportional to the velocity (Spijkers, et al., 2005). The damping value is often expressed as a percentage of the critical damping, the dimensionless damping ratio ξ. The critical damping is the damping required to bring the system to its equilibrium state in exactly one period. This phenomenon is called aperiodic motion (Metrikine, n.d.). For a single-degree-of-freedom system, the critical damping is given by: $2\sqrt{km}$. Thus, if the damping ratio ξ is assumed, and the stiffness and mass are known, the damping value can be calculated.

It should be emphasized that the aim of this research is not to accurately predict the damping in high-rise buildings, but to provide insight in the influence of the assumed damping. Therefore, whether or not the assumed damping ratio is accurate for a particular building, is not of great importance for this research. Yet, to be able to provide insight in the influence of damping, the considered range of damping ratios should be somehow realistic.

Proposed values of the damping ratio of structural damping from different references are shown in Table 7. The damping ratio is depending on the structural material and ranges between 0.2% ($h = 300$) and 5%.

Besides these proposed values, measurements of completed buildings help to make a reasonable assumption, see Figure 54. Both worldwide, as in the Netherlands, buildings are being monitored for their dynamic response. Using sensors, the dynamic properties of the building, like natural frequency and damping ratio, can be measured. Different relations are made between the building dimensions, structural materials and dynamic properties. Yet, there is still a large scatter in the measured data concerning the damping ratio, see Figure 54. (Geurts, et al., 2015) (Smith & Willford, 2008)

Mainly based on the measured data in the Netherlands, a damping ratio range of the superstructure of 0.5% to 4.0% is considered.

Reference	Damping ratio ξ	Structural material
NEN 6702	0.010	Steel structures
	0.020	Concrete structures
	0.050	Wood structures
NEN-EN 1991-1-4	0.008	Steel structures
	0.016	Reinforced concrete
	0.013	Steel and concrete structures
CNR-DT 207/2008	$\frac{1}{100}\frac{56}{h} \geq 0.008$	Steel structures ($h \geq 30$ m)
	$\frac{1}{100}\frac{68}{h} \geq 0.010$	Reinforced concrete ($h \geq 30$ m)

Table 7: Proposed damping ratios of structural damping from different references
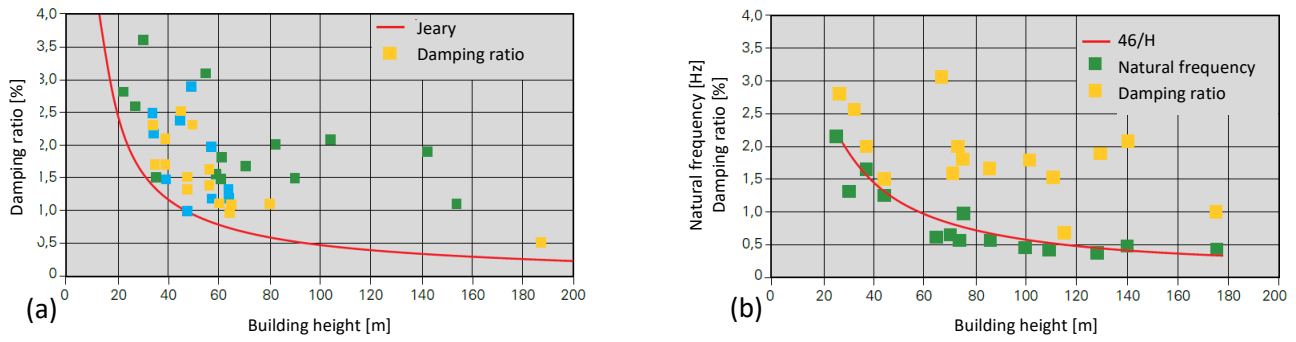
Figure 54: Damping ratio against building height measured in the UK (a) and natural frequency and damping ratio against building height measured in the Netherlands (b) (Geurts, et al., 2015)

5.4   SUMMARY

Discussed in previous sections, the three main parameters of the superstructure are varied within certain ranges in this research. The determined ranges are summarized in Table 8.

Parameter	Symbol	Units	Parameter range
Stiffness	EI	Nm^2	$0.2\ EI_{initial} - 5.0\ EI_{initial}$
Mass density	ρ	kg/m^3	$200 - 500$
Damping ratio	ξ	%	$0.5 - 4.0$

Table 8: Overview of parameter ranges of the superstructure
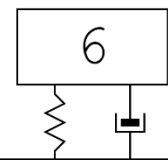
CHAPTER | 6 |

INPUT PARAMETERS FOUNDATION

The model variables for the rotational and translational stiffness and damping value of the foundation are discussed in this chapter. Three representative soil profiles are determined. The analytical expressions of two references are compared with the results from time history analyses. Also, the contribution of the foundation piles to the model variables is investigated.

6.1   INTRODUCTION

When a high-rise building is excited by a wind load, the response of the structure is affected by the interaction of three linked systems: the superstructure, the foundation and the soil surrounding the foundation. The term soil-structure interaction (SSI) is often used for the analysis of the interaction between the different systems. (National Institute of Standards and Technology, 2012)

When a high-rise building starts to vibrate due to wind, base shear, moment and torsion forces develop at foundation level. Due to these forces, displacements and rotations will occur at the soil-foundation interface. These displacements and rotations are only possible, when a certain flexibility is present in the soil-foundation system. This flexibility has to be combined with the flexibility of the superstructure and therefore can have a significant influence on the overall behaviour. Also, the deformations at foundation level result in energy dissipation via radiation damping and hysteretic damping, which influences the overall damping of the structure. (National Institute of Standards and Technology, 2012)

From above, it is clear that SSI can have a significant influence on the total response of a structure and can therefore not be disregarded. This is emphasised by the statement of (National Institute of Standards and Technology, 2012), that SSI effects tend to be significant for stiff structures located on softer soils, which is generally the case for buildings in the Netherlands. Yet, SSI is a very complex subject and literature is often difficult to understand due to its complex arithmetic to formulate solutions (National Institute of Standards and Technology, 2012). Different calculation procedures are developed to estimate the stiffness and damping in the soil-foundation system. These procedures range from analytical expressions (National Institute of Standards and Technology, 2012) (Wolf & Deeks, 2004) to numerical programs using finite element models (Kocak & Mengi, 2000).

As earlier emphasised, the aim of this research is not to accurately predict the values of certain parameters for a high-rise building. If this would be the case, a numerical program would be the best choice for the SSI parameters, to have the most accurate estimation. Different programs are available which can handle all aspects like foundation dimensions, pile configurations and soil layers. Due to the three-dimensional nature of SSI, a three-dimensional numerical program would be necessary to make accurate predictions. Also, the non-linear soil behaviour should be taken into account.

Since in this research a linear model is used, this assumption is maintained in the foundation. A linear elastic estimation of the foundation parameters is therefore used in this research. Analytical expressions for the stiffness and damping in the soil-foundation system are available in literature.

Analytical formulas for the soil-foundation interaction have been presented by Veletsos and Nair (1975), Bielak (1975 and 1976), Roesset (1980), Wolf (1985), Aviles and Perez-Rocha (1996), Maravas et al. (2007), Givens (2013), Gazetas (1991) (Gazetas & Tassoulas, 1987) (Gazetas, 1991), and Pais and Kausel (1988), among others (National Institute of Standards and Technology, 2012). Their solutions show many similarities and the existing differences are caused by different assumptions. In (National Institute of Standards and Technology, 2012), the most important differences are discussed and the solutions of Gazetas and Pais and Kausel are recommended. This is confirmed by engineers from practice with a preference for the formulations of Gazetas.

The structure-foundation-soil model (3DoF model) adopted in this research is introduced already. A more elaborate description of this model is given in section 8.1. To solve this system, the parameters associated to the foundation-soil system should be estimated: K_x, C_x, K_r, C_r. The foundation is assumed to be rigid. Therefore, the stiffness and dissipation capacities are provided by the soil only.

6.2   TYPICAL SOIL PROFILES

As will be explained in following sections, the SSI-parameters are determined using a foundation resting on a single homogeneous soil layer. To give an indication of the soil characteristics of this homogeneous layer,

representative soil profiles are obtained for three big cities in the Netherlands: Rotterdam, Amsterdam and The Hague. These three cities are chosen because they have the largest number of high-rise buildings in the Netherlands. The soil profiles are obtained via DINOloket, by making sections through the cities. For each layer of the soil profiles, representative soil characteristics have been assumed. This is done using multiple CPT's (Cone Penetration Tests) which are relatively close to the sections. Since there are no rules of thumb for the depth to consider, the top 30 meters of the subsoil is used, which is common practice in earthquake engineering.

The equivalent parameters G, ρ_s and v of the homogeneous layer have to be determined. Since most of the layers will be saturated, the Poisson's ratio will be relatively high. The assumption is made that the Poisson's ratio is equal to 0.45 for all layers.

To calculate the equivalent shear modulus and mass density, the equivalent shear wave velocity is obtained by: (Vijayendra, et al., 2010)

$$\frac{1}{V_{s,eq}} = \frac{1}{H}\left(\sum_{i=1}^{m} \frac{h_i}{(V_s)_i}\right) \tag{6.1}$$

$V_{s,eq}$ is the equivalent shear wave velocity
H is the total depth (30 m)
h_i is the uniform thickness of the ith layer
$(V_s)_i$ is the shear wave velocity of the ith layer: $(V_s)_i = \sqrt{G_i/\rho_i}$

To calculate the equivalent G and ρ_s, for one of the two parameters an assumption has to be made. Therefore, the equivalent mass density is determined as the weighted average of the mass densities of the soil layers with:

$$\rho_{eq} = \frac{1}{H}\left(\sum_{i=1}^{m} h_i \rho_i\right) \tag{6.2}$$

ρ_{eq} is the equivalent mass density
ρ_i is the mass density of the ith layer

Finally, the equivalent shear modulus is determined using the equivalent shear wave velocity and the equivalent mass density. All sections can be found in Appendix . Here, an overview of the soil profiles and equivalent soil characteristics is provided, see Figure 55.

Three different soil profiles are introduced (Table 9) which cover the range of soil characteristics as shown in Figure 55:

Soil profile	Flexibility	Shear modulus G [$\cdot 10^6$ N/m^2]	Mass density ρ_s [kg/m^3]	Poisson's ratio v [-]	Shear wave velocity V_s [m/s]
1	"Soft"	20	1700	0.45	108.5
2	"Medium"	40	1900	0.45	145.1
3	"Stiff"	60	2000	0.45	173.2

Table 9: Equivalent soil properties of 3 soil profiles used in this research
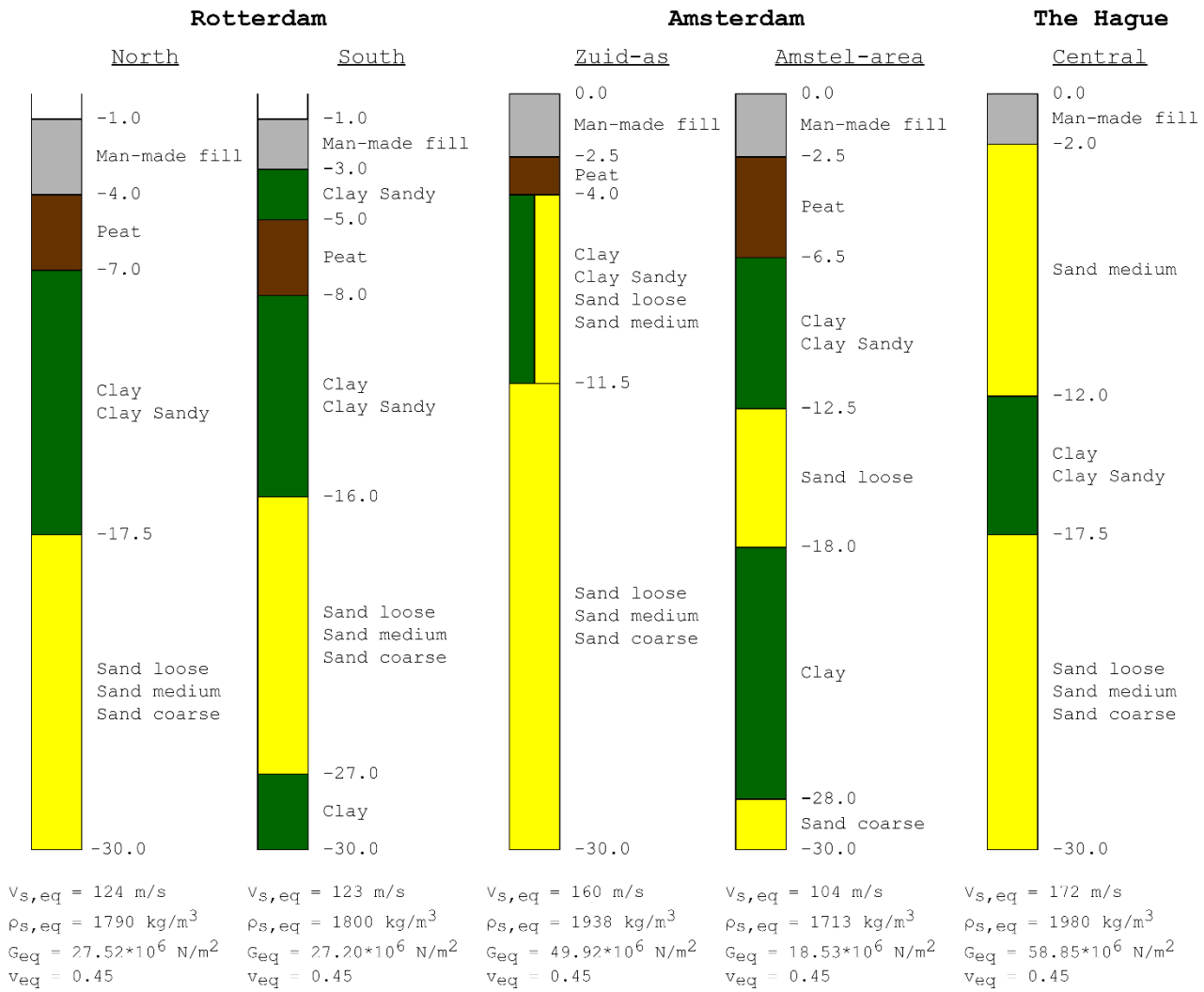
Figure 55: Representative soil profiles and equivalent soil characteristics of five areas in three big cities in the Netherlands

6.3 FOUNDATION STIFFNESS

The calculation procedure for the stiffness parameters (K_i), with i is x for translation and r for rotation, is typically described with the static stiffness at zero frequency of a rigid rectangular foundation resting on the surface of a uniform half-space ($K_{sur,i}$), see Figure 56(a). This static stiffness is then multiplied by a dynamic stiffness modifier (α_i), which is related to the dimensionless frequency $a_0 = \omega B/V_s$. B is half of the width of the foundation as shown in Figure 56, V_s is the shear wave velocity, and ω is the angular frequency. The shear wave velocity is calculated with the shear modulus G and soil mass density ρ_s as: $V_s = \sqrt{G/\rho_s}$. The shear modulus should be taken as the so-called small strain shear modulus. In the case of an embedded foundation (Figure 56 (b)), the static stiffness should also be multiplied by an embedment modifier (η_i), since the embedment increases the static foundation stiffness. Consequently, the stiffness parameters of the foundation-soil system are given by:

$$K_i = K_{sur,i} \cdot \alpha_i \cdot \eta_i \tag{6.3}$$
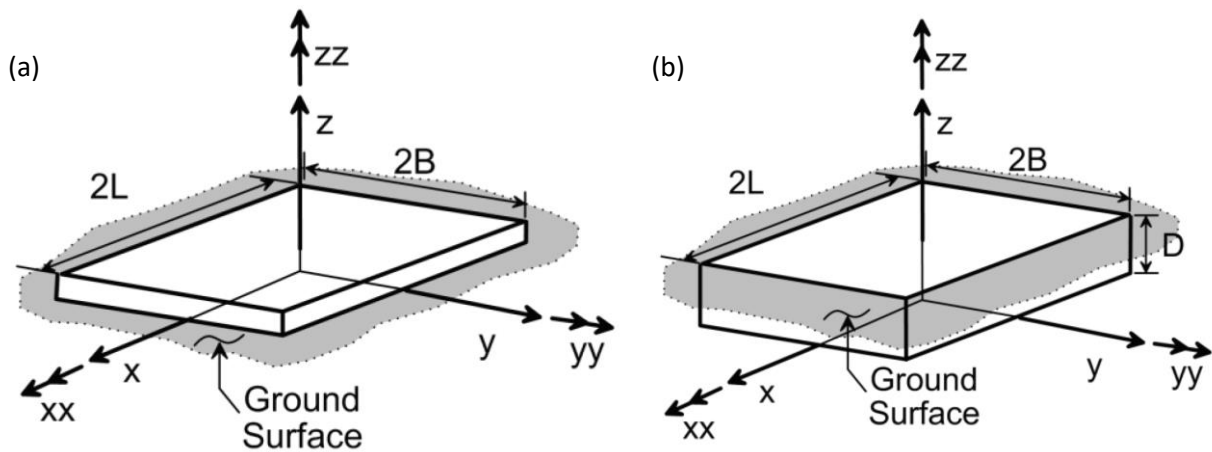
Figure 56: Rigid rectangular foundation resting on the surface (a) and embedded foundation (b), both over a uniform half-space (National Institute of Standards and Technology, 2012)

As mentioned earlier, the formulas from Gazetas (1991) and Pais and Kausel (1988) are recommended in literature. In (National Institute of Standards and Technology, 2012), all expressions available from Gazetas and Pais and Kausel are provided in four tables. For the static stiffness and the embedment modifier, both Gazetas as Pais and Kausel provide analytical expressions. Yet, for the dynamic modifier, only Pais and Kausel provide analytical expressions. The dynamic modifiers from Gazetas are only provided in the form of graphs in (Gazetas & Tassoulas, 1987) and (Gazetas, 1991). A study into the different expressions turns out that the difference between both references are mainly in the dynamic modifiers. The graphs provided in (Gazetas, 1991) are fitted with formulas to be able to calculate the stiffness for different foundation dimensions. The two procedures (Gazetas and, Pais and Kausel) to determine the horizontal and rotational stiffness are described in Appendix .

The horizontal and rotational stiffness of a surface foundation (Depth = 0 m) and embedded foundation (Depth = 15 m) with a depth of 30 meters (B=15 m), and different width (L=15, 30, 60 m) on a homogeneous half space are calculated according to Gazetas and Pais and Kausel. The soil parameters for a typical soil profile in Rotterdam are used.

The results, shown in Figure 57, show that both references provide results of the same order. Yet, for certain L/B ratio's, there is a significant difference between the two references (up to ~50%). Because of this difference, more research into the expected stiffness is performed using PLAXIS 2D (PLAXIS, 2019). This research is discussed in section 6.5.

Figure 57: Horizontal stiffness for surface foundation (a) and embedded foundation (b) and rotational stiffness for surface foundation (c) and embedded foundation (d) as a function of dimensionless frequency a_0, according to Gazetas and Pais and Kausel, for different L/B ratio's

6.4   FOUNDATION DAMPING

As mentioned before, both radiation damping as hysteretic material damping in the soil will contribute to the overall damping of the system. Yet, the analytical expressions provided in literature (National Institute of Standards and Technology, 2012) (Gazetas & Tassoulas, 1987) (Gazetas, 1991), only account for radiation damping. Since the expressions are providing a rough estimate anyway, and to not complicate the estimation procedures even more, it is decided to not consider material damping of the soil in this research.

In (National Institute of Standards and Technology, 2012), the radiation damping ratios (β_i) of Pais and Kausel are provided, for both rigid foundations at the ground surface as embedded foundations. In order to obtain the damping values (C_i), the following equation is provided in (National Institute of Standards and Technology, 2012):

$$\beta_i = \frac{\omega C_i}{2K_i} \quad \rightarrow \quad C_i = 2K_i \frac{\beta_i}{\omega} \tag{6.4}$$

Gazetas uses a different approach using a damping modifier. Therefore, different formulas are provided to determine the damping values (C_i): (Gazetas, 1991)

$$C_{x,sur} = \rho_s V_s A_b \tilde{c}_i$$
$$C_{r,sur} = \rho_s V_{La} I_x \tilde{c}_{r,i}$$
$$C_{x,emb} = C_{x,surf} + 4\rho_s V_s BD + 4\rho_s V_{La} LD$$

$$C_{r,emb} = C_{r,surf} + \rho_s I_x \left(\frac{D}{B}\right)\left(V_{La}\left(\frac{D^2}{B^2}\right) + 3V_s + V_s\left(\frac{B}{L}\right)\left(1 + \left(\frac{D^2}{B^2}\right)\right)\right)n_r \tag{6.5}$$

A_b is the surface area
I_x is the area moment of inertia
V_{La} is the Lysmer's analog wave velocity: $(3.4/(\pi(1-v)))\, V_s$
$\tilde{c}_i$ is the damping modifier for horizontal damping
$\tilde{c}_{r,i}$ is the damping modifier for rotational damping
n_r is: $0.25 + 0.65\sqrt{a_0}(D/B)^{-1/4}$

The two procedures (Gazetas and, Pais and Kausel) to determine the horizontal and rotational damping values are described in Appendix .

The graphs for the damping modifiers are fitted by formulas to be able to calculate the damping values according to Gazetas. The same study as performed for the stiffness in the previous section, is performed for the damping values from the expressions of Gazetas and Pais and Kausel, see Figure 58.

Even bigger differences between the two references are found for the damping values. Especially for the rotational damping, large deviations between the two procedures are observed. Therefore, more research is performed into the expected damping values as well. The same models in PLAXIS 2D, which are used for the research into the expected stiffness values, are used. This is discussed in section 6.5.
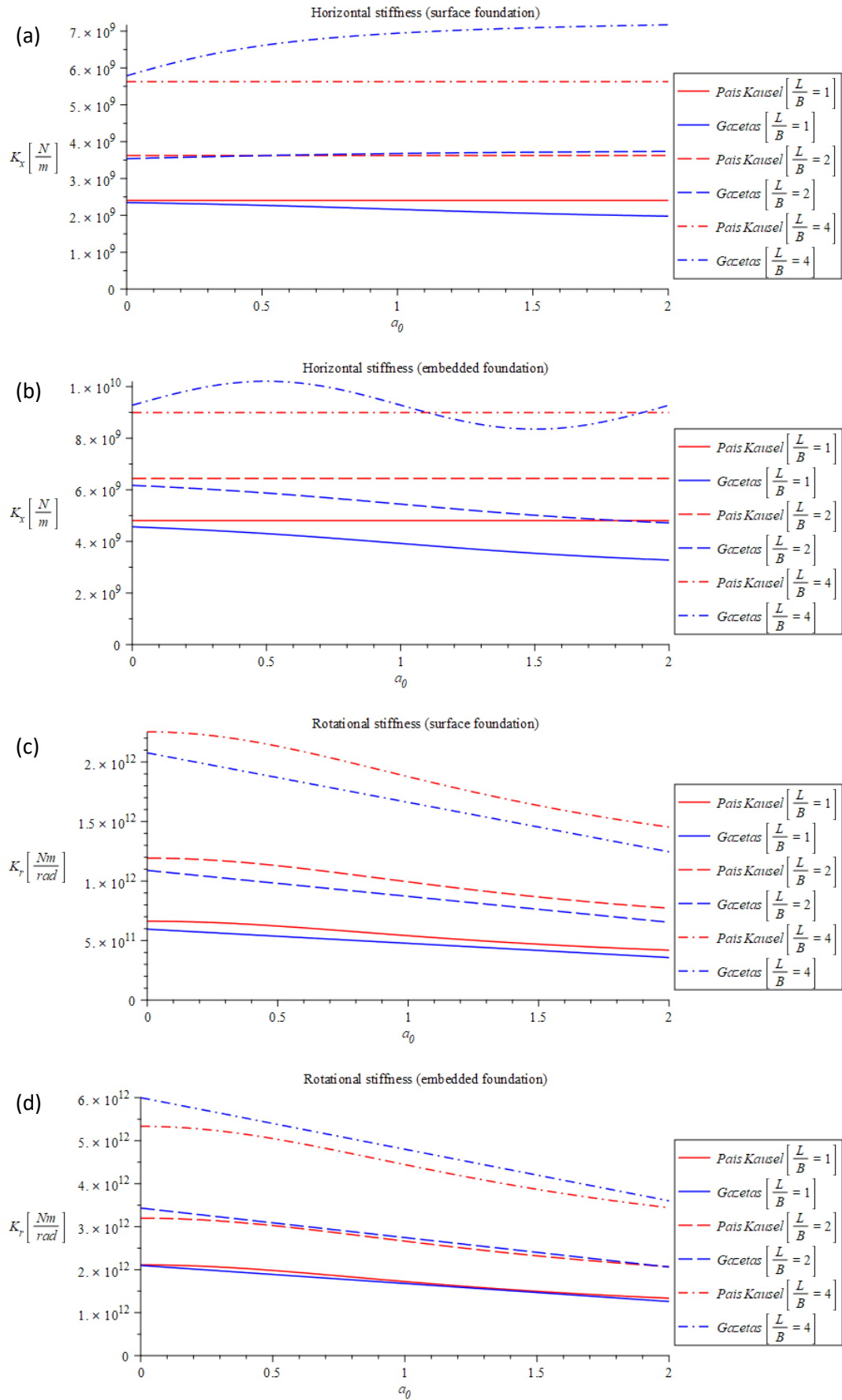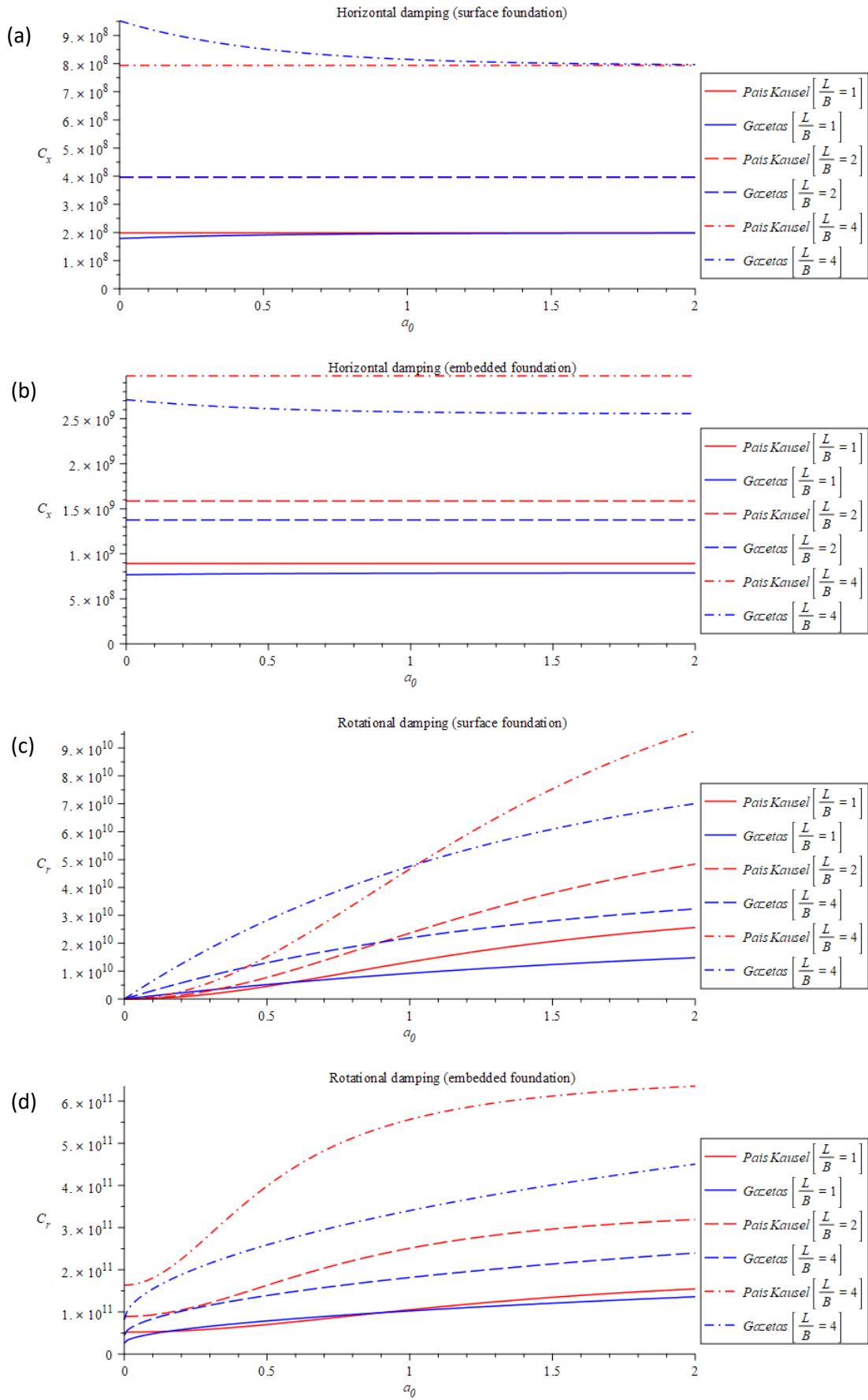
Figure 58: Horizontal damping for surface foundation (a) and embedded foundation (b) and rotational damping for surface foundation (c) and embedded foundation (d) as a function of dimensionless frequency a_0, according to Gazetas and Pais and Kausel, for different L/B ratio's

6.5 VERIFICATION OF ANALYTICAL EXPRESSIONS

As discussed in previous section, the existing expressions for the foundation parameters of Gazetas and, Pais and Kausel, show deviations for certain foundation dimensions. To verify which expressions show more accurate values, PLAXIS 2D is used (PLAXIS, 2019). PLAXIS 2D is a finite element package intended for two-dimensional analysis for geotechnical engineering. The Dynamics add-on to PLAXIS 2D is used to model the dynamic loads. The choice for the two-dimensional package is made to limit the required computation time. Three-dimensional finite element calculations require significantly more computation time than two-dimensional calculations.

A couple notes should be made related to the use of the 2D finite element program:

- The three-dimensional behaviour of the soil cannot be considered
  The 2D package considers an infinite length in the orthogonal direction. This means that all results are per meter length in the orthogonal direction. To make a valid comparison, the analytical expressions should also be considered for infinite length ($L = \infty$). Since this will result in infinite values, a relatively large value for L is chosen instead: $L = 300$ m.
- Linear elastic behaviour of the soil
  Since the analytical expressions are derived for foundations on a linear elastic half-space, this assumption is maintained in the FEM-program.
- Massless and rigid foundation
  This is also an assumption used for the derivation of the analytical expressions and therefore maintained in the FEM-program.

The verification process is performed for two cases:

- A surface foundation: $L = 300$ m, $B = 15$ m, $D = 0$ m
- An embedded foundation: $L = 300$ m, $B = 15$ m, $D = 15$ m

In both cases, the same soil characteristics are used. The soil properties of a homogeneous soil, equivalent to a typical soil profile for Rotterdam, are used: $G = 27 \cdot 10^6$ N/m, $\rho_s = 1800$ kg/m^3, $v = 0.45$. These parameters are explained in section 6.2.

The boundary conditions in the dynamic phase are free + dashpot. This is a different boundary condition than for the static load case, where the boundaries are fixed. The free + dashpot boundaries are chosen to prevent reflections at the boundaries.

The verification is performed using a time history analysis. The procedure to determine the stiffness and damping values is as follows, see Figure 59:

1. Create the homogeneous soil;
2. Install the rigid and massless foundation (either a surface foundation or an embedded foundation) and initialize the stress field in the homogeneous soil;
3. Reset all deformations to zero to start from neutral position (important in case of excavation);
4. Load the structure with a harmonic (sinusoidal) load with specific loading frequency (horizontal load or moment) for a duration of five periods. The five periods is necessary to reach the steady state vibration;
5. Remove the dynamic load and let the foundation return to neutral position in free vibration;
6. Extract the displacement curves and determine the associated stiffness and damping values for the specific loading frequency.

This procedure is repeated for eight loading frequencies which cover the a_0-range of the analytical expressions. How to determine the dynamic stiffness and damping values from the displacement curves, is demonstrated in Appendix .

	Surface foundation	Embedded foundation
1		
2		
3		
4	Horizontal load or moment	Horizontal load or moment
5		
6		
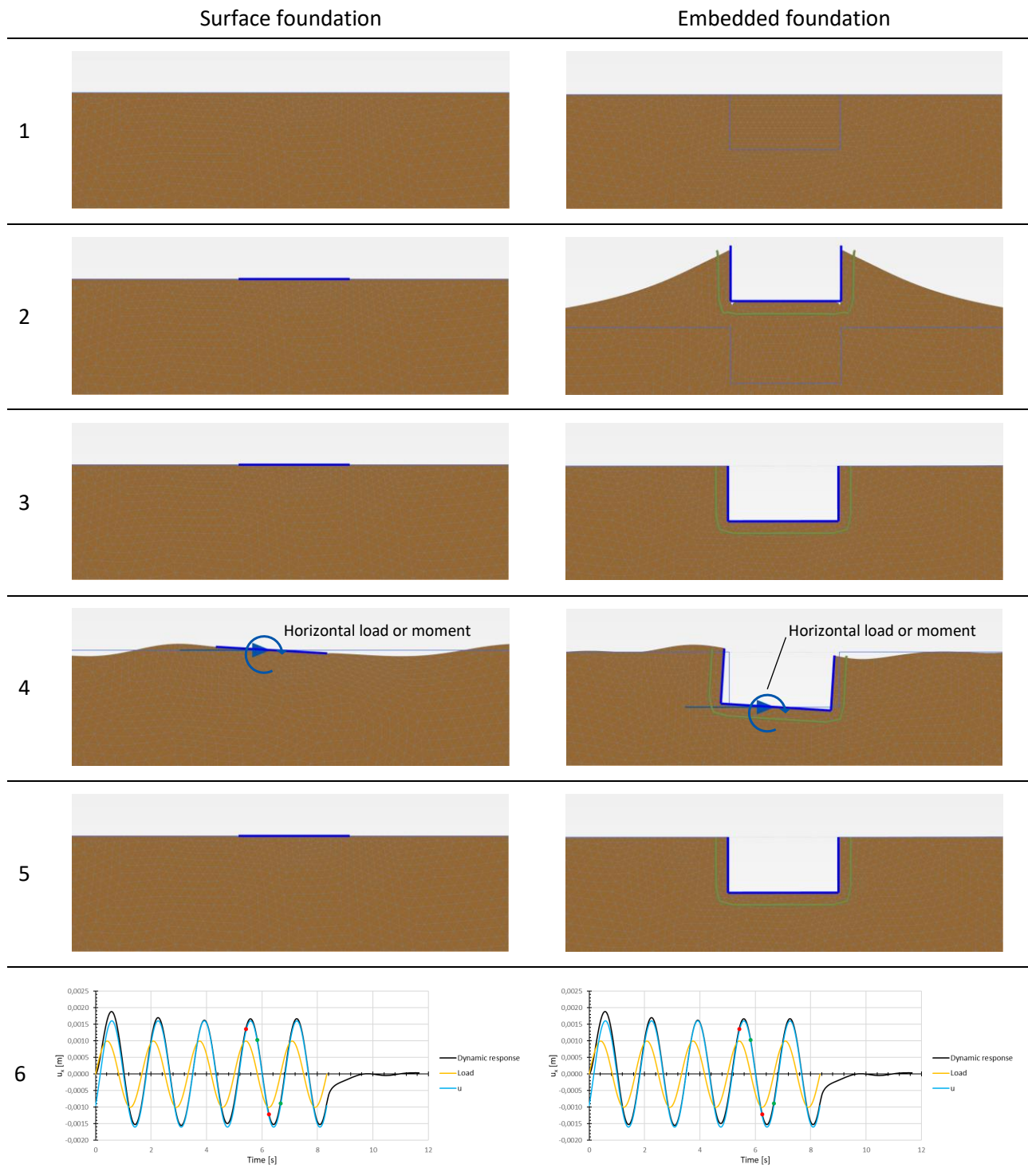
Figure 59: Procedure to determine the dynamic stiffness and damping using the FEM-program

During the verification process, multiple issues were encountered with the finite element model. The most important ones are summarized here:

- Creating a linear elastic half-space with the finite element method is difficult, since there should always be boundary conditions. It turned out that the boundaries have a large influence on the behaviour of the model, even in the static load case. To reduce this influence, the boundaries are placed far away from the foundation. Eventually, the influence was negligible at a horizontal distance of over 13 times the total width of the foundation to both sides and over 6 times the total width in vertical direction;

- The element size needs to be small enough. As indication the following is used:

$$\text{element size} < \frac{\lambda_{min}}{10}, \lambda_{min} = \frac{V_s}{f_{max}}, f_{max} = \text{maximum loading frequency [Hz]}$$

  This indication recommends to sample 10 nodes in one wavelength. For this study, this means that the element size should be smaller than 4 meters. A element size of circa 2 meters is used around the foundation and circa 5 meters at the boundaries.;

- The time step needs to be small enough. The standard recommendation is, that the stress wave does not skip one element of the mesh in one time step. For this study, this would mean a time step of 0.016 seconds. A time step of 0.05 seconds, which is considered to produce sufficiently accurate results, is used, to reduce computation time;

- Finally, it is found to be important to always have a timestep at the peak of the harmonic load.

The results of the verification process are shown in Figure 60 for the foundation stiffness and in Figure 61 for the foundation damping.

The following can be observed from the results of the verification process:

- Horizontal stiffness
  The horizontal stiffness is much better in line with Gazetas. There is an underestimation for both the surface foundation as the embedded foundation. Two hypothesis, both linked to the boundary conditions, are likely to explain the differences:
  1. The relaxation of the boundary conditions from fixed (in the static phase prior to the dynamic phase) to free + dashpot could produce extra displacement and therefore lower stiffness. This is not considered in the Gazetas formulation and not realistic, since there is actually soil next to the boundaries;
  2. The free + dashpot boundaries intend to simulate so-called silent boundaries. Yet, the non-reflective boundaries only work perfectly for one-dimensional wave propagation (Metrikine & Vrouwenvelder, n.d.). Thus, there might still be reflections affecting the stiffness, even though the boundaries are far away.

- Rotational stiffness
  The rotational stiffness is in line with both Gazetas as with Pais and Kausel for both the surface foundation as the embedded foundation. The observed differences are relatively small.

- Horizontal damping
  The horizontal damping is much better in line with Gazetas for both the surface foundation as the embedded foundation. For the embedded foundation, Gazetas results in higher damping values than the PLAXIS results, but the difference is relatively small.

- Rotational damping
  Also for the rotational damping, the PLAXIS results look more similar to the Gazetas curves than those from Pais and Kausel. Yet, for the surface foundation, much higher values are found with the PLAXIS model. The reason for this overestimation is hard to identify, especially because the values for the embedded foundation match quite well. A possible reason can be the sensitivity of the calculation procedure to determine the dynamic damping from the displacement curve. This procedure is explained in Appendix . It is observed that the calculated damping value is very sensitive to where the points for the u-curve are chosen. A smaller time step could result in a better estimation of the u-curve and therefore possibly a lower damping value.

From the verification process, it can be concluded that the Gazetas formulas are much better in line with the obtained numerical results. Therefore, the provided expressions and fitted curves of the Gazetas' dynamic modifiers are used in this research.
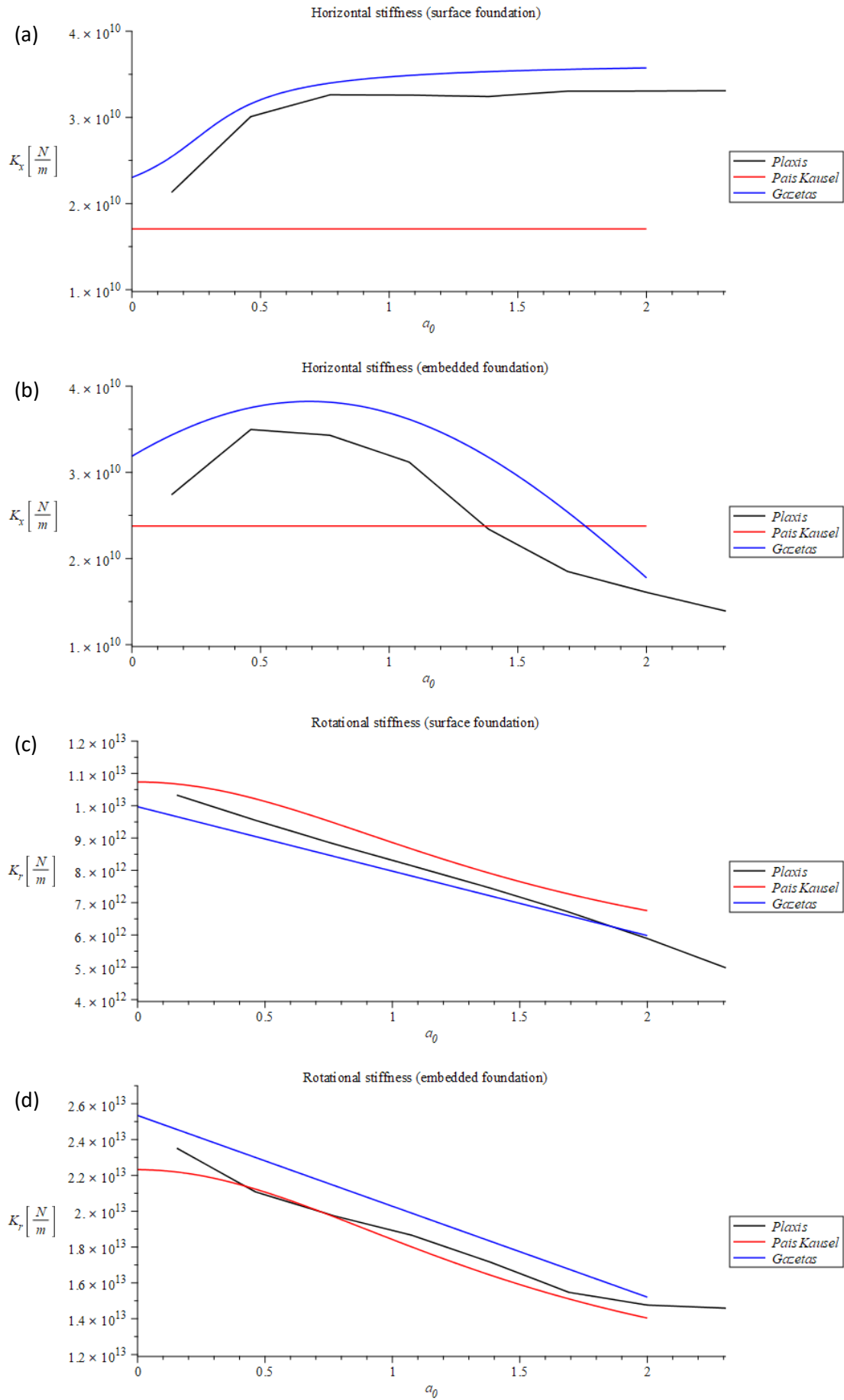
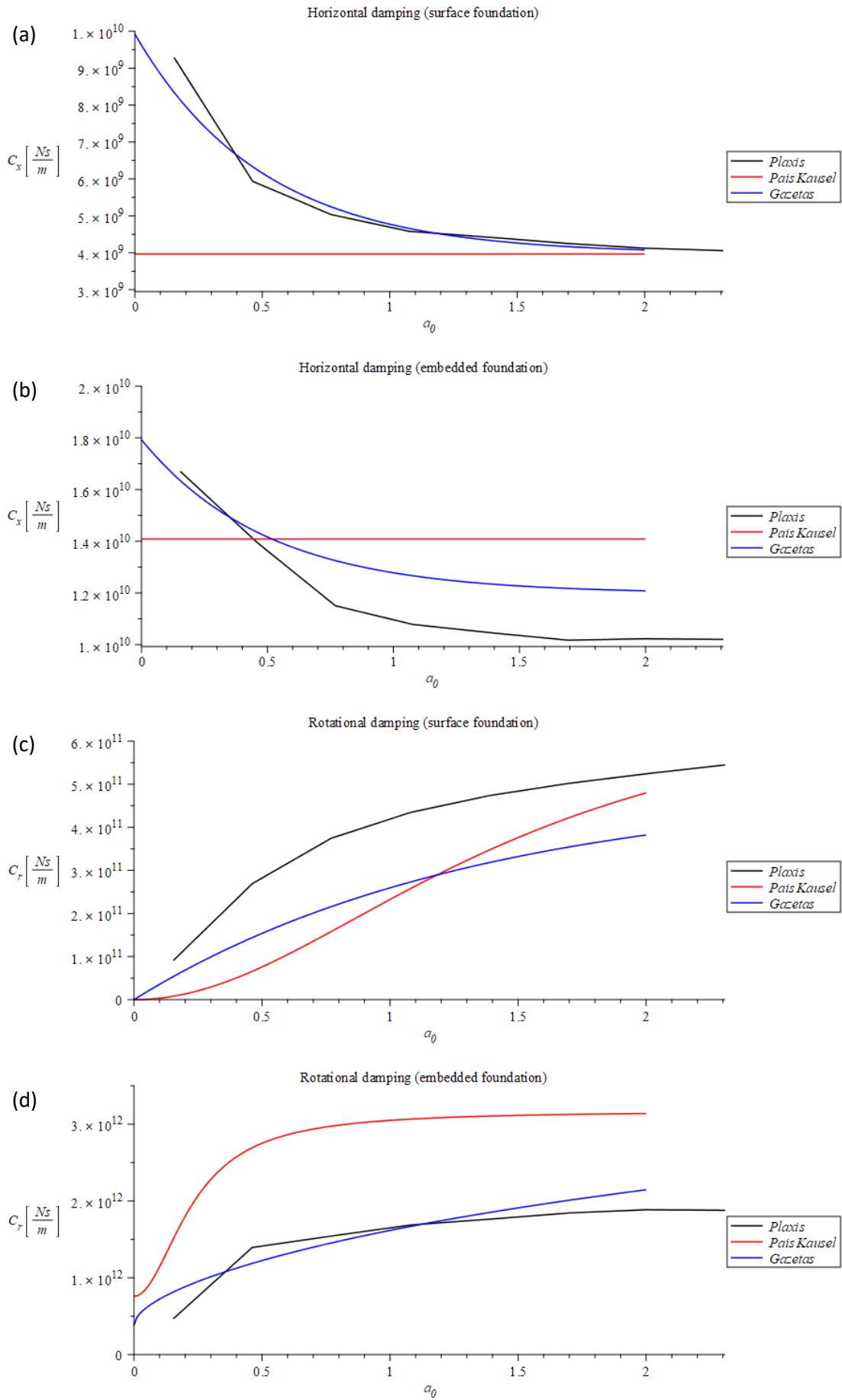Figure 60: Results of the verification process for the stiffness parameters

Figure 61: Results of the verification process for the damping parameters

6.6   PILE FOUNDATION VS SHALLOW FOUNDATION

An important drawback of all previously discussed models and expressions, is that none of these methods consider the contribution of foundation piles. High-rise buildings, especially in the Netherlands, will have pile foundations. Therefore, the contribution of the piles to the dynamic stiffness and damping should be considered. In (National Institute of Standards and Technology, 2012), guidelines for single piles and piles groups up to 4x4 piles are provided. Yet, it does not give any analytical expressions for pile foundations as a whole.

The contribution of the piles is depending on many different aspects. Among others, the ground conditions, pile characteristics and foundation dimensions all have an influence. In addition, different phenomena can influence the contribution of the piles as well. A good example is the contact area of the foundation with the soil. It can happen that a small gap occurs between the bottom face of the foundation and the soil, resulting in a loss of soil stiffness and damping on the bottom interface. This small gap can be caused by consolidation of soft soil layers due to, for example, lowering the hydraulic head of underlying aquifers. Since all these influencing aspects cannot be accounted for separately, it should be emphasised that the correction factor introduced hereafter, is a rough estimate and could change significantly under specific circumstances.

A study into the contribution of the piles is made by (Gómez, 2019), based on the comparison of the cone model by Wolf, without piles, with a numerical program including piles, Dynapile. The numerical model does not account for embedment where the cone model does. The results from (Gómez, 2019) show, that only the rotational stiffness (K_r) obtained with the analytical model significantly deviates from the values obtained by the numerical program. The other three parameters (K_x, C_x, C_r) show comparable results. The results are explained by stating that the horizontal stiffness of the piles is nearly negligible, but they do contribute significantly to the rotational stiffness. Therefore, a correction factor is used for only the rotational stiffness to overcome the differences. Unfortunately, the used value of the correction factor is not mentioned.

Another study is made based on the comparison of (National Institute of Standards and Technology, 2012) between the stiffness and damping ratio of a 3x3 pile group and that of a shallow foundation with equivalent dimensions, shown in Figure 62. It is recognized that a 3x3 pile group is not equivalent to a complete pile foundation. The contribution of the piles for a 3x3 pile group will be higher because the contact area of the footing and the soil is relatively small. Yet, it will give an indication of the contribution of the piles. The results from this comparison should be interpreted in the context of a complete pile foundation, meaning reducing the observed correction factors.

The graphs shown in Figure 62, are presented relative to the common normalized frequency:

$$a_0 = a_0^p \frac{B}{d} = \frac{\omega d}{V_s}\frac{B}{d} = \frac{\omega B}{V_s} \tag{6.6}$$

By assuming a reasonable width of the 3x3 pile group foundation of 4 meters, so: $B = 2$ m, a shear wave velocity of: $V_s = 120$ m/s, and a frequency range up to 2 Hz (low frequency range of the wind), so $\omega = 12.6$ rad/s, this results in a a_0-range from 0 to 0.21. In this range, Figure 62 shows more or less constant stiffness ratios. From this, it can be concluded that the contribution of the piles is not frequency dependent for the low frequency range of the wind loading. The factor is depending on the ratio E_p/E_s. For concrete piles and common soil properties in the Netherlands, this ratio is between 100 and 3000. The dashed line in Figure 62 will give a reasonable estimate.
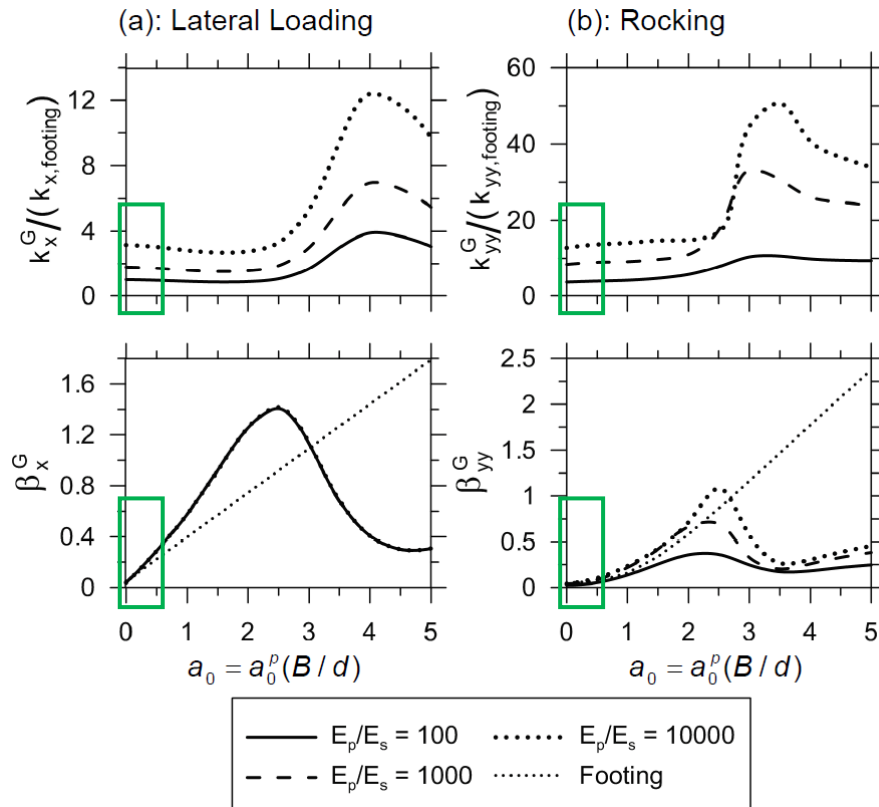
Figure 62: Comparison between the stiffness and damping ratios of a 3x3 pile group and an equivalent shallow foundation by (National Institute of Standards and Technology, 2012)

The stiffness factor is around 2 for horizontal stiffness and around 9 for rotational stiffness. This is not in line with the statement of (Gómez, 2019), which concluded that the piles only have an influence on the rotational stiffness. The influence of the piles on the damping values is very small in the low frequency range. This is in line with the statement of (Gómez, 2019), that the damping in the foundation is governed by the soil surrounding the foundation and the damping contribution of the piles is negligible.

Both studies discussed before, considered a foundation at the ground surface. Logically, it can be argued that the relative contribution of the piles will decrease with increasing embedment depth, since the contact area of the foundation and the surrounding soil will increase, resulting in a higher stiffness from the soil. The effect of embedment is not studied in the referenced literature. Therefore, another study is performed using PLAXIS 2D. Since the contribution of the piles is not frequency dependent in the low frequency range, and more or less equal to the case of $\omega = 0$, the contribution of the piles can be estimated with a static load case.

A pile foundation is effective when the tip of the piles are situated in a strong and stiff layer. In this way, they can transfer the axial forces to, usually deeper, layers. This behaviour cannot be simulated in the PLAXIS model with homogeneous soil properties used before, since there are no layers. Adding the piles in the model will increase the stiffness values ($\sim$50%), but not in the range observed in the previously discussed studies. Therefore, a PLAXIS model, including layers based on a representative soil profile of Rotterdam (see section 6.2), is used instead. The pile contribution is calculated for a surface foundation and 4 embedment depths (7.5, 15.0, 22.5, 30.0 m), with and without piles, for both the horizontal and rotational stiffness. The results are shown in Figure 63.
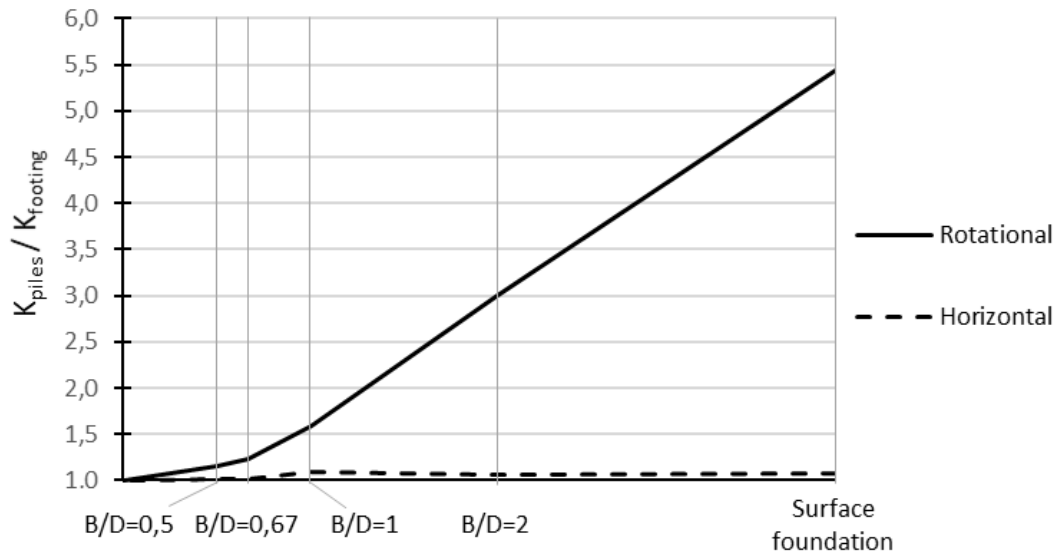
Figure 63: Pile contribution for both the horizontal as the rotational stiffness for a surface foundation and 4 B/D ratio's

As can be seen in Figure 63, the horizontal stiffness is hardly effected by the piles. This is in line with the statement of (Gómez, 2019). The fact that it is much lower than the study of (National Institute of Standards and Technology, 2012), where a factor of 2 is found, can be explained by the much larger contact area of the foundation and the soil, compared to the amount of piles. Also, the stiffness of the top layers has an influence on the contribution of the piles.

The factor for the rotational stiffness for the surface foundation is almost 5.5. This is in line with the statement of (Gómez, 2019) and the study of (National Institute of Standards and Technology, 2012), since the value is a bit lower (5.5 < 9.0). The factor is decreasing for higher embedment depths, which is expected as explained before.

Based on the discussed studies in literature ((National Institute of Standards and Technology, 2012) (Gómez, 2019)), and the performed study in the finite element program, the following is concluded for the considered embedment depths:

- The piles have a negligible contribution to the damping values. The damping values are determined by the radiation damping of the soil;
- The horizontal stiffness is hardly effected by the foundation piles because of the relatively large contact area between the soil and the foundation. The horizontal stiffness is determined by the horizontal stiffness of the soil;
- The rotational stiffness is significantly affected by the foundation piles. A correction factor of 5.5 is found for surface foundations. It is found that the correction factor decreases with increasing embedment depth. This decrease it assumed to be linear, reaching a value of 1.0 at D=30 m.

6.7   SUMMARY

It should be emphasised that all findings are based on the assumptions described in previous sections. It is likely that the results will change for different assumptions. The assumptions that will most likely change the results are:

- No gap between the foundation and the soil is considered in this research. When this is considered, a reduction of soil stiffness and radiation damping is expected, meaning the foundation piles will have larger contribution to both the stiffness as damping;
- No stiffness degradation of the soil is considered;
- No material damping of the soil is considered.

Concluding from the previous sections, the expressions and factors shown in Table 10, are used for the foundation parameters in this research.

Parameter	Surface stiffness	Dynamic modifier	Embedment modifier	Pile correction factor
K_x	Gazetas (1991) Equation (E.2)	Gazetas (1991) Fitted curves (Figure 125)	Gazetas (1991) Equation (E.10)	1
K_r	Gazetas (1991) Equation (E.6)	Gazetas (1991) Equation (E.22)	Gazetas (1991) Equation (E.14)	$5.5 - 0.15\,D$

Parameter	Damping value	Damping modifier		Pile correction factor
C_x	Gezetas (1991) Equation (6.5)	Gazetas (1991) Fitted curves (Figure 126)		1
C_r	Gezetas (1991) Equation (6.5)	Gazetas (1991) Fitted curves (Figure 127)		1

Table 10: Expressions and factors used for the foundation parameters in this research

CHAPTER $\quad$ 7
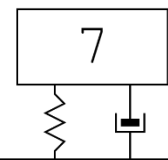
DISTRIBUTION OF MASS AND STIFFNESS OVER HEIGHT

This chapter elaborates on one of the limitations of the three-degree-of-freedom model. The consequences of non-constant mass and/or stiffness over the height of the structure on the first two natural frequencies of a clamped beam system are shown. Also, an analysis procedure is proposed to estimate the equivalent parameters to be used in the model.

7.1   INTRODUCTION

In the preliminary design stage, the structure is often simplified to have constant parameters over height. This is convenient for the calculation procedures, but is not always in line with the design. A good example is the Montevideo tower in Rotterdam, see Figure 64. This building consists of a concrete structure below, with a steel structure on top. The mass and stiffness of both parts are significantly different from each other.
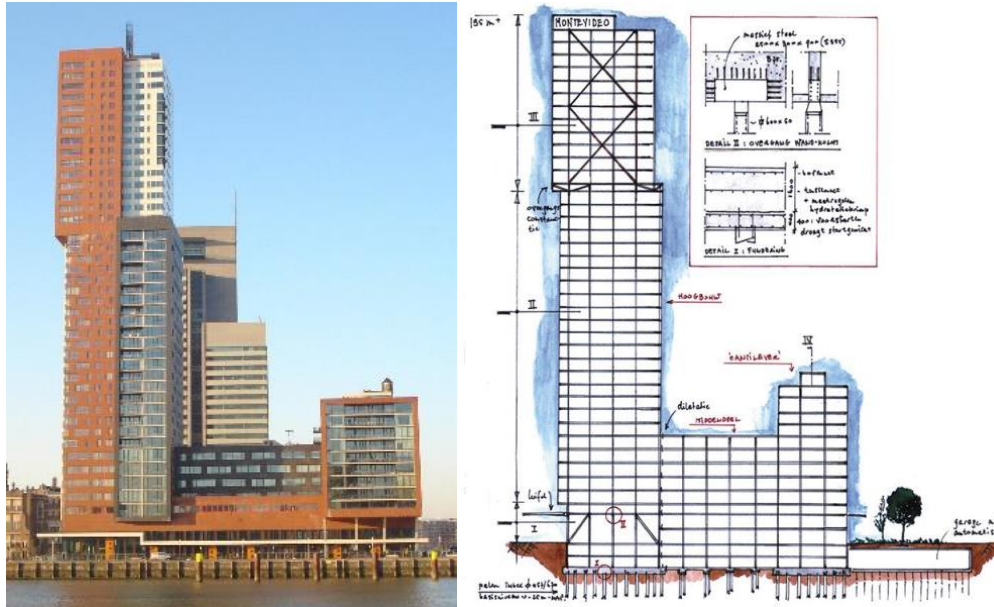
Figure 64: Montevideo tower in Rotterdam (Spangenberg, 2002)

From a dynamic point of view, the mass and stiffness of the structure play an important role. Therefore, it is important to have a good understanding of the consequences of non-constant parameters over height. The natural frequency is an important property of the structure. Being able to predict the natural frequency of the system accurately, enables for a more precise dynamic analysis.

For the model used in this research, described in section 8.1, equivalent stiffness, mass and damping values are determined for the superstructure. This is done in such a way that the SDoF system that represents the superstructure, has the same natural frequency as the superstructure with a clamped foundation. The described method to determine these equivalent properties, uses the assumption of constant parameters over height. This chapter shows how this procedure can still be used in the case of non-constant parameters over height, and the same analysis procedure can be applied to assess the dynamic behaviour of the structure.

First, the model is explained. Then, the analysis procedure to determine the natural frequencies of a separated parameter system is shown. Following, the results for only a stiffness variation or mass variation are discussed in respectively section 7.4 and 7.5. In section 7.6, the case of both stiffness and mass variation is discussed. Section 7.7 elaborates on the verification of the results. Finally, general conclusions and a proposed analysis procedure are provided.

7.2   THE MODEL

To analyse the consequences, the structure is simplified as a fixed beam consisting of two separate parts. Each part having its own parameter values. In this research, the separation height is considered to be a fraction of the total height. Nine different separation heights are considered: $(i/10) \cdot h$ with i from 1 to 9. In the case of $i = 0$ or 10, the structure has constant parameters associated to the top or bottom part respectively. The used model is a clamped beam with total height h, as shown in Figure 65.
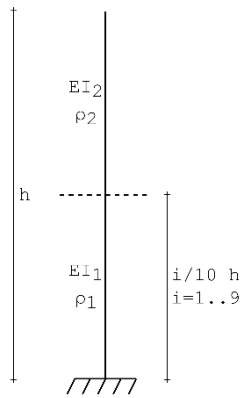
Figure 65: Clamped beam model with 9 separation heights

The natural frequency is governed by stiffness and mass. The aim is to find a design rule that can be used to calculate the natural frequency of the separated parameter system using a non-separated parameter system, see Figure 66. This will simplify calculations, because for the non-separated parameter system the equations for the natural frequencies are known, see Appendix A.
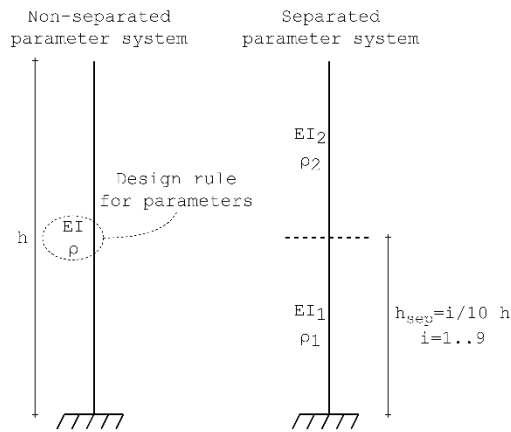
Figure 66: Non-separated and separated parameter system

The values for the stiffness and mass of the bottom and top part are chosen such that the average of both is always the same. This is convenient since the parameters can then be determined with α_{EI} and α_ρ, which are the ratios of the bottom and top stiffness and mass respectively: $\alpha_{EI} = EI_1/EI_2$ and $\alpha_\rho = \rho_1/\rho_2$. The stiffness and mass values are obtained using the following equations:

$$EI_1 = \frac{2}{\frac{1}{\alpha_{EI}} + 1} EI_{average} \qquad\qquad \rho_1 = \frac{2}{\frac{1}{\alpha_\rho} + 1} \rho_{average}$$
$$EI_2 = \frac{2}{\alpha_{EI} + 1} EI_{average} \qquad\qquad \rho_2 = \frac{2}{\alpha_\rho + 1} \rho_{average} \qquad (7.1)$$

The results are normalised such, that the normalized frequency is 1.0 for an α-value of 1.0. By doing so, a good comparison between the different separation heights can be made, since they will all go through the same point for an α-value of 1.0. Also, by normalizing the frequency, the results are valid for every total height (h), stiffness (EI) or mass (ρ) of the structure. Instead of the "actual" natural frequency of the system, a factor (B) is obtained with which the "actual" natural frequency can be calculated using the standard formulas given in Appendix A. Since the stiffness and mass are considered separately, two frequency factors are provided in the form of graphs: $B_{EI,i}$ for a difference in stiffness and $B_{\rho,i}$ for a difference in mass. These frequency factors can be used to calculate the natural frequencies of a separated parameter system. The expressions are provided in the following sections. The i is the mode of vibration. In this research, the first two modes of vibration of the superstructure are considered ($i = 1$ or 2).

7.3 NATURAL FREQUENCIES OF THE SEPARATED PARAMETER SYSTEM

Every part of the separated parameter system has its own equation of motion. These are obtained with Newton's second law and the kinematic and constitutive relation from the Euler-Bernoulli model. This results in the following equations of motion:

$$EI_1 \frac{\partial^4}{\partial z^4} u_1(z,t) + \rho_1 A \frac{\partial^2}{\partial t^2} u_1(z,t) = q(z,t)$$
$$EI_2 \frac{\partial^4}{\partial z^4} u_2(z,t) + \rho_2 A \frac{\partial^2}{\partial t^2} u_2(z,t) = q(z,t)$$

(7.2)

For the free vibration, using the method of separation of variables, the eigen value problems can be obtained:

$$\frac{d^4}{dz^4} u_1(z) - \beta_1^4 u_1(z) = 0 \qquad\qquad \beta_1^4 = \frac{\rho_1 A \omega_1^2}{EI_1}$$
$$\frac{d^4}{dz^4} u_2(z) - \beta_2^4 u_2(z) = 0 \qquad\qquad \beta_2^4 = \frac{\rho_2 A \omega_2^2}{EI_2}$$

(7.3)

By assuming a solution for the eigenvalue problem ($u_i(z) = e^{\lambda z}, i = 1, 2$) and substitution in the characteristic equation, the solution for the free vibration is obtained. Rewriting the solution results in:

$$u_1(z) = D_{11} \cosh(\beta_1 z) + D_{21} \sinh(\beta_1 z) + D_{31} \cos(\beta_1 z) + D_{41} \sin(\beta_1 z)$$
$$u_2(z) = D_{12} \cosh(\beta_2 z) + D_{22} \sinh(\beta_2 z) + D_{32} \cos(\beta_2 z) + D_{42} \sin(\beta_2 z)$$

(7.4)

To find the 8 undetermined constants, 8 equations are needed. The boundary and interface conditions used are:

$$z = 0 \qquad \begin{cases} u_1(0) = 0 \\ \frac{d}{dz} u_1(0) = 0 \end{cases}$$

$$z = h_{sep} \qquad \begin{cases} u_1(h_{sep}) = u_2(h_{sep}) \\ \frac{d}{dz} u_1(h_{sep}) = \frac{d}{dz} u_2(h_{sep}) \\ EI_1 \frac{d^2}{dz^2} u_1(h_{sep}) = EI_2 \frac{d^2}{dz^2} u_2(h_{sep}) \\ EI_1 \frac{d^3}{dz^3} u_1(h_{sep}) = EI_2 \frac{d^3}{dz^3} u_2(h_{sep}) \end{cases}$$

$$z = h \qquad \begin{cases} EI_2 \frac{d^2}{dz^2} u_2(h) = 0 \\ EI_2 \frac{d^3}{dz^3} u_2(h) = 0 \end{cases}$$

(7.5)

The 8 equations can be written in matrix notation ($\mathbf{M} \cdot \underline{D} = \underline{0}$) resulting in $\mathbf{M}$ to be an 8x8 matrix:

$$\begin{bmatrix} 1 & 0 & 1 & 0 & 0 & 0 & 0 & 0 \\ 0 & \beta_1 & 0 & \beta_1 & 0 & 0 & 0 & 0 \\ \cosh(\beta_1 h_{sep}) & \sinh(\beta_1 h_{sep}) & \cos(\beta_1 h_{sep}) & \sin(\beta_1 h_{sep}) & -\cosh(\beta_2 h_{sep}) & -\sinh(\beta_2 h_{sep}) & -\cos(\beta_2 h_{sep}) & -\sin(\beta_2 h_{sep}) \\ \sinh(\beta_1 h_{sep})\beta_1 & \cosh(\beta_1 h_{sep})\beta_1 & -\sin(\beta_1 h_{sep})\beta_1 & \cos(\beta_1 h_{sep})\beta_1 & -\sinh(\beta_2 h_{sep})\beta_2 & -\cosh(\beta_2 h_{sep})\beta_2 & \sin(\beta_2 h_{sep})\beta_2 & -\cos(\beta_2 h_{sep})\beta_2 \\ EI_1 \cosh(\beta_1 h_{sep})\beta_1^2 & EI_1 \sinh(\beta_1 h_{sep})\beta_1^2 & -EI_1 \cos(\beta_1 h_{sep})\beta_1^2 & -EI_1 \sin(\beta_1 h_{sep})\beta_1^2 & -EI_2 \cosh(\beta_2 h_{sep})\beta_2^2 & -EI_2 \sinh(\beta_2 h_{sep})\beta_2^2 & EI_2 \cos(\beta_2 h_{sep})\beta_2^2 & EI_2 \sin(\beta_2 h_{sep})\beta_2^2 \\ EI_1 \sinh(\beta_1 h_{sep})\beta_1^3 & EI_1 \cosh(\beta_1 h_{sep})\beta_1^3 & EI_1 \sin(\beta_1 h_{sep})\beta_1^3 & -EI_1 \cos(\beta_1 h_{sep})\beta_1^3 & -EI_2 \sinh(\beta_2 h_{sep})\beta_2^3 & -EI_2 \cosh(\beta_2 h_{sep})\beta_2^3 & -EI_2 \sin(\beta_2 h_{sep})\beta_2^3 & EI_2 \cos(\beta_2 h_{sep})\beta_2^3 \\ 0 & 0 & 0 & 0 & EI_2 \cosh(\beta_2 h)\beta_2^2 & EI_2 \sinh(\beta_2 h)\beta_2^2 & -EI_2 \cos(\beta_2 h)\beta_2^2 & -EI_2 \sin(\beta_2 h)\beta_2^2 \\ 0 & 0 & 0 & 0 & EI_2 \sinh(\beta_2 h)\beta_2^3 & EI_2 \cosh(\beta_2 h)\beta_2^3 & EI_2 \sin(\beta_2 h)\beta_2^3 & -EI_2 \cos(\beta_2 h)\beta_2^3 \end{bmatrix}$$

(7.6)

The non-trivial solution is found by setting the determinant of $\mathbf{M}$ equal to zero and solving the equation. Because the continuous model has infinite natural frequencies, a numerical solver is used to find the first two solutions which are the first two natural frequencies of the system.

7.4 STIFFNESS VARIATION

In this case, the stiffness of the bottom and top part is altered according to equation (7.1), using α_{EI}-values ranging from 0.2 to 5.0. The mass of the bottom and top part is taken constant and equal.

For all considered separation heights, the results for the frequency factor ($B_{EI,i}$) are shown in Figure 67 for the first natural frequency and in Figure 68 for the second natural frequency. In these graphs, the limit cases are added where the system has either EI_1 or EI_2 over the total height of the structure (separation heights with $i = 0$ or 10).

The frequency factors ($B_{EI,i}$) given in the Figure 67 and Figure 68, result in the exact frequency of the separated parameter system in the case that the mass of the bottom and top part is equal. The first two natural frequencies of a separated parameter system with different stiffness of the bottom and top part can be obtained by equation (7.7).

From Figure 67, it becomes clear that the first natural frequency is dominated by the bottom part of the structure, because the solid lines tend to approach the dashed line associated to EI_1. The dominance of the bottom part is decreasing for smaller separation heights.

From Figure 68, it can be seen that the dominance of the bottom part is less apparent for the second natural frequency. For separation heights lower than $0.8 \, h$, both parts have a significant contribution.
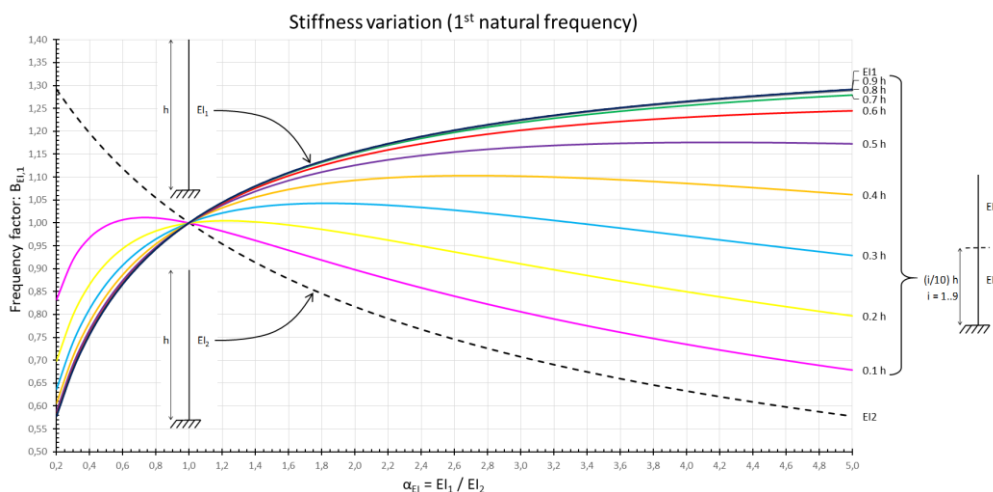

Figure 67: Frequency factor ($B_{EI,1}$) as function of the stiffness ratio α_{EI} for the first natural frequency of a separated parameter system for 9 separation heights

Figure 68: Frequency factor ($B_{EI,2}$) as function of the stiffness ratio α_{EI} for the second natural frequency of a separated parameter system for 9 separation heights

$$\omega_i = B_{EI,i}\, C_i \sqrt{\frac{EI_{average}}{\rho\, A\, h^4}} \qquad\qquad i = 1,2 \quad (mode\ of\ vibration) \tag{7.7}$$

$B_{EI,i}$ is the frequency factor according to Figure 67 ($i = 1$) or Figure 68 ($i = 2$)
C_i is 3.516 for $i = 1$ or 22.034 for $i = 2$
$EI_{average}$ is the average stiffness of the structure: $(EI_1 + EI_2)/2$
ρ is the mass density of the structure
A is the cross-sectional area of the structure
h is the total height of the structure

The distance between the lines, for a certain α- value, indicates how much the mode shapes look similar. This is only true if the system remains the same for different separation heights. This is the case here, namely a clamped beam. If the mode shapes of two separation heights look similar, the integrals of the mode shapes over the height are close to each other as well. This results in similar modal stiffness and modal mass, resulting in similar natural frequency.

The second natural frequency for stiffness variation is used to explain this because, for $\alpha_{EI} = 5.0$, the frequency factor for separation height $0.3\,h$ and $0.4\,h$ are close to each other, see Figure 68. The second natural frequency of the system (ω_2) can also be found using the modal stiffness (k_e) and modal mass (m_e) of the second mode of vibration:

$$\omega_2 = \sqrt{\frac{k_{e,2}}{m_{e,2}}} \tag{7.8}$$

The second natural frequency for separation height $0.3\,h$ and $0.4\,h$ are only similar if the ratio of $k_{e,2}/m_{e,2}$ of both cases are similar. These modal parameters for a separated parameter system can be determined with:

$$k_{e,2} = \rho\, A\, \omega_2^2 \left(\int_0^{h_{sep}} U_2^{bottom}(z)^2\, dz + \int_{h_{sep}}^{h} U_2^{top}(z)^2\, dz \right)$$

$$m_{e,2} = \rho\, A \left(\int_0^{h_{sep}} U_2^{bottom}(z)^2\, dz + \int_{h_{sep}}^{h} U_2^{top}(z)^2\, dz \right) \tag{7.9}$$

A is the cross-sectional area of the structure
ρ is the mass density of the structure
$U_2^{bottom}(z)$ is the second mode shape of the bottom part
$U_2^{top}(z)$ is the second mode shape of the top part

Again, the results of above equations are normalized to have a normalized value of 1.0 for an α-value of 1.0. The normalised modal stiffness ($k_{e,2}$), normalised modal mass ($m_{e,2}$) and normalised frequency factor ($\sqrt{k_{e,2}/m_{e,2}}$) for stiffness variation with an $\alpha_{EI} = 5.0$ are obtained in this way.

In Figure 69, it is visible that the normalised second natural frequency for two different separation heights is close to each other, if the ratio of modal stiffness and modal mass of two different separation heights is close to each other. In this case, the same clamped cantilever beam model is used, which means the modes shapes look similar.

The mode shapes for separation heights $0.1\,h$ to $0.5\,h$ are shown in Figure 70, which shows that the second mode shapes of $0.3\,h$ and $0.4\,h$ are very similar. The second mode shape of $0.2\,h$ also looks quite similar, which is correct since the normalised natural frequency for separation height $0.2\,h$ is not far from the ones of $0.3\,h$ and $0.4\,h$, see Figure 69.
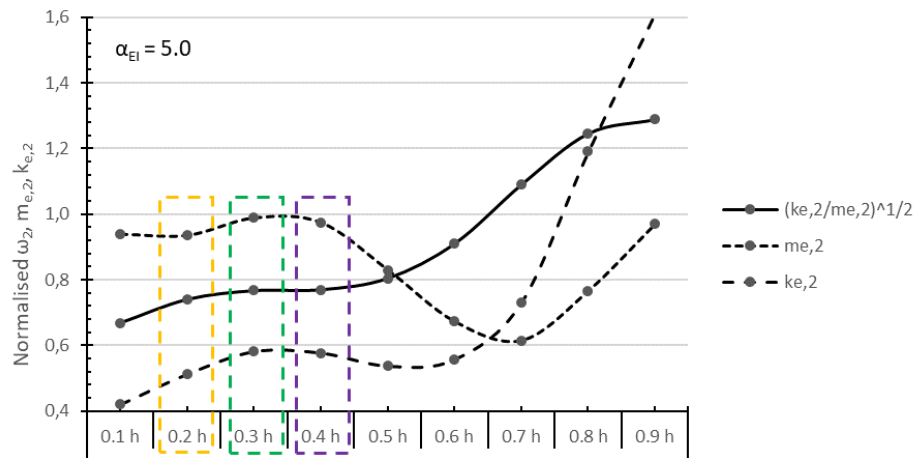
Figure 69: Normalised modal stiffness ($k_{e,2}$), normalised modal mass ($m_{e,2}$) and normalised frequency factor ($\sqrt{k_{e,2}/m_{e,2}}$) for stiffness variation with an $\alpha_{EI} = 5.0$ for 9 different separation heights
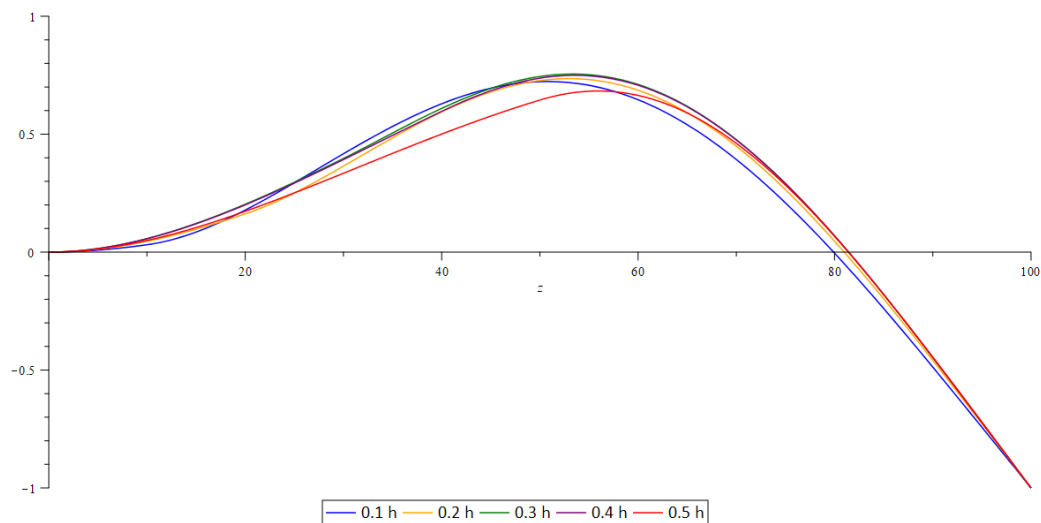
Figure 70: Second mode shapes for separation heights $0.1\ h$ to $0.5\ h$ for $\alpha_{EI} = 5.0$

7.5   MASS VARIATION

For the mass variation, the stiffness is taken constant and equal and the mass is altered according to equation (7.1), using α_ρ-values ranging from 0.2 to 5.0. The same type of graphs are created for the mass variation for the first and second natural frequency, showing the mass factor ($B_{\rho,i}$). Again, the limit cases are added where the system has either ρ_1 or ρ_2 over the total height of the structure.

The frequency factors ($B_{\rho,i}$) given in Figure 71 and Figure 72, result in the exact frequency of the separated parameter system in the case that the stiffness of the bottom and top part is equal and constant. The first two natural frequencies of a separated parameter system with different mass of the bottom and top part can be obtained by equation (7.10).

Opposite to the stiffness variation, the first natural frequency is dominated by the top part in the case of mass variation, as can be seen in Figure 71. The dominance of the top part is decreasing for larger separation heights.

As with the stiffness variation, the second natural frequency is not fully dominated by one part in the case of mass variation, see Figure 72. For separation heights larger than $0.2\ h$, the contribution of the bottom part becomes significant.

The same reasoning as with the stiffness variation is valid here for the distance between the lines. The fact that lines 0.6 h and 0.7 h are now close to each other is in line with expectations since the variation of mass is inversely related to the variation of stiffness.
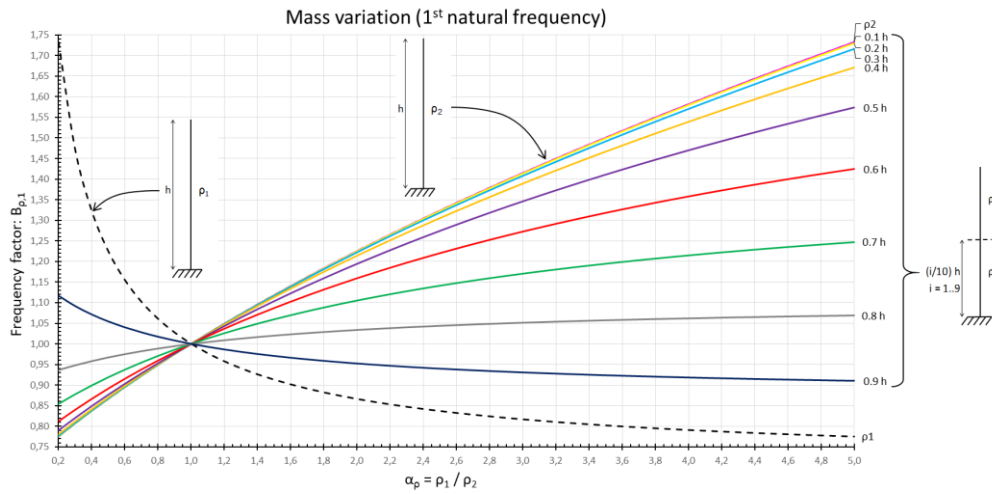
Figure 71: Frequency factor ($B_{\rho,1}$) as function of the mass ratio α_ρ for the first natural frequency of a separated parameter system for 9 separation heights
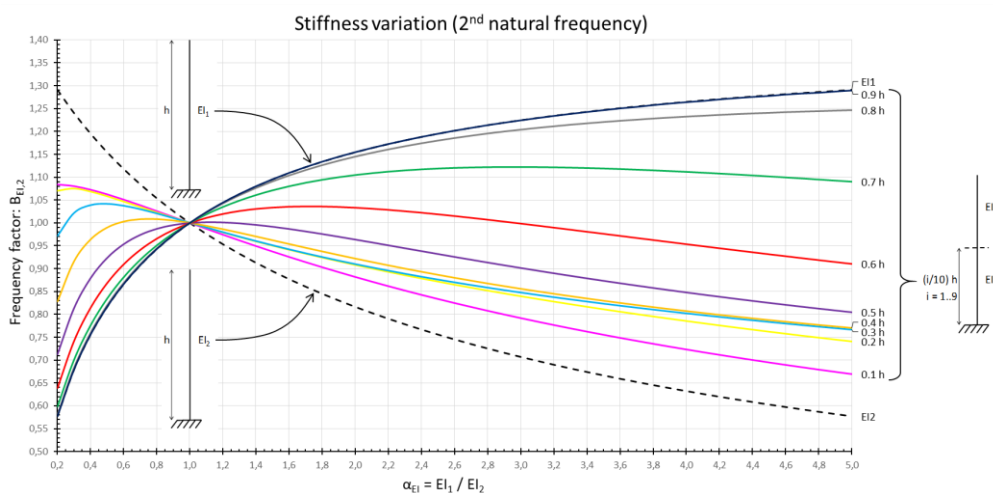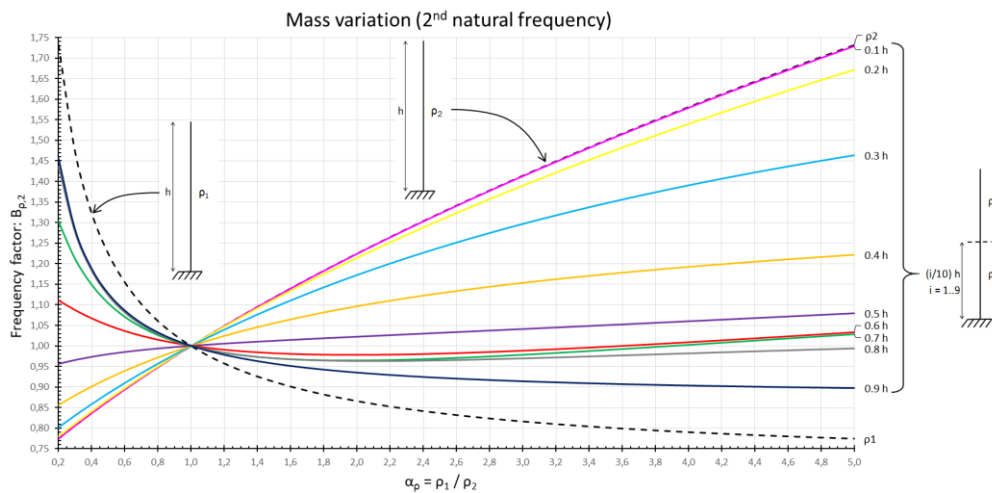

Figure 72: Frequency factor ($B_{\rho,2}$) as function of the mass ratio α_ρ for the second natural frequency of a separated parameter system for 9 separation heights

$$\omega_i = B_{\rho,i}\, C_i \sqrt{\frac{EI}{\rho_{average}\, A\, h^4}} \qquad i = 1,2 \quad (mode\ of\ vibration) \qquad (7.10)$$

$B_{\rho,i}$ is the frequency factor according to Figure 71 (i = 1) or Figure 72 (i = 2)
C_i is 3.516 for i = 1 or 22.034 for i = 2
EI is the stiffness of the structure
$\rho_{average}$ is the average mass density of the structure: $(\rho_1 + \rho_2)/2$
A is the cross-sectional area of the structure
h is the total height of the structure

7.6 STIFFNESS AND MASS VARIATION

Till now, only the stiffness or the mass was altered according to the associated α-value. Yet, it is a realistic situation that both the stiffness and the mass of the bottom and top part are different. In this situation, the frequency factors shown before are not exact anymore. Still, the first and second natural frequency of a

separated parameter system can be estimated by combining the frequency factors. Yet, this will result in a certain error.

The first and second natural frequency of a separated parameter system with different stiffness and mass of the bottom and top part can be obtained by:

$$\omega_i = B_{EI,i}\, B_{\rho,i}\, C_i \sqrt{\frac{EI_{average}}{\rho_{average}\, A\, h^4}} \qquad i = 1,2 \quad (mode\ of\ vibration) \qquad (7.11)$$

$B_{EI,i}$ is the stiffness factor according to Figure 67 (i = 1) or Figure 68 (i = 2)
$B_{\rho,i}$ is the mass factor according to Figure 71 (i = 1) or Figure 72 (i = 2)
C_i is 3.516 for i = 1 or 22.034 for i = 2
$EI_{average}$ is the average stiffness of the structure: $(EI_1 + EI_2)/2$
$\rho_{average}$ is the average mass density of the structure: $(\rho_1 + \rho_2)/2$
A is the cross-sectional area of the structure
h is the total height of the structure

The frequency factors, related to stiffness or mass variation, are exact if the other parameter, stiffness or mass, is constant and equal. A certain error occurs when the other parameter is not equal anymore. So, the error is zero for an equal other parameter and starts to increase for a larger difference of the other parameter. Therefore, the error of estimation will be largest for the largest or smallest α-values, biggest difference of the other parameter. This results in the following four limit cases:

- $\alpha_{EI,i} = 0.2$ and $\alpha_{\rho,i} = 0.2$;
- $\alpha_{EI,i} = 0.2$ and $\alpha_{\rho,i} = 5.0$;
- $\alpha_{EI,i} = 5.0$ and $\alpha_{\rho,i} = 0.2$;
- $\alpha_{EI,i} = 5.0$ and $\alpha_{\rho,i} = 5.0$;

These four cases will provide the upper and lower bounds of the error of estimation using equation (7.11), for both the first as the second natural frequency of a separated parameter system and are shown in Figure 73 and Figure 74.

As can be seen from Figure 73, the error of estimation of the first natural frequency is small with a maximum error of +2.8 %. This error is small considering the fact that measurements of high-rise buildings in the Netherlands show large deviations from system parameters up to 50%. Therefore, a certain amount of conservatism should be accounted for in the design. An error of 2.8% on the first natural frequency will therefore not have a significant influence on the final response of the structure.

The error of estimation of the second natural frequency can become more significant as the maximum error is −18.0 %, see Figure 74. A generally applicable judgement about this error cannot be made because, whether or not this error is significant for the final response, depends on the value of the second natural frequency. For example, if the second natural frequency is far outside the wind frequency domain, the error of −18.0% will not have a significant influence, since the second natural frequency will not contribute significantly to the total response anyway. Yet, the second mode of vibration of the superstructure can have a significant contribution to the total response in certain cases, as shown in section 0. When this is the case, an error of 18% in the determination of the second natural frequency of the superstructure, can result in inaccurate results. The judgment of the error of the determination of the second natural frequency should be made for every individual case, when equation (7.11) is used.
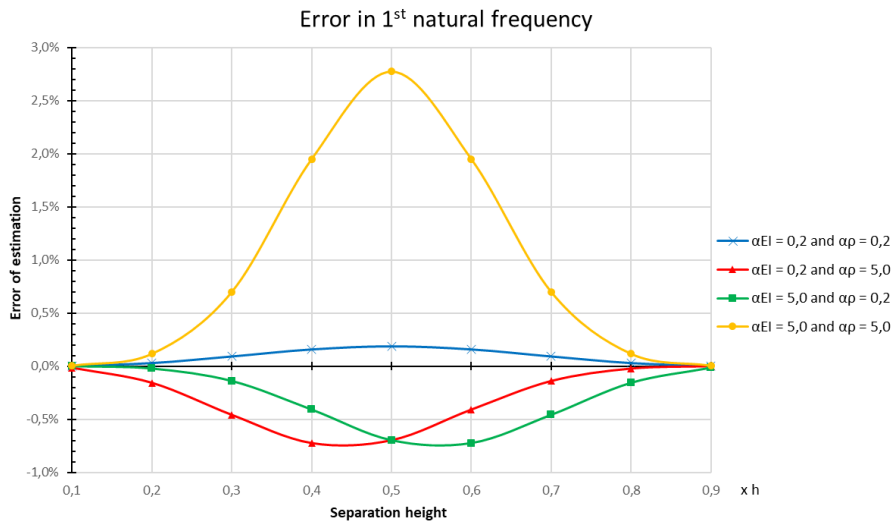
Figure 73: Error of estimation of the first natural frequency of a separated parameter system using equation (7.11)
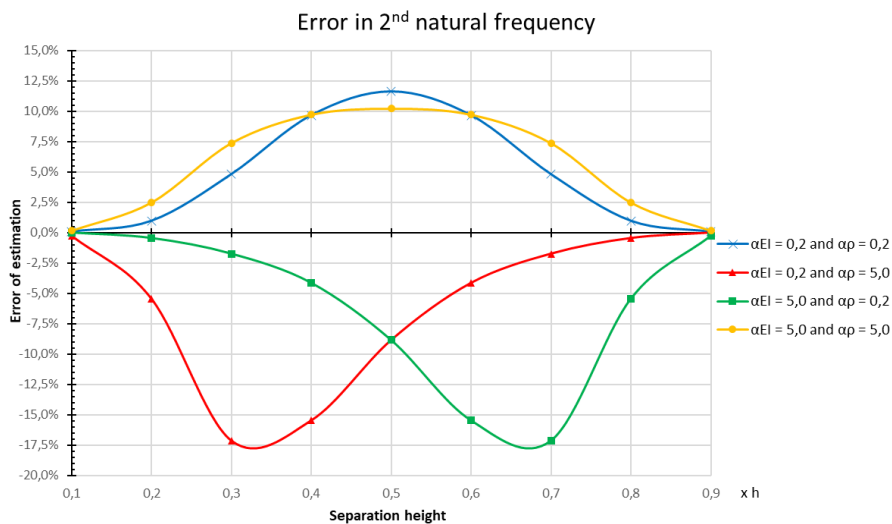
Figure 74: Error of estimation of the second natural frequency of a separated parameter system using equation (7.11)

7.7   VERIFICATION OF RESULTS

To verify the obtained results from the analytical approach described in section 7.3, the finite element program SOFiSTiK is used. SOFiSTiK is a finite element program which can perform all kinds of dynamic analysis, from modal analysis to time history analysis.

For this verification, a modal analysis is used for the first and second natural frequency of the analytical approach. A homogeneous cross-section of 5x5 meter is used for the bottom part and 4x4 meter for the top part. To match the stiffness (EI) and mass (ρA) values of the analytical approach, the elastic modulus E and the mass density ρ of the material for the bottom and top part are modified accordingly.

Multiple configurations of the building parameters are compared with the finite element model and show similar results. Negligible errors ($\sim 0.3\%$) are obtained between the FEM and the analytical model due to rounding errors.

To illustrate the verification, the results from the analytical approach and finite element program are shown in Table 11, for the case of different stiffness and mass of the bottom and top part. Also, the results from the approximation with equation (7.11) are added for comparison. The approach with the approximation formula is explained hereafter.

$h = 100 \text{ m}$
$h_{sep} = 60 \text{ m} \quad (0.6 \text{ h})$
$b = d = 30 \text{ m}$
$A = 900 \text{ m}^2$
$EI_1 = 8.325 \cdot 10^{12} \text{ Nm}^2$
$EI_2 = 2.775 \cdot 10^{12} \text{ Nm}^2$ $\Big\}$ $\alpha_{EI} = 3.00$
$\rho_1 = 400 \text{ kg/m}^3$
$\rho_2 = 300 \text{ kg/m}^3$ $\Big\}$ $\alpha_\rho = 1.33$
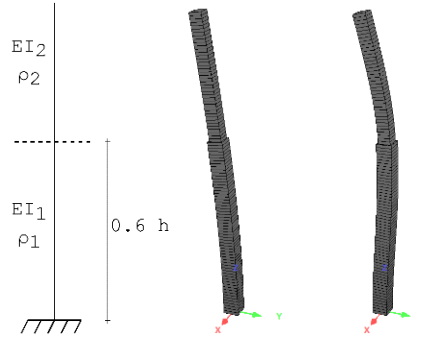
Figure 75: Model (left) and FEM results from SOFiSTiK (right)

	f$_1$ [Hz]	error f$_1$ [%]	f$_2$ [Hz]	error f$_2$ [%]
FEM	0.300	—	1.471	—
Analytical	0.300	0.0	1.475	0.3
Approximation	0.298	0.7	1.451	1.4

Table 11: Results from the finite element program, analytical approach and approximation approach. Errors are given relative to the FEM results

Example of approximation approach

The example parameters are:

$h = 100 \, m$
$h_{sep} = 60 \, m \quad (0.6 \, h)$
$b = d = 30 \, m$
$A = 900 \, m^2$
$EI_1 = 8.325 \cdot 10^{12} \, Nm^2$
$EI_2 = 2.775 \cdot 10^{12} \, Nm^2$ $\Big\}$ $\alpha_{EI} = 3.00$ $\rho_1 = 400 \, kg/m^3$
$\rho_2 = 300 \, kg/m^3$ $\Big\}$ $\alpha_\rho = 1.33$
$EI_{average} = 5.55 \cdot 10^{12} \, Nm^2$ $\rho_{average} = 350 \, kg/m^3$

From Figure 67, Figure 68, Figure 71 and Figure 72 the frequency factors are obtained:

$B_{EI,1} = 1.203$
$B_{\rho,1} = 1.054$
$B_{EI,2} = 0.999$
$B_{\rho,2} = 0.987$

The first natural frequency of the system is calculated with equation (7.11) as:

$$\omega_1 = 1.203 \cdot 1.054 \cdot 3.516 \sqrt{\frac{5.55 \cdot 10^{12}}{350 \cdot 900 \cdot 100^4}} = 1.871 \, rad/s \; \rightarrow \; f_1 = 0.298 \, Hz$$

And the second natural frequency is calculated with equation (7.11) as:

$$\omega_2 = 0.999 \cdot 0.987 \cdot 22.034 \sqrt{\frac{5.55 \cdot 10^{12}}{350 \cdot 900 \cdot 100^4}} = 9.116 \, rad/s \; \rightarrow \; f_2 = 1.451 \, Hz$$

7.8   SUMMARY

From Figure 67 till Figure 72, it becomes clear that the first and second natural frequency of a separated parameter system are depending on the separation height, the stiffness ratio and/or the mass ratio. The presented graphs can be used to calculate the first and second natural frequency using the formulas given in equations (7.7) and (7.10). Equations (7.7) and (7.10) give an exact result for the first and second natural frequency only, if the mass (equation (7.7)) or stiffness (equation (7.10)) of the bottom and top part is constant and equal.

For situations where both the stiffness and mass of the bottom and top part are different, equation (7.11) can be used to estimate the first and second natural frequency. The error of estimation for the first natural frequency can be neglected for the studied domain in this research. For the second natural frequency, a judgment should be made about the significance of the error. Figure 73 and Figure 74 provide the lower and upper bound of the error of estimation using equation (7.11) for the domain of this research.

When the natural frequencies of the separated-parameters system are determined, these can be used to determine the equivalent mass and stiffness for the dynamic analysis using the analysis procedure described in section 8.1. When a constant parameter approach is used for this, the stiffness or the mass should be determined to calculate the other, since the natural frequency is known. From practice, the mass of the building is usually better predicted, since the stiffness contains many different aspects which have a large uncertainty, e.g. the Young's modulus of concrete. Therefore, it is recommended to calculate the modal mass per vibration mode of the superstructure, and match the modal stiffness in such a way that the natural frequencies are equal to the obtained natural frequencies of the separated-parameter system.
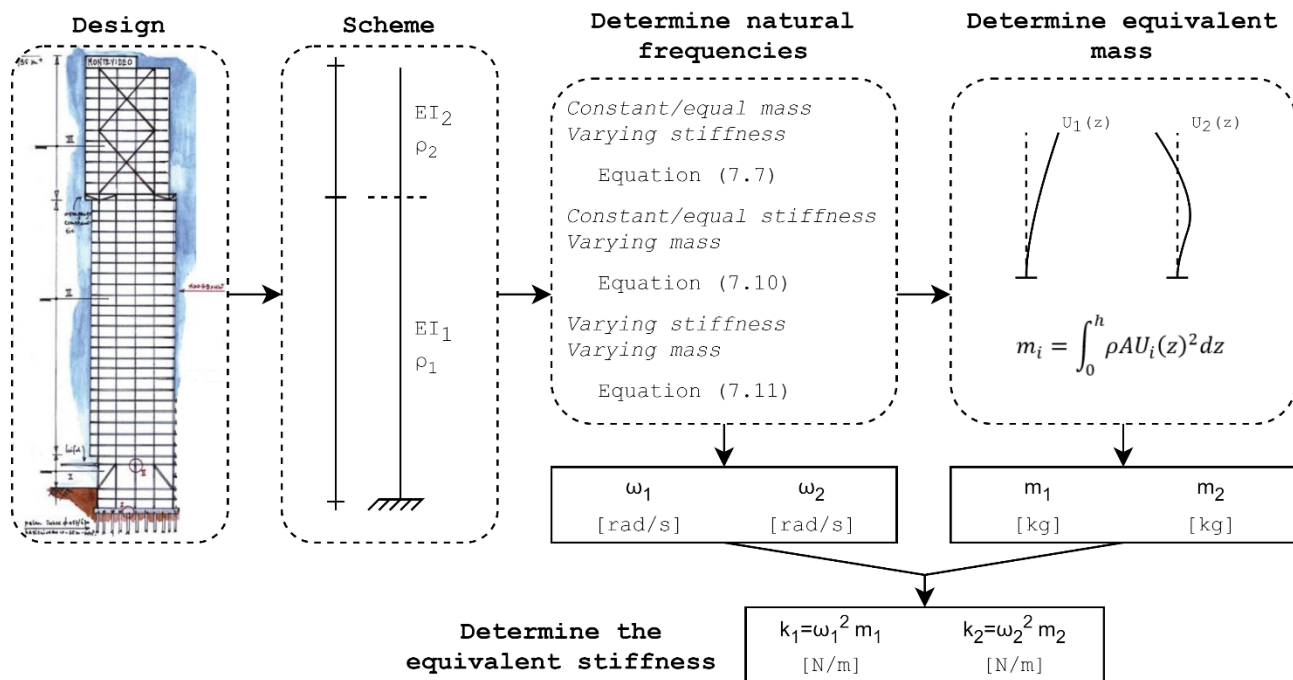
Figure 76: Analysis procedure to determine the equivalent mass and stiffness for the dynamic analysis using the model as described in section 8.1

CHAPTER $\boxed{8}$
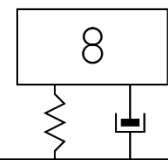
PARAMETER INFLUENCE STUDIES

This chapter provides insight into the influence of the main parameters in the structural design on the maximum acceleration of the structure. This can be used to obtain insight into the influence of design changes on the maximum acceleration at the top of the building. For example, changing the floor system will result in a change in the mass density of the building. The influence of the main parameter for mass density ρ, provides insight into the consequences of a changing floor system.

First, the model is shown and the assumptions and analysis procedure are explained. Then, the calculation procedure to determine the maximum acceleration at the top of the building is shown. After, the contribution of the second run, with different equivalent parameters of the superstructure, to the maximum acceleration is presented. Following, the influence of the geometrical dimensions, the foundation parameters and the superstructure parameters are determined. The significance of a flexible foundation is mentioned and the effective modal damping ratios are discussed.

8.1 THE MODEL

To analyse the response due to wind load, the analysis procedure as shown in Figure 77, is used. A three-degree-of-freedom model is used in this research. This discrete model is adopted from (Gómez, et al., 2018). The stiffness and damping of the superstructure and the soil are represented by means of springs and dashpots, assuming small displacements. The determination of the equivalent superstructure parameters are explained hereafter. The parameters related to the foundation are determined using analytical expressions by (Gazetas, 1991), as explained in chapter 6.

In the 3DoF model, equivalent parameters ($K_{b,equi}$, $C_{b,equi}$, $m_{b,equi}$), which are representative for the superstructure in the 3DoF model, are determined. The modal stiffness, modal mass and modal damping value, for a particular mode of vibration of a continuous clamped beam, are used for these equivalent parameters. These modal properties are determined using the mode shapes of the first and second mode of vibration of a continuous beam model, clamped at the foundation (see Appendix A). In this way, the equivalent parameters are such that they have the same natural frequency as the particular bending mode of vibration of the clamped beam. Following this procedure, the response of the three-degree-of-freedom model is considered representative for the particular mode of vibration of the superstructure including a flexible foundation. This assumption is further discussed in section 8.3.

In general, the total response of a system is the summation of all modes of vibration. The modes can be summed up, in the case of linear models. However, not all modes contribute equally to the total response. The amount of modes necessary to estimate the total response sufficiently accurate, differs for different fields of application.

In this research, the first two modes of the clamped beam model are used. The 3DoF model is used twice with different input parameters. First, with the modal parameters of the first mode of vibration of the clamped beam model (Run 1). Then, with the modal parameters of the second mode of vibration of the clamped beam model (Run 2). The response functions and total variance of acceleration from both runs are superimposed to find the combined response. This is further discussed in section 8.3.

The analysis procedure using the discrete 3DoF model twice, as shown in Figure 77, is always applied in this research.
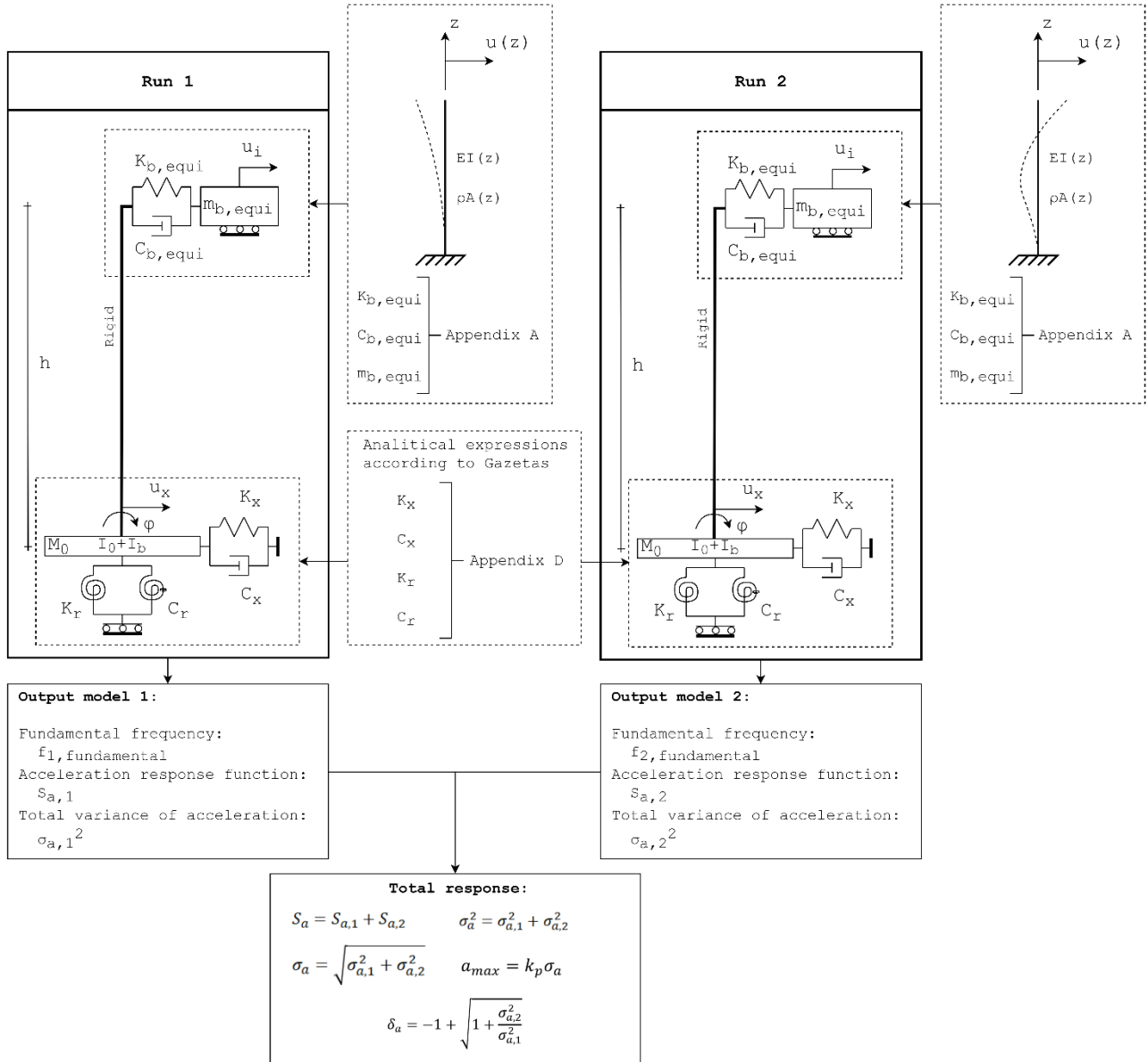
Figure 77: Analysis procedure for the calculation of the maximum acceleration (a_{max}) and the contribution of the second run to the maximum acceleration (δ_a)

8.2 CALCULATION OF THE RESPONSE

The equations of motion of the model, form a system of equations. The equations represent the horizontal force equilibrium of the structure, the horizontal force equilibrium of the soil-foundation interaction and the moment equilibrium of the soil foundation interaction of the system. This system of equations can be rewritten in matrix form as follows:

$$\mathbf{M}\,\ddot{U}(t) + \mathbf{C}\,\dot{U}(t) + \mathbf{K}\,U(t) = F(t) \tag{8.1}$$

$$\mathbf{M} = \begin{bmatrix} m_{b,equi} & 0 & 0 \\ 0 & M_0 & 0 \\ 0 & 0 & I_0 + I_b \end{bmatrix}$$

$$\mathbf{K} = \begin{bmatrix} K_{b,equi} & -K_{b,equi} & -K_{b,equi}h \\ -K_{b,equi} & K_{b,equi} + K_x & K_{b,equi}h \\ -K_{b,equi}h & K_{b,equi}h & K_{b,equi}h^2 + K_r \end{bmatrix}$$

$$\mathbf{C} = \begin{bmatrix} C_{b,equi} & -C_{b,equi} & -C_{b,equi}h \\ -C_{b,equi} & C_{b,equi} + C_x & C_{b,equi}h \\ -C_{b,equi}h & C_{b,equi}h & C_{b,equi}h^2 + C_r \end{bmatrix}$$

$$F(t) = \begin{bmatrix} f(t) \\ 0 \\ 0 \end{bmatrix} \qquad U(t) = \begin{bmatrix} u(t) \\ u_x(t) \\ \varphi(t) \end{bmatrix} \qquad \dot{U}(t) = \begin{bmatrix} \dot{u}(t) \\ \dot{u}_x(t) \\ \dot{\varphi}(t) \end{bmatrix} \qquad \ddot{U}(t) = \begin{bmatrix} \ddot{u}(t) \\ \ddot{u}_x(t) \\ \ddot{\varphi}(t) \end{bmatrix}$$

Equation (8.1) can be transformed to the frequency domain as follows:

$$\mathbf{A}(\omega)\,\tilde{U}(\omega) = F(\omega) \tag{8.2}$$

The matrix $\mathbf{A}(\omega)$ is a matrix that contains the mass, damping and stiffness coefficients. The complex valued natural frequencies are obtained by setting the determinant of $\mathbf{A}$ equal to zero and solving for the roots of the obtained equation. Since a spectral analysis is used, the transfer function of the system is needed. To find this function, the term in the forcing vector associated to the superstructure is forced to be equal to 1:

$$F(\omega) = \begin{bmatrix} 1 \\ 0 \\ 0 \end{bmatrix} \tag{8.3}$$

Now the system can be solved which results in the transfer functions for displacements: $H_u, H_{x,u}, H_{r,u}$. The subscript u describes the response at height h in terms of displacement. The subscript x, u describes the response of the translational degree-of-freedom of the foundation and the subscript r, u describes the response of the rotational degree-of-freedom of the foundation. The transfer functions for acceleration are found by multiplication with ω^2. In the subscript, the u is replaced by an a. Now, the response functions for acceleration are found by:

$$S_a(\omega) = |H_a|^2 S_{FF}$$
$$S_{x,a}(\omega) = |H_{x,a}|^2 S_{FF} \tag{8.4}$$
$$S_{r,a}(\omega) = |H_{r,a}|^2 S_{FF}$$

The variance of the acceleration at the top of the building is found by:

$$\sigma_a^2 = \int_0^\infty S_a(\omega)\, d\omega \tag{8.5}$$

As explained, the 3DoF model is used twice. The variance of the combined response is given by:

$$\sigma_a^2 = \sigma_{a,1}^2 + \sigma_{a,2}^2 \tag{8.6}$$

And the standard deviation of the combined response is:

$$\sigma_a = \sqrt{\sigma_{a,1}^2 + \sigma_{a,2}^2} \tag{8.7}$$

As described in section 4.3, the maximum acceleration is found by multiplying the standard deviation by a peak factor. So, the maximum acceleration of the combined response is given by:

$$a_{max} = k_p \sigma_a \tag{8.8}$$

For the contribution of the second run of the analysis procedure to the combined response, the variance of the combined response can be rewritten as:

$$\sigma_a^2 = \sigma_{a,1}^2 \left(1 + \frac{\sigma_{a,2}^2}{\sigma_{a,1}^2} \right) \tag{8.9}$$

The contribution of the second run of the analysis procedure to the maximum acceleration is therefore:

$$\delta_a = -1 + \sqrt{1 + \frac{\sigma_{a,2}^2}{\sigma_{a,1}^2}} \quad [\%] \tag{8.10}$$

The contribution of the second run to the maximum acceleration of the structure is relative to the maximum acceleration of the structure when only the first run is considered. This means that if the maximum acceleration from only the first run is considered to be 100%, the maximum acceleration when both runs are considered is above 100%. For example, the maximum acceleration, considering only the first run, is 100%. The maximum acceleration, considering both runs, is 130%. Then, the contribution of the second run to the maximum acceleration is: $\delta_a = 30\%$. Meaning, a 30% higher maximum acceleration, relative to the maximum acceleration if only the first run is considered.

8.3 CONTRIBUTION OF THE SECOND RUN

The importance of the interaction between superstructure and foundation is emphasised before. From a dynamic point of view, the interaction is studied in literature and the main conclusion is that the contribution of the foundation can be significant (Bronkhorst & Geurts, 2018) (Gómez, et al., 2018). However, the significance of higher modes of vibration, analysed with a model including the foundation, is not found in literature.

Continuous systems have infinite modes of vibration and the total response is the summation of all modes. But, not all modes of vibration contribute significantly to the total response of the structure. Generally for high-rise buildings, the lower the natural frequency of the mode of vibration, the higher the contribution to the total response. This is true because the energy content of the wind spectrum is higher for lower frequencies, see Figure 78.
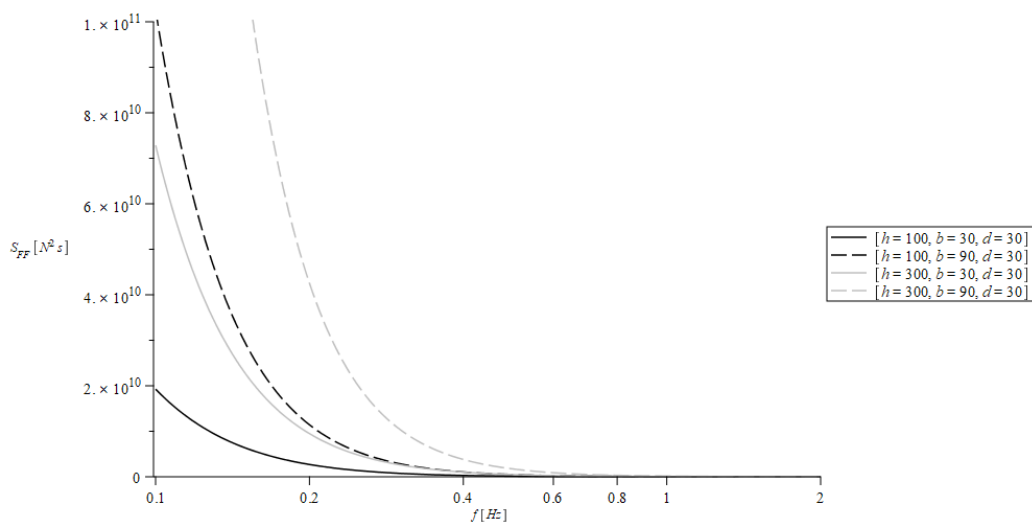
Figure 78: Wind load spectrum for the geometrical dimension boundary cases studied in this research

In the Eurocode, only the first mode of vibration is considered. In addition, the NTA 4614-3 states that higher modes of vibration only have to be considered in a dynamic analysis, if their natural frequency is below 1 Hz. This statement is valid looking at the energy content of the wind load spectrum in Figure 78. It

can be seen that the energy content for frequencies higher than 1 Hz is negligible compared to frequencies lower than 1 Hz.

Since current methods, often applied for high-rise buildings in the Netherlands, only consider the first mode of vibration, the aim of this section is to give an indication of the contribution of the second mode of vibration to the maximum acceleration, including the influence of the foundation in the analysis.

The first run of the model is assumed to be representative for the first mode of vibration of a high-rise building, including a flexible foundation. The second run of the model is assumed to be representative for the second mode of vibration of a high-rise building, including of a flexible foundation. Therefore, it is also assumed that the contribution of the second run to the maximum acceleration gives an indication of the contribution of the second mode of vibration of a high-rise building, including a flexible foundation.
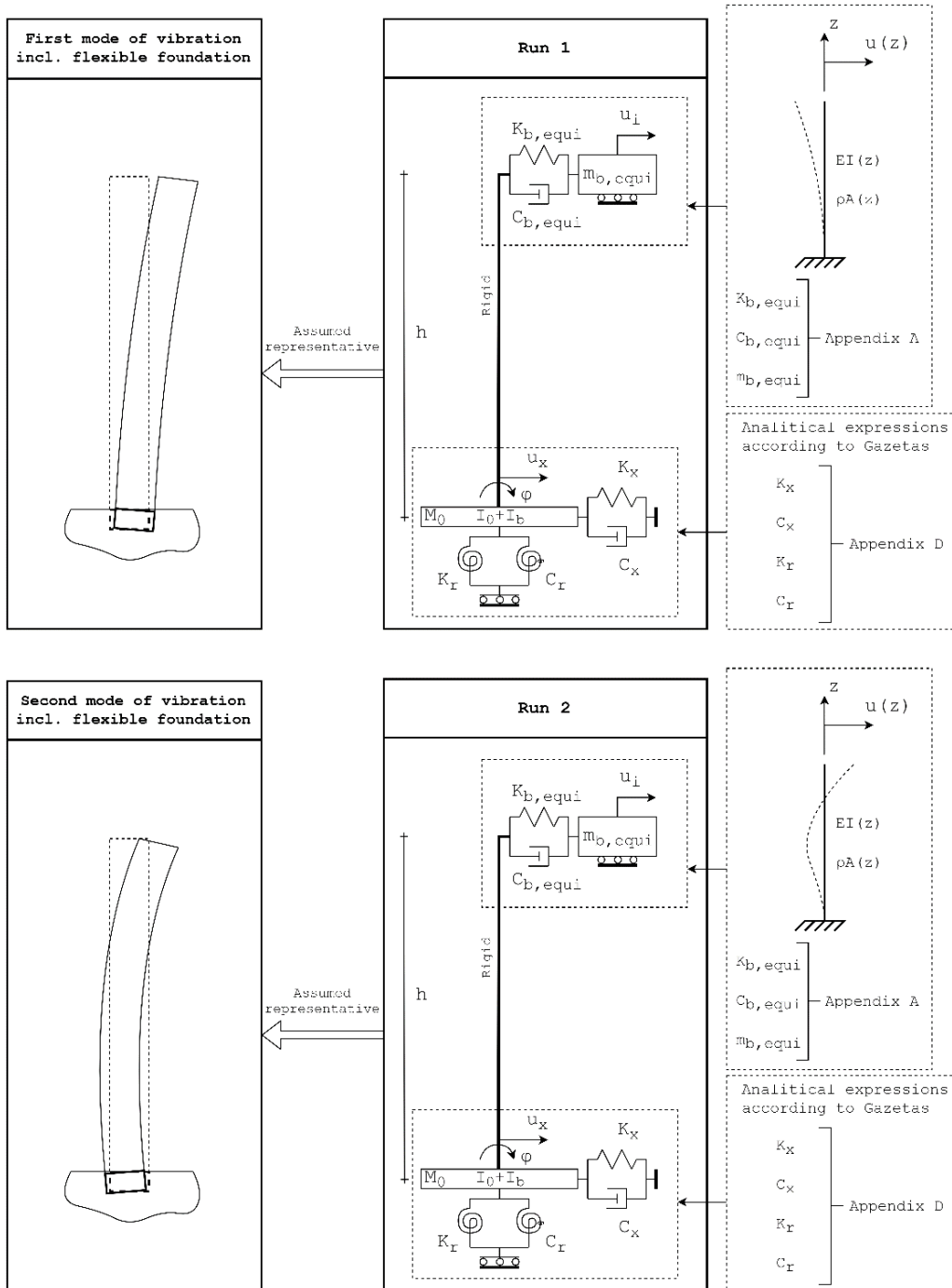
Figure 79: Assumption that run 1 and run 2 are representative for the first and second mode of vibration of a high-rise building with a flexible foundation

It should be emphasized that the use of a 3DoF model limits the amount of modes that can be captured to three. It is assumed that the procedure adopted in this research, provides an indication of the contribution of the second mode of vibration to the maximum acceleration. However, this assumption is not verified in this research. A different model, which can capture higher modes of vibration, is required to investigate the contribution of higher modes of vibration to the maximum acceleration more accurately. A suitable model to investigate the contribution of higher modes would a continuous beam model, including the rotational and translational springs and dashpots, representing the foundation.

The contribution of the second run to the maximum acceleration of the building is investigated by analysing multiple variants with different geometrical dimensions, different foundation depths and different ground conditions. The following dimensions are used for the analysis:

- Height of the building: $h = 100, 150, 200, 250, 300$ m;
- Width of the building: $b = 30, 40, 50, 70, 90$ m;
- Depth of the building: $d = 30, 40, 50, 70, 90$ m;
- Foundation depth: $D = 3.5, 7.0, 10.5, 14.0$ m.

Besides the different dimension parameters, three soil profiles are used. The three soil profiles are categorised as soft, medium and stiff as shown in Table 9. Besides these, a clamped foundation is considered to verify the conclusions of earlier research. Consequently, a total of 2000 variants are analysed.

The stiffness ($EI(z)$) is determined based on the height as described in section 5.1. The mass ($\rho A(z)$) is calculated by multiplying a constant mass density ($\rho = 350 \text{ kg/m}^3$) with the associated cross-sectional area (A). The damping ratio is considered constant for both runs ($\xi = 1.5\%$). The parameters related to the foundation are determined accordingly for both runs as described in chapter 6 and Appendix E.

Results clamped foundation

As studied and concluded by (Oosterhout, 1996), the contribution of the second mode of vibration of the superstructure to the maximum acceleration is small ($< 1\%$). Yet, this conclusion is based on a model with a clamped foundation. To compare the model used in this research with the results by (Oosterhout, 1996), the results of a model with a clamped foundation are discussed first. The clamped foundation is reached by forcing the foundation stiffness parameters to be very high (10^{20}) and the foundation damping parameters to be zero. The maximum contribution of the second run to the maximum acceleration, for a clamped foundation, is 4.3%, and is found for: $h = 300$ m, $b = 30$ m, $d = 90$ m. This is slightly higher than the value found by (Oosterhout, 1996). This is probably the case because larger heights are considered in this research. Yet, the contribution is still small. Also, the shift in natural frequency for different geometrical dimensions is equal for both the first as second fundamental frequency, indicated by the arrows in Figure 80. This is in line with the theoretical derivation of the natural frequencies of a clamped beam, see Appendix C. Also, the influence of the geometrical dimensions (h, b and d) is equal for both runs (the b- and d-variation plots have the same shape). There is no large difference between the influence of b and d on the contribution.

Based on the results from this investigation, the contribution of the second run to the maximum acceleration of the structure can be neglected for a clamped foundation within the considered domain in this research.
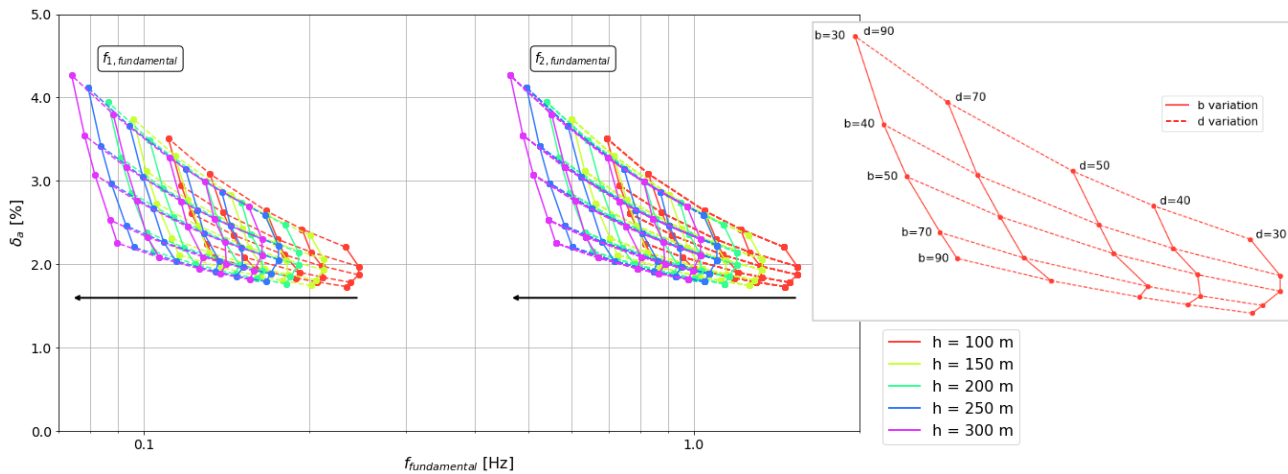
Explanation of graph:

On the x-axis, the fundamental frequency. The first and second fundamental frequency (first and second run) are both plotted. On the y-axis, the contribution of the second run to the maximum acceleration, relative to the maximum acceleration when only the first run is considered. The dots are the different geometrical dimensions considered. The solid and dashed lines show the influence of changing parameter values, b- and d-variation respectively. The colors indicate a variation in height h. The black arrows indicate the shift of the first and second fundamental frequency.

Figure 80: Contribution of the second run to the maximum acceleration (δ_a) against the fundamental frequency of the first and second run, for a clamped foundation, for different geometrical dimensions

Results flexible foundation

When a flexible foundation is considered, the contribution of the second run to the maximum acceleration can become large. A similar plot of the results for the case of a flexible foundation (soil profile 1 and foundation depth of 3,5 m) is shown in Figure 81. This is the most flexible foundation case, and will therefore give an upper limit of the contribution. The highest value is 55.1%, and is found for: $h = 300$ m, $b = 30$ m, $d = 30$ m.

It should be mentioned that this investigation may provide a distorted image of the reality. The main reason for this is that the used parameter values result in unacceptable maximum accelerations for higher buildings (300 meters) on soft foundation conditions. This is shown and discussed in the next section. This means that for higher structures, the maximum acceleration should be lowered by, for example, increasing the stiffness in the foundation and/or superstructure. This will increase the natural frequencies of the building and therefore lower the contribution of the second run as well. Besides, from the comparison with measurement, it is observed that the first natural frequency of high-rise buildings in the Netherlands is often underestimated. This means that the building is more stiff in reality than estimated up front. This is also observed in the case-study, discussed in chapter 9. Overall, the results of this investigation give an indication of the contribution of the second run, but should not be considered as actual truth. The contribution is expected to be lower in reality.

It is found that the shift of the fundamental frequencies is not equal anymore. The second fundamental frequency is influenced more than the first fundamental frequency. This is one of the reasons that the contribution is increasing, since the second fundamental frequency is shifting more towards a lower frequency range, compared to the clamped situation, which has a higher energy content in the load spectrum. Also, the influence of the geometrical dimensions (h, b and d) is not equal anymore (the b- and d- variation plots do not have the same shape). A large difference between the influence of b and d is visible. The building depth d has a much larger influence on the contribution than the building width b, in the case of a flexible foundation. The influence of d is larger because the depth d has a larger influence on the foundation parameters. The influence of depth d on the foundation parameters and effective modal damping ratios is more elaborated discussed in section 8.4.
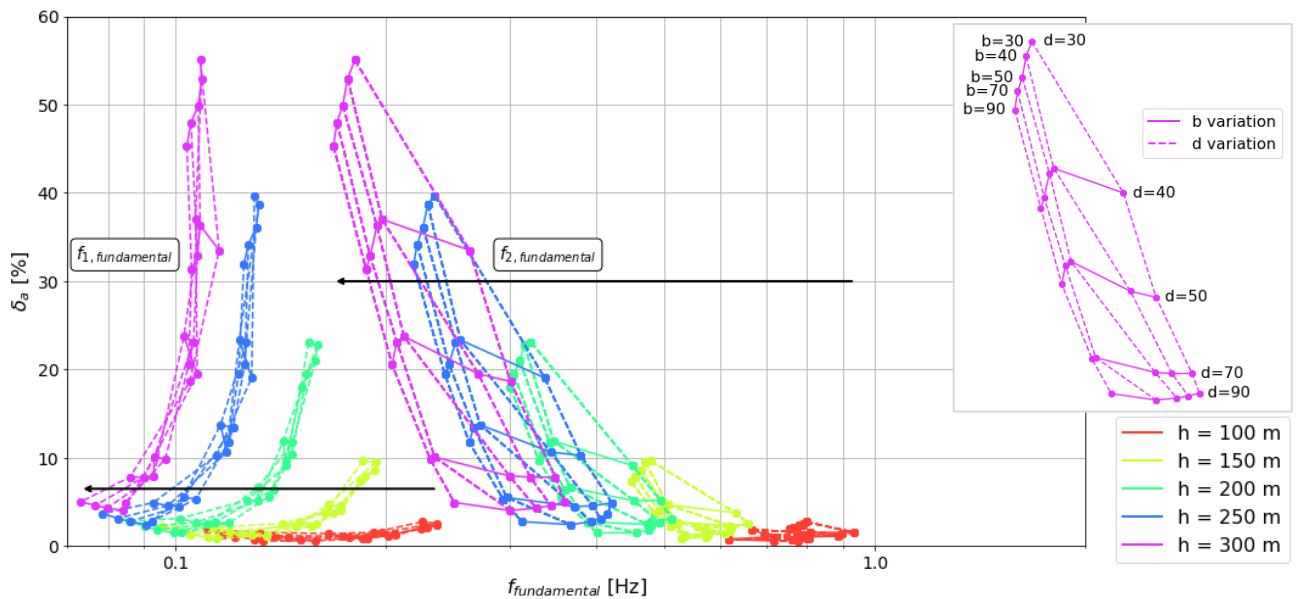
Figure 81: Contribution of the second run to the maximum acceleration (δ_a) against the fundamental frequency of the first and second run, for a flexible foundation (soil profile "soft" and D=3,5 m), for different geometrical dimensions

For this analysis, the geometrical parameters h, b, and d, and the foundation parameters D and the soil profile are deviated. The variation of these five parameters results in 1500 combinations. The contribution of the second run to the maximum acceleration for these 1500 combinations, depending on the variables: h, b, d, D and the soil profile, are presented in a table in Appendix H. This table can be used to lookup the contribution of the second run to the maximum acceleration for each combination of parameters considered in this research. The highest and lowest value found are shown in Table 12. The total difference between the highest and lowest value, due to the variation of the five parameters, is 54.6%.

	δ_a [%]	Height h [m]	Width b [m]	Depth d [m]	Foundation depth D [m]	Soil profile [-]
Lowest	0.5	100	90	70	14.0	Soft
Highest	55.1	300	30	30	3.5	Soft
Difference	54.6					

Table 12: Highest and lowest contribution of the second run to the maximum acceleration for variation of five parameters (h, b, d, D and the soil profile) in the parameter ranges considered in this research

From Figure 81 it becomes clear that the contribution of the second run to the maximum acceleration is never higher than 5% for buildings of 100 meters high. The contribution is higher than 5% for buildings of at least 150 meters. To be able to give a general statement about when the second run becomes significant from the obtained data in this investigation, the slenderness ratio h/d is introduced. The contribution is plotted against this slenderness ratio, for both a clamped and flexible foundation in Figure 82(a). An exponential increase of the contribution with the slenderness ratio is visible. The large spread of datapoints for the different slenderness ratios, are variations in b, D and the soil profile. Also, the same h/d-ratio can be reached with different values for h and d. The influence of the soil profile and foundation depth are shown in respectively Figure 82(c) and (d). From Figure 82(b) it can be seen that the contribution can become larger than 5% for slenderness ratios larger than 3.5. A total of 720 combinations have a contribution always lower than 5%. This is 48% of all combinations considered. A total of 180 combinations have a contribution always higher than 5%. This is 12% of all combination and those combinations always

have a slenderness larger than 7.0. The remaining 40% (600 combinations between h/d is 3.5 and 7.0) has a contribution higher or lower than 5%, depending on the variation of b, D and the soil profile.
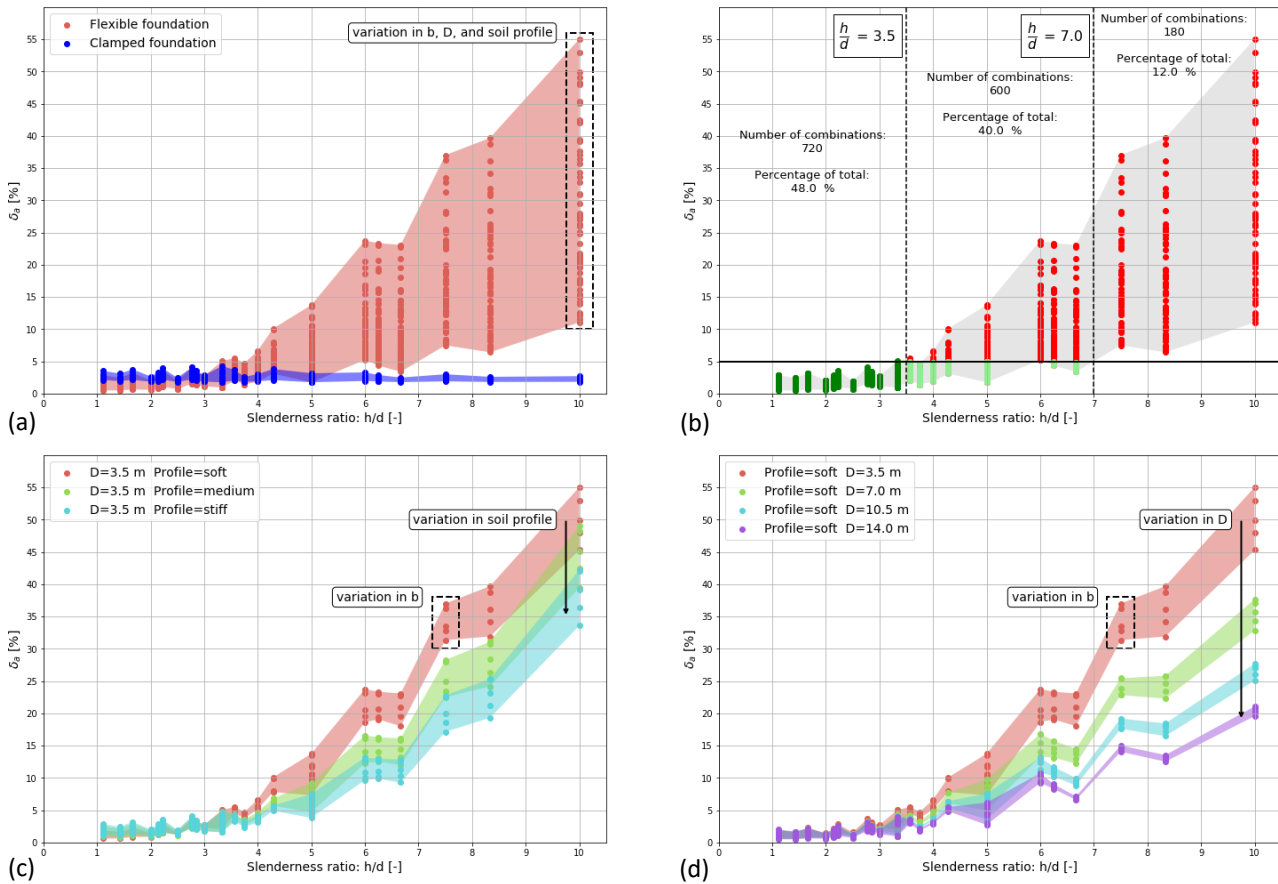
Explanation of graph:
On each x-axis, the slenderness ratio h/d. On each y-axis, the contribution of the second run to the maximum acceleration, relative to the maximum acceleration when only the first run is used. The dots are the different combinations of parameters considered. For each slenderness, the different dots are variations in b (30, 40, 50, 70, 90 m), D (3.5, 7.0, 10.5, 14.0 m) and the soil profile ("soft", "medium", "stiff"). The shaded areas show the trend of the data. The arrows indicate an increasing stiffness of the soil profile and an increasing foundation depth in respectively (c) and (d).

Figure 82: The contribution of the second run to the maximum acceleration, plotted against the slenderness ratio h/d

By introducing the slenderness ratio h/d, the contribution of the second run is still depending on three parameters. Also, a particular slenderness can be reached with different values for h and d. This results in the increasing spread of datapoints in Figure 82(b). The spread of data is plotted against the slenderness ratio h/d in Figure 83. It reaches a maximum of 44% for a slenderness ratio of 10. At h/d of 3.5, the spread is 5%. At h/d is 7.0, the spread is 22.3%.
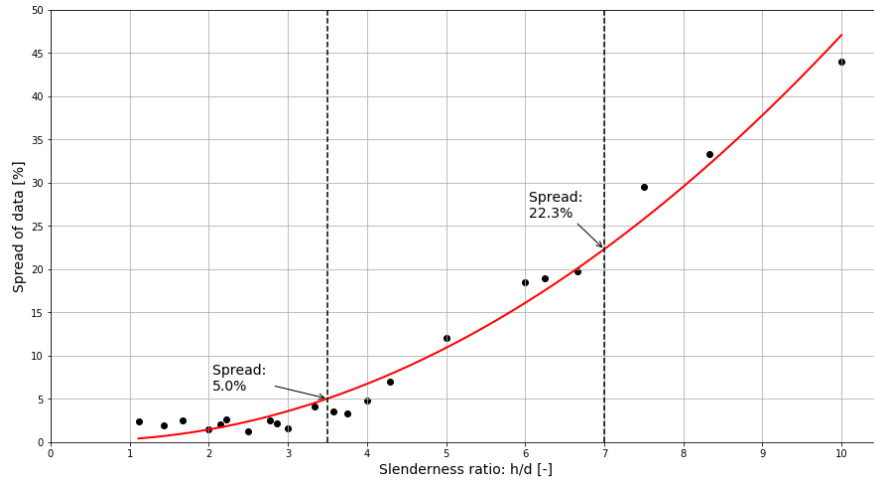
Figure 83: The spread of data due to the variation in parameters b, D and the soil profile, plotted against the slenderness ratio h/d

The spread of data will reduce when certain parameters are fixed, or when the bandwidth of variation is reduced. For example, the following parameters are assumed to be known in the design: $h = 200$ m, $b = 40$ m, $d = 40$ m, $D = 7.0$ m and soil profile "medium". From Table 18 in Appendix H, the contribution of the second run is: $\delta_a = 6\%$. If, for example, the bandwidth of parameters d and D is now reduced to d: [30, 40, 50] m and D: [3.5, 7.0, 10.5] m, keeping the other parameters fixed, the spread of data will reduce to 6.5% and 3.9%, for respectively d-variation and D-variation, see Figure 84.
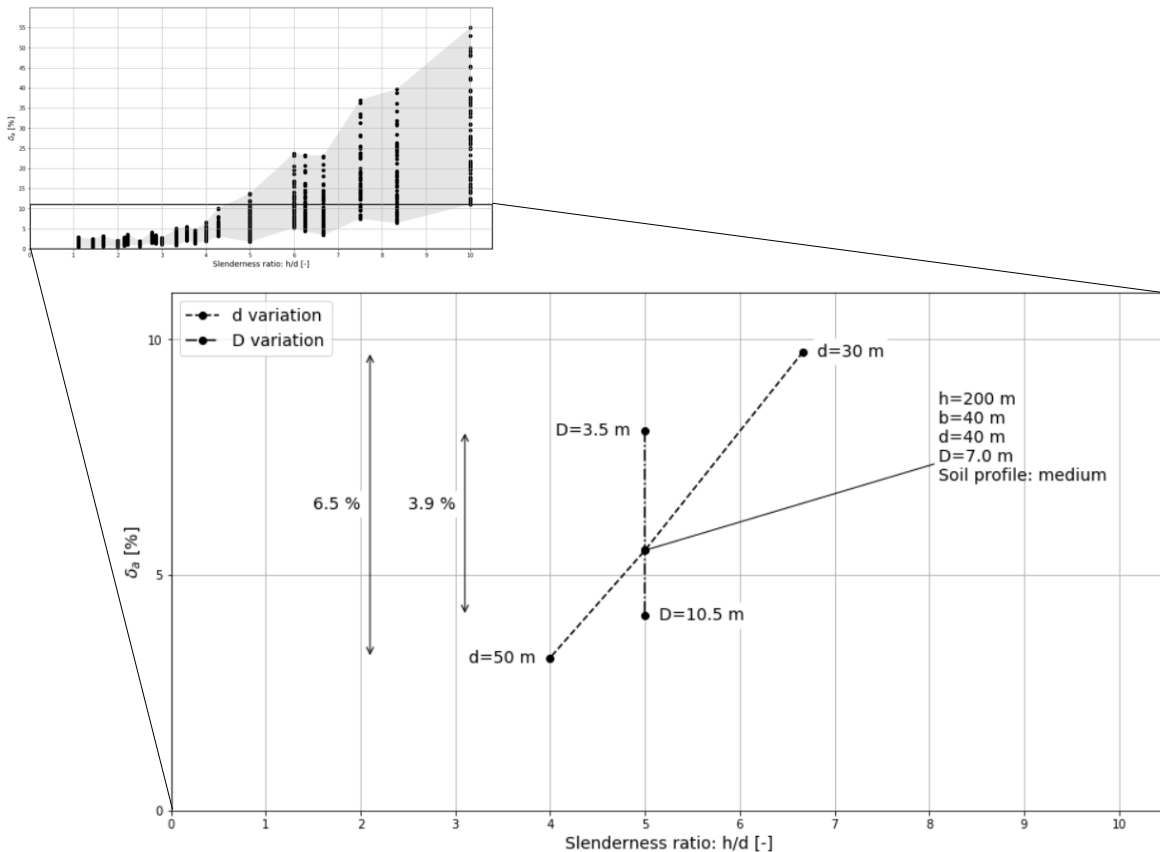
Explanation of graph:
On the x-axis, the slenderness ratio h/d. On the y-axis, the contribution of the second run to the maximum acceleration, relative to the maximum acceleration when only the first run is used. The dots are the different combinations of parameters considered. The dashed lines indicate a variation in parameters d or D. The relative difference (the spread in data) is indicated with the arrows.

Figure 84: Example of fixed parameters and reduced bandwidth for $h = 200\ m$, $b = 40\ m$, $d = 40\ m$, $D = 7.0\ m$ and soil profile "medium"

8.4 INFLUENCE STUDY GEOMETRICAL DIMENSIONS

The geometrical dimensions are the dimensions of the superstructure, covered by the parameters height h, width b, and depth d. In previous chapter, the influence of the geometrical dimensions is already introduced. Here, the focus will be on the influence of the geometrical dimensions on the maximum acceleration, which is presented against two maximum limits from the NTA 4614-3.

The same dataset as described in previous section is used. This dataset contains variations in geometrical dimensions, foundation depth and soil profile. The stiffness of the superstructure is linked to the height as described in section 5.1, and the mass density (350 kg/m^3) and damping ratio (1.5%) of the superstructure are taken constant. The complete dataset (1500 combinations) can be generated for each value of the mass and damping ratio. Considering the limited time for this research, this is not performed in this research.

As in the previous section, the foundation depth D and the soil profile have an influence on the maximum acceleration. This influence is described in more detail in the following section. Here, the most flexible foundation case ($D = 3.5 \text{ m}$, soil profile: "soft") and most stiff foundation case ($D = 14.0 \text{ m}$, soil profile: "stiff") are used for visualisation.

The maximum acceleration (a_{max}) is plotted against the first fundamental frequency for both foundation cases in Figure 85.
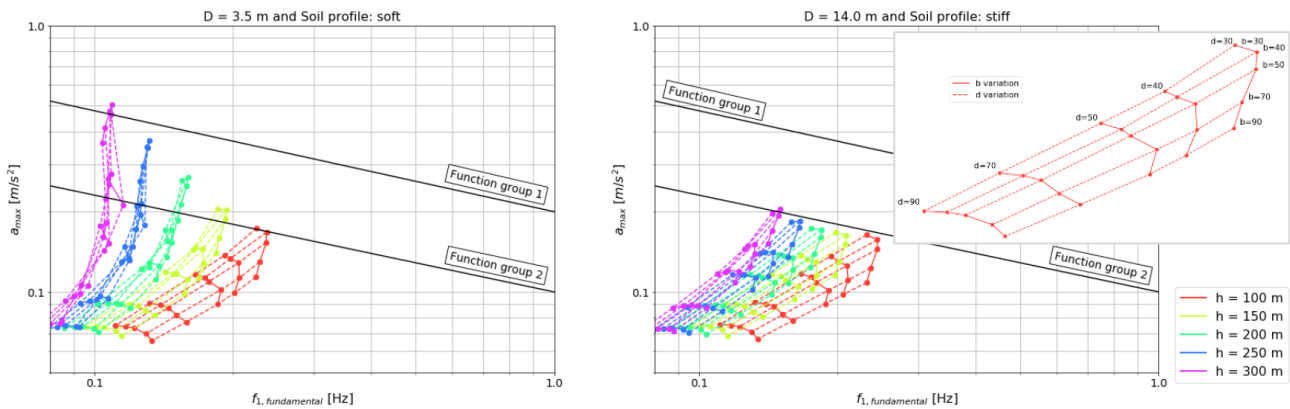
Explanation of graph:
On the x-axis, the first fundamental frequency. On the y-axis, the maximum acceleration at the top of the structure. The solid and dashed lines indicate a variation in parameters b and d respectively. The colors indicate different heights h. The maximum lines are from the NTA 4614-3. Function group 1: Office, education, industrial and others. Function group 2: Public, residential, lodging, prison, healthcare, sports and retail.

Figure 85: Maximum acceleration, plotted against the first fundamental frequency, for different geometrical dimensions, for two foundation cases

From Figure 85, it can be seen that not all variants are below one or both of the maximum lines. This is especially true for higher buildings on the most flexible foundation case. Also, it becomes clear that the influence of the dimensions is different for the different foundation cases. For example, the influence of the building depth d, is much larger for the most flexible foundation case than for the most stiff foundation case. This makes it impossible to provide always applicable recommendations and insight into the influence of the geometrical dimensions. Yet, some general trends can be distinguished. In general it can be stated that the influence of the geometrical dimensions becomes larger for softer foundations.
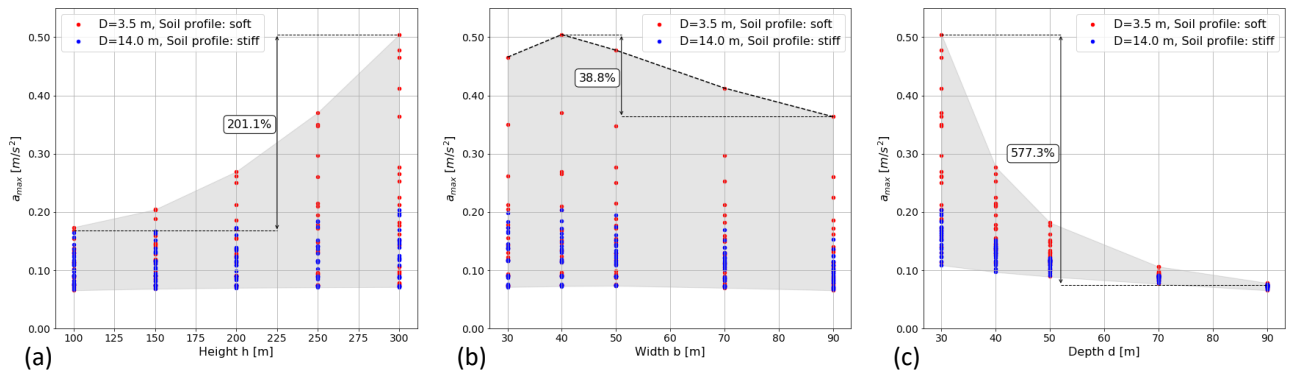
Figure 86: Influence of the height h (a), width b (b) and depth d (c) on the maximum acceleration for two foundation cases

The influence of the geometrical dimensions is alternatively plotted in Figure 86. The influence of the height h is in line with expectations. The higher the building, the more vulnerable it becomes for lateral motions. The largest influence of the height on the maximum acceleration is 201.1%, relative to the minimum value.

The influence of the width b and depth d, cannot be allocated to a single aspect. The following aspects are affected by a changing width b or depth d:

1. The shape factor C_f. The shape factor is depending on the ratio d/b as described in section 3.3.2;
2. The total mass per unit length of the building. By changing the width or depth, the cross-sectional area of the building will change what results in a different mass per unit length, although a constant mass density is considered;
3. The stiffness of the building is linked to a static load, as described in section 5.1. This static load is depending on the height of the building, but also on the width of the building. A changing width of the building will therefore result in a changing stiffness of the superstructure;
4. The foundation parameters are also influenced by the width and depth of the building.

Looking at the influence of the width, there is a peak at a width of 40 meters. The peak is the highest for $h = 300\ m$ and $d = 30\ m$, shown as the dashed line in Figure 86(b). This shape is mainly to be appointed to the shape factor. The shape factor is the highest for $d/b = 30/40 = 0.75$, see Figure 21, hence the peak at $b = 40\ m$. The largest influence of the width on the maximum acceleration is 38.8% relative to the minimum value.

The influence of the depth d on the maximum acceleration is mainly to be appointed to the increasing foundation stiffness with increasing depth. This is further discussed hereafter. The largest influence of the depth on the maximum acceleration is 577.3%, relative to the minimum value.

A building with a height of 300 meters, width of 40 meters and depth of 30 meters is the most vulnerable for changing geometrical dimensions.

It is clear that the height h and depth d, have a larger influence on the maximum acceleration than the with b. The following two statements are true:

- The larger the height h, the larger the maximum acceleration;
- The larger the depth d, the lower the maximum acceleration.

Foundation variables

As explained, there are multiple aspects that cause the depth d to have an influence on the maximum acceleration. The most influential one is linked to the foundation parameters. The larger the building depth, the larger the rotational stiffness and damping value of the foundation. Because the foundation parameters are frequency dependent, the rotational stiffness and damping value at the first fundamental frequency are plotted Figure 87. The largest influence of d is 1680% and 1000% for the rotational stiffness and damping

value respectively, compared to the lowest value. This means the rotational stiffness is almost 18 times larger for a depth of 90 meters compared to a depth of 30 meters. The influence of d on the translational parameters is much lower, and not plotted here (30% and 60% for the translational stiffness and damping value respectively, compared to the lowest value).
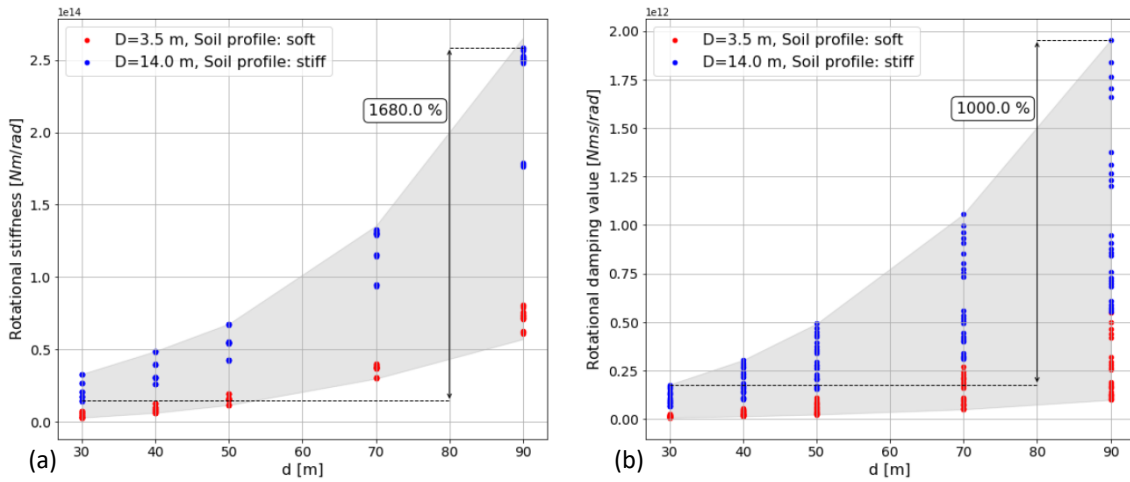
Figure 87: Rotational stiffness (a) and rotational damping value (b) of the foundation at the first fundamental frequency, plotted against the building depth d, for two foundation cases

The large increasing of the rotational foundation parameters with increasing depth, is the most import reason of the large decrease of the maximum acceleration. The maximum acceleration is plotted against the rotational stiffness and damping value at the first fundamental frequency in Figure 88. The steep decrease of the maximum acceleration is clearly visible.
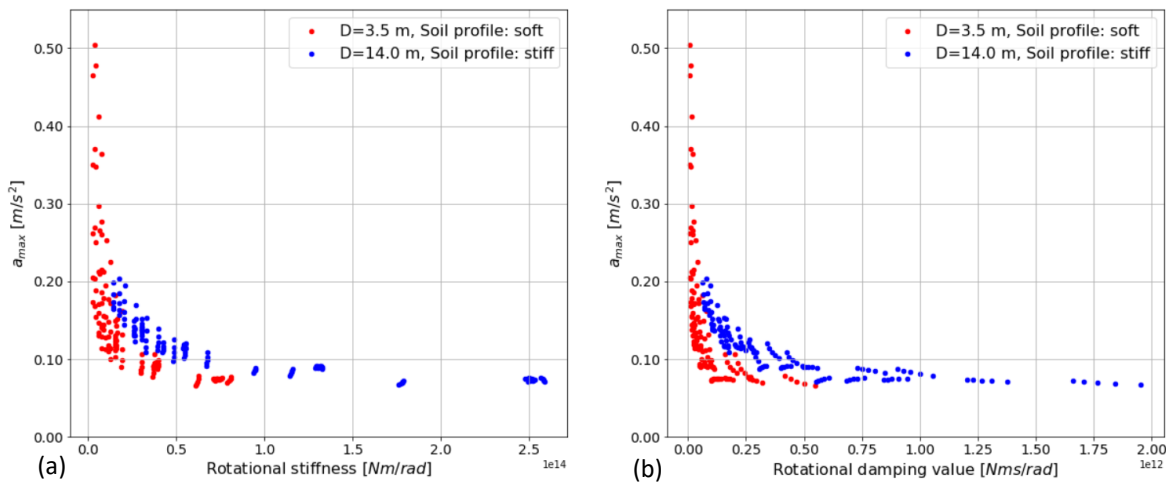
Figure 88: Rotational stiffness (a) and rotational damping value (b) of the foundation at the first fundamental frequency, plotted against the maximum acceleration, for two foundation cases

Effective modal damping ratios

The system's effective modal damping ratio, indicates how much the motions are damped out in that particular mode. In the 3DoF model, the fundamental mode (associated to the lowest natural frequency), is dominant for the total response at the top of the building in terms of acceleration (the peak in the frequency response function is significantly higher than the other two peaks). Therefore, the effective modal damping ratio of the first mode of the 3DoF model, provides a good estimate of the overall damping ratio of the system. Recall that it is assumed that the first run is representative for the first mode of vibration of a high-rise building including a flexible foundation, and the second run for the second mode of vibration of a high-rise building including a flexible foundation (Figure 79). Therefore, the effective modal

damping of the first run in the fundamental mode provides an equivalent first effective modal damping ratio, and the effective modal damping of the second run in the fundamental mode an equivalent second effective modal damping ratio.

The complex valued fundamental frequencies are used to compute these equivalent modal damping ratios, assuming single-degree-of-freedom dynamics (Gómez, 2019). The system's effective modal damping ratio is given by:

$$\xi_n = \frac{\Im(\omega_{n,\text{fundamental}})}{\sqrt{\Re(\omega_{n,\text{fundamental}})^2 + \Im(\omega_{n,\text{fundamental}})^2}} \tag{8.11}$$

The equivalent effective modal damping ratios of both the first and second run are plotted against the height for two foundation cases in Figure 89. The different coloured lines show the different building depths d and the coloured areas show the deviations in building width b for that specific depth. The input damping ratio of the superstructure is in all cases 1.5% for both runs.
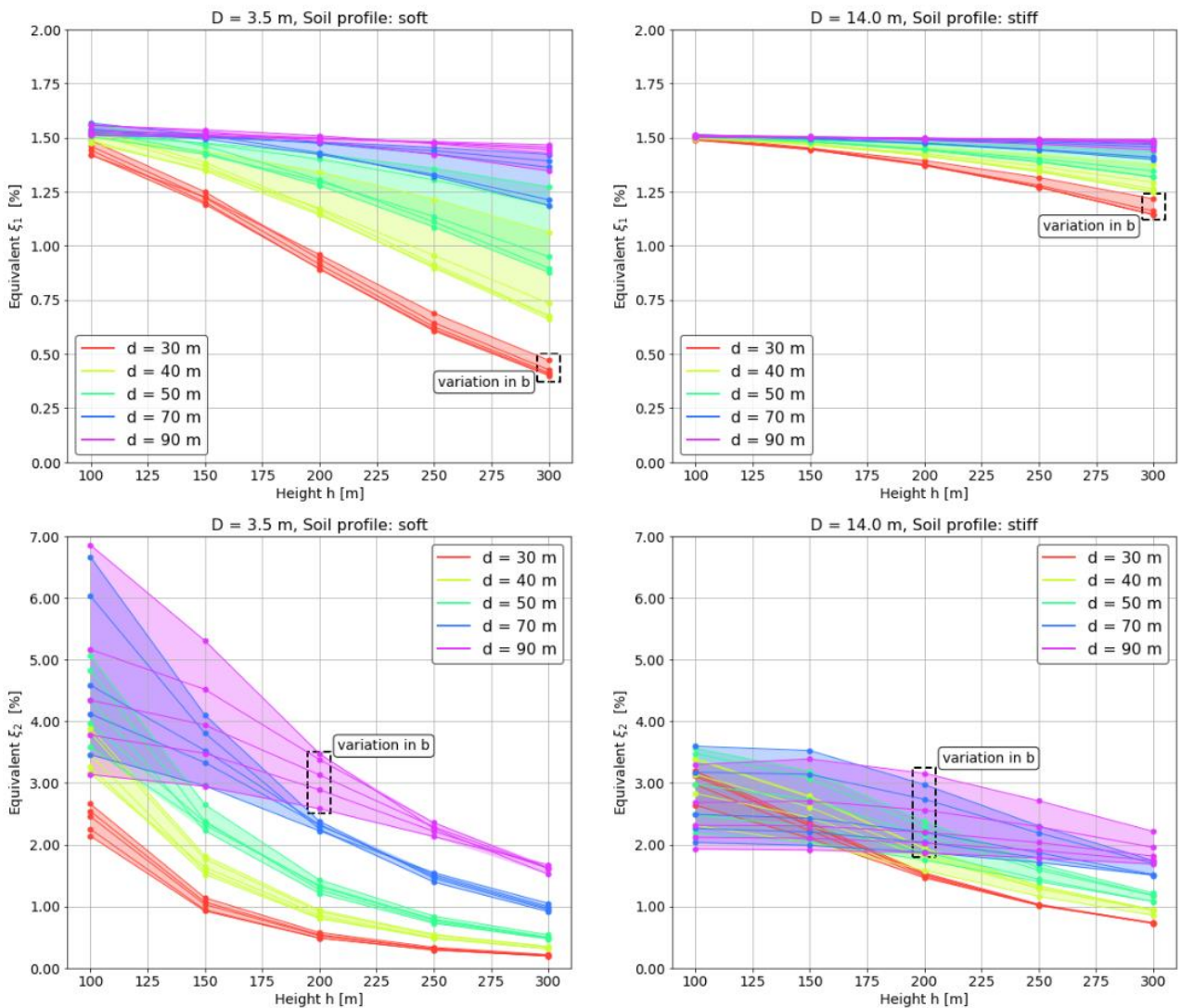
Explanation of graph:
On the x-axis, height of the building. On the y-axis, the equivalent effective modal damping ratio of run 1 or run 2. The colored lines show the different building depths *d* and the colored areas show the deviations in building width *b* [30, 40, 50, 70, 90 m] for that specific depth. Note: the scale of the y-axis is different for the top and bottom plots.

Figure 89: Equivalent effective modal damping ratio for the first and second run, plotted against the height h for two foundation cases

It becomes clear that the equivalent effective modal damping ratio of both runs is affected in all cases due to a flexible foundation. A reduction of the equivalent damping ratio of the first run is visible for increasing height, for both foundation cases. For the most flexible foundation case, for large building depth d and small heights h, a small increase of the damping ratio, relative to the damping ratio of the superstructure, is visible. This is in line with presumptions in literature that the soft soil and pile foundation of Dutch high-rise buildings, have a beneficial effect on the damping ratio (Treels, 2019). However, Figure 89 shows that these presumptions do not hold for larger building heights. For larger building heights h, the equivalent damping ratio of the system becomes smaller than the input damping ratio of the superstructure. The reduction becomes larger for smaller building depth d. The same trends are visible for the most stiff foundation case, but less significant.

The equivalent damping ratio of the second run is much more affected by the flexible foundation. Especially for lower buildings on a soft soil, the equivalent damping ratio of the second run increases significantly, relative to the damping ratio of the superstructure. From this it can be concluded that the system in the second run is much more damped out than the first run, especially for lower heights, even though an equal damping ratio of the superstructure is assumed.

The reduction in equivalent damping ratio with increasing height is in line with damping predictors in literature. For example, Jeary's empirical damping predictor (used in (Gómez, et al., 2018)) also accounts for SSI-effects in which damping decreases for increasing building height, because the lower the frequency of vibration, the smaller the radiation and material damping provided by the SSI-effects (Gómez, et al., 2018). However, the analytical expressions from (Gazetas, 1991) are used for the foundation parameters in this research. These expressions do only account for radiation damping, and therefore material damping of the soil is not taken into account in this research. Due to this fact, the results presented in Figure 89, may underestimate the actual effective modal damping ratio of a high-rise building with a flexible foundation.

Dimensionality of graphs

The presented graphs for the influence of the geometrical dimensions have a relatively high dimensionality. For example, the graphs in Figure 85 show 5-dimensional data. The other 5 parameters for the shown variants are constant. By fixing 5 parameters, the influence of a changing height, width and depth of the superstructure can be plotted. This is shown for a particular foundation depth and soil profile. To present the influence of the geometrical dimensions for all possible foundation depths and soil profiles within this research, 12 of these plots are needed.

This kind of graphs, as in Figure 85, is difficult to comprehend and it takes time to understand all information inside the graph. Also, the influence can be hard to read because the influence lines are crossing each other. Reducing the dimensionality can be done by fixing more parameters to a certain value. This is illustrated in Figure 90. The dimensionality of Figure 85 is reduced to 4 by fixing the height (Figure 90(a)) and to 3 by fixing the width (Figure 90(b)). The influence of the foundation depth becomes clear when the dimensionality is reduced to 3. However, to present the same amount of information with 3-dimensional graphs as captured in the original 5-dimensional graph in Figure 85, 25 different graphs are needed. For the total influence of the geometrical dimensions this would result in $12 \cdot 25 = 300$ different graphs. Those 300 graphs are only covering the influence of the geometrical dimensions. Hundreds of extra graphs are necessary to cover the influence of the other parameters as well. This is considered to be unrealistic for working practice and is therefore not generated.
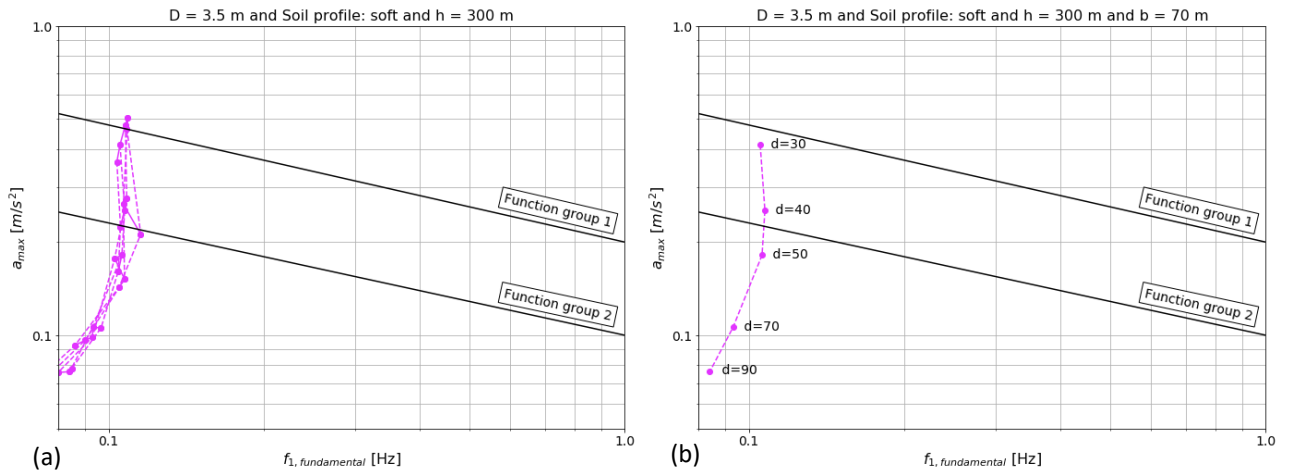
Figure 90: Reduction of the dimensionality of Figure 85 by fixing the height (a) and the height + width (b)

Example of case-specific approach

To provide an example of how the case-specific influence of the geometrical dimensions on the maximum acceleration can look like, two example buildings for two foundation cases are provided in Figure 91. The maximum acceleration is plotted against the first fundamental frequency, together with the variation lines for the height, width and depth. Each line shows the influence of changing only that parameter, keeping all other parameters unchanged.
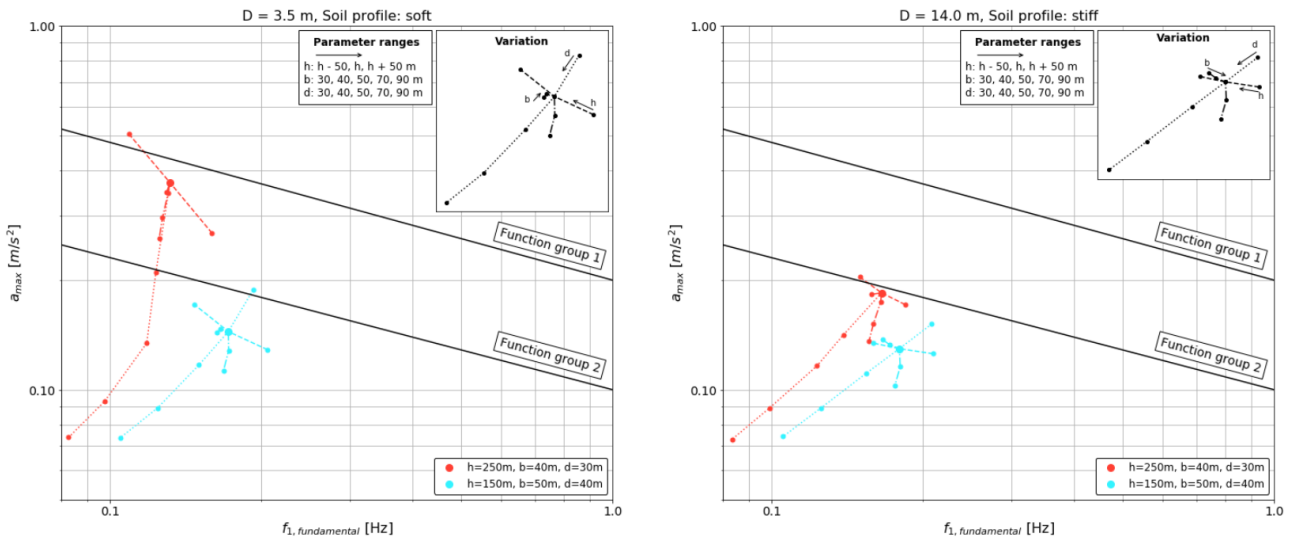
Explanation of graph:
On the x-axis, the first fundamental frequency. On the y-axis, the maximum acceleration at the top of the structure. The dots indicate different geometrical dimensions. The dashed lines indicate a variation in parameters h, b and d. The maximum lines are from the NTA 4614-3. Function group 1: Office, education, industrial and others. Function group 2: Public, residential, lodging, prison, healthcare, sports and retail. Arrows points in the direction of increasing parameter value.

Figure 91: Maximum acceleration plotted against the fundamental frequency of two example buildings and two foundation cases, together with their influence lines of height, width and depth

8.5 INFLUENCE STUDY FOUNDATION PARAMETERS

In previous chapter, the importance of the foundation is already mentioned. Yet, there is a difference between the translational parameters of the foundation and the rotational parameters of the foundation. As already mentioned before, the four foundation parameters (K_x, K_r, C_x, C_r) are frequency dependent. The value at the first fundamental frequency is plotted against the maximum acceleration for all combinations in Figure 92. Because the dominant peak in the transfer function of the 3DoF model is located at the

fundamental frequency, the parameter values at this frequency will provide a good indication of the influence on the maximum acceleration. The rotational foundation parameters clearly have a larger influence, since the plots show a much steeper inverse power trendline. Also, the translational parameters show a much larger spread around the trendline than the rotational parameters.
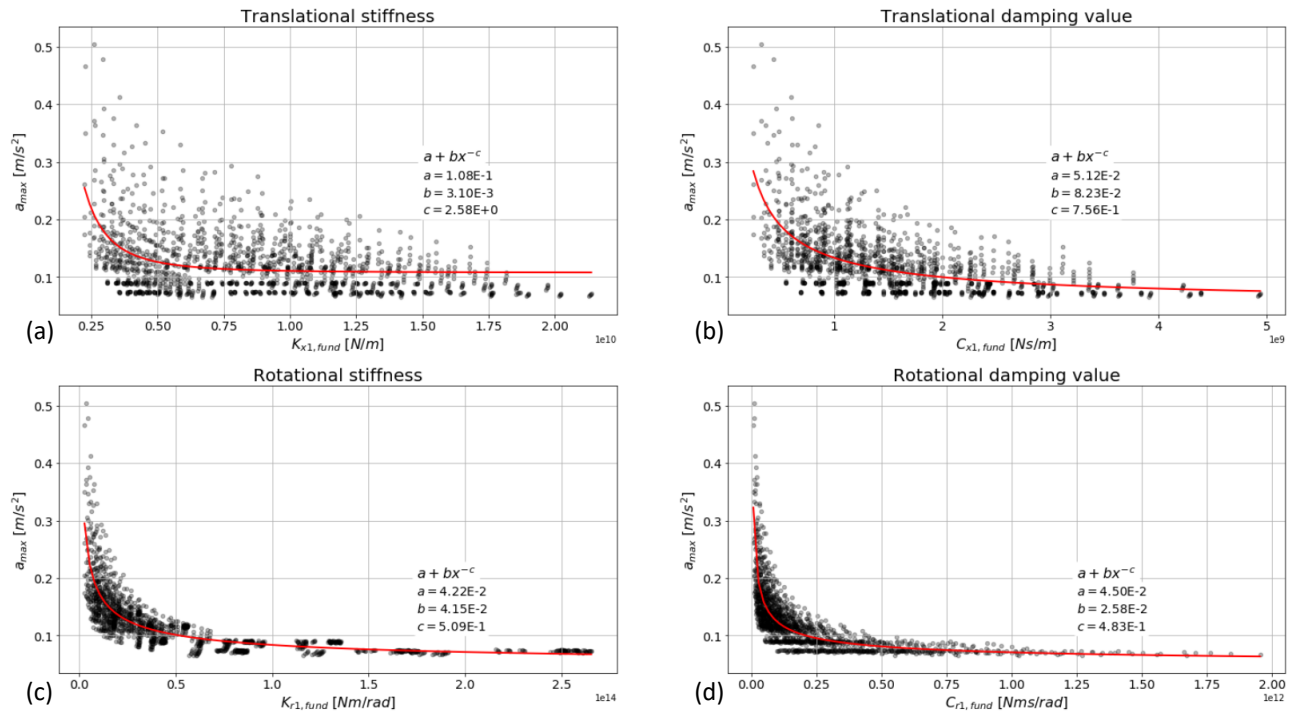
Explanation of graph:
On the x-axis, the foundation parameter values at the first fundamental frequency. On the y-axis, the maximum acceleration at the top of the structure. The dots indicate different parameter combinations. The red lines indicate the fitted inverse power trendline, together with the fitted formula and variable values. Note: the x-axes have different scales, multiplied by different 10^i-values.

Figure 92: Translational stiffness (a), translational damping value (b), rotational stiffness (c) and rotational damping value (d) at the first fundamental frequency, plotted against the maximum acceleration, with fitted inverse power trendline

A more flexible foundation results in a higher maximum acceleration. First of all, this is due to the fact that a more flexible support, results in a more flexible system compared to a clamped situation, resulting in larger motions. Second, the flexible foundation results in a so-called period-lengthening. A larger period means a lower frequency which results in a shift to the left in the spectrum. The lower the frequency, the higher the energy content in the load spectrum. To illustrate the difference between a relatively flexible foundation and a relatively stiff foundation, the period lengthening ($T_1/T_{1,\text{clamped}}$) for both foundation cases is plotted against the height h for different building depths, in Figure 93. The filled area shows the variation in width b.
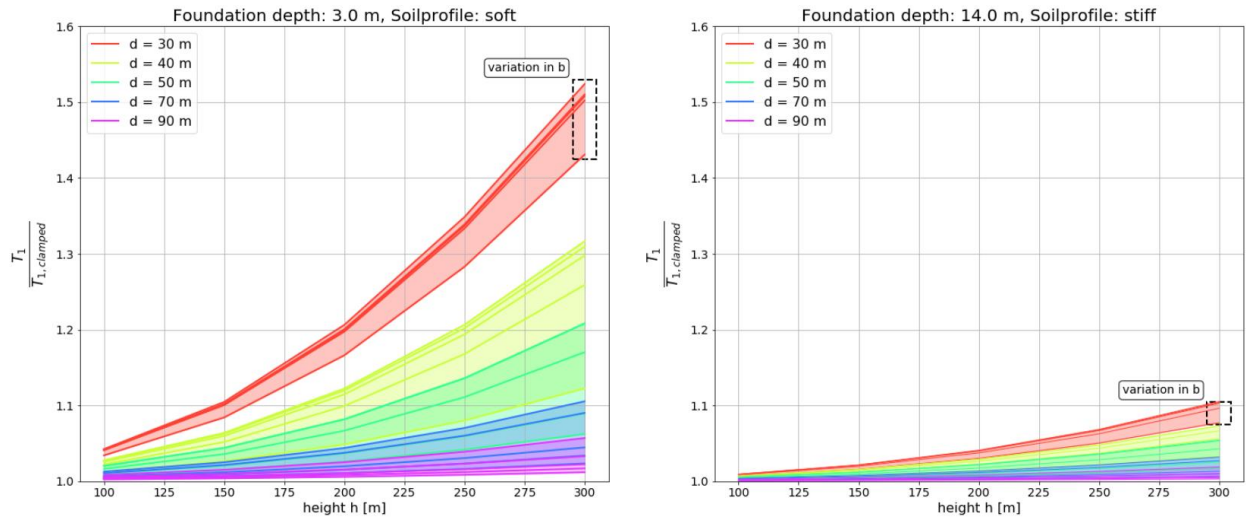
Explanation of graph:
On the x-axis, height of the building. On the y-axis, the ratio between the period of the structure with a flexible foundation and a clamped foundation. The colored lines show the different building depths d and the colored areas show the deviations in building width b [30, 40, 50, 70, 90 m] for that specific depth.

Figure 93: Period lengthening, plotted against the height, for two foundation cases

Also, the damping in the foundation reduces the motions of the system. In the case of an infinitely stiff foundation with no damping (a clamped foundation), the overall damping in the system is equal to the damping in the superstructure. Yet, when a flexible foundation with damping is considered, the total damping in the system is a combination of the damping in the superstructure and the damping in the foundation and surrounding soil. The fact that the overall damping ratio of the system is changing, is already shown in the previous section.

The consequence of a flexible foundation on the maximum acceleration, compared to the maximum acceleration of a clamped foundation is shown in Figure 94. The ratio between the maximum acceleration with a flexible foundation and the maximum acceleration with a clamped foundation ($a_{max}/a_{max,clamped}$) is plotted against the height for different building depths. The filled area shows the variation in width b.
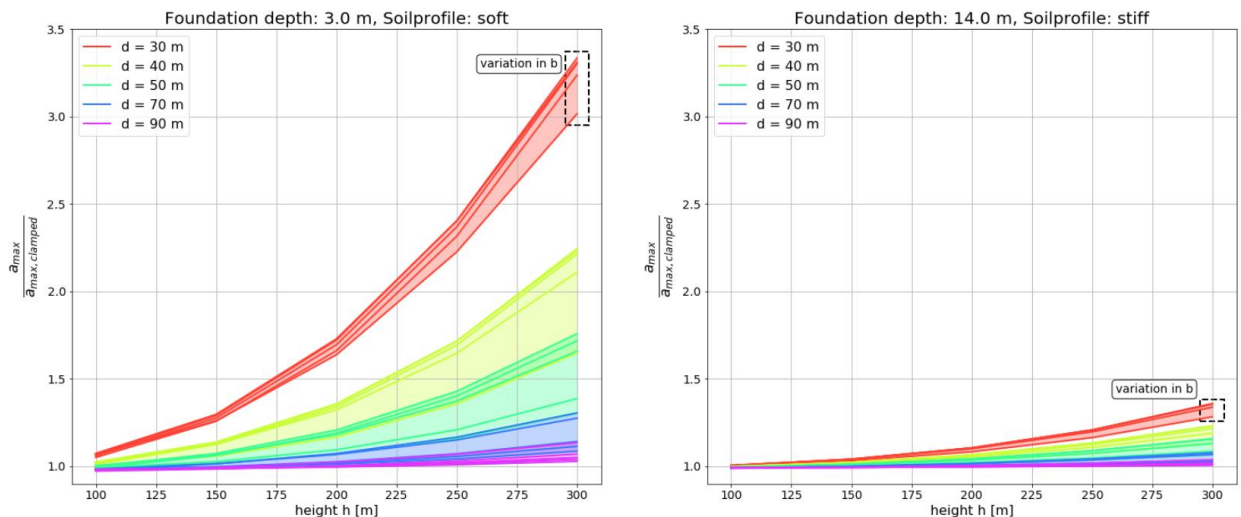
Explanation of graph:
On the x-axis, height of the building. On the y-axis, the ratio between the maximum acceleration of the structure with a flexible foundation and a clamped foundation. The colored lines show the different building depths d and the colored areas show the deviations in building width b [30, 40, 50, 70, 90 m] for that specific depth.

Figure 94: Maximum acceleration with a flexible foundation over maximum acceleration with a clamped foundation, plotted against the height, for two foundation cases

The difference between relatively flexible foundation conditions, and relatively stiff foundation conditions, is clearly visible in Figure 94. The relatively flexible foundation conditions result in up to 3.3 times the maximum acceleration of the clamped situation for a height of 300 meters. This emphasises that a flexible foundation can have a significant contribution to the maximum acceleration of the structure. The flexibility of the foundation is determined by the geometrical dimensions, the foundation depth and the soil profile. To provide insight into the significance of the foundation flexibility, the ratio of the maximum acceleration with a flexible foundation over the maximum acceleration with a clamped foundation, is plotted against the slenderness ratio h/d, for the three soil profiles in Figure 95. The coloured areas show the variation in building width b. Clearly visible, the more stiff the soil profile, and the larger the foundation depth, the smaller the ratio.

For design purposes, the maximum acceleration can be determined with a clamped foundation. Subsequently, this maximum acceleration can be multiplied by the factor provided in Figure 95, depending on the soil profile and foundation depth. The upper limit can be used to have a conservative value. This will give an indication of the maximum acceleration of the structure including a flexible foundation. However, the spread of the data is still such, that it is not recommended to use the graphs for the final comfort checks. To check the maximum acceleration of the structure more accurately, a model including the effects of SSI is advised.
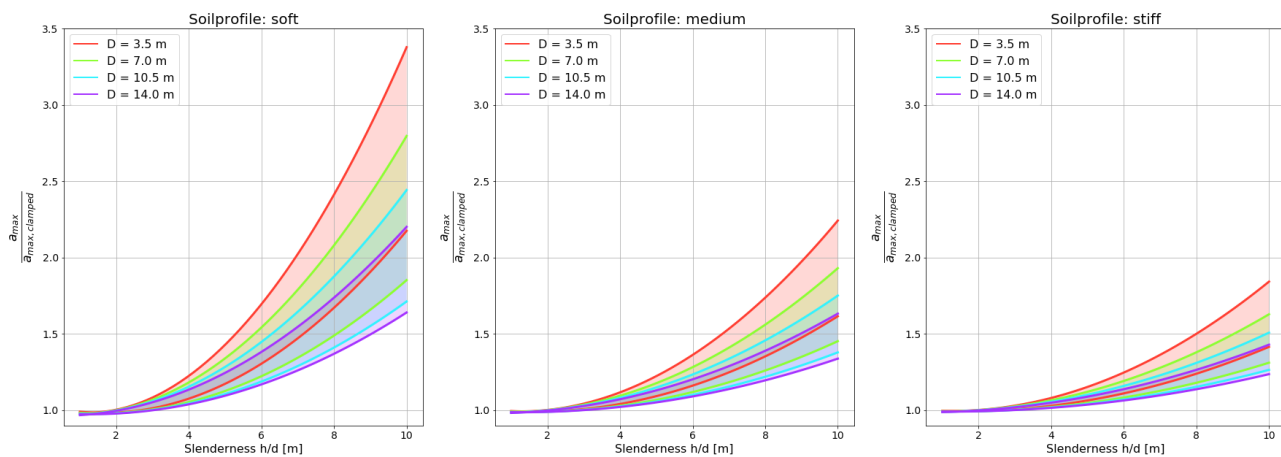
Figure 95: Maximum acceleration with a flexible foundation over maximum acceleration with a clamped foundation, plotted against the slenderness h/d, for three soil profiles

To illustrate the use of the graphs in Figure 95, an example is provided. A building with the following parameters is considered: $h = 150 \text{ m}, b = 40 \text{ m}, d = 30 \text{ m}, D = 3.5 \text{ m}$ and soil profile: soft. The slenderness is: $h/d = 150/30 = 5$. The maximum acceleration, calculated with a clamped foundation, is: $a_{max,clamped} = 0.157 \text{ m/s}^2$. From Figure 95, the upper limit of the factor to take into account the flexible foundation is 1.43. This results in a maximum acceleration of: $a_{max} = 1.43 \cdot 0.157 = 0.224 \text{ m/s}^2$. The maximum acceleration is 43% higher with a flexible foundation than with a clamped foundation. The maximum acceleration, calculated with the model including the SSI effects, is: $a_{max} = 0.203 \text{ m/s}^2$. The conservative approach of using the upper limit value from the graphs results in a overestimation of 10% for this particular case.

The influence of the mass of the foundation, represented by M_0 in the model (see Figure 77), is negligible in all cases. From this, it can be concluded that this parameter can be disregarded in the design process, regarding the maximum acceleration of the structure. Therefore, the influence of the mass of the foundation is left out of all graphs.

The influence of the foundation depth and the soil profile is shown in Figure 96. The different points for each depth or profile are variations in geometrical dimensions and the foundation depth or soil profile. The maximum influence of the foundation depth, relative to the minimum, is 74.8%. This maximum is found for

a building of 300 meters high, 40 meter width, 30 meters depth and a soft soil profile. The maximum influence of the soil profile, relative to the minimum, is 72.1%. This maximum is found for the same building, with a foundation depth of 3.5 meters.
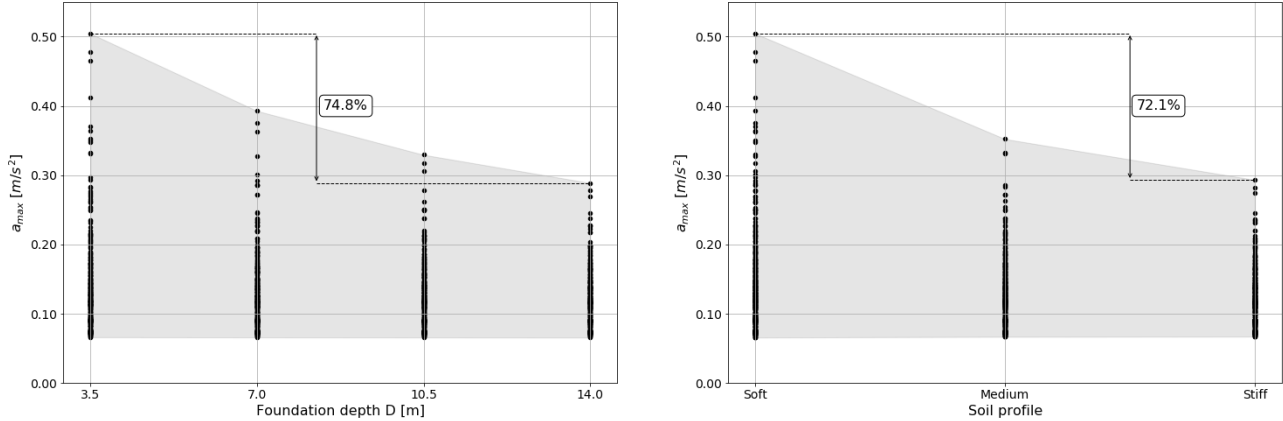
Figure 96: Influence of the foundation depth and soil profile on the standard deviation of the acceleration

Example of case-specific approach

Again, two example buildings are chosen to illustrate the influence of the foundation depth and soil profile, see Figure 97. The different influence of the soil profile and the foundation depth for buildings with a different height, is clearly visible.
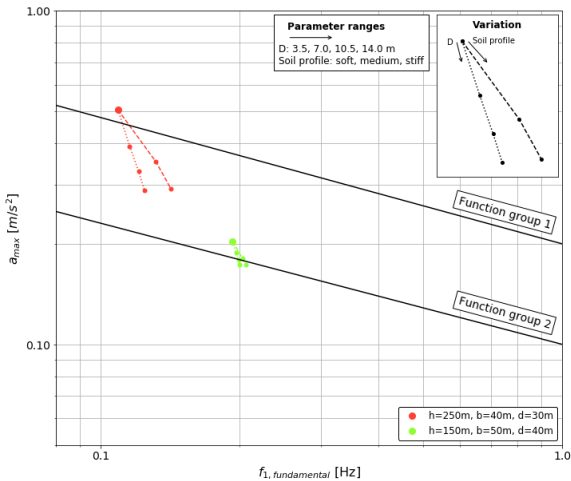
Explanation of graph:
On the x-axis, the first fundamental frequency. On the y-axis, the maximum acceleration at the top of the structure. The dots indicate different geometrical dimensions. The dashed lines indicate a variation in parameters D and the soil profile. The maximum lines are from the NTA 4614-3. Function group 1: Office, education, industrial and others. Function group 2: Public, residential, lodging, prison, healthcare, sports and retail. Arrows points in the direction of increasing parameter value.

Figure 97: Maximum acceleration plotted against the fundamental frequency of two example buildings, together with their influence lines of soil profile and foundation depth

8.6   INFLUENCE STUDY SUPERSTRUCTURE PARAMETERS

In a previous sections, the parameters of the superstructure, namely the stiffness EI, mass density ρ and damping ratio of the superstructure ξ, are kept constant. In this section, the influence of these parameters is investigated. This is done by changing these three parameters separately, within a certain range, as described in chapter 5. Multiple variants with different geometrical dimensions and foundation cases are considered.

To limit computation time, not all variants of previous analysis are analysed in this part. It is shown in previous section that, from the geometrical dimensions, the height h and depth d have the largest influence on the maximum acceleration. Also, the largest deviations are found for a width of 40 meters. Therefore, only a width of 40 meters, depth of 30 and 90 meters, and height of 100, 200 and 300 meters are considered here.

- $h = 100, 200, 300$ m;
- $b = 40$ m;
- $d = 30, 90$ m.

Also shown in a previous section, the foundation conditions, foundation depth and soil profile, have an influence. Yet, to reduce computation time again, only the boundary cases are considered here.

- $D = 3.0, 14.0$ m;
- Soil profile: soft, stiff.

This results in a total of 576 combinations for the variation of the parameters stiffness (EI), mass density (ρ) and damping ratio of the superstructure (ξ). The influence of the superstructure parameters for the six variants analysed, are plotted for two foundation cases in Figure 98. The maximum acceleration is plotted against the fundamental frequency together with two maximum lines from literature. Each dashed or dotted line shows the influence of one of the parameters, with the arrows pointing towards increasing parameter value. The initial stiffness, the stiffness of the reference building under consideration, is multiplied with a factor to show the influence of a reducing or increasing stiffness. The other two parameters show the influence of a changing parameter value, as described in chapter 5 and shown in the plots.
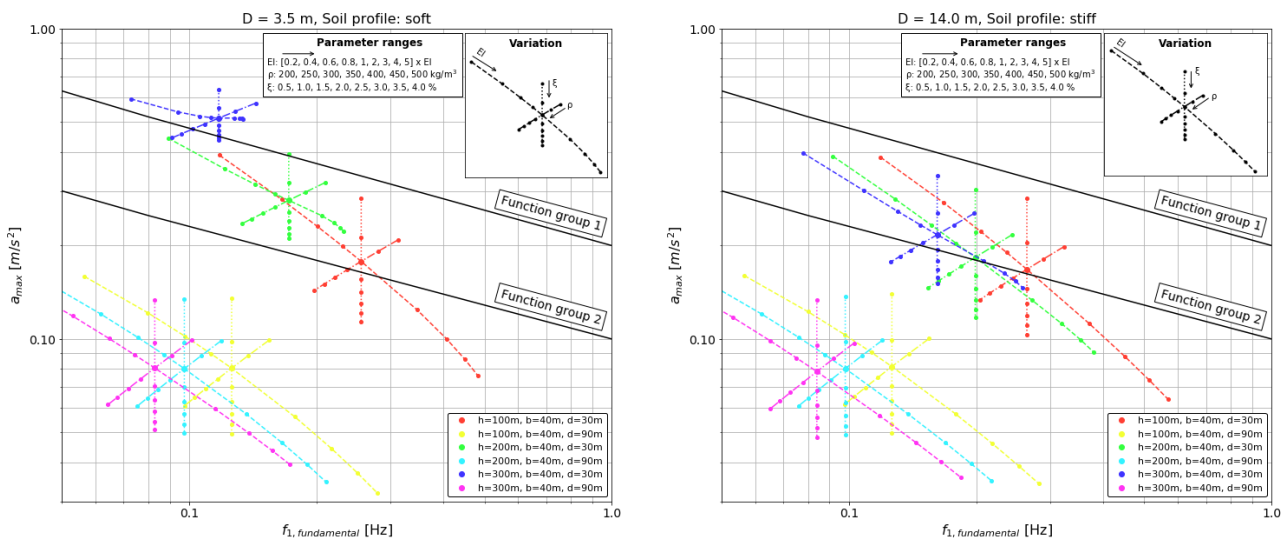
Explanation of graph:
On the x-axis, the first fundamental frequency. On the y-axis, the maximum acceleration at the top of the structure. The dots indicate different geometrical dimensions. The dashed lines indicate a variation in parameters EI, ρ and ξ. The maximum lines are from the NTA 4614-3. Function group 1: Office, education, industrial and others. Function group 2: Public, residential, lodging, prison, healthcare, sports and retail. Arrows points in the direction of increasing parameter value.

Figure 98: Maximum acceleration plotted against the fundamental frequency of six buildings and two foundation cases, together with their influence lines of stiffness, mass density and damping ratio

The influence of the three parameters on the maximum acceleration is different for every single case. The dependency of the height is clearly visible in Figure 98, as the steepness of the influence lines changes for different heights. Yet, this dependency is much smaller for cases with a large depth d, and/or a stiff soil profile and larger foundation depth.

The steepness of the influence lines of the mass density and the damping ratio, is not changing significantly for the different cases. Yet, the length of the lines do change for certain cases. On the other hand, the steepness of the influence line of the stiffness does change. And also the length of the influence lines of the stiffness change. In general, it can be stated that the influence lines of the mass density and the damping ratio follow the same direction and decrease in length for increasing height, yet only for smaller building depths. The influence lines for stiffness do change in direction and length for increasing height, but also only for smaller building depths.

The factor, the ratio between the considered and reference case, due to a changing stiffness, mass density or damping ratio, is alternatively plotted in Figure 99. For each parameter it is shown that the influence is almost equal for every situation, in the case of a large building depth ($d = 90$ m). The dependency of height or the foundation conditions is small in this case. Yet, for the cases of small building depth ($d = 30$ m), the dependency of height and foundation conditions is present. In the plots, the solid lines show the average for each height considered. The coloured areas show the deviations from the average, due to changing foundation conditions (foundation depth and/or soil profile). The deviations from the average are relatively small for a changing mass density. On the other hand, the deviations are relatively large for a changing stiffness or damping ratio.

(a)

(b)

(c)
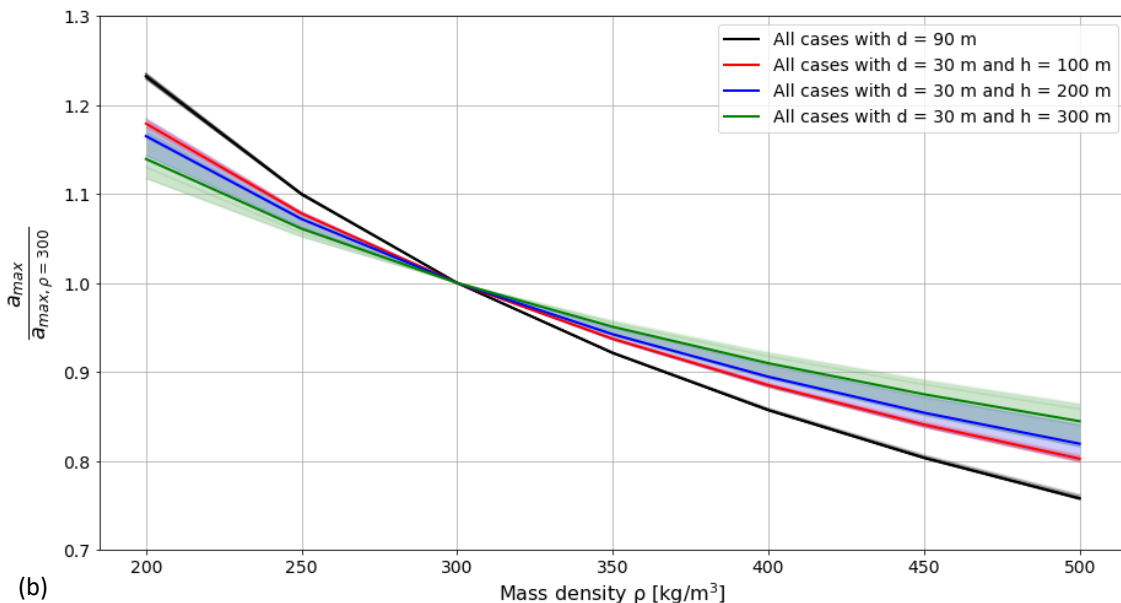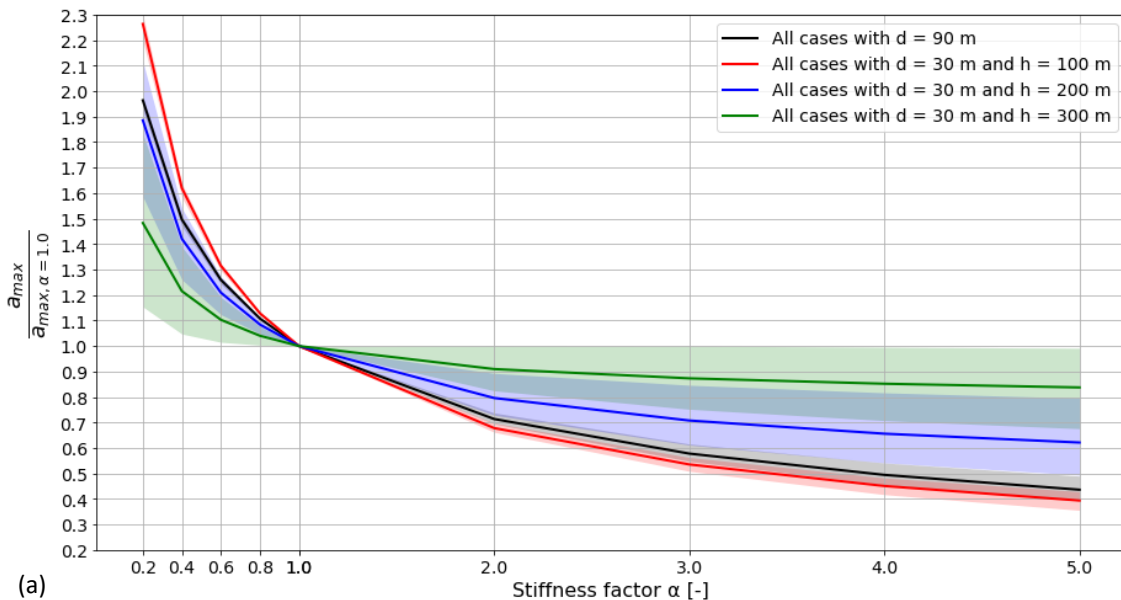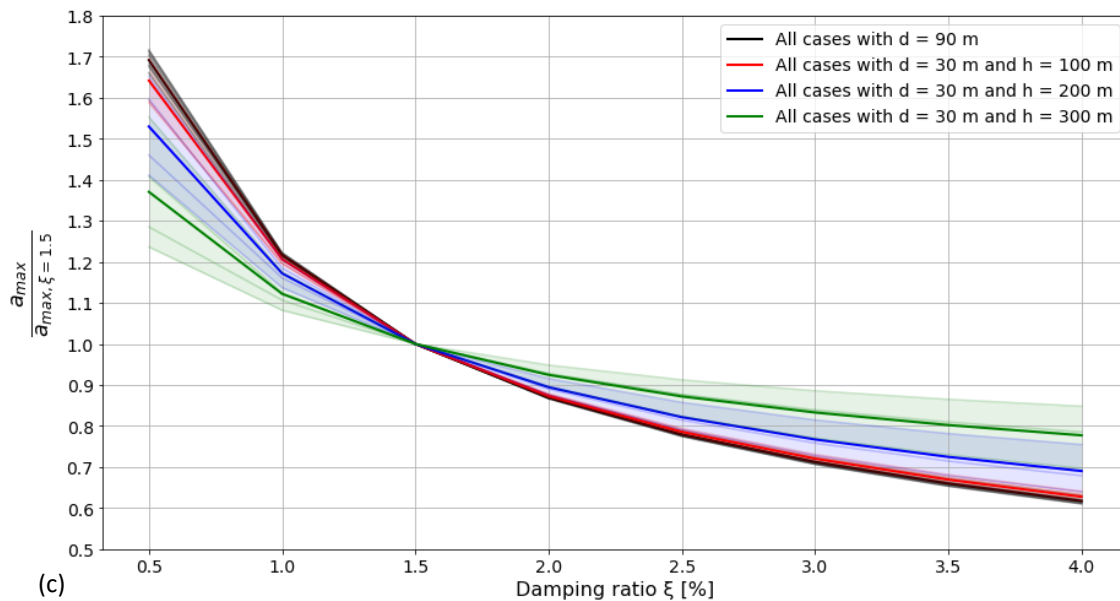
Explanation of graph:
On the x-axis, the stiffness factor (a), the mass density (b) and the input damping ratio of the superstructure (c). On the y-axis, the maximum acceleration of the considered building over the maximum acceleration of the reference building. The lines indicate the average per height. The colored areas show deviations in foundation conditions (foundation depth: 3.0 or 14.0 m, soil profile: soft or stiff). Note: the axes have different scales.

Figure 99: Maximum acceleration of considered case over reference case due to a changing stiffness (a), mass density (b) or damping ratio (c)

The presented graphs in Figure 98 and Figure 99 can be used to come up with an indication of the influence of a changing stiffness, mass density or damping ratio, while keeping all other parameters equal. Yet, it must be emphasised that these graphs are only valid for the considered foundation conditions and reference values of the parameters (EI linked to the height according to section 5.1, $\rho = 300 \text{ kg/m}^3$ and $\xi = 1.5\%$ for both runs). When a building has different geometrical dimensions, different foundation conditions or different reference values, the presented graphs will not be accurate. The graphs can be generated for every combination of parameters. As mentioned before, a digital platform will be a good solution for practice.

The maximum and minimum values of the influence of the three superstructure parameters (from Figure 99), for different geometrical dimensions and two foundation conditions, are shown in Table 13. The combinations for which the change in influence for increasing height is more than 0.05, 0.10 and 0.20, are indicated respectively light grey, grey and dark grey. From Table 13, it can be seen that the influence of the three superstructure parameters on the maximum acceleration for cases with $d = 90$ m, is hardly influenced by the height in almost all cases. This is also the case for the influence of the mass density on the maximum acceleration for cases with $d = 30$ m. However, the influence of the damping ratio and, especially, the stiffness of the superstructure on the maximum acceleration, is changing for different heights.

For example, the maximum acceleration due to a five times larger stiffness than the reference stiffness of a building with: $h = 100$ m, $b = 40$ m, $d = 30$ m, $D = 3.5$ m on a soft soil profile, is: $1/0.43 = 2.3$ times smaller than the reference case. For the same case with a height of 300 meters this is: $1/0.99 = 1.0$ times smaller. Meaning, a higher stiffness for this case will not results in lower accelerations. It should be mentioned that this case is a boundary case within this research and the maximum accelerations are too high according to the maximum lines of the NTA 4614-3. Yet, it does illustrate how the influence of the stiffness of the superstructure can reduce significantly for large heights on soft foundation conditions. The same comparison is made for: $h = 100 / 300$ m, $b = 40$ m, $d = 30$ m, $D = 14.0$ m on a stiff soil profile. The influence

of the stiffness is: $1/0.38 = 2.6$ times (h = 100 m) and: $1/0.68 = 1.5$ times (h = 300 m) smaller than the reference value. This shows that the decrease of the influence of the stiffness for increasing height, for stiff foundation conditions is still significant. Keep in mind, to reach such a high decrease of the maximum acceleration, the stiffness of the superstructure is five times larger than the reference value.

Parameter		Stiffness EI			Mass density ρ			Damping ratio ξ		
		Height h			Height h [m]			Height h [m]		
		100	200	300	100	200	300	100	200	300
d = 30 m	Max. Ratio	2.20	1.59	1.15	1.17	1.14	1.12	1.59	1.41	1.24
D = 3.5 Soil profile: soft	Min. Ratio	0.43	0.80	0.99	0.81	0.84	0.86	0.64	0.75	0.85
d = 30 m	Max. Ratio	2.30	2.12	1.83	1.18	1.19	1.17	1.69	1.65	1.55
D = 14.0 Soil profile: stiff	Min. Ratio	0.38	0.49	0.68	0.80	0.80	0.82	0.62	0.64	0.70
d = 90 m	Max. Ratio	1.98	1.97	1.93	1.23	1.23	1.23	1.68	1.68	1.66
D = 3.5 Soil profile: soft	Min. Ratio	0.40	0.43	0.49	0.76	0.76	0.76	0.62	0.62	0.63
d = 90 m	Max. Ratio	1.96	1.97	1.96	1.23	1.23	1.24	1.72	1.71	1.70
D = 14.0 Soil profile: stiff	Min. Ratio	0.42	0.44	0.46	0.76	0.76	0.76	0.61	0.61	0.61

Explanation of table:
The maximum and minimum value of the ratio: $a_{max}/a_{max,ref}$, for different geometrical dimensions and two foundation conditions. The two foundation conditions are: $D = 3.5\ m$ and soil profile "soft" and $D = 14.0\ m$ and soil profile "stiff". The maximum values are for the lowest stiffness ($\alpha_{EI} = 0.2$), mass density ($\rho = 200\ kg/m^3$) or damping ratio ($\xi = 0.5\%$). The minimum values are for the highest stiffness ($\alpha_{EI} = 5.0$), mass density ($\rho = 500\ kg/m^3$) or damping ratio ($\xi = 4.0\%$).

Table 13: Maximum and minimum ratio of the influence of the superstructure parameters on the maximum acceleration for different geometrical dimensions and two foundation conditions

Finally, the comparison is made with the existing influence studies discussed in section 2.2. The results found in this research are similar to the ones found by (Oosterhout, 1996). The different influence of the superstructure parameters for different building dimensions is the most important similarity. This different influence is amplified by the flexible foundation considered in this research. Similar results were expected since the same analysis procedure is applied.

The results found by (Berg, 2012), are based on the procedure described by the NEN-EN 1991-1-4, using the $c_s c_d$-factor. The results show a more or less equal influence of the three parameters on the maximum acceleration. This is not in line with the results found in this research. No judgement can be made which analysis procedure results in more accurate results, but it does show that the different methods do not result in the same conclusions.

8.7 SUMMARY

The conclusions and recommendations in this research are based on the results of a simplified representation of a high-rise building. In the analysis procedure, multiple assumptions and simplifications are made. This should always be kept in mind when using the results of this research.

Before performing the influence studies of the main parameters in the design, the contribution of the second run is investigated. The assumption is made that the contribution of the second run of the 3DoF model to the maximum acceleration of the structure, is representative for the contribution of the second mode of vibration to the maximum acceleration of the structure. The contribution is relative to the maximum acceleration when only the first run is used, which is assumed representative for the maximum acceleration in only the first mode of vibration.

The contribution of the second run to the maximum acceleration is investigated for both a clamped foundation and a flexible foundation. For the clamped foundation, the maximum contribution is found to be 4.3%. This is in the same range as found by previous research (e.g. (Oosterhout, 1996)). Therefore, based on the results from this investigation, the contribution of the second run to the maximum acceleration of the structure can be neglected for a clamped foundation in the considered domain in this investigation.

In the case of a flexible foundation, the upper limit of the contribution of the second run is found to be 55.1%. The lowest value found for the contribution of the second run is 0.5%. This results in a total difference, due to the variation of the parameters h, b, d, D and the soil profile, of 54.6%. The contribution of the second run is higher than 5% for buildings of at least 150 meters high. The h/d-ratio is introduced to provide an indication of the contribution of the second run. This results in the indication that the contribution of the second run to the maximum acceleration of the structure, can become larger than 5% for buildings of at least 150 meters high, and a h/d-ratio of at least 3.5. The spread in the data is 5% for a h/d-ratio of 3.5. The contribution of the second run is always lager than 5% for h/d-ratios larger than 7.0. The spread in the data is 22.3% for a h/d-ratio of 7.0. The maximum spread of the data, due to the variation of the parameters b, D and the soil profile, is found to be 44%, for a h/d-ratio of 10. The spread in the data can be reduced when parameters are fixed to a certain value. This is shown via an example. The example ($h = 200\,\text{m}, b = 40\,\text{m}, d = 40\,\text{m}, D = 7.0\,\text{m}$ and soil profile "medium") has a h/d-ratio of 5.0 and contribution of the second run of: $\delta_a = 6\%$. The reduced bandwidth of variation for d (30, 40 and 50 m) and D (3.5, 7.0, 10.5 m) results in a reduced spread of 6.5% and 3.9% respectively.

It is emphasised that the results from this analysis may provide a distorted view of the reality. Especially for higher structures (300 meters), it is expected that the used parameters are not realistic since unacceptable maximum accelerations are found. As a solution, the overall stiffness of the system can be increased. This will increase the natural frequencies and lower the contribution of the second run. High-rise buildings in the Netherlands are often more stiff in reality than calculated upfront. Therefore, the results of this investigation give an indication of the contribution of the second run, but should not be considered as actual truth. The contribution is expected to be lower in reality.

Because the contribution of the second run can become significant ($> 5\%$), the contribution of the second run is always considered in this research to make valid comparisons.

The increasing maximum acceleration due to a flexible foundation can mainly be appointed to two aspects. First, the overall stiffness of the system becomes smaller when a flexible foundation is considered, resulting in larger motions. Second, the flexible foundation results in a period lengthening which shifts the system towards a domain with higher energy content in the load spectrum, also resulting in larger motions. The maximum period lengthening of a system with a flexible foundation is found to be 1.52, compared to a system with a clamped foundation. This maximum period lengthening is found for the most soft foundation conditions ($D = 3.5\,\text{m}$, soil profile: soft), a height of 300 meters, a width of 50 meters and a depth of 30 meters. For the most stiff foundation conditions ($D = 14.0\,\text{m}$, soil profile: stiff), the period lengthening is up to 1.11, found for a height of 300 meters, width of 90 meters and depth of 30 meters.

The two aspects together can result in much larger maximum accelerations for a system with a flexible foundation, compared to a system with a clamped foundation. Values up to 3.3 times the maximum acceleration of the clamped system are found. This emphasises the significance of the foundation flexibility. Design graphs are provided which can be used to estimate the increase factor for a flexible foundation based on the maximum acceleration of a clamped foundation. Using the upper limit in the graphs will result in a conservative estimation of the maximum acceleration. However, it is not recommended to use these graphs for the final comfort checks, since there can be a relatively large spread in the data (up to a ratio of 1.1). Instead, it is recommended to calculate the final maximum acceleration with a model including the effects of SSI, when a large amount of the parameters are set. The example of the conservative method with the design graphs showed an increase of 43% of the maximum acceleration due to the flexible

foundation. The conservative method resulted in an overestimation of 10% in this example.
For the conclusions of the influence studies, a flexible foundation is always considered.

The influence of the geometrical dimensions is very dependent on the foundation conditions. In general it can be stated that the influence of the geometrical dimensions becomes larger for softer foundation conditions. It is found that the height (100 to 300 meters) and the depth (30 to 90 meters) of the building, have the largest influence on the maximum acceleration with a maximum of respectively 201.1% and 577.3% relative to the minimum value. The building width (30 to 90 meters) has a maximum influence of 38.8%, relative to the minimum value. The following two statements are true: the larger the height h, the larger the maximum acceleration, and, the larger the depth d, the lower the maximum acceleration. The large influence of the building depth d is mainly to be appointed to the increasing rotational stiffness and damping value for increasing d. The largest influence of d on the rotational stiffness and damping is 1680% and 1000% respectively, relative to the minimum value. Meaning, the rotational stiffness is almost 18 times higher for a depth of 90 meters than for a depth of 30 meters. The translational parameters are only influenced for maximum 30% (stiffness) and 60% (damping), relative to the minimum value. It is shown that the rotational foundation parameters are dominant for the SSI-effects.

Regarding the effective modal damping ratios, the assumption is maintained that the first run is representative for the first mode of vibration and the second run is representative for the second mode of vibration. It is found that both the first and the second effective modal damping ratio is influenced by the effects of the SSI. Both show a decreasing trend with increasing height. It is found that the first effective modal damping ratio shows a trend of becoming smaller than the input damping ratio for larger heights. The point where it becomes unfavourable, is depending on the depth of the building. The smallest value is over 3 times smaller than the input damping ratio, and is found for a depth of 30 meters, a height of 300 meters, a foundation depth of 3.5 meters and a "soft" soil profile. In general, this would mean that the effects of the SSI have an increasing unfavourable effect on the first effective modal damping ratio of the structure for increasing height. The unfavourable effects become larger for more soft foundation conditions. The second effective modal damping ratio is much more influenced by the flexible foundation. The results show values over 4 times larger than the input damping ratio for small heights (100 meters), and values over 3 times smaller for large heights (300 meters). The SSI effects in this research, do only account for radiation damping in the soil. Material damping from the soil is therefore not taken into account. Due to this fact, the results may underestimate the actual effective modal damping ratio of a high-rise building including a flexible foundation.

For the foundation design, the mass of the foundation has no influence on the maximum acceleration of the structure. From this, it can be concluded that this parameter can be disregarded in the design process, regarding the maximum acceleration of the structure. The foundation depth has a maximum influence of 74.8%, relative to the minimum value (from 3.5 m to 14.0 m), and is found for: $h = 300 \, \text{m}, b = 40 \, \text{m}, d = 30 \, \text{m}$ and a soft soil profile. The maximum influence of the soil profile is found to be 72.1%, relative to the minimum value (soil profiles "soft", "medium" and "stiff"), found for the same building with a foundation depth of 3.5 meters.

Finally, the influence of the superstructure parameters (stiffness, mass density and damping ratio) on the maximum acceleration is shown using six variants. The influence of the stiffness, mass density and damping ratio of the superstructure is different for every single case. However, it is shown that the influence lines become similar for more stiff foundation cases. For example, for large building depths ($d = 90 \, \text{m}$), the factor for stiffness, mass density and damping ratio are very similar. Also, the influence is not changing significantly for increasing height for these cases. The influence of the mass density is also not changing significantly for increasing height for $d = 30 \, \text{m}$. However, the influence of the damping ratio and, especially, the stiffness of the superstructure is changing for different heights. Using an example ($D = 3.5 \, \text{m}$ and a soft soil profile), the decrease in maximum acceleration for a five times larger stiffness of the superstructure

than the reference case, is shown to change from 2.3 times smaller, for $h = 100$ m, to 1.0 times smaller, for $h = 300$ m. Meaning, a five times higher stiffness for the case that $h = 300$ m, will not result in lower accelerations. The general conclusion can be made that, for stiff foundation conditions, the influence of the superstructure parameters is relatively large. The more flexible the foundation, the lower the influence of the superstructure parameters.

For the considered combinations in this research, the stiffness has the largest influence range for the majority of combinations. Only for the case of $h = 300$ m, $d = 30$ m, $D = 3.5$ m on a soft soil profile, the damping ratio has the largest influence range. However, with this conclusion it should be remembered that the stiffness ranges from five times smaller to five time larger than the reference value. This is a relatively large range and it may be required to make major changes to the design (e.g. different stability system) to reach such an increase or decrease in stiffness. The input damping ratio range is 0.5% to 4.0%. This is already a relatively high upper limit, since current measurements show damping ratio's up to 3.0%, for relatively low buildings ($\sim < 150$ m), knowing that the overall damping ratio is generally decreasing for larger heights. To reach the upper limit of the influence ranges used in this research, additional damping devices may be needed. The influence of the mass density is relatively low. This is mainly caused by the limited input range of 200 to 500 kg/m^3.

CHAPTER 9
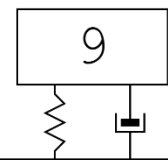
CASE STUDY: MONTEVIDEO

In this chapter, the Montevideo tower is used as a case study. A description of the building, including the structural design, is provided. The original design procedure regarding the dynamic response of the building is discussed and compared to the procedure used in this research. Finally, the structure is schematized as described in this research and the influences of the different parameters is shown.

The case-study is used to illustrate the case-specific approach to draw conclusions. Smaller bandwidths of the parameters are used and case-specific influence lines are generated.

9.1   INTRODUCTION

The Montevideo tower is chosen because the stability system consist of two parts. Therefore, the system has non-constant parameters over the height of the structure and the procedure described in chapter 7 can be demonstrated. Also, the building has a relatively large height (currently for the Netherlands) and is situated on a relatively soft soil in Rotterdam. The structural design of the building is designed by ABT and therefore, the original calculations are used.

The design of the 140 meters high Montevideo tower is inspired by the skyscrapers in New York from the '20s and '30s of the last century. The building is located at the end of the Wilhelminapier in Rotterdam. The building consists of four parts: "the Tower", "the Plint", "the Cantilever" and "the Parking". Beside the parking below the square next to the building, there is a two-storey parking garage underneath the whole building. (Bos, 2006)
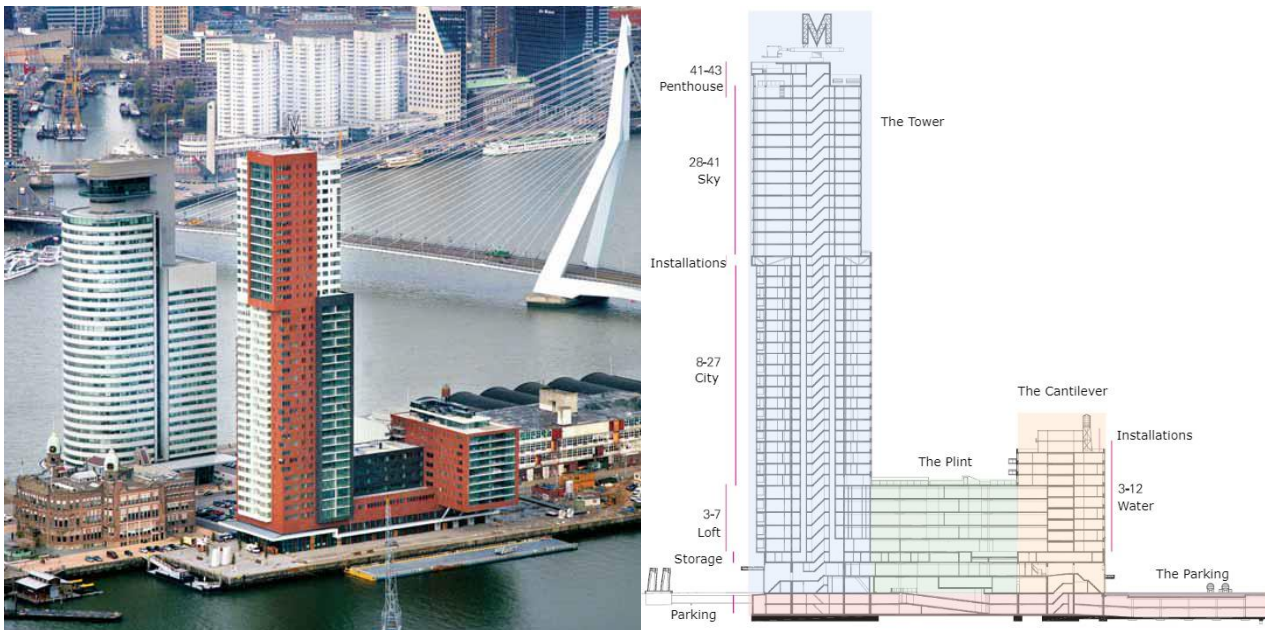
Figure 100: The Montevideo tower in Rotterdam (Bos, 2006)

The tower consists of 42 storeys and reaches a height of ca. 140 meters. The ground floor and 1st floor have a general/commercial function. The 27th floor is used for installations. All other floors in the tower have a residential function. The tower has a base of approximately 27x28 m^2. The "Plint" connects the "Tower" and the "Cantilever". The ground floor and 1st floor have a commercial function. The 2nd and 3rd floor are used for a swimming pool and storages boxes. On floors 4 till 8, offices are situated. The total height of the "Plint" is ca 29 meters and has a base of approximately 27x39 m^2. The "Cantilever" has 11 storeys with a total height of ca. 37 meters. The bottom two floors are commercial, and the remaining floors are residential. Floors 2 till 11 are cantilevering over the quay with a length of 16 meters. The base on the ground floor is approximately 23x27 m^2 and at the 2nd floor approximately 23x44 m^2. The parking garage is extended next to the cantilever below the square. The parking garage has two basement levels and has dimensions of approximately 42x32 m^2. (Rozemeijer, 2002)

Because the focus of this case study is on the "Tower", further description and elaboration will only consider the tower of the building.

9.2   STRUCTURAL DESIGN

9.2.1   Load bearing structure

The tower consists of three different structural systems. The top part, floor 28 till 42, the middle part, floor 2 till 27, and the bottom part, ground floor and 1st floor.
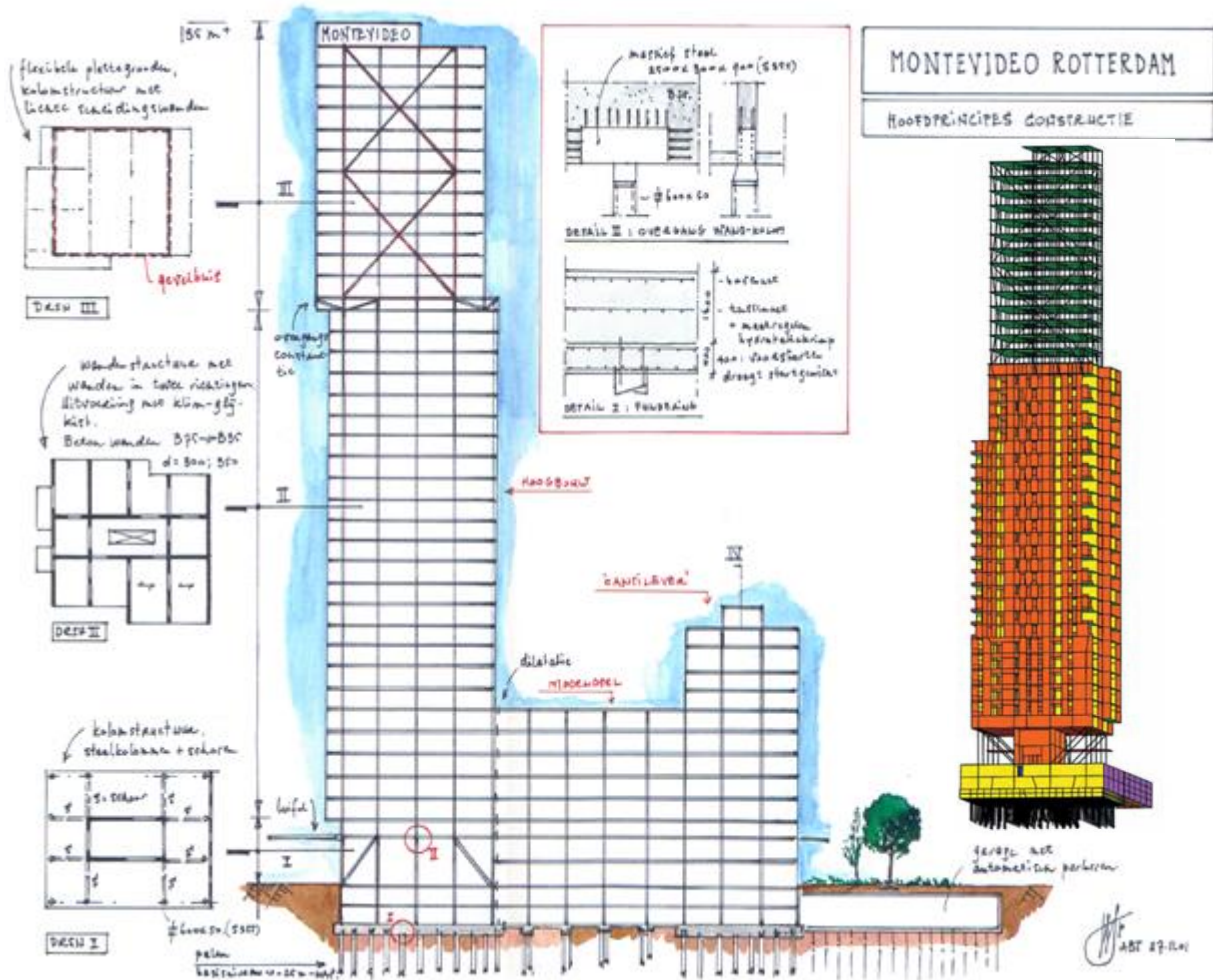
Figure 101: Overview of structural system (Spangenberg, 2002) (Bos, 2006)

The top of the tower is designed in steel. The stability is secured by a tube-structure. The tube-structure is realized by adding large steel bracings in the façade. The steel columns support steel beams which are integrated in the concrete floor ($t = 220$ mm). The steel columns are supported by the concrete structure underneath at the 27th floor.
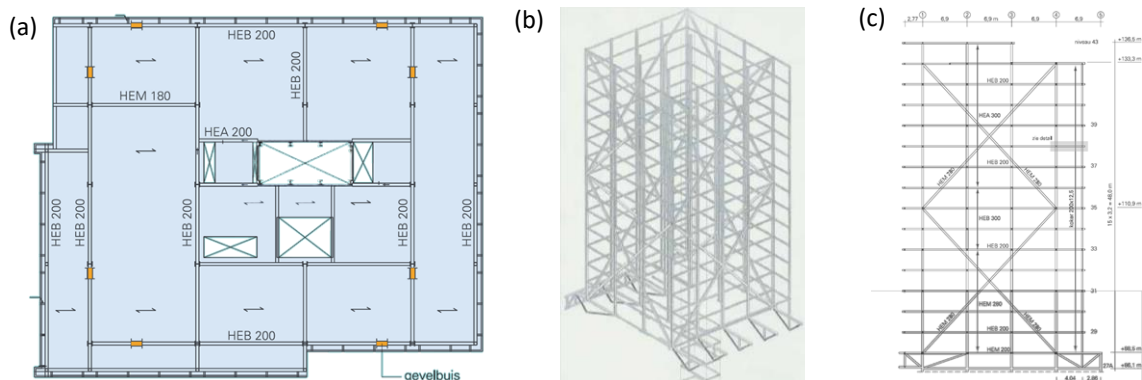
Figure 102: Floor plan (a), 3D image tube-structure (b) and side view tube structure (c) of the top part (Bos, 2006)

The middle of the tower is designed in concrete. The stability is secured by concrete shear walls ($t = 300/350$ mm), which support the concrete floors ($t = 220$ mm). The concrete floors act as a diaphragm and transfer the loads to the walls.
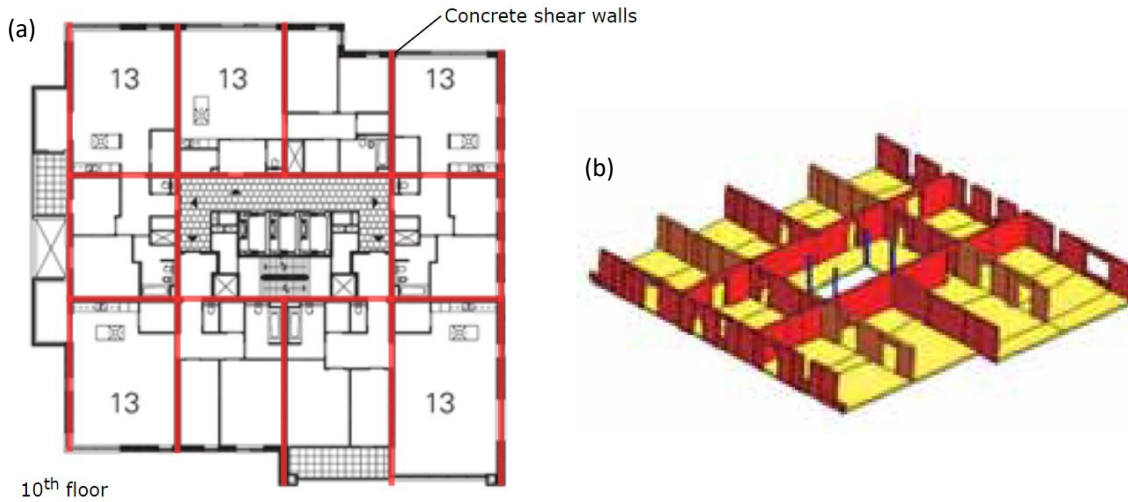
Figure 103: Floor plan (a) and 3D image of the concrete structure of the middle part (Bos, 2006)

The bottom part of the tower has a concrete core and a steel braced structure. The concrete core has walls with a thickness of 500 mm. The steel columns are connected to the concrete core with steel diagonals.
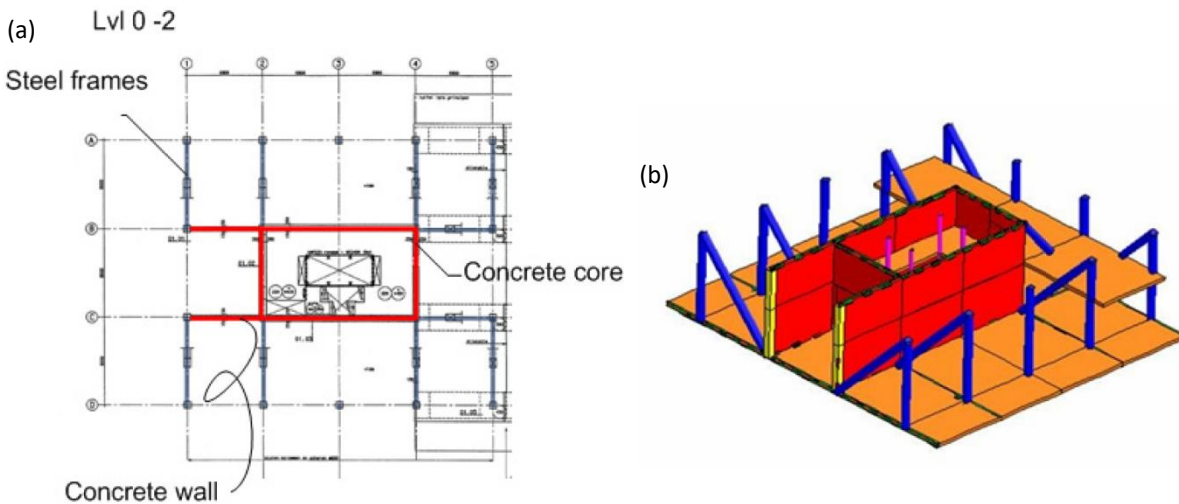
Figure 104: Floor plan (a) and 3D image of the concrete core and braced steel structure of the bottom part (Berg, 2012)

9.2.2 Foundation

Underneath the whole building, a two layer parking garage is realized. The basement levels are cast in situ concrete. The bottom floor is a 2 meters thick concrete slab. The concrete core is extended until this slab. Concrete columns ($d = 750$ mm) with steel HD-profiles inside and concrete walls ($t = 500 - 600$ mm) support the tower.

The subsoil of the top 30 meters, is characterized by four layers. A weakly compacted sand layer on top, a weak clay and peat layer till 17 m -NAP, a sand layer till 30 m -NAP and a very stiff clay layer below 30 meters. The prefabricated concrete piles have their tip in the sand layer at 25 m -NAP. A large part of the piles have been installed under an angle to transfer horizontal forces into the subsoil.
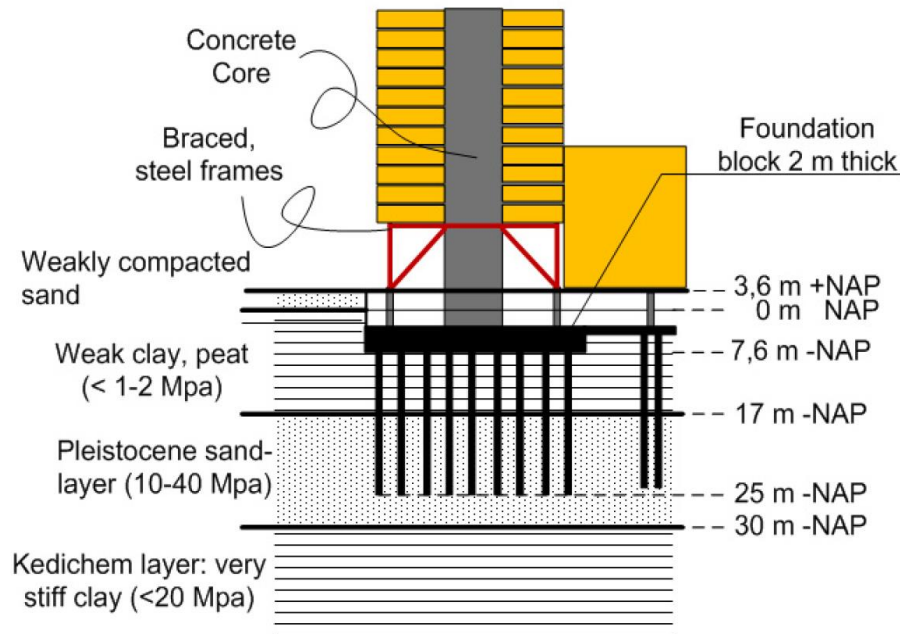
Figure 105: Overview of the foundation and subsoil (Berg, 2012)

9.3 DESIGN PROCEDURE

A three dimensional model of the structure has been made in DIANA by ABT in the design process. This 3D model has been used to determine the forces on the foundation piles and to perform checks regarding the horizontal deflection.

The dynamic behaviour of the structure is taken into account with a dynamic amplification factor, as described in the NEN6702, annex A.4. This is done for the most critical direction, the direction parallel to the letter axis in above figures. To determine the dynamic amplification factor, the natural frequency of the building is estimated. This is done by the method described in NEN6702. The following formula is used to determine the first natural frequency of the structure:

$$f_1 = \sqrt{\frac{a}{\delta}} \tag{9.1}$$

a is the vibration acceleration, depending on static system and distribution of mass
δ is the deflection due to the "momentane" load combination

The value of a for a clamped beam with equally distributed mass is used ($a = 0.384$). The deflection due to a "momentane" load combination, is determined with a beam model, including the foundation stiffness. For the foundation stiffness, a value of $1.42 \cdot 10^{19}$ Nmm^2 is used. For the stiffness of the structure, the same beam model is used. A wind load is applied and the stiffness is determined by matching the total deflection equal to the total deflection from the DIANA model. The stiffness value found is: $EI = 2.79 \cdot 10^{19}$ Nmm^2. Finally, the first natural frequency of the structure is estimated to be: $f_1 = 0.19$ Hz, resulting in a dynamic amplification factor of 1.34. (Rozemeijer, 2002)

According to (Berg, 2012), the designers of the building have indicated that the maximum acceleration of the building was not governing for the design. Therefore, the design was based on the maximum allowable deflection of the structure.

9.4 INFLUENCE STUDY

9.4.1 Input parameters

Not all parameters that are required for the model in this research are reported. The missing parameters are estimated based on the available information. Also, the available reports ((Rozemeijer, 2002), (Rozemeijer, 2002), (Rozemeijer, 2003)) contain hand calculations and DIANA output, which show different values. Therefore, two parameter sets are used in this case study:

1. Parameter set 1: Values from hand calculations;
2. Parameter set 2: Values from DIANA calculations.

The hand calculations simplify the structure to a system with constant parameters. This simplification is maintained in the first parameter set. The DIANA calculations result in different parameter values for the different parts of the structure. Therefore, a separated parameter system, as described in chapter 7, is used for this parameter set.

Superstructure

Parameter set 1

As described in previous section, a beam model is used to calculate the stiffness of the superstructure. This is done by matching the top displacement of the beam model with the maximum displacement from the DIANA model, resulting in an overall EI-value of the superstructure. The rotational stiffness of the foundation is taken into account in this calculation.

The mass density of the building is not calculated in the original reports. Therefore, an estimation is made based on the available information. This calculation can be found in Appendix D. The weighted average of the two parts is taken as representative mass density for the whole building.

The damping ratio is used to determine the dynamic amplification factor. This is done separately for the steel part and the concrete part. A damping ratio of 2% is assumed for the steel part and 1% for the concrete part. Subsequently, the weighted average of both amplification factors is determined. Since in parameter set one constant parameters are considered, the weighted average of the assumed damping ratios is used.

$$EI = 2.79 \cdot 10^{13} \text{ Nm}^2$$

$$\rho = \frac{309 \cdot 56 + 493 \cdot 84}{140} = 420 \text{ kg/m}^3$$

$$\xi_1 = \xi_2 = \frac{2\% \cdot 56 + 1\% \cdot 84}{140} = 1.4\%$$

Parameter set 2

The stiffness values for the different parts of the structure are given by the DIANA calculations. This is simplified to a system with two parts. For every part, the average of the DIANA values is taken as representative stiffness value.

As mentioned, the mass density is calculated in Appendix D.

From measurements, it is know that the overall damping ratio of the first mode of vibration of the complete structure is 1%. This includes all phenomena that contribute to the overall damping, e.g. damping from the subsoil. The damping ratio of the superstructure is matched such, that the overall damping of the first mode of vibration of the superstructure is 1%.

$$EI_1 = \frac{4.291 \cdot 8.1 + 3.837 \cdot 64.3 + 3.835 \cdot 5.8 + 4.159 \cdot 5.8}{84} \cdot 10^{13} = 3.903 \cdot 10^{13} \text{ Nm}^2$$

$$EI_2 = 3.179 \cdot 10^{13} \text{ Nm}^2$$

$$\rho_1 = 493 \text{ kg/m}^3$$

$$\rho_2 = 309 \text{ kg/m}^3$$

$$\xi_1 = \xi_2 = 1.3 \text{ \%}$$
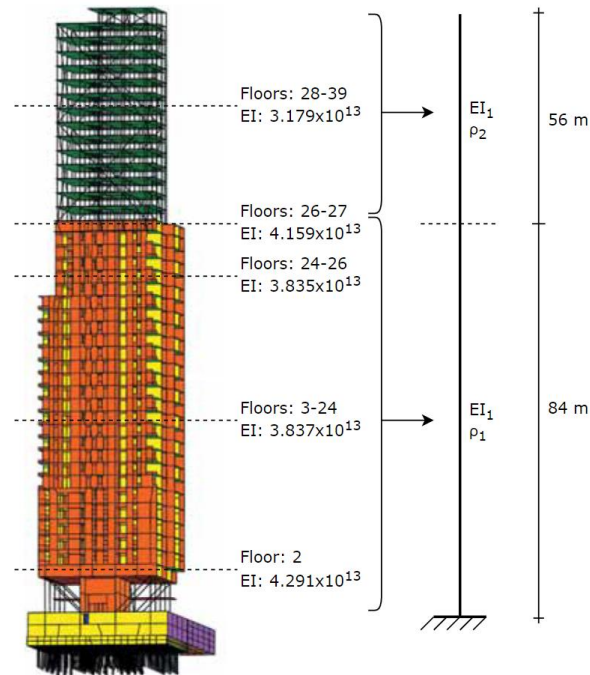
Figure 106: Stiffness values of the DIANA calculation, together with the separated parameter system

Foundation

The previously described soil profile is used to determine the soil characteristics of a homogeneous soil layer, as described in section 6.2. This results in the following soil characteristics:

Soil profile	Flexibility	Shear modulus G [$\cdot 10^6$ N/m^2]	Mass density ρ_s [kg/m^3]	Poisson's ratio v [-]	Shear wave velocity V_s [m/s]
1	"Soft"	20	1726	0.45	108

Regarding the previously determined flexibility of three representative soil profiles in the Netherlands, this soil profile is "soft".

From the existing reports, the only information available regarding the foundation parameters is the rotational stiffness. The rotational stiffness is determined to be: $K_r = 1.42 \cdot 10^{12}$ Nm/rad. When the rotational stiffness value, of the first mode of vibration of the superstructure at the first resonance frequency, is determined according to the discussed method and assumptions in chapter 6, the value is significantly larger: $K_r = 3.97 \cdot 10^{12}$ Nm/rad. The large difference is probably due to different assumptions for the contribution of the soil to the rotational stiffness. To consider both cases, the reported rotational stiffness value is used for parameter set one, and the calculated rotational stiffness according to the assumptions in this research in parameter set two.

To match the rotational stiffness values for parameter set one, the pile factor is modified. For a foundation depth of 7.5 m, the pile factor is reduced from 4.375 to 1.555. In this way, the rotational stiffness of the foundation at the first resonance frequency is equal to $1.42 \cdot 10^{12}$ Nm/rad. The other foundation parameter values are not modified.

9.4.2   Natural frequencies

Parameter set 1

For parameter set 1, constant parameters over height are considered. Therefore, the natural frequencies of a clamped situation can be determined using the formulas given in Appendix C. This results in:

$$\omega_{1,clamped} = 1.68 \, rad/s \quad \rightarrow \quad f_{1,clamped} = 0.27 \, Hz$$

$$\omega_{2,clamped} = 10.54 \, rad/s \quad \rightarrow \quad f_{2,clamped} = 1.68 \, Hz$$

The flexible foundation results in a period lengthening. The discrete model, as described in section 8.1, is used to determine the fundamental frequencies of the system. This results in:

$$\omega_{1,fundamental} = 1.33 \, rad/s \quad \rightarrow \quad f_{1,fundamental} = 0.21 \, Hz$$

$$\omega_{2,fundamental} = 2.41 \, rad/s \quad \rightarrow \quad f_{2,fundamental} = 0.38 \, Hz$$

Parameter set 2

For parameter set 2, a separated parameter system is used. The procedure, as described in chapter 7, is used to find the natural frequencies of a clamped situation. The separation height is 0.6 h.

The stiffness of the bottom and top part are:

$$\left.\begin{array}{l} EI_1 = 3.903 \cdot 10^{13} \, Nm^2 \\ EI_2 = 3.179 \cdot 10^{13} \, Nm^2 \end{array}\right\} \quad EI_{average} = 3.541 \cdot 10^{13} \, Nm^2$$

$$\alpha_{EI} = \frac{3.903}{3.179} = 1.23$$

The frequency factors $B_{EI,i}$ are obtained from Figure 67 and Figure 68:

$$B_{EI,1} = 1.05$$

$$B_{EI,2} = 1.02$$

The mass density of the bottom and top part are:

$$\left.\begin{array}{l} \rho_1 = 493 \, kg/m^3 \\ \rho_2 = 309 \, kg/m^3 \end{array}\right\} \quad \rho_{average} = 401 \, kg/m^3$$

$$\alpha_{EI} = \frac{493}{309} = 1.60$$

The frequency factors $B_{\rho,i}$ are obtained from Figure 71 and Figure 72:

$$B_{\rho,1} = 1.10$$

$$B_{\rho,2} = 0.98$$

The first and second natural frequency of the clamped separated parameter system are now estimated using equation (7.11):

$$\omega_{1,clamped} = 2.239 \, rad/s \quad \rightarrow \quad f_{1,clamped} = 0.36 \, Hz$$

$$\omega_{2,clamped} = 12.145 \, rad/s \quad \rightarrow \quad f_{2,clamped} = 1.93 \, Hz$$

The equivalent mass of the superstructure for the first and second run are:

$$m_{1,equivalent} = 10.61 \cdot 10^6 \, kg$$

$$m_{2,equivalent} = 5.52 \cdot 10^6 \, kg$$

The equivalent stiffness of the superstructure for the first and second run are:

$$k_{1,equivalent} = 5.32 \cdot 10^7 \text{ N/m}$$

$$k_{2,equivalent} = 81.38 \cdot 10^7 \text{ N/m}$$

These equivalent mass and stiffness values are used for the analysis procedure as shown in Figure 77. Again, the flexible foundation results in a period lengthening. This results in the fundamental frequencies of the system:

$$\omega_{1,fundamental} = 1.93 \text{ rad/s} \quad \rightarrow \quad f_{1,fundamental} = 0.31 \text{ Hz}$$

$$\omega_{2,fundamental} = 3.95 \text{ rad/s} \quad \rightarrow \quad f_{2,fundamental} = 0.63 \text{ Hz}$$

Comparison of natural frequencies

The original calculated natural frequency of the design, the fundamental frequencies from the analysis procedure used in this research with two parameter sets, and the measured natural frequency (Geurts, et al., 2015) are shown in Figure 107. There are some significant deviations between the different values. Especially the original calculated value is much lower than the measured value. This emphasises that simplified methods can results in large deviations from reality. Also the values from the analysis procedure in this research, result in lower values than measured. This means that the total system is more stiff in reality than estimated up front. Unfortunately, it is not possible to determine exactly why the structure is more stiff in reality, based on the available data. The system can have a larger stiffness of the superstructure, e.g. a larger young's modulus of the concrete or additional stiffness due to secondary structures, but also the foundation can be more stiff than estimated.
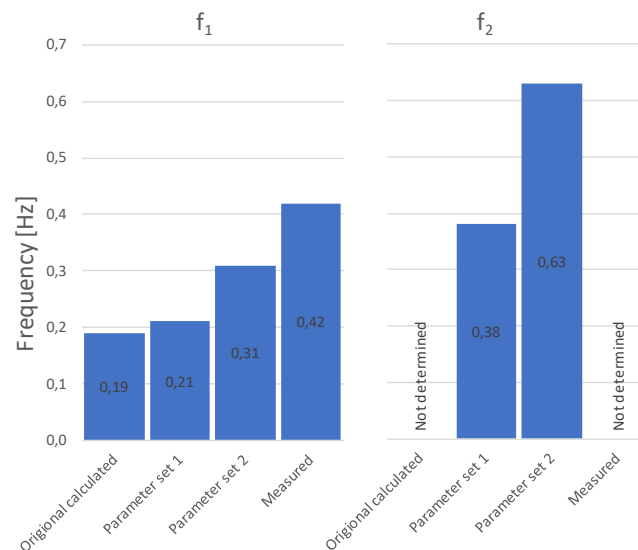
Figure 107: Comparison between originally calculated value, calculated values in this research (parameter set 1 and 2) and measured value (Geurts, et al., 2015) of the first two natural frequencies of the Montevideo tower

A lower natural frequency causes the system to have a peak in the transfer function in a domain with higher energy content in the load spectrum. Therefore, underestimating the natural frequency can be considered conservative. However, underestimation of the natural frequency can also result in an over-dimensioned and uneconomic structure, especially when the structure is designed based on the dynamic behaviour. The originally calculated estimation of the natural frequency of the Montevideo (0.19 Hz) is much lower than the measured natural frequency (0.42 Hz). The wind load, from the wind load spectrum considered in this research, results in a 12.3 times higher load at a frequency of 0.19 Hz than for a frequency of 0.42 Hz. The load is 4.6 times higher for a frequency of 0.31 Hz. For the case of 0.19 Hz, this does not mean that the maximum acceleration is also 12 times larger, but it does show the importance of a good estimate of the natural frequency.

9.4.3   Contribution of the second run

As general statement, the second mode of vibration in a translational direction is most of the time not significant in measurements of Dutch high-rise buildings (not quantified by data). To show whether this general observation is in line with the results of the analysis approach in this research, the contribution of the second mode of vibration of the superstructure is determined. For this, the assumption that the first and second run are representative for the first and second mode of vibration is maintained here. The contribution of the second run to the maximum acceleration is determined as described in section 8.2.

Parameter set 1

The contribution of the second run to the maximum acceleration, for parameter set 1, is: $\delta_a = 10.0\%$.

Parameter set 2

The contribution of the second run to the maximum acceleration, for parameter set 2, is: $\delta_a = 7.1\%$.

Because the natural frequency of parameter set 2 is closer to the measured value, parameter set 2 is assumed to be more representative for the actual building. According to the calculations, the contribution of the second run is relatively small (7.1%). For design purposes, this contribution can be neglected. For the final comfort check, the contribution of the second mode of vibration might be considered, to have a more precise estimation.

The relatively low contribution of the second mode of vibration is in line with the general statement that the second translational mode of vibration is most of the time not significant in measurements. A reason can be that the contribution is of such magnitude, that it falls within the noise of the measurement.

Since the contribution of the second mode of vibration of the superstructure is taken into account in this entire research, this is done here as well for both parameter sets.

9.4.4   Influence geometrical dimensions

In the design process of a building, the geometrical dimensions are one of the first parameters which are fixed. They are determined by many different aspects, e.g. the dimensions of the plot, restrictions of municipalities or the demands of the client. To show the influence of relatively small deviations in the geometrical dimensions, the following parameter ranges are considered:

- Height h: $120, 130, 140, 150, 160$ meters;
- Width b: $23, 25, 27, 29, 31$ meters;
- Depth d: $24, 26, 28, 30, 32$ meters.

This analysis shows the influence of a changing geometrical dimension on the maximum acceleration. For example, what happens if the stability system was not changed, so equal stiffness, but the building was designed 20 meters higher.

Parameter set 1

Parameter set 1 is based on a constant parameter system as described in previous sections. The equivalent mass, stiffness and damping values are determined with a clamped beam model, as described in section 8.1. However, the EI-value is not linked to the height, but a constant value is considered ($EI = 2.79 \cdot 10^{13}\ \text{Nm}^2$). Therefore, the equivalent stiffness value is constant for changing geometrical dimensions. The mass density is kept constant ($\rho = 420\ \text{kg/m}^3$), but does result in a changing equivalent mass for changing geometrical dimensions, since the cross-sectional area will change. The damping ratio of the superstructure is considered constant ($\xi_1 = \xi_2 = 1.4\%$) for changing geometrical dimensions.

Parameter set 2

Parameter set 2 is based on the separated parameter system as described in previous sections. The equivalent stiffness is matched with the equivalent mass and found natural frequency of the superstructure. Since the geometrical dimensions influence the equivalent mass, the equivalent stiffness is kept equal to the reference value. The reference value is the equivalent stiffness related to the existing geometrical dimensions ($h = 140$ m, $b = 27$ m, $d = 28$ m). The equivalent mass is changed due to changing geometrical dimensions. The damping ratio of the superstructure is considered constant ($\xi_1 = \xi_2 = 1.3\%$) for changing geometrical dimensions.

Case-specific influence lines

The influence of changing the geometrical dimensions on the maximum acceleration of the building are shown in Figure 108.
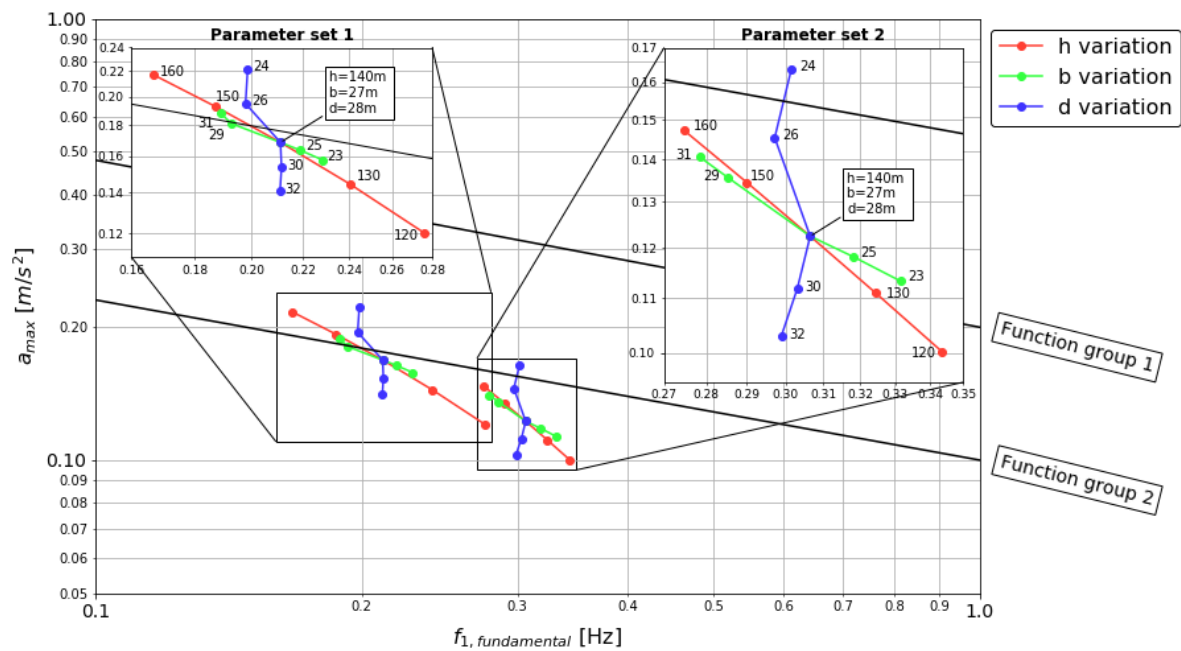
> Explanation of graph:
> On the x-axis, the first fundamental frequency. On the y-axis, the maximum acceleration at the top of the structure. The dots indicate different geometrical dimensions. The colored lines indicate a variation in parameters h, b and d. The maximum lines are from the NTA 4614-3. Function group 1: Office, education, industrial and others. Function group 2: Public, residential, lodging, prison, healthcare, sports and retail. Arrows points in the direction of increasing parameter value.

Figure 108: Influence of geometrical dimensions on the maximum acceleration of two parameter sets associated to the case study

The maximum acceleration of both parameter sets are below the limit line for function group 2 (residential). From this, one can say that both parameter sets satisfy the comfort requirements. However, it should be mentioned again that the maximum values indicate a level of accelerations that will be experienced by the inhabitants of the building on the top floor. Since the measured natural frequency of the building is higher than both parameter sets, the existing building behaves stiffer, which will results in lower accelerations.

The influence lines for height deviation in Figure 108 look similar to the ones shown in Figure 91. A larger height results in a lower fundamental frequency and an increase in the maximum acceleration. The influence lines for width deviation, look different. The reason for this, is that the width is not linked to the stiffness in this case study. A larger width results in a larger mass and therefore a lower fundamental frequency. The larger width also results in a higher load. Because the stiffness remains constant, this results in a larger maximum acceleration. The influence lines for depth deviation look different as well. The

fundamental frequency is not changing significantly for increasing depth. A larger depth results in a higher mass and therefore a lower frequency. However, the larger depth also results in a larger foundation stiffness which increases the natural frequency. Therefore, the fundamental frequency is not changing significantly. The larger foundation stiffness and damping does results in lower values of the maximum acceleration.

The change in the maximum acceleration relative to the reference value due to changing geometrical dimensions is given by the following formula, and shown in Table 14.

$$\Delta a_{max} = -1 + \frac{a_{max}}{a_{max,ref}} \tag{9.2}$$

It becomes clear that the height, but especially the depth of the building, have a large influence on the maximum acceleration of the building.

Height h [m]	Δa_{max} [%]		Width b [m]	Δa_{max} [%]		Depth d [m]	Δa_{max} [%]	
	Parameter set 1	Parameter set 2		Parameter set 1	Parameter set 2		Parameter set 1	Parameter set 2
120	-28.5	-18.2	23	-6.3	-7.5	24	31.4	33.7
130	-14.4	-9.3	25	-2.9	-3.5	26	15.5	18.7
140	0.0	0.0	27	0.0	0.0	28	0.0	0.0
150	14.3	9.8	29	7.3	10.7	30	-8.9	-8.7
160	28.6	20.1	31	11.6	14.7	32	-16.6	-15.9

Table 14: Change in the maximum acceleration relative to the reference value (in grey) due to changing geometrical dimensions

9.4.5   Influence foundation parameters

Because the soil profile will not change for the case study, a different parameter is varied to show its influence. The pile factor γ is already mentioned before, and is included in this influence study. The pile factor takes into account the contribution of the piles to the rotational stiffness of the foundation. Therefore, the influence of the pile factor is equivalent for the influence of a changing rotational stiffness of the foundation. In section 6.6, the pile factor is determined to be a function of the foundation depth D. It has a value of 5.5 for a surface foundation and a value of 1.0 for a foundation depth of 30 meters. This results in a value of 4.375 for a foundation depth of 7.5 m.

In parameter set 1, the pile factor is altered to match the original calculated rotational stiffness, which results in a pile factor of 1.555. In parameter set 2, the default pile factor is maintained (4.375).

The foundation depth is changed with steps of 2.8 meter, the height of a basement level. In this way, the influence of one, two, three or four basement levels is shown. The Montevideo tower has two basement levels.

Case-specific influence lines

The influence of a changing pile factor and foundation depth are shown in Figure 109.
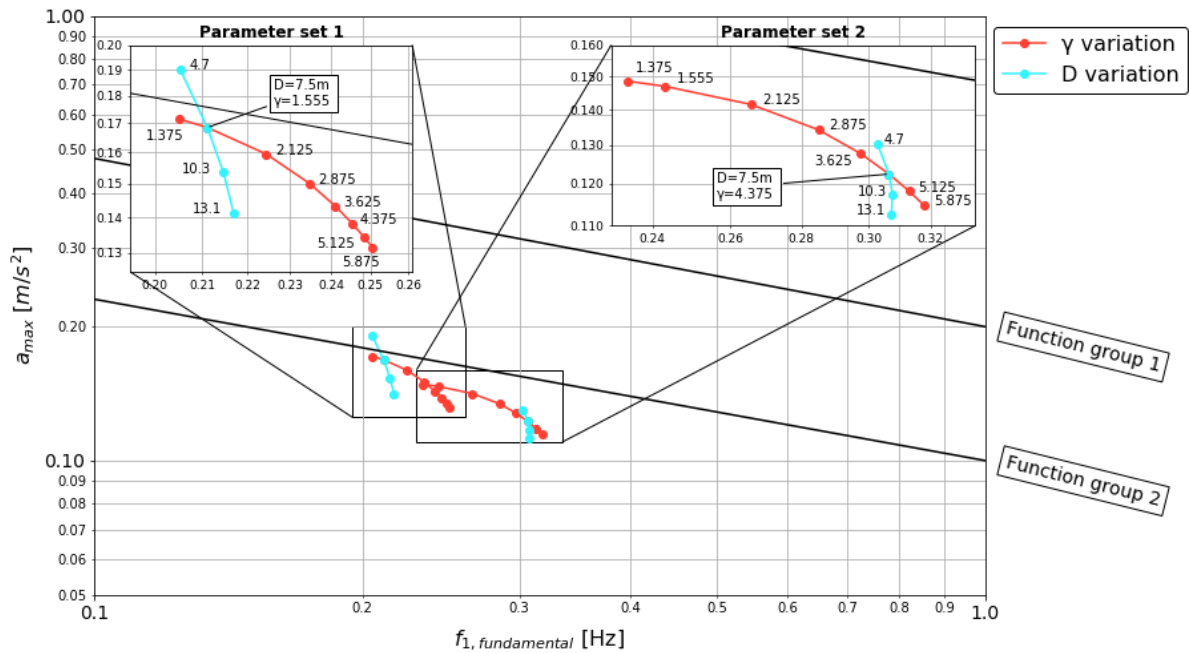
Explanation of graph:
See explanation of Figure 108. The colored lines indicate a variation in parameters D and γ.

Figure 109: Influence of the pile factor and foundation depth on the maximum acceleration of two parameter sets associated to the case study

The influence line of the foundation depth D, looks similar to the one shown in Figure 97. A larger foundation depth results in a larger foundation stiffness and damping. The natural frequency is not affected much by the increased foundation stiffness. On the other hand, the maximum acceleration is decreasing, which is caused by the increasing stiffness and damping value for larger foundation depths.

The influence lines of the pile factor is not shown before. Because the pile factor only increases the rotational stiffness of the foundation, the translational stiffness and damping values are unchanged. An increasing pile factor results in an increasing natural frequency, due to the increasing rotational stiffness. In other words, the period lengthening becomes smaller due to a more stiff foundation. Together with the shift in natural frequency, the maximum acceleration decreases due to the increasing rotational stiffness.

The change in the maximum acceleration relative to the reference value due to changing foundation depth and pile factor is shown in Table 15. The change for the foundation depth for parameter set 1 is double the change for parameter set 2. This is in line with previous observations that the influence of the foundation is larger for more flexible systems. The change for the pile factor becomes significant (e.g. $> 10\%$), for pile factors, and therefore for a rotational stiffness, of at least twice/half the reference value.

Foundation depth D [m]	Δa_{max} [%]		Pile factor γ [m]	Δa_{max} [%]	
	Parameter set 1	Parameter set 2		Parameter set 1	Parameter set 2
4.7	12.9	6.3	1.375	1.7	18.5
7.5	0.0	0.0	1.555	0.0	17.5
10.3	-8.9	-4.4	2.125	-5.3	14.0
13.1	-16.2	-8.3	2.875	-10.9	8.8
			3.625	-15.0	4.0
			4.375	-18.0	0.0
			5.125	-20.3	-3.3
			5.875	-22.0	-6.0

Table 15: Change in maximum acceleration relative to the reference value (in grey) due to changing foundation depth and pile factor

9.4.6 Influence superstructure parameters

The parameters related to the superstructure are the stiffness (EI), the mass density (ρ) and the damping ratio (ξ). The three parameters are altered according to the described parameter ranges in chapter 5.

Case-specific influence lines

The influence of a changing stiffness, mass density and damping ratio of the superstructure are shown in Figure 110.
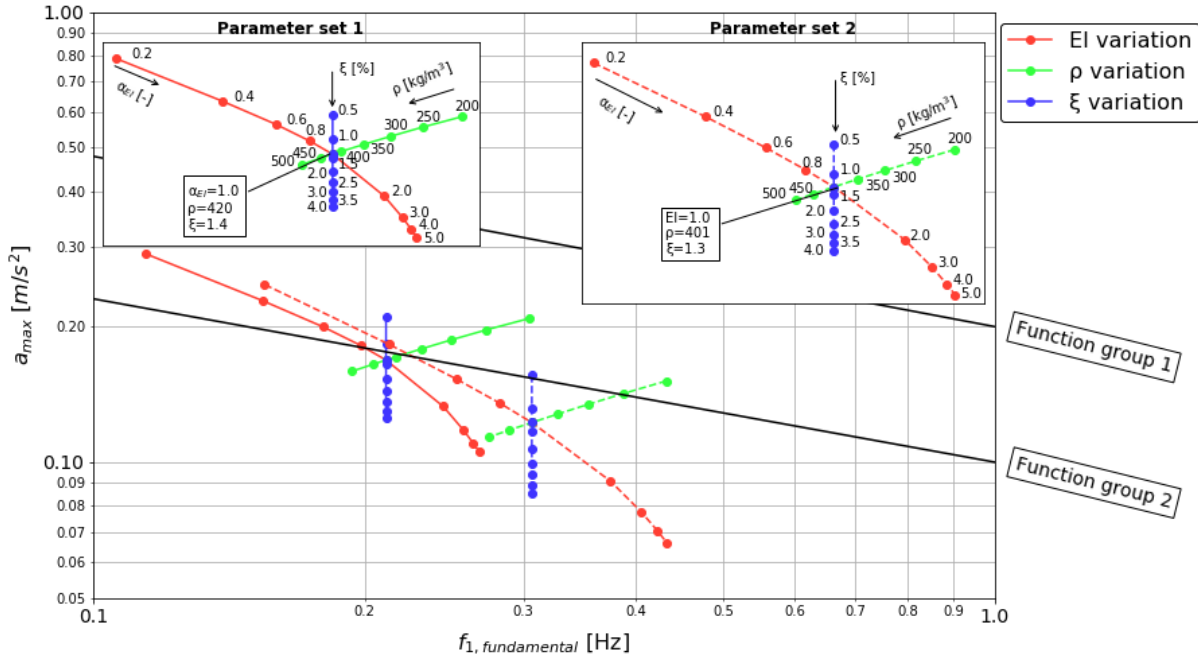
Figure 110: Influence of the stiffness, mass density and damping ratio of the superstructure on the maximum acceleration of two parameter sets associated to the case study

The influence lines of all parameters are similar to the ones shown in Figure 98. Also, the lines show the same trend for both parameter sets. From this, it can be concluded that the higher rotational foundation stiffness of parameter set 2, does not results in significantly different influence lines for the superstructure parameters.

The change in the maximum acceleration relative to the reference value due to changing stiffness, mass density and damping ratio of the superstructure is shown in Table 16.

Stiffness factor [-]	Δa_{max} [%] Parameter set 1	Δa_{max} [%] Parameter set 2	Mass density ρ [kg/m³]	Δa_{max} [%] Parameter set 1	Δa_{max} [%] Parameter set 2	Damping ratio ξ [%]	Δa_{max} [%] Parameter set 1	Δa_{max} [%] Parameter set 2
0.2	72.1	102.4	200	23.8	23.7	0.5	24.7	27.5
0.4	35.4	49.3	250	16.7	16.0	1.0	8.6	7.8
0.6	18.5	25.0	300	10.8	9.7	1.3	-	0.0
0.8	7.8	10.2	350	5.9	4.5	1.4	0.0	-
1.0	0.0	0.0	400/401	1.6	0.0	1.5	-1.8	-4.2
2.0	-21.1	-25.8	420	0.0	-	2.0	-9.2	-12.6
3.0	-30.1	-36.7	450	-2.2	-3.8	2.5	-14.8	-18.7
4.0	-34.7	-42.4	500	-5.6	-7.2	3.0	-19.2	-23.5
5.0	-37.5	-45.9				3.5	-22.8	-27.3
						4.0	-25.7	-30.5

Table 16: Change in the standard deviation of the acceleration relative to the reference value (in grey) due to changing stiffness, mass density and damping ratio of the superstructure
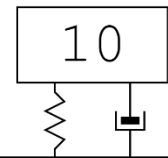
CHAPTER 10

APPLICATION IN TWO RESPONSE DIRECTIONS

This chapter serves as an extension to the research. The analysis procedure is applied in the two orthogonal translational response directions. The comparison of the maximum acceleration in both directions is made for square cross-sections. Also, this chapter provides an indication when the load from vortex shedding can become significant for the maximum acceleration of the structure.

10.1   INTRODUCTION

The analysis procedure used in this research is based on the assumption of uncoupled response directions. In this way, each response direction can be analysed separately and combined accordingly. Up until now, only the alongwind response is analysed. In this chapter, the same analysis procedure is used to analyse also the across-wind response.

In previous chapters, the along wind response for many different building dimensions is analysed. It is shown that the depth of the building is very influential on the maximum acceleration at the top of the structure. When two directions are considered, it is safe to assume that the direction with the largest h/d-ratio is critical for the maximum acceleration of the structure. However, in the case of square cross-sections, the h/d-ratio is equal in both directions. This chapter will investigate which response direction results in larger maximum accelerations.

For the across-wind response, the v-component of the wind load spectrum is used. In addition, an extra load from vortex shedding can occur. This load is depending on the wind velocity and the dimensions of the building.

10.2   THE MODEL

The same model, as described in chapter 8, is used for the across-wind response. Both response directions are analysed separately. The wind is considered in one direction. This results in the loading spectra, described in section 3.4.2, shown in Figure 111. Additional to the fluctuating part of the wind in y-direction, a force due to vortex shedding can occur, which is described in section 4.1.2.
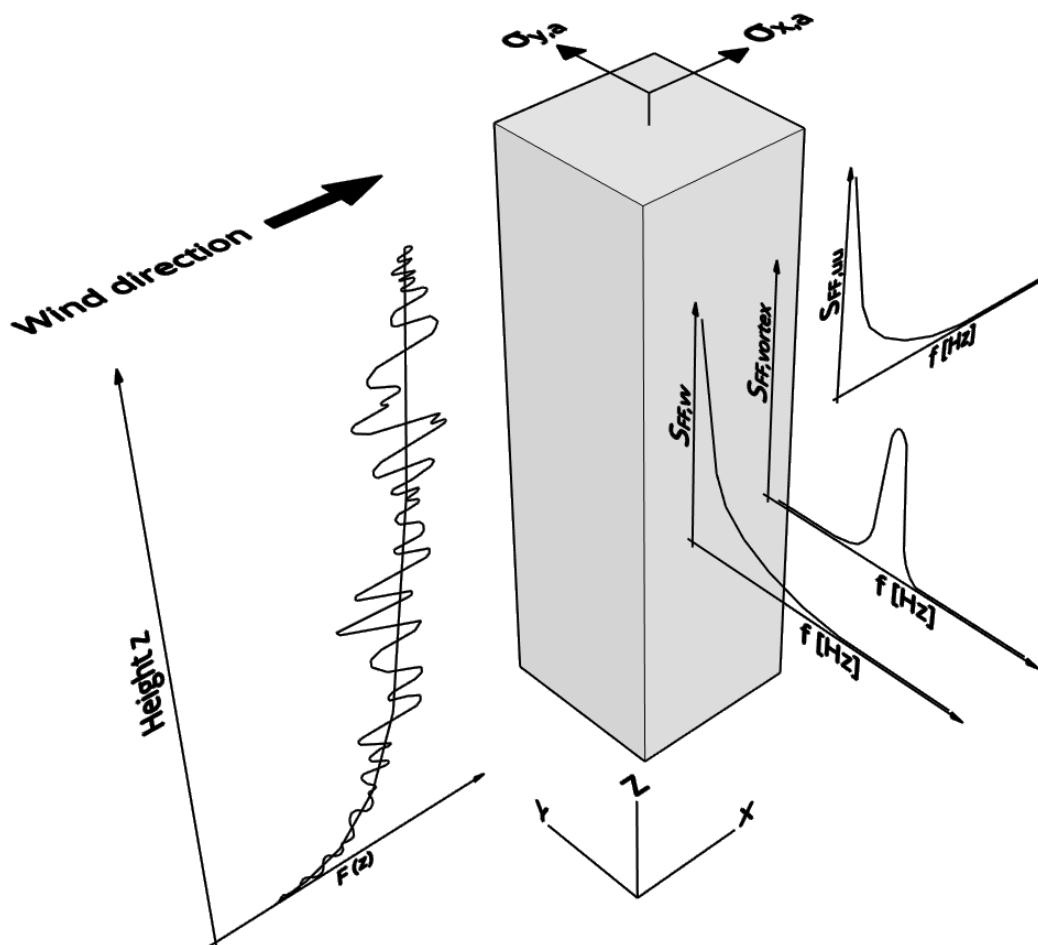
Figure 111: Three dimensional representation of dynamic wind load, alongwind and acrosswind load spectra and the alongwind and acrosswind response ($\sigma_{x,a}$ and $\sigma_{y,a}$ respectively)

The parameters of the superstructure are based on the same assumptions for both directions. The mass density is equal ($\rho = 350\ \text{kg/m}^3$). The damping ratio of the superstructure is assumed to be equal in both direction ($\xi = 1.5\%$). The stiffness in linked to the height and a static load, as described in section 5.1, which results in an equal stiffness in both direction when $b = d$.

The same combinations of parameters, as used for the analysis described in section 8.3, is used here. This dataset consists of variations in geometrical dimensions, foundation depths and soil profiles. All together this results in a total of 2000 combinations.

The foundation parameters are determined with the analytical expressions from (Gazetas, 1991), as described in chapter 6 and given in Appendix E. The expressions provide the stiffness and damping values for both directions, considering a load in one direction. Since the main wind direction will produce the largest load on the building (constant mean and fluctuating part), the foundation parameters are determined using this load in one direction. This results in different stiffness and damping values for both directions, even in the case that $b = d$. The expressions in the xy-coordinate system are given for $L \geq B$. Therefore, the coordinate system is adjusting accordingly for either $b \geq d$ or $b < d$.

10.3 CALCULATION OF THE RESPONSE

The calculation procedure is the same as described in section 8.2. The only difference is that all formulas get an extra subscript for the direction. The procedure is repeated twice in the y-direction. One time with a loading spectrum excluding the vortex shedding load, and one time including the vortex shedding load. The response functions given by equation (8.4) change for the three cases in:

$$
\begin{array}{ccc}
\text{x-direction} & \text{y-direction (without vortex)} & \text{y-direction (with vortex)} \\[4pt]
S_{x,a}(\omega) = |H_{x,a}|^2 S_{FF,uu} & S_{y,a}(\omega) = |H_{y,a}|^2 S_{FF,vv} & S_{yv,a}(\omega) = |H_{y,a}|^2 S_{FF,vv+vortex}
\end{array}
\tag{10.1}
$$

This results in the standard deviation of the acceleration for the three cases:

$$
\begin{array}{ccc}
\text{x-direction} & \text{y-direction (without vortex)} & \text{y-direction (with vortex)} \\[4pt]
\sigma_{x,a} = \sqrt{\sigma_{x,a,1}^2 + \sigma_{x,a,2}^2} & \sigma_{y,a} = \sqrt{\sigma_{y,a,1}^2 + \sigma_{y,a,2}^2} & \sigma_{yv,a} = \sqrt{\sigma_{yv,a,1}^2 + \sigma_{yv,a,2}^2}
\end{array}
\tag{10.2}
$$

Finally, the maximum acceleration of the combined response for the three cases is given by:

$$
\begin{array}{ccc}
\text{x-direction} & \text{y-direction (without vortex)} & \text{y-direction (with vortex)} \\[4pt]
a_{x,max} = k_p \sigma_{x,a} & a_{y,max} = k_p \sigma_{y,a} & a_{yv,max} = k_p \sigma_{yv,a}
\end{array}
\tag{10.3}
$$

The significance of the vortex shedding load is calculated by:

$$
\Delta_{yv,a} = \frac{a_{yv,max} - a_{y,max}}{a_{y,max}} \quad [\%]
\tag{10.4}
$$

10.4 COMPARISON BETWEEN RESPONSE DIRECTIONS

Since the load spectrum and parameters are dependent on the geometrical dimensions, a valid comparison between the response in x-direction and the response in y-direction can only be made for the cases where $b = d$.

10.4.1 Comparison of the model variables

When $b = d$, all parameters of the superstructure are equal. However, the foundation parameters are not equal. This originates in the analytical expressions of (Gazetas, 1991). When loading the structure, with

equal width and depth, in a certain direction, the foundation stiffness and damping values for the translational and rotational degree of freedom, in the two orthogonal directions, are not equal.

The different stiffness and damping values at the first fundamental frequency for both orthogonal response directions is visualized in Figure 112, by the ratios of the stiffness and damping in both directions. The height of the structure and the soil profile have only a small influence on these ratios. Therefore, the ratios are only shown for a height of 100 meters and a medium soil profile. The parameters which do have an influence on these ratios are the width b and depth d, which are equal, and the foundation depth D.

The rotational damping value and translational stiffness are almost the same for both directions. The translational damping value is higher in y-direction with a maximum of $1.16 \cdot C_{x1}$. The rotational stiffness value varies the most, and is larger in y-direction. The maximum value in the y-direction is $1.47 \cdot K_{rx1}$.
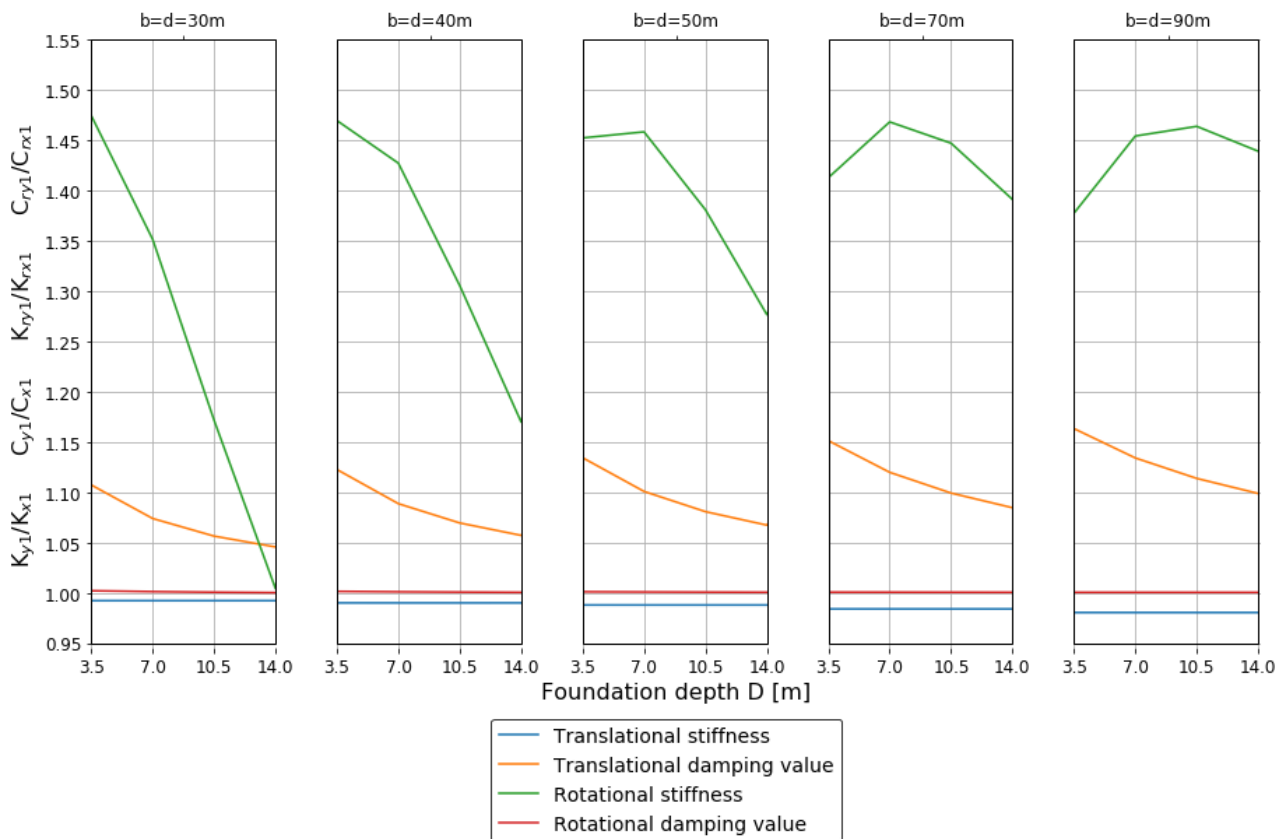
Figure 112: Stiffness and damping ratios of the horizontal and rotational degree of freedom of the foundation at the first fundamental frequency for a height of 100 meters and soil profile "medium" for both orthogonal response directions

10.4.2 Comparison of the load spectra

Besides the different foundation parameters, the load spectra in x- and y-direction are also different. The difference between the spectra is clearly visible for lower frequencies in Figure 25. The spectrum of the v-component (y-direction) takes lower values in the low frequency range. However, the first fundamental frequency of high-rise buildings in the Netherlands is usually between 0.1 Hz and 1.0 Hz. In this domain, the spectrum of the v-component takes larger values than the u-component for square cross-sections. This is hardly visible in Figure 25, but comes clear by plotting the ratio of the v-component over the u-component, as shown in Figure 113. For frequencies larger than 0.022 Hz, the load spectrum for the v-component takes larger values than the load spectrum of the u-component, reaching an asymptote at a ratio of 1.36.
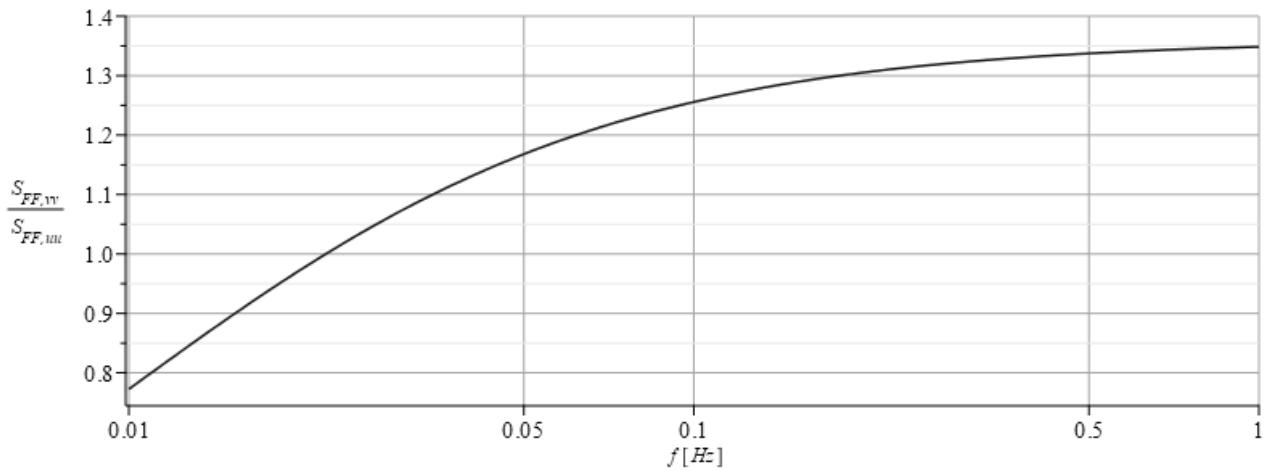
Figure 113: Ratio of the load spectrum of the v-component over load spectrum of the u-component

10.4.3 Comparison of the maximum acceleration

As discussed in previous sections, the input parameters and loading spectra are different for the two orthogonal response directions. This also results in a different response in the two response directions. The ratio of the maximum acceleration in the y-direction over the maximum acceleration in the x-direction for square cross-sections is shown in Figure 114. The height of the building and the soil profile have an influence on the ratio of the dynamic response in the two directions. The different heights are shown in Figure 114. However, to keep the graph readable, the results are only shown for a 'medium' soil profile. The force from vortex shedding is not included in this analysis.
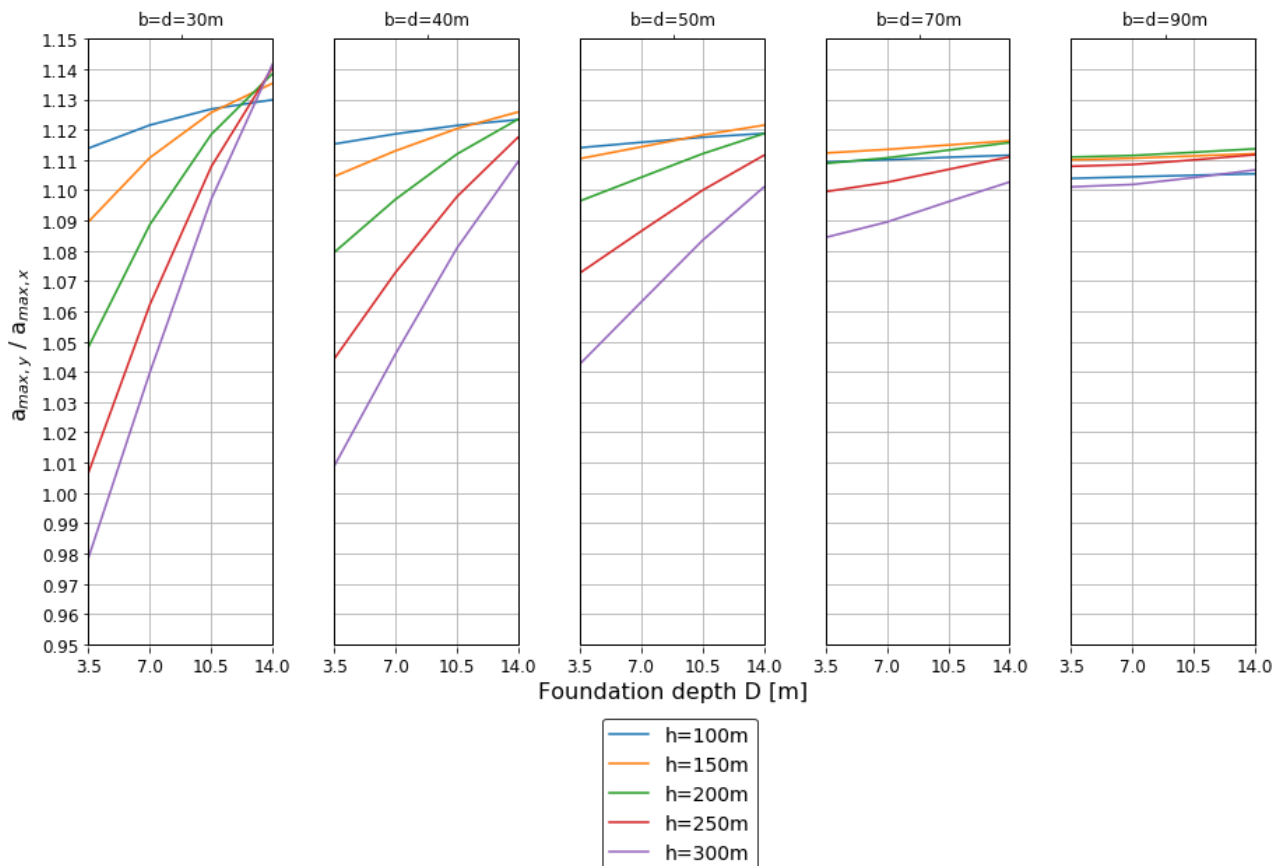
Figure 114: Ratio of the maximum acceleration in the y-direction over the maximum acceleration in x-direction for different heights and a "medium" soil profile

From Figure 114, it becomes clear that the response in the y-direction is larger than the response in x-direction in 99% of the cases (for square cross-sections on a medium or stiff soil profile). For a soft soil profile, this is for 95% of the cases. The ratio is increasing for an increasing foundation depth. This is caused by the decreasing rotational stiffness ratio for increasing foundation depth, while the load in y-direction stays higher than the load in x-direction.

10.5 SIGNIFICANCE OF VORTEX SHEDDING

The significance of the phenomena of vortex shedding is investigated by analysing the dynamic response in the y-direction due to a loading spectrum with and without a peak at the vortex shedding frequency, see Figure 111. All combinations with a flexible foundation are considered with this investigation. This means that a total of 1500 combinations is used to provide an indication of the significance of vortex shedding.

It should be mentioned that this investigation only provides an indication about the significance of vortex shedding. The occurrence of vortex shedding is a complex phenomenon which is still hard to predict. Also, accurate analysis procedure are still lacking (National Research Council of Italy, 2008). Therefore, using assumptions, this research provides an indication of the significance which can be used in preliminary design. Also, this can be used to proceed with more detailed analysis procedure in later design stages.

10.5.1 The vortex shedding frequency

The vortex shedding frequency is given by equation (4.2), which depends on the Strouhal number, the wind velocity and the width of the building. The Strouhal number depends on the ratio d/b, and the wind velocity on the height h. The dependency of the wind velocity on the height is relatively small. Therefore, the vortex shedding frequency is mainly depending on the width and depth of the building, see Figure 115.
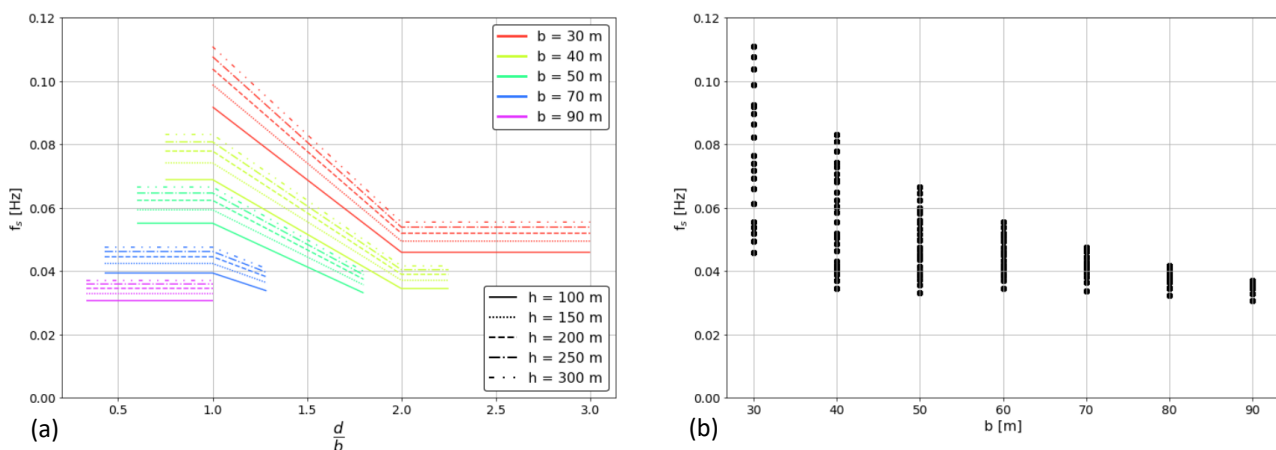
Figure 115: Vortex shedding frequency plotted against the d/b ratio (a) and the building width b (b)

Within the domain studied in this research, the vortex shedding frequency has a value within a certain frequency domain. Also, the first fundamental frequency of the building of all variants studied in this research, are within a certain frequency domain. The density of the number of variants of both is shown in Figure 116.
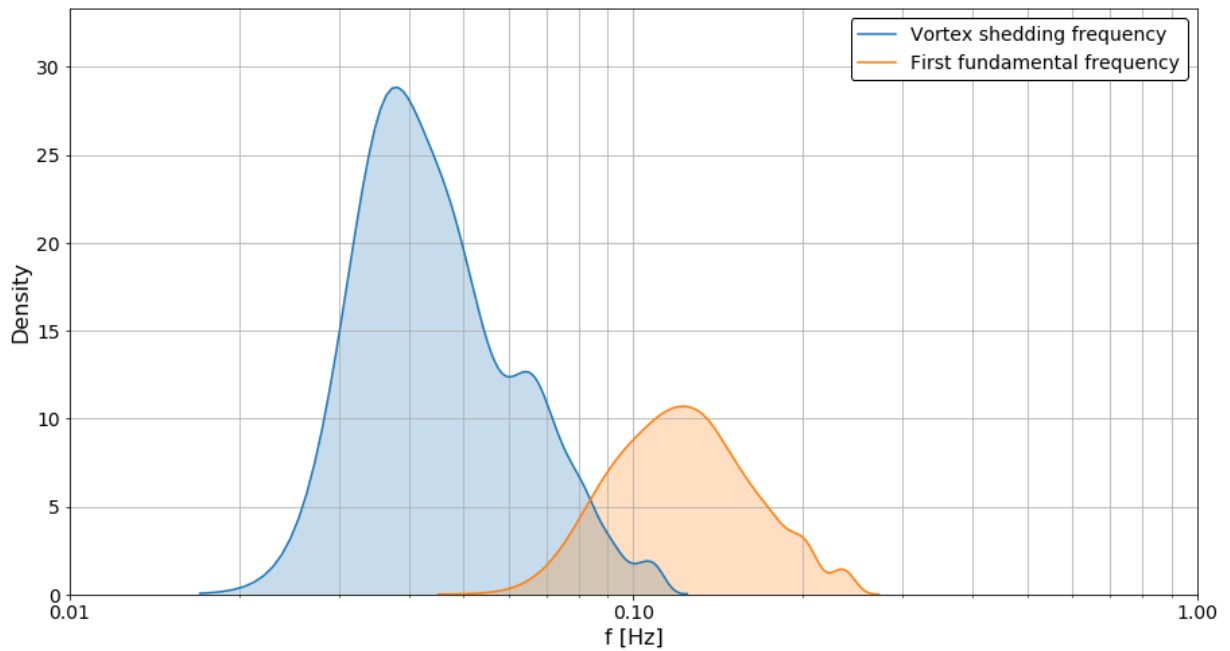
Figure 116: Density plot of the vortex shedding frequency and the first fundamental frequency of the building of all variants studied in this research

In general, the closer the first fundamental frequency is to the vortex shedding frequency, the higher the response due to the vortex shedding load. From Figure 116, it becomes clear that in many cases, the vortex shedding frequency is far from the first fundamental frequency of the building, and therefore, the response due to the vortex shedding load can be neglected. However, the question is: how far should the vortex shedding frequency and the first fundamental frequency be apart to neglect the contribution due to the vortex shedding load? And: How significant is the response due to a vortex shedding load in the case that the frequencies are close together? These two questions will be answered in the next section.

10.5.2 Results

The ratio of the difference between the maximum acceleration with and without a vortex shedding load, to the maximum acceleration without a vortex shedding load, is given by $\Delta_{yv,a}$, see equation (10.4). Therefore, a $\Delta_{yv,a}$ of, for example a 100%, means that the maximum acceleration with the vortex shedding load is double the maximum acceleration without the vortex shedding load in the y-direction.

As mentioned before, the closer together the vortex shedding frequency and the fundamental frequency of the building are, the larger the contribution of the vortex shedding load to the maximum acceleration. This is shown in Figure 117. The contribution of the vortex shedding load to the maximum acceleration is plotted against the ratio of the fundamental frequency of the building over the vortex shedding frequency. The fundamental frequency of the building is larger than the vortex shedding frequency in all cases (ratio $>$ 1). The large amplification of the response ($>$ 100%) is visible for cases where both frequencies are close together (ratio $<$ 1.5). The extreme cases show values up to 950%. This means that the maximum acceleration including a vortex shedding load is 9.5 times larger than the maximum acceleration without a vortex shedding load. Situations where both frequencies are this close together, should always be avoided. From Figure 117, it can also be seen that the contribution is always lower than 5% for building of 100 meters high. For buildings of at least 150 meters high, the contribution is always lower than 5% if the fundamental frequency is at least 3 times larger than the vortex shedding frequency. This results in the general conclusion that the phenomenon of a vortex shedding load can become significant for buildings of at least 150 meters high. And, that it is safe to neglect the contribution of a vortex shedding load to the maximum acceleration at the top of the building, if the fundamental frequency of the building is at least 3 times larger than the vortex shedding frequency.
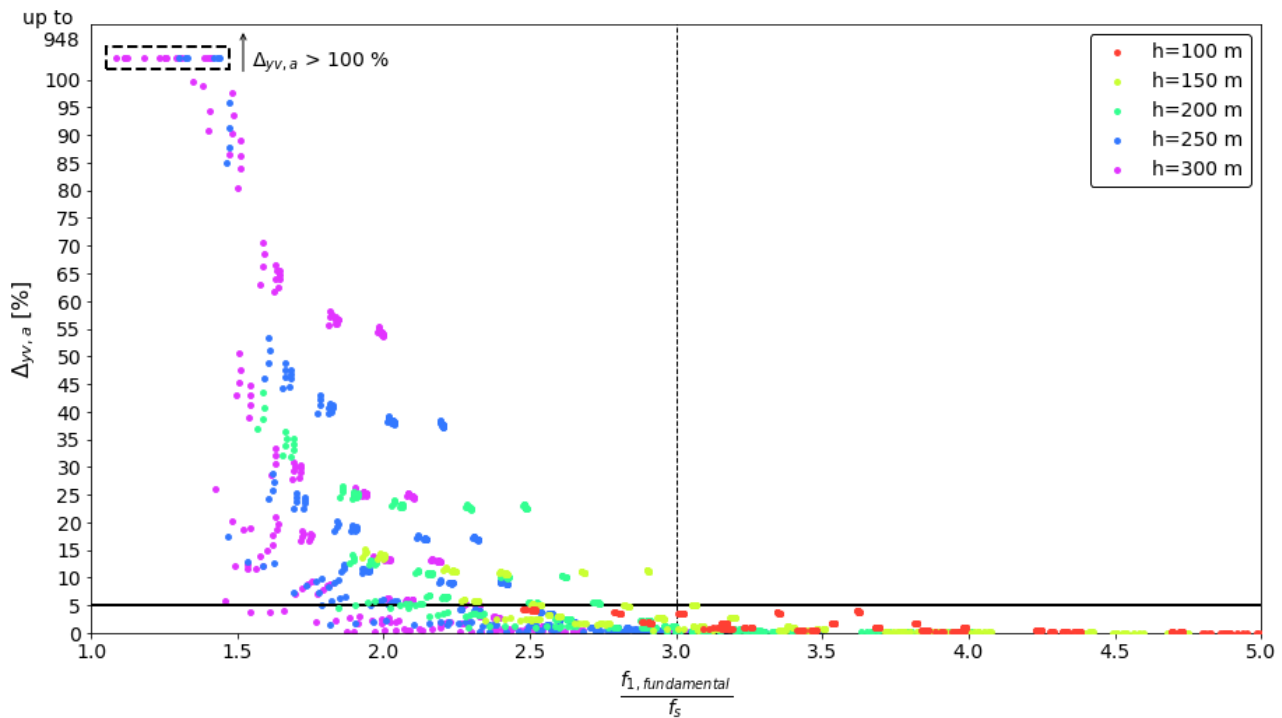
Figure 117: Contribution of the vortex shedding load to the maximum acceleration, plotted against the ratio of the fundamental frequency of the building over the vortex shedding frequency

As can be seen in Figure 117, when the fundamental frequency is less than 3 times the vortex shedding frequency, the contribution can still be lower than 5%. This mainly has to do with the slenderness. The contribution is plotted against the slenderness ratio h/d in Figure 118. It can be seen that the contribution increases with increasing slenderness ratio. The maximum value (948%) is reached for a slenderness of 10. Zooming in to a contribution till 100%, shows that the contribution can become larger than 5% for slenderness ratios larger than 3.5. The contribution is always larger than 5% for slenderness ratios larger than 6.0. It also shows that the contribution is larger than 50% for a slenderness ratio of 10. From this it is concluded, the more slender the structure, the more vulnerable the structure becomes to a vortex shedding load.
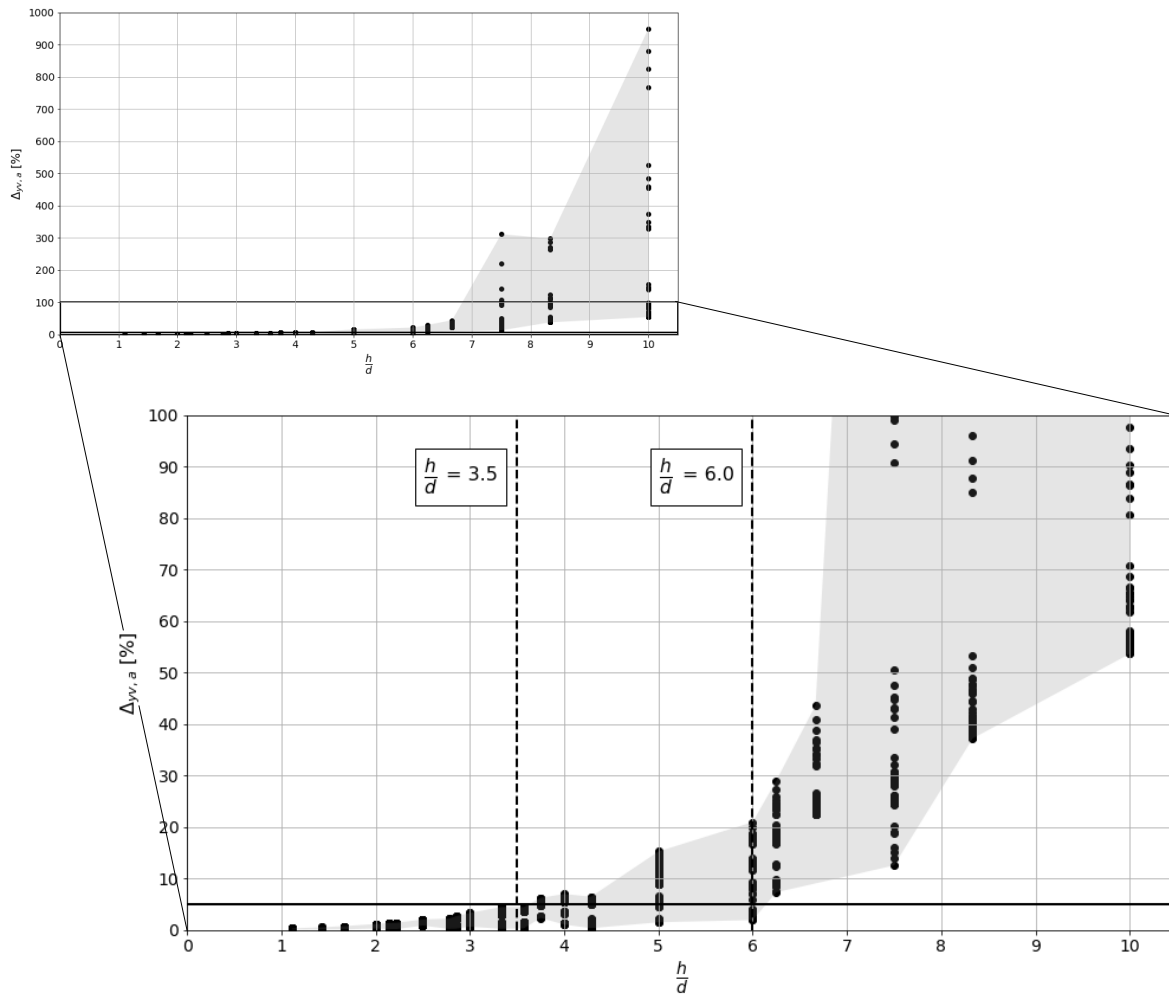
Figure 118: Contribution due to the vortex shedding load to the maximum acceleration, plotted against the slenderness ratio h/d

10.6 SUMMARY

The conclusions and recommendations in this research are based on the results of a simplified representation of a high-rise building. In the analysis procedure, multiple assumptions and simplifications are made. This should always be kept in mind when using the results of this research.

This chapter shows the results of the application of the analysis procedure in the two orthogonal response directions. The two response directions are analysed separately, under the assumption of uncoupled response directions.

First, the comparison between the x- and y-direction for square cross-sections is made. It is shown that the analytical expressions used for the SSI model variables, do not result in equal stiffness and damping values in the two directions. The rotational damping value (C_r) and the translational stiffness value (K_x) show almost equal values for both directions. The translational damping value (C_x) shows larger values in y-direction. The largest difference is 1.16 times larger in y-direction than in x-direction, and is decreasing for larger foundation depth and increasing for larger building width/depth. The rotational stiffness value (K_r) is also larger in y-direction with the largest differences of 1.47 times. It is also influenced by the foundation depth and the building width/depth.

The different wind load spectra in both directions also show differences. It is shown that the u-component of the wind load spectrum (along wind) is larger than the v-component of the wind load spectrum (across wind) for low frequencies ($< 0.022\ \text{Hz}$). However, for frequencies larger than $0.022\ \text{Hz}$, the v-component of

the wind load spectrum takes larger values than the u-component of the wind load spectrum. This means, the dynamic load for the across-wind response is larger than the dynamic load for the along-wind response for frequencies larger than 0.022 Hz.

The differences in parameters in both directions result in a difference in the maximum acceleration of the structure in both directions. It is shown that, for square cross-sections, the maximum acceleration in the y-direction is larger than the maximum acceleration in the x-direction, in 99% of the cases for a medium or stiff soil profile and 95% of the cases for a soft soil profile. The difference goes up to a maximum acceleration which is 1.14 times larger in y-direction than in x-direction. The soil profile has an influence on the ratio between the maximum acceleration in both directions. For a soft soil profile, the ratio decreases. It should be emphasized that these results are mainly caused by the difference in the wind load spectra and the foundation variables on both directions. Especially the differences in the wind load spectra are determinative for the results. Also, the coupling between the response directions is not taken into account in this analysis. Further research is needed to verify the results of this investigation. Based on the results on this research, it is recommended to analyse both directions (along wind and across wind) to find the maximum acceleration of the structure.

Second, the significance of vortex shedding is investigated. The maximum acceleration is determined with a wind load spectrum with and without a vortex shedding load. In this way, the contribution of the vortex shedding load to the maximum acceleration is determined. It is shown that the contribution can become large when the vortex shedding frequency and the fundamental frequency of the building are close together. The maximum acceleration is up to 9.5 times larger in particular cases. In these cases, a large amplified response is present, which should always be avoided. When the fundamental frequency is at least 3 times larger than the vortex shedding frequency, the contribution of the vortex shedding load can be neglected ($< 5\%$). When they are closer together, the contribution is mainly determined by the slenderness ratio h/d. For buildings of 100 meters high, the contribution is always lower than 5%. When the h/d-ratio is larger than 3.5, the contribution can become larger than 5%. When the h/d-ratio is larger than 6.0, the contribution is always larger than 5%. In general, the phenomena of vortex shedding can become significant for buildings of at least 150 meters high, with a h/d-ratio larger than 3.5 and a fundamental frequency lower than 3 times the vortex shedding frequency. Also this general indication is based on an analysis procedure including many assumptions and simplifications and should not be considered as a "general truth".

CHAPTER $\boxed{11}$

DISCUSSION, CONCLUSIONS, RECOMMENDATIONS AND FUTURE RESEARCH

This chapter provides a discussion about the results and the most important assumptions made in this research. After, the conclusions are summarized and future research is proposed.

11.1 DISCUSSION

The design of a high-rise building is a complex task in which many disciplines come together. The preliminary design is characterized by many design alternatives, many design changes and the availability of relatively limited amount of time. The structural engineer should be able to make informed and well-argued recommendations and come up with the best possible solution. This is true for all aspects related to the structural design. For higher and more slender structures, the wind-induced dynamic behaviour of the structure becomes more and more important. To secure the comfort of the inhabitants of the building, the maximum acceleration of the structure should be controlled and limited to certain levels. Due to the complex nature of the dynamic behaviour of high-rise buildings, capturing the complete dynamic response and obtaining insight into the consequences of design decisions, may require advanced dynamic analysis. The limited time in the preliminary stage of design may not allow for such type of analysis procedures. For practice, this creates the demand for a quick insight into the influence of the main parameters in design on the maximum acceleration, without performing a complete dynamic analysis. This insight will allow for well-argued design decisions and a better control of the wind-induced dynamic response, already in the preliminary stage. This is where the generated data in this research can add its value for practice.

To obtain this insight, the analysis procedure as shown in Figure 11, is performed. The maximum acceleration of the structure is determined with a spectral analysis, using a three-degree-of-freedom model representing a high-rise building including a flexible foundation. This model is able to analyse the dynamic response in one response direction per iteration. This means that the two orthogonal response directions can be analysed separately by applying the analysis procedure in each direction. In this way, the coupling between the response directions is not taken into account. The significance of this coupling is still unknown. The simplified representation is chosen to be able to isolate the dependency of the main parameters, by limiting the amount of model variables. The more variables are incorporated in the analysis, the harder it becomes to isolate dependencies. Taking into account the coupling between the response directions, will result in more model variables.
Another limitation of the three-degree-of-freedom model is, that it is able to capture only three modes of vibration. Therefore, the model is not suitable to provide accurate predictions for higher modes of vibration. In this research, a fundamental assumption is made to consider the first two modes of vibration of a building with a flexible foundation. This assumption will be discussed later.

In a spectral analysis, the wind load is represented in the form of a wind load spectrum. A literature study is performed to determine the most representative wind load spectra for the Netherlands for both the fluctuating part of the wind in alongwind and acrosswind direction, as the load from vortex shedding. For the determination of these spectra, multiple assumptions are made, e.g. the logarithmic relation of the wind velocity over the height, the turbulence intensity of the wind, the shape factor, the spectral density functions, the bandwidth of the vortex shedding load and the standard deviation of the vortex shedding load. This has the consequence that the results of this research, are depending on these assumptions. Therefore, the maximum values of acceleration itself, may deviate when other assumption are applied. However, the main focus of this research is to provide inside into the influence of the main parameters instead of the accurate prediction of the maximum acceleration. This insight is presented relative to a reference value. When different assumption for the wind load spectra are applied, both values will change. For the fluctuating part of the wind load, it is expected that the influence of the main parameters on the maximum acceleration will not change dramatically. The choice for the spectral density function will have the largest influence on the results because it defines the energy content in the frequency domain. The results regarding the phenomenon of vortex shedding, should be handled with more suspicion. This phenomenon in itself is very complex and is represented in a simplified manner in this research. The results are expected to change if different assumptions are made. Especially the bandwidth and the standard

deviation of the vortex shedding load are determinative for the results. The conclusions regarding this topic, should solely be used as indication.

Realistic ranges for the main parameters, as shown in Table 2, are determined based on literature and hand calculations. To be able to provide insight into the influence of changes in the main parameters, reference values are chosen. In this way, the influence is always relative to the reference value. Choosing a different reference value will result in a different influence. It is not expected that a different reference value for the stiffness, mass or damping value of the superstructure will result in significantly different influence lines. However, to provide the exact influence lines, the analysis procedure should be re-performed with different reference values.

The indirect model variables related to the superstructure (equivalent stiffness, mass and damping value), are determined using the modal properties of a clamped beam. The analysis procedure is applied twice, with the modal properties of the clamped beam of the first and second mode of vibration. The assumption is made that the first run is representative for the first mode of vibration, and the second run for the second mode of vibration, of a high-rise building including a flexible foundation. It should be emphasized that, due to this assumption, the conclusions related to different modes of vibration provide an indication instead of an accurate prediction. This is especially important to keep in mind for the results regarding the contribution of the second run, and the effective modal damping ratios.

The SSI-effects are taken into account by the model variables related to the foundation (rotational and translational stiffness and damping value). Because it is not the aim of this research to accurately predict parameter values, the foundation variables are determined by analytical expressions from (Gazetas, 1991), shown in Table 10. The analytical expressions from (Gazetas, 1991) are compared with other references and show best resemblance with 2D PLAXIS calculations. These expressions are based on multiple assumptions. The most important are: linear elastic soil behaviour, no material damping of the soil, no stiffness degradation of the soil and no gap between the soil and the foundation. The foundation variables are expected to change when different assumptions are made. This change in foundation variables may result in different conclusions. Especially a change in the rotational foundation parameters (stiffness and/or damping value) may result in different conclusions, because these are dominant for the maximum acceleration of the structure.

The cross-sectional dimensions of the foundation are always equal to the cross-sectional dimensions of the building in this research. This is done to limit the amount of variants in this research, but does not necessarily have to be the case in reality. Especially the horizontal depth of the foundation (d) plays an important role for the maximum acceleration of the structure. A larger horizontal depth enables a larger rotational stiffness and damping value, resulting in a lower maximum acceleration. Considering larger cross-sectional dimensions of the foundation than of the superstructure, can be an effective option to increase the rotational parameters of the foundation. In practice, this might be hard to realize considering the often limited available space in the densely urbanised cities. Another option to increase the rotational foundation variables are the foundation piles. In this research, only the rotational stiffness is increased by a pile factor. The influence of the pile factor is shown in the case-study. This pile factor is highly dependent on the type and amount of piles, the depth of the pile tip and the soil conditions, amongst others. The contribution of the piles to the horizontal, but especially the rotational foundation variables should be determined carefully in the design process. This is especially important for higher and more slender structures, because the foundation has an increasing influence on the maximum acceleration for higher and more slender structures.

Three representative soil profiles ("soft", "medium" and "stiff") are determined based on information from sections and CPT's of the three cities with currently the largest number of high-rise buildings in the Netherlands (Rotterdam, Amsterdam and The Hague). It is likely that future high-rise buildings will be located in similar urban areas. When the equivalent soil characteristics are similar to those of the three

representative soil profiles, the results from this research can be used. When ground conditions are significantly different, it is advised to re-perform the analysis procedure with adjusted soil conditions.

The equivalent stiffness, mass and damping ratio of the superstructure are determined using the modal properties of a clamped beam model. In this model, the bending stiffness and mass density are considered constant over the height of the structure. The consequences of non-constant mass and stiffness over the height of the structure on the first two natural frequencies of the system are shown in this research (chapter 7). The use of the clamped beam model results in the fact that the foundation flexibility is not taken into account in the consequences for the first two natural frequencies of the system. It is expected that this fact has no large influence on the accuracy of the total analysis procedure because the foundation flexibility is taken into account in the three-degree-of-freedom model.

The research question is answered using three separate influence studies. Each influence study focusses on a particular group of parameters. By doing so, the influence of each parameter on the maximum acceleration of the structure is isolated. As extension of the research, the complete analysis procedure is applied in the two orthogonal translational response directions. A comparison between the maximum acceleration in the two response direction is made for square cross-sections. As mentioned, the two response directions are analysed separately and therefore the coupling between the two directions is not taken into account. However, the coupling might have a significant influence on the response in both directions.

Also, an exploratory investigation is performed into the significance of the phenomenon of vortex shedding. The simplifications and assumptions of the vortex shedding load are already discussed. The response due to the vortex shedding load is only considered at the top of the structure. However, it can also cause a peak acceleration at a different height, as explained in section 4.1.2. Besides, the assumption is made that the movement of the building does not influence the vortex shedding load. These kind of assumptions and simplifications may result in conclusions that are not entirely in line with reality. The phenomenon of vortex shedding is very complex and could be a topic for a thesis on its own. Therefore, the results shown in this thesis should solely be used as indication.

11.2   CONCLUSIONS AND RECOMMENDATIONS

As discussed in previous section, multiple assumptions and simplifications are made in this research. The resulting conclusions and recommendations are based on the results of a simplified representation of a high-rise building in the Netherlands. The fact that this representation does not exactly reflect the reality, should always be kept in mind when using the results of this research.

The literature study and generated data in this research are used to answer the research question. The main research question is as follows:

What are the influences of the parameters: geometrical dimensions, mass, stiffness, and damping ratio, of both the superstructure as the foundation, on the wind-induced dynamic response of high-rise buildings in the Netherlands?

First, the main conclusions of the analysis procedure are given. Then, the answer on the main research question and main conclusions of the influence studies are provided. Finally, the conclusions of the comparison of the maximum acceleration in the two orthogonal response directions and the exploratory investigation into the significance of the phenomenon of vortex shedding are summarized.

As explained in the introduction, two approaches are used in this research to draw conclusions: a generic approach and a case-specific approach. The reason why these two approaches are used is explained hereafter. The general conclusions and recommendations resulting from the generic approach are summarized in this section.

The analysis procedure

- The structural design of a high-rise building is a multi-variable problem with a large amount of parameters. This research has reduced the number of input parameters to the nine main parameters of the structural design, as shown in Table 2. Assuming a realistic step size for each parameter, the total number of combinations is around 25 million. This number of combinations is too large to be analysed. Therefore, three different influence studies are performed. Each influence study focusses on a different parameter group. The number of combinations per influence study goes up to 2000. The average calculation time for each iteration is approximately 30 seconds. The calculation time of 30 seconds is reached by optimizing the calculation process. Initially, the calculation time was up to two minutes per iteration. The optimized calculation process resulted in a total computation time of approximately 17 hours per influence study. The computation time can be reduced by making use of faster computers. Besides the input parameters, the generated datasets also contains indirect parameters. Those indirect parameters, like the slenderness h/d, are generated to be used to isolate dependencies. Also the model variables are used for this purpose. In total, the datasets contain around 20 attributes that are used to determine the dependencies of the main parameters. This high dimensionality of data results in the general conclusion that not all information obtained within this research can be presented by the medium of a report. The influence of the different parameters can be plotted together. However, the higher the dimensionality of the data plotted in one graph, the more difficult it becomes to understand the message. In this research, plots with a dimensionality up to seven are presented (e.g. Figure 98). A graph with a dimensionality of seven is found to be difficult to comprehend. Especially for working practice, graphs with a dimensionality higher than four are not recommended. To reduce the dimensionality of data, certain parameters have to be fixed. Throughout this research, multiple examples have shown that the dependencies and influence of the main parameters can be presented when particular parameters are fixed or grouped/clustered. For the design process this is also realistic, because certain parameters are fixed in early design stages. For example, the geometrical dimensions of the building are one of the first parameters which are usually fixed in the design. In section 8.4, this is illustrated with an example. For plotting the influence of the geometrical dimensions, 12 different 5-dimensional plots are necessary. By reducing the dimensionality of the plots to 3, to make them suitable for practice, 300 different plots are necessary. Hundreds of different plots needs to be generated to present the influence of all parameters. This is considered as not realistic for working practice. Therefore, the best solution to obtain all knowledge from the datasets generated in this research, is a digital environment/ platform. By the use of filters, the dimensionality can be reduced and the influence of the main parameters can be visualised for every single case within the domain of this research. This allows for a quick insight into the influence of the main parameters, with which informed decisions can be made in practice.
- The use of simplified models to understand and estimate the complex reality is inevitable in many fields of engineering. This is especially true for the analysis of the dynamic behaviour of structural systems. In this research, it is encountered that it is sometimes unavoidable to run large amounts of iterations to completely understand the behaviour of the model and detect errors in the programming. This ultimately results in a better analysis procedure, but requires time. In practice, in the preliminary stage of design, it might be the case that this time is not available. This strengthens the demand for well-established and verified methods or instant insight without performing a complete dynamic analysis, for which the iteration process is not required. This second option is where this research can add its value for the structural engineer in practice.

Parameter influence studies

- The model used in this research is a simplified representation of a high-rise building including a flexible foundation. To identify the consequences of simplifications, two limitations of the analysis procedure are investigated in this research.
    - o The superstructure is represented by a mass with 1 degree-of-freedom, connected to the foundation by a spring and a dashpot on height h. Therefore, only one representative stiffness, mass and damping value can be used for the superstructure. To be able to use this model in the case of unequal mass and/or stiffness over the height of the structure, the consequences of this unequal mass and/or stiffness on the first two natural frequencies of a clamped beam system are investigated. The results are presented by means of frequency factors. These frequency factors take into account the consequences of a unequal mass and/or stiffness on the first two natural frequencies of the clamped system. Simple formulas can be used to estimate the first two natural frequencies. These frequency factors take values up to 1.74, which means a 74% higher frequency than if the average values of the system are used. This maximum value is found for a five times larger mass of the bottom part than the top part and a separation height of $0.1h$. This influence is of such magnitude, that it can have a significant influence on the maximum acceleration of the structure. The importance of an accurate prediction of the natural frequency of the system is illustrated with the case-study in this research. The difference in the fundamental frequency, of the two parameter sets considered for the case-study, is 45% relative to the smallest value. Ultimately, the difference in the maximum acceleration between the two parameters sets is 38%, relative to the smallest value. This difference is not entirely to be appointed to the higher fundamental frequency, but it does play an important role. An analysis procedure is proposed to estimate the equivalent parameters to be used in the model, in the case of unequal mass and/or stiffness over the height of the structure.
    - o The contribution of the second run of the analysis procedure to the maximum acceleration of the structure is investigated. The contribution is defined as the percentual increase of the maximum acceleration considering both runs, relative to the maximum acceleration if only the first run is considered. The determinative assumption underlying this analysis, is already discussed in previous section. For a clamped foundation, the maximum contribution is found to be 4.3%. Therefore, the contribution of the second run can be neglected in the case of a clamped foundation. In the case of a flexible foundation, the maximum contribution is found to be 55.1%. This high contribution value may provide a distorted view of the reality. It is expected that the used parameters are not realistic for structures with large heights (300 meters), since unacceptable maximum accelerations are found. The results of this investigation provide an indication of the contribution of the second run, but should not be considered as actual truth. The results can be considered as conservative, since the contribution is expected to be lower in reality. This maximum value is found for a h/d-ratio of 10. The slenderness ratio h/d is introduced to provide a general indication of the contribution of the second run to the maximum acceleration. Due to the variation of the other seven input parameters, there is an increasing spread in the data for increasing h/d-ratios. This spread ranges from 5% for a h/d-ratio of 3.5, to 44% for a h/d-ratio of 10.0. It is observed that the contribution is always lower than 5% for buildings of 100 meters high or buildings with a h/d-ratio lower than 3.5. For buildings with a h/d-ratio larger than 7.0, the contribution is always higher than 5%. In this latter case, it is recommended to always consider the second mode of vibration. The general recommendation is provided to take the second mode of vibration into account for buildings of at least 150 meters high, with a h/d-ratio of at least 3.5.

- The significance of a flexible foundation is shown in section 8.5. The maximum acceleration of a system with a flexible foundation is found to be up to 3.3 times larger than for a clamped foundation. This emphasises the importance to take into account the flexible foundation and the soil-structure interaction effects in the dynamic analysis. Design graphs are provided which can be used to estimate the increase factor of the maximum acceleration for a flexible foundation based on the maximum acceleration of a clamped foundation. Using the upper limit in the graphs will result in a conservative estimation of the maximum acceleration, which can be used for design purposes. However, it is not recommended to use these graphs for the final comfort checks because there can be a relatively large spread in the data (up to a difference in increase factor of 1.1). This may result in a significant overestimation of the maximum acceleration. To prevent this overestimation, a dynamic analysis including the effects of a flexible foundation and the soil-structure interaction effects should be performed. An example of such analysis is the calculation procedure used in this research. This kind of analysis is recommended for the final comfort check.

- The influence of the main parameters is shown by three separate influence studies. Each influence study isolates the influence of a particular group of parameters (1: geometrical dimensions, 2: foundation parameters, 3: superstructure parameters). As mentioned before, the influence cannot be shown in a generic manner. Therefore, particular cases are visualised in this research. Here, the general trends and maximum influence values are summarized:

    1. From the geometrical dimensions, the height and the depth of the building have the largest influence on the maximum acceleration with maximum values up to 201% and 577% respectively, relative to the lowest value. The building width has the lowest influence with a maximum value of 39%, relative to the lowest value. The depth of the building has such a high influence due to the increasing rotational stiffness and damping value in the foundation. In general, it can be stated that the influence of the geometrical dimensions increases for softer foundation conditions.

    2. Regarding the foundation, the rotational variables (K_r, C_r) are dominant over the translational variable (K_x, C_x) and can have a large influence on the maximum acceleration of the structure. The influence is increasing for increasing height. Any possible way to increase the rotational stiffness and damping value can therefore lead to a significant reduction in the maximum acceleration. For example, the variation of the pile factor in the case study results in a maximum decrease in the maximum acceleration of 22%. Is should be mentioned that higher pile factors than applied in this research are possible. The contribution of the piles to the rotational model variables can be increased by, for example, extending the piles to deeper sand layers. The foundation depth and the soil profile have more or less the same influence with maximum values of respectively 75% and 72%, relative to the lowest value. The soil profile, and therefore indirect the location of the building, has a determinative influence on the dynamic behaviour. However, the soil profile is not something that can be changed in the design for a fixed location.

    3. From the superstructure parameters, the stiffness has the largest influence on the maximum acceleration for lower buildings (100 meters). Although this parameter also has the largest range. The influence of the stiffness decreases for increasing height, resulting in almost no decrease of the maximum acceleration for a building of 300 meters high on soft foundation conditions. For buildings with such height, an increased stiffness of the superstructure is not recommended as effective solution. An increased damping value will be a more efficient option, although artificial damping devices might be needed for this. The damping value has the second largest influence and is also depending on the height of the structure on soft soil conditions. The mass density has the lowest influence, which is partly to be appointed to the relatively small parameter range.

Application in two response directions

- The comparison between the two orthogonal translational response directions is made for square cross-sections. The comparison is based on the calculated maximum acceleration in both directions due to the u- and v-component of the wind load spectrum. The results show that the maximum acceleration in the y-direction (acrosswind) is larger than the maximum acceleration in x-direction (alongwind), in 94% of the cases for a soft soil profile, and even 99% of the cases for a medium or stiff soil profile. A maximum ratio between the two maximum accelerations of 1.14 is found, for a foundation depth of 14.0 meters. This means that the maximum acceleration is 14% larger in y-direction than in x-direction. The coupling of the two response directions is not taken into account in this research but is expected to have an influence on the results. Based on the results of this investigation, the general recommendation is provided to analyze both the alongwind response and the across wind response for buildings with square cross-sections.
  The differences in the wind load spectra are determinative for the results. The v-component (across-wind) of the wind load spectrum takes larger values, up to 1.36 times the u-component (along-wind) of the wind load spectrum, for frequencies larger than 0.022 Hz. This is a result of the used wind load spectra from literature. The foundation variables also take different values in the two response directions for square cross-sections. This is the result of the analytical expressions used for the foundation variables. These two observations are the result of the chosen wind load spectra and expressions and are not further investigated in this research.
- The significance of the phenomenon of vortex shedding is investigated by comparing the maximum acceleration of the structure due to a load spectrum with and without the vortex shedding load. Theoretically, the contribution of the vortex shedding load may become large when the vortex shedding frequency and one of the natural frequencies of the building are close together. This is confirmed by the results of the analysis, which show maximum accelerations up to 9.5 times larger when the vortex shedding frequency is close to the fundamental frequency of the building. It is shown that the contribution due to the vortex shedding load can be neglected ($< 5\%$), if the fundamental frequency of the building is at least three times larger than the vortex shedding frequency. The h/d-ratio has a large influence on the contribution of the vortex shedding load. In general, the higher this ratio, the higher the contribution of the vortex shedding load. It is concluded that the phenomenon of vortex shedding can become significant for buildings of at least 150 meters high, with a h/d-ratio larger than 3.5 and a fundamental frequency lower than three times the vortex shedding frequency. This conclusion should solely be used as an indication.

As overall conclusion of the research, the importance of taking into account the flexibility and damping of the foundation should be emphasized. The rotational stiffness and damping value of the foundation can have a large influence on the dynamic response of high-rise buildings. This is especially true for higher and more slender structures. This research has shown that the influence of the superstructure parameters is decreasing with increasing height. This automatically results in an increasing influence of the foundation flexibility and damping for higher and more slender structure.

11.3   FUTURE RESEARCH

The following topics are proposed for further research:

- For a more accurate prediction of the maximum acceleration of the structure, it is recommended to do more research into the determination of the wind load spectra. This can be done by real time measuring of the wind, using wind tunnel testing or with advanced CFD techniques. Building and location specific aspects may can be taken into account.
  A determinative characteristic of the u- and v-component of the wind load spectra used in this research, is that the v-component takes larger values than the u-components for frequencies

higher than 0.022 Hz. This is partly the reason why the maximum across-wind acceleration is larger than the maximum along-wind acceleration in the majority of cases in this research. Further research into the determination of the wind load spectra is recommended to verify if, and for which cases, the v-component is actually larger than the u-component;

- For the creation of all variants analysed in this research, parameter ranges are determined based on literature and hand calculations. These ranges are assumed to be realistic in a design situation. However, for large heights and soft foundation conditions, the calculated maximum accelerations exceed the maximum lines. For these cases, measurement need to be taken to limit the maximum accelerations. Also, from the comparison of the originally calculated values and measurements, deviations are found. More research into a more accurate prediction of the design parameters, may lead to a better estimation and control of the dynamic response. This is especially true for the stiffness and damping ratio of the superstructure, because these two parameters include many uncertainties;

- Further research into the SSI-effects is advised. The consequences of the assumption made in this research are recommended to investigate thoroughly. This would mean that the following aspects are considered for the SSI-effects: non-linear soil behaviour, material damping of the soil, stiffness degradation of the soil and the occurrence of a gap between the soil and the foundation. From further research, it can also be verified if, and for which cases, it is actually true that the rotational stiffness is larger in y-direction than in x-direction for a main load in x-direction;

- For the indication of the contribution of the second mode of vibration of a building with a flexible foundation, one fundamental assumption is made in this research. It is assumed that the first run of the analysis procedure is representative for the first mode of vibration of the building including a flexible foundation, and the second run of the analysis procedure is representative for the second mode of vibration of the building with a flexible foundation. Further research is recommended to verify this assumption with a model that is capable of capturing more/higher modes of vibration. The contribution can be estimated more accurately with a model that can capture more/higher modes of vibration. A continuous beam model including the foundation stiffness and damping can be a suitable model for this;

- In this research, the different response directions are considered separately. Therefore, the coupling between the response directions is not taken into account. Investigating the coupling of the response directions may lead to a better understanding of the dynamic behaviour of high-rise buildings. However, even more parameters need to be included in the model to investigate the behaviour. Isolating the different influences of the parameters has been one of the most difficult issues in this research. This will become even harder when the response directions are combined in one model. More research is needed to tackle this problem;

- As mentioned throughout this research, a different medium is proposed to be able to extract and transfer all knowledge from the generated data in this research. A digital platform/environment is proposed. Due to the limited available time for this research, this platform is not developed within this research. Further research is advised to investigate the best possible way to extract and present all knowledge from the generated data in this research for working practice.

NORMATIVE REFERENCES

Eurocode	Description
NEN-EN 1991-1-4	Eurocode 1: Actions on structures – Part 1-4: General actions – Wind actions

Other	Description
NTA 4614-3	Covenant high-rise buildings – Part 3: Structural safety
CNR-DT 207-2008	National Research Council of Italy Advisory committee on technical recommendations for construction Guide for the assessment of wind actions and effects on structures

REFERENCES

Abspoel, R., 2013. *Building Structures 2 - Steel part,* Delft: Delft University of Technology.

Ali, M. M. & Sun Moon, K., 2007. Structural Developments in Tall Buildings: Current Trends and Future Prospects. *Architectural Science Review,* pp. 205-223.

Balendra, T., 1993. *Vibrations of Buildings to Wind and Earthquake Loads.* 1st ed. s.l.:Springer-Verlag.

Berg, R. v. d., 2012. *Investigation of damping in high-rise buildings (appendices),* Delft: Delft University of Technology.

Berg, R. v. d., 2012. *Investigation of damping in high-rise buildings (report),* Delft: Delft University of Technology.

Bos, F., 2006. *Hybride constructie van staal en beton optimaal benut in een gestapelde opbouw,* Zoetermeer: Bouwen met Staal.

Bronkhorst, A. & Geurts, C., 2018. Slappe onderfgrond dempt trillingen van hoogbouw. *Bouwen met staal,* Issue 266, pp. 40-44.

Council on Tall Buildings and Urban Habitat, 2018. *CTBUH Year in Review: Tall Trends of 2018.* [Online]
Available at: http://www.skyscrapercenter.com/year-in-review/2018
[Accessed 28 February 2019].

Council on Tall Buildings and Urban Habitat, 2019. *CTBUH Height Criteria.* [Online]
Available at: http://www.ctbuh.org/criteria/
[Accessed 27 May 2019].

Davenport, A. & Novak, M., 2002. Vibration of structures induced by wind. In: *Harris' shock and vibration handbook.* s.l.:McGraw-Hill, pp. 29.21-29.46.

Fu, F., 2018. *Design and analysis of tall and complex structures.* s.l.:Matthey Deans.

Gazetas, G., 1991. Formulas and Charts for Impedances of Surface and Embedded Foundationa. *Journal of Geotechnical Engineering,* 117(9), pp. 1363-1381.

Gazetas, G., Dobry, R. & Tassoulas, J. L., 1985. Vertical Response of arbitrarily Shaped Embedded Foundations. *Journal of Geotechnical Engineering,* 111(6), pp. 750-771.

Gazetas, G. & Tassoulas, J., 1987. Horizontal Stiffness of Arbitrarily Shaped Embedded Foundation. *Journal of Geotechnical Engineering,* 113(5), pp. 440-457.

Geurts, A., Bentum, C. v. & Sanchez, S., 2015. Demping hoogbouw voorspeld. *Cement,* Volume 3, pp. 60-65.

Geurts, C., 1997. *Wind-Induced Pressure Fluctuations on Building Facades,* Eindhoven: Technische Universiteit Eindhoven.

Geurts, C., Sanchez, S., Dijk, S. v. & Bentum, C. v., 2015. Trilling voorspellen en dempen. *Bouwen met Staal,* Issue 243, pp. 52-55.

Gómez, S., 2019. *Energy flux method for identification of damping in high-rise buildings subject to wind.* [Online]
Available at: https://doi.org/10.4233/uuid:bc4fe937-2711-4ee0-95b7-baad7c5d234c

Gómez, S., Geurts, C. & Metrikine, A., 2018. On the importance of soil damping for tall buildings loaded by wind. *Engineering Structures,* Volume 163, pp. 426-435.

Kayvani, K., 2014. *Design of high-rise buildings: past, present and future.* Byron Bay, Southern Cross University, pp. 15-20.

Kocak, S. & Mengi, Y., 2000. A simple soil±structure interaction model. *Applied Mathematical Modelling,* Issue 24, pp. 607-635.

Koninklijk Nederlands Meteorologisch Instituut, 2011. *Windrozen van de Nederlandse hoofdstations.* [Online]
Available at: https://www.knmi.nl/nederland-nu/klimatologie/grafieken/maand/windrozen
[Accessed 2019].

Kooiman, N., Jong, A. d., Duinen, C. v. & Stoeldraijer, L., 2016. *PBL/CBS Regionale bevolkings- en huishoudensprognose 2016-2040: sterke regionale verschillen,* s.l.: Planbureau voor de Leefomgeving.

Metrikine, A., n.d. *Dynamics of Mechanical Systems and Slender Structures.* Delft: Delft University of Technology.

Metrikine, A. & Vrouwenvelder, A., n.d. *Dynamics of Structures - Part 2 - Wave Dynamics.* Delft: Delft University of Technology.

Mooneghi, M. & Kargarmoakhar, R., 2016. Aerodynamic Mitigation and Shape Optimization of Buildings: Review. *Journal of Building Engineering,* Volume 6, pp. 225-235.

National Institute of Standards and Technology, 2012. *Soil-Structure Interaction for Building Structures,* s.l.: U.S. Department of Commerce.

National Research Council of Italy, 2008. *Guide for the assessment of wind actions and effects on structures,* Rome: Italian National Research Council.

Oosterhout, G. v., 1996. *Wind-induced Dynamic Behaviour of Tall Buildings,* Delft: Delft University of Technology.

Oosterhout, G. v. & Geurts, C., 2001. Trillingen en hoogbouw: comfort en demping. *Cement,* pp. 73-75.

PLAXIS, 2019. *Manual PLAXIS 2D.* [Online]
Available at: www.plaxis.nl
[Accessed 2019].

Rana, N., 2014. Structural Forms Systems for Tall Building Structures. *SSRG International Journal of Civil Engineering (SSRG-IJCE),* pp. 33-36.

Rozemeijer, G.-J., 2002. *WRMC - 7280 Deel A: Algemene gegevens en overzicht belastingen,* Delft: abt.

Rozemeijer, G.-J., 2002. *WRMC - 7280 Deel B-1: Gewichts- & stabiliteitsberekening Toren,* Delft: ABT.

Rozemeijer, G.-J., 2003. *WRMC - 7280 Deel C-1: Fundering Toren; poeren, funderingsbalken, keldervloer, kelderwanden,* Delft: ABT.

Smith, R. & Willford, M., 2008. *Damping in tall buildings - uncertainties and solutions.* Chicago, s.n.

Spangenberg, W., 2002. *ABT.* [Online]
Available at: https://www.abt.eu/projecten/montevideo-rotterdam.aspx

Spijkers, J., Vrouwenvelder, A. & Klaver, E., 2005. *Structural Dynamics CT 4140 - Part 1 - Structural Vibrations.* Delft: Delft University of Technology.

Stathopoulos, T., 2007. Introduction to Wind Engineering, Wind Structure, Wind-Building Interaction. In: *Wind effects on buildings and design of wind-sensitive structures.* Montreal: SpringerWienNewYork, pp. 1-30.

StatisticsHowTo, 2016. *Dimensionality & High Dimensional Data: Definition, Examples, Curse of.* [Online]
Available at: https://www.statisticshowto.datasciencecentral.com/dimensionality/
[Accessed 28 October 2019].

Steenbergen, R. & Geurts, C., 2011. Praktische handvaten voor eigenfrequencies. *Bouwen met Staal,* Volume 219, pp. 46-47.

Steenbergen, R., Geurts, C. & Bentum, C. v., 2008. Trillingen veroorzaakt door fluctuerende windbelasting. *Bouwen met staal,* Issue 204, pp. 56-62.

Strathopoulos, T. & Baniotopoulos, C., 2007. *Wind effects on building and design of wind-sensitive structures.* s.l.:SpringerWien NewYork.

Treels, R., 2019. Berekeningsmethoden dynamische responsies hoogbouw. *Cement,* 6(7), pp. 29-37.

Treels, R., 2019. *Wind en slanke hoogbouw, norm overstijgend?,* Rotterdam: IMd Raadgevende Ingenieurs.

Tsukagoshi, H., Tamura, Y., Sasaki, A. & Kanai, H., 1993. Response analysis on along-wind and across-wind vibrations of tall buildings in time domain. *Journal of Wind Engineering and Industrial Aerodynamics,* pp. 497-506.

United Nations, Department of Economic and Social Affairs, 2017. *World Population Prospects 2017.* [Online]
Available at: https://population.un.org/wpp/DataQuery/
[Accessed 22 May 2019].

Vijayendra, K., Prasad, S. & Nayak, S., 2010. *Computation of Fundamental Period of Soil Deposit: A Comparative Study.* Mumbai, s.n.

Vrouwenvelder, A. & Geurts, C., 2006. Dynamica, windbelasting en voorschriften. *Cement,* pp. 20-24.

Wisse, J. & Staalduinen, P. v., 1992. Dynamische belastingen (VI). *Cement,* Volume 12, pp. 52-58.

Wolf, J. & Deeks, A. J., 2004. *Foundation Vibration Analysis: A Strength-of-Materials Approach.* Burlington: Elsevier.

Woudenberg, I. & Vambersky, J., 2003. Windbelasting, hoogbouw en regelgeving. *Cement,* Issue 6, pp. 89-94.

Zandbelt&vandenBerg, 2008. *Een studie naar Nederlandse hoogbouwcultuur,* Rotterdam: Zandbelt&vandenBerg.

APPENDICES

Appendix A

Re-writing the spectral density functions of the load

Appendix B

The derivation of the response and frequency response function of a multi-degree-of freedom system and modal properties

Appendix C

Natural frequencies, mode shapes and modal properties of a clamped beam model

Appendix D

Rough mass density calculation of the Rembrandt Tower, Zalmhaven Tower and Montevideo tower

Appendix E

Analytical expressions and graphs for the foundation stiffness values and damping values

Appendix F

Determination of the dynamic stiffness and damping value from displacement curves

Appendix G

Typical soil profiles of Rotterdam, Amsterdam and The Hague

Appendix H

Contribution of the second run to the maximum acceleration, depending on the variables: h, b, d, D and the soil profile

APPENDIX A

Re-writing the spectral density functions of the load

The spectral density functions are:

$$\frac{f\,S_{uu}}{\sigma_u^2} = \frac{36.19\,f_L}{(1 + 54.31\,f_L)^{5/3}} \qquad\qquad \frac{f\,S_{vv}}{\sigma_v^2} = \frac{11.71\,f_L}{(1 + 17.56\,f_L)^{5/3}} \tag{A.1}$$

with:

$$f_L(z) = \frac{f\,z}{\bar{u}(z)} \tag{A.2}$$

This yields:

$$S_{uu}(z,f) = \frac{\sigma_u^2}{f}\frac{36.19\,\dfrac{f\,z}{\bar{u}(z)}}{\left(1 + 54.31\,\dfrac{f\,z}{\bar{u}(z)}\right)^{5/3}} \qquad\qquad S_{vv}(z,f) = \frac{\sigma_v^2}{f}\frac{11.71\,\dfrac{f\,z}{\bar{u}(z)}}{\left(1 + 17.56\,\dfrac{f\,z}{\bar{u}(z)}\right)^{5/3}} \tag{A.3}$$

The area under the spectrum should be equal, therefore:

$$\sigma_u^2 = \int S_{uu}(z,\omega)\,d\omega = \int S_{uu}(z,f)\,df \qquad\qquad \sigma_v^2 = \int S_{vv}(z,\omega)\,d\omega = \int S_{vv}(z,f)\,df \tag{A.4}$$

Using $f = \frac{\omega}{2\pi}$, the transformation is:

$$S_{uu}(z,\omega) = S_{uu}(z,f)\frac{df}{d\omega} = \frac{1}{2\pi}S_{uu}(z,f) \qquad\qquad S_{vv}(z,\omega) = S_{vv}(z,f)\frac{df}{d\omega} = \frac{1}{2\pi}S_{vv}(z,f) \tag{A.5}$$

Thus:

$$S_{uu}(z,\omega) = \sigma_u^2\frac{36.19\,\dfrac{z}{\bar{u}(z)}}{2\pi\left(1 + 54.31\,\dfrac{\omega}{2\pi}\dfrac{z}{\bar{u}(z)}\right)^{5/3}} \qquad\qquad S_{vv}(z,\omega) = \sigma_v^2\frac{11.71\,\dfrac{z}{\bar{u}(z)}}{2\pi\left(1 + 17.56\,\dfrac{\omega}{2\pi}\dfrac{z}{\bar{u}(z)}\right)^{5/3}} \tag{A.6}$$

The standard deviations are given by the turbulence intensities:

$$\sigma_u(z) = \frac{1}{ln\left(\dfrac{z}{z_0}\right)}\,\bar{u}(z) \qquad\qquad\qquad \sigma_v(z) = \frac{0.8}{ln\left(\dfrac{z}{z_0}\right)}\,\bar{u}(z) \tag{A.7}$$

This yields:

$$S_{uu}(z,\omega) = \left(\frac{1}{ln\left(\dfrac{z}{z_0}\right)}\,\bar{u}(z)\right)^2 \frac{36.19\,\dfrac{z}{\bar{u}(z)}}{2\pi\left(1 + 54.31\,\dfrac{\omega}{2\pi}\dfrac{z}{\bar{u}(z)}\right)^{5/3}} \tag{A.8}$$

and:

$$S_{vv}(z,\omega) = \left(\frac{0.8}{ln\left(\dfrac{z}{z_0}\right)}\,\bar{u}(z)\right)^2 \frac{11.71\,\dfrac{z}{\bar{u}(z)}}{2\pi\left(1 + 17.56\,\dfrac{\omega}{2\pi}\dfrac{z}{\bar{u}(z)}\right)^{5/3}} \tag{A.9}$$

APPENDIX B

The derivation of the response and frequency response function of a multi-degree-of-freedom system and modal properties
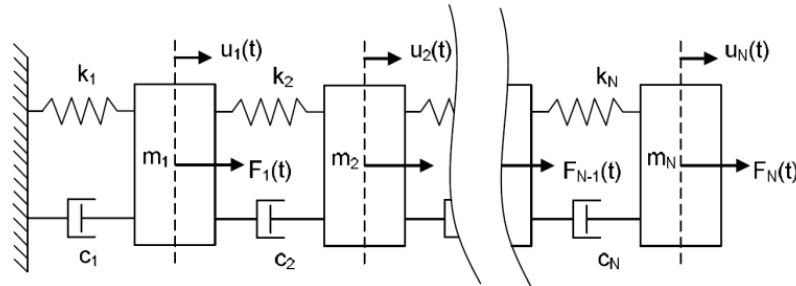
Figure 119: N-degree-of-freedom system (Berg, 2012)

The matrix notion is used for multi-degree-of-freedom systems. For this, matrices are depicted as bold capital letters (e.g. **M**) and vectors as underlined letters (e.g. $\underline{u}$ or $\underline{F}$).

The equation of motion of the system is:

$$\boldsymbol{M}\underline{\ddot{x}} + \boldsymbol{C}\underline{\dot{x}} + \boldsymbol{K}\underline{x} = \underline{F}(t) \tag{B.1}$$

The general solution is again the summation of the homogeneous and particular solution. The modal analysis method, makes it possible to find the solution. This analysis uses a superposition of the different modes of vibration. The modes of vibration are obtained by considering the free vibration of the un-damped system. (Berg, 2012)

The homogeneous solution for an undamped system is described by the coupled differential equations:

$$\boldsymbol{M}\underline{\ddot{x}} + \boldsymbol{K}\underline{x} = \underline{0} \tag{B.2}$$

As homogeneous solution, a harmonic motion is assumed, which means that all degrees of freedom vary in time in the same manner (Spijkers, et al., 2005):

$$\underline{x}(t) = \underline{\hat{x}} \sin(\omega t + \varphi) \tag{B.3}$$

Substituting the homogeneous solution into the equation of motion lead to the following requirement:

$$(-\omega^2 \boldsymbol{M} + \boldsymbol{K})\underline{\hat{x}} = \underline{0} \tag{B.4}$$

This set of equations is called the generalised eigenvalue problem. Setting the determinant of the matrix of coefficients to zero leads to the characteristic polynomial of which the natural frequencies can be found. With the natural frequencies, the associated eigenvectors can be found.

The free vibration is found as the summation of all possible eigenmodes:

$$\underline{x}(t) = \sum_{i=1}^{n} \underline{\hat{x}_i} A_i \sin(\omega_i t + \varphi_i) \tag{B.5}$$

The constants A_i and φ_i are found with the prescribed initial conditions.

The free vibration can be written as:

$$\underline{x}(t) = \sum_{i=1}^{n} \underline{\hat{x}_i} u_i(t) \tag{B.6}$$

in matrix notation:

$$\underline{x}(t) = \boldsymbol{E}\,\underline{u}(t) \tag{B.7}$$

The matrix $\boldsymbol{E}$ is called the eigenmatrix and contains the eigenvectors as columns.

Each of the time functions $u_{i,\text{hom}}(t)$ satisfies a homogeneous differential equation of the form:

$$\ddot{u}_i + \omega_i^2\,u_i = 0 \qquad\qquad\qquad i = 1,2\dots n \tag{B.8}$$

From orthogonality conditions (fully described in (Spijkers, et al., 2005)), the following matrices are introduced:

$$\boldsymbol{M}^* = \boldsymbol{E}^T\,\boldsymbol{M}\,\boldsymbol{E} \tag{B.9}$$

$$\boldsymbol{K}^* = \boldsymbol{E}^T\,\boldsymbol{K}\,\boldsymbol{E} \tag{B.10}$$

And the relation between matrices $\boldsymbol{M}^*$ and $\boldsymbol{K}^*$ is obtained:

$$\boldsymbol{\Omega}^2\,\boldsymbol{M}^* = \boldsymbol{K}^* \tag{B.11}$$

The summation of synchronised motions is the essence of the so-called Modal Analysis (Spijkers, et al., 2005). This assumption is also made for forced vibrations.

$$\boldsymbol{M}\,\boldsymbol{E}\,\underline{\ddot{u}} + \boldsymbol{K}\,\boldsymbol{E}\,\underline{u} = \underline{F}(t) \tag{B.12}$$

By making use of the found relations from the orthogonality conditions:

$$\boldsymbol{M}^*\underline{\ddot{u}} + \boldsymbol{M}^*\boldsymbol{\Omega}^2\,\underline{u} = \boldsymbol{E}^T\underline{F}(t) \tag{B.13}$$

Expression (B.13) represents a set of decoupled differential equations in the variable $\underline{u}(t)$ since the $\boldsymbol{M}^*$ and $\boldsymbol{\Omega}^2$ are diagonal matrices.

The solution of the coupled inhomogeneous systems can be found with the decoupled set of inhomogeneous differential equations:

$$\ddot{u}_i + \omega_i^2\,u_i = \frac{F_i^*(t)}{m_{ii}^*} \tag{B.14}$$

$$\begin{aligned}
F_i^*(t) &= \underline{\hat{x}}_i^T\,\underline{F}(t)\\
m_{ii}^* &= \underline{\hat{x}}_i^T\,\boldsymbol{M}\,\underline{\hat{x}}_i
\end{aligned}$$

Using the initial conditions, the undetermined constants can be found.

So, the particular solution can again be found as the summation:

$$\underline{x}_{part}(t) = \sum_{i=1}^{n}\underline{\hat{x}_i}\,u_{i,part}(t) \tag{B.15}$$

The total solution is finally the sum of the homogeneous solution and the particular solution:

$$\underline{x}(t) = \underline{x}_{hom}(t) + \underline{x}_{part}(t) \tag{B.16}$$

If the load is assumed to be a harmonic function, $\underline{F}(t) = \hat{\underline{F}} \sin(\Omega t)$, the solution also should be a harmonic function:

$$u_i(t) = \hat{u}_i \, sin(\Omega t) \tag{B.17}$$

The amplitude $\hat{u}_i$ is found by substitution in to the decoupled system:

$$\hat{u}_i = \frac{1}{\omega_i^2 - \Omega^2} \frac{\hat{\underline{x}}_i^T \, \hat{\underline{F}}}{\hat{\underline{x}}_i^T \, \boldsymbol{M} \, \hat{\underline{x}}_i} \tag{B.18}$$

If it is assumed that there is only one harmonic load active at the position of the degree of freedom p, the amplitude can be written as:

$$\hat{u}_i = \frac{1}{1 - (\Omega/\omega_i)^2} \frac{1}{\omega_i^2} \frac{\hat{x}_{pi} \, \hat{F}_p}{\hat{\underline{x}}_i^T \, \boldsymbol{M} \, \hat{\underline{x}}_i} \tag{B.19}$$

And the frequency response function is defined as:

$$H_{u_i F_p}(\Omega) = \frac{\hat{u}_i}{\hat{F}_p} = \frac{1}{1 - (\Omega/\omega_i)^2} \frac{1}{\omega_i^2} \frac{\hat{x}_{pi}}{\hat{\underline{x}}_i^T \, \boldsymbol{M} \, \hat{\underline{x}}_i} \tag{B.20}$$

The total frequency response matrix is then given by:

$$\boldsymbol{H_{u_i F_p}} = \begin{bmatrix} H_{u_1 F_1} & H_{u_1 F_2} & \cdots & H_{u_1 F_n} \\ H_{u_2 F_1} & H_{u_2 F_2} & \cdots & H_{u_2 F_n} \\ \vdots & \vdots & \ddots & \vdots \\ H_{u_n F_1} & H_{u_n F_2} & \cdots & H_{u_n F_n} \end{bmatrix} \tag{B.21}$$

The harmonic response is obtained as:

$$u_i(t) = \hat{u}_i \, sin(\Omega t) = H_{u_i F_p}(\Omega) \, \hat{F}_p \, sin(\Omega t) \tag{B.22}$$

The response in the degrees of freedom $\underline{x}(t)$ is then:

$$\underline{x}(t) = \sum_{i=1}^{n} \hat{\underline{x}}_i \, H_{u_i F_p}(\Omega) \, \hat{F}_p \, sin(\Omega t) \tag{B.23}$$

This is the steady state response, since only the particular solution is considered. This vector describes the dynamic behaviour of the whole system. Looking at one specific degree of freedom q, the individual frequency response functions can be plotted, see Figure 120.
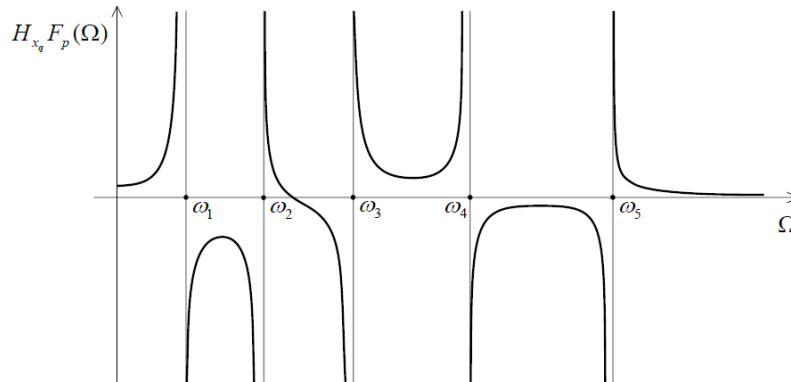

Figure 120: Frequency response function of degree of freedom q (Spijkers, et al., 2005)

Maxwell's reciprocal theorem holds (Metrikine, n.d.), therefore:

$$H_{x_q F_p}(\Omega) = H_{x_p F_q}(\Omega) \tag{B.24}$$

Using this theorem, the frequency response matrix is:

$$H_{x_q F_p} = \begin{bmatrix} H_{x_1 F_1} & H_{x_1 F_2} & \cdots & H_{x_1 F_n} \\ H_{x_2 F_1} & H_{x_2 F_2} & \cdots & H_{x_2 F_n} \\ \vdots & \vdots & \ddots & \vdots \\ H_{x_n F_1} & H_{x_n F_2} & \cdots & H_{x_n F_n} \end{bmatrix}$$

(B.25)

The following relation is found:

$$\underline{x}(t) = \boldsymbol{H}_{x_q F_p}\, \underline{F}(t)$$

(B.26)

Since harmonic time functions are present:

$$\underline{x}(t) = \underline{\hat{x}}\, sin(\Omega t) \qquad\qquad \underline{F}(t) = \underline{\hat{F}}\, sin(\Omega t)$$

(B.27)

the following is obtained:

$$\underline{\hat{x}} = \boldsymbol{H}_{x_q F_p}\, \underline{\hat{F}}$$

(B.28)

For the damped system, the equation of motion of equation (B.1) is used. For the damped vibrations, the modal analysis can be adopted as well and the forced vibration can be expanded in eigenvectors which are known from the undamped system, equation (B.6). Substitution results in:

$$\boldsymbol{M}\,\boldsymbol{E}\,\underline{\ddot{u}} + \boldsymbol{C}\,\boldsymbol{E}\,\underline{\dot{u}} + \boldsymbol{K}\,\boldsymbol{E}\,\underline{u} = \underline{F}(t)$$

(B.29)

Pre-multiplying with $\boldsymbol{E}^{\mathbf{T}}$ and using the orthogonality conditions, results in:

$$\boldsymbol{M}^*\,\underline{\ddot{u}} + \boldsymbol{C}^*\,\underline{\dot{u}} + \boldsymbol{K}^*\,\underline{u} = \boldsymbol{E}^T\,\underline{F}(t)$$

(B.30)

In equation (4.26), the $\boldsymbol{C}^*$ is called the modal damping matrix and is defined by:

$$\boldsymbol{C}^* = \boldsymbol{E}^T \boldsymbol{C}\,\boldsymbol{E}$$

(B.31)

Generally speaking, the eigenvectors are not orthogonal with respect to the damping matrix $\boldsymbol{C}$. Therefore, the modal damping matrix is not diagonal. The consequence is that the set of differential equations is only partly uncoupled, so-called damping coupling is present. Because of this coupling, the simple solution-method described before is not applicable anymore. The so-called complex modal analysis can be used to solve systems with damping coupling. It uses the assumption of non-synchronous motion of the degrees of freedom. When the damping matrix is forced to be a diagonal matrix, the simple modal analysis can be applied. (Spijkers, et al., 2005)

Proceeding with equation (B.30) with the assumption of a forced diagonal damping matrix. Using $\boldsymbol{K}^* = \boldsymbol{M}^*\boldsymbol{\Omega}^2$ and pre-multiplying with $(\boldsymbol{M}^*)^{-1}$, equation (B.30) can be written as:

$$\boldsymbol{I}\,\underline{\ddot{u}} + (\boldsymbol{M}^*)^{-1}\,\boldsymbol{C}^*\,\underline{\dot{u}} + \boldsymbol{\Omega}^2\,\underline{u} = (\boldsymbol{M}^*)^{-1}\,\boldsymbol{E}^T\,\underline{F}(t)$$

(B.32)

The decoupled system can be written as follows:

$$\ddot{u}_i + \frac{\hat{x}_i^T\,\boldsymbol{C}\,\hat{x}_i}{\hat{x}_i^T\,\boldsymbol{M}\,\hat{x}_i}\dot{u}_i + \omega_i^2\,u_i = \frac{\hat{x}_i^T\,\underline{F}(t)}{\hat{x}_i^T\,\boldsymbol{M}\,\hat{x}_i}$$

(B.33)

A relative damping ratio ξ_i per uncoupled degree of freedom is defined as:

$$2\xi_i\omega_i = \frac{\hat{x}_i^T\,\boldsymbol{C}\,\hat{x}_i}{\hat{x}_i^T\,\boldsymbol{M}\,\hat{x}_i}$$

(B.34)

And the decoupled system can be written as:

$$\ddot{u}_i + 2\xi_i\omega_i\dot{u}_i + \omega_i^2\,u_i = \frac{\hat{\underline{x}}_i^T\,\underline{F}(t)}{\hat{\underline{x}}_i^T\,\boldsymbol{M}\,\hat{\underline{x}}_i} \tag{B.35}$$

From equation (B.34), the following is determined:

$$\boldsymbol{C} = \boldsymbol{M}\,\boldsymbol{E}\,[2\xi_i\omega_i]\,\boldsymbol{E}^{-1} \qquad\qquad or \qquad\qquad \boldsymbol{C} = \boldsymbol{M}\,\boldsymbol{E}\,[2\xi_i\omega_i]\,(\boldsymbol{M}^*)^{-1}\,\boldsymbol{E}^T\,\boldsymbol{M} \tag{B.36}$$

In practice, the damping ratios ξ_i are often assumed based on experience and chosen equal for all modes. After numerical evaluation it should become apparent whether or how far the damping matrix is realistic in a physical sense. A possible conclusion can be that damping decoupling cannot be used as an assumption. Generally speaking, damping decoupling provides reasonably accurate results for structures with more or less uniform distributed damping and low damping (Spijkers, et al., 2005). This statement should be checked in analysis procedures where damping decoupling is applied.

For the forced vibrations, proceeding with equation (B.35) and a harmonic load:

$$\underline{F}(t) = \hat{\underline{F}}\,sin(\Omega t) \tag{B.37}$$

The particular solution is assumed to be:

$$u_i(t) = \hat{u}_i\,sin(\Omega t - \varphi_i) \tag{B.38}$$

The amplitude and phase shift are known from a damped single degree of freedom system:

$$\hat{u}_i = \frac{1}{\sqrt{(1 - (\Omega/\omega_i)^2)^2 + (2\xi_i\Omega/\omega_i)^2}}\frac{1}{\omega_i^2}\frac{\hat{\underline{x}}_i^T\,\hat{\underline{F}}}{\hat{\underline{x}}_i^T\,\boldsymbol{M}\,\hat{\underline{x}}_i} \tag{B.39}$$

$$tan(\varphi_i) = \frac{2\xi_i\Omega/\omega_i}{1 - (\Omega/\omega_i)^2} \tag{B.40}$$

As with the free vibrations, the frequency response function is found for a load only at point p:

$$H_{u_iF_p}(\Omega) = \frac{\hat{u}_i}{\hat{F}_p} = \frac{1}{\sqrt{(1 - (\Omega/\omega_i)^2)^2 + (2\xi_i\Omega/\omega_i)^2}}\frac{1}{\omega_i^2}\frac{\hat{x}_{pi}}{\hat{\underline{x}}_i^T\,\boldsymbol{M}\,\hat{\underline{x}}_i} \tag{B.41}$$

The frequency response matrix can again be written as:

$$\boldsymbol{H}_{u_iF_p} = \begin{bmatrix} H_{u_1F_1} & H_{u_1F_2} & \cdots & H_{u_1F_n} \\ H_{u_2F_1} & H_{u_2F_2} & \cdots & H_{u_2F_n} \\ \vdots & \vdots & \ddots & \vdots \\ H_{u_nF_1} & H_{u_nF_2} & \cdots & H_{u_nF_n} \end{bmatrix} \tag{B.42}$$

The response $u_i(t)$ can be found as:

$$u_i(t) = H_{u_iF_p}(\Omega)\hat{F}_p\,sin(\Omega t - \varphi_i) \tag{B.43}$$

And the response in the degrees of freedom $x(t)$:

$$\underline{x}(t) = \sum_{i=1}^{n}\hat{\underline{x}}_i H_{u_iF_p}(\Omega)\hat{F}_p\,sin(\Omega t - \varphi_i) \tag{B.44}$$

From equation (B.44), it can be concluded: the maximum displacement in point q is a summation of displacements in q from every mode of vibration caused by a load at p.

Because of the phase shift, the frequency response function for a specific degree of freedom $x_q(t)$, can not be found in the same simple manner as with the undamped system. Some extra work is necessary.

Ultimately, the frequency response function for a specific degree of freedom $x_q(t)$ is given by:

$$H_{x_q F_p}(\Omega) = \frac{\hat{x}_q}{\hat{F}_p} = \sqrt{\left(\sum_{i=1}^{n} \hat{x}_{qi} H_{u_i F_p}(\Omega)\cos(\varphi_i)\right)^2 + \left(\sum_{i=1}^{n} \hat{x}_{qi} H_{u_i F_p}(\Omega)\sin(\varphi_i)\right)^2} \qquad (B.45)$$

Figure 121 shows an example of the frequency response function $H_{x_q F_p}$.

The response amplitude is:

$$\hat{x}_q = H_{x_q F_p}(\Omega)\,\hat{F}_p \qquad (B.46)$$

Ultimately, the response can be found as:

$$x_q(t) = H_{x_q F_p}\,\hat{F}_p\,sin(\Omega t - \theta_q) \qquad (B.47)$$

In which:

$$tan(\theta_q) = \frac{\sum_{i=1}^{n} \hat{x}_{qi} H_{u_i F_p}(\Omega)\sin(\varphi_i)}{\sum_{i=1}^{n} \hat{x}_{qi} H_{u_i F_p}(\Omega)\cos(\varphi_i)} \qquad (B.48)$$

The frequency response matrix can again be written as:

$$\boldsymbol{H_{x_q F_p}} = \begin{bmatrix} H_{x_1 F_1} & H_{x_1 F_2} & \cdots & H_{x_1 F_n} \\ H_{x_2 F_1} & H_{x_2 F_2} & \cdots & H_{x_2 F_n} \\ \vdots & \vdots & \ddots & \vdots \\ H_{x_n F_1} & H_{x_n F_2} & \cdots & H_{x_n F_n} \end{bmatrix} \qquad (B.49)$$

As can be seen from equation (B.47), it is concluded: the response in point q is the summation of responses due to a load in all points. The amplitude of the response has a linear relation with the amplitude of the load.
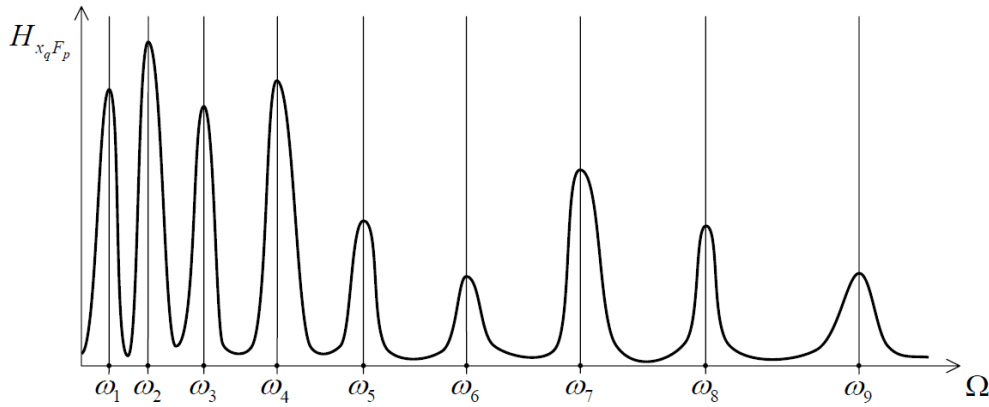
Figure 121: Example of frequency response function (Spijkers, et al., 2005)

Modal properties of discrete systems

A structure can vibrate in multiple modes of vibrations. For multi-degree-of-freedom systems, this is illustrated in Figure 122. Based on the modal analysis, the response can be derived as a summation of uncoupled modes of vibration. Therefore, the response for every mode of vibration has to be determined.

The amplitude of response for the ith mode, due to a load at all points, can be obtained by equation (B.39):

$$\hat{u}_{i,q} = \sum_{p=1}^{n} \hat{x}_{i,q} \frac{1}{\sqrt{\left(1-(\Omega/\omega_{n,i})^2\right)^2 + (2\xi_i \Omega/\omega_{n,i})^2}} \frac{1}{\hat{\underline{x}}_i^T \boldsymbol{M}\,\hat{\underline{x}}_i\,\omega_{n,i}^2} \hat{x}_{i,p}\,\hat{F}_p \qquad (B.50)$$
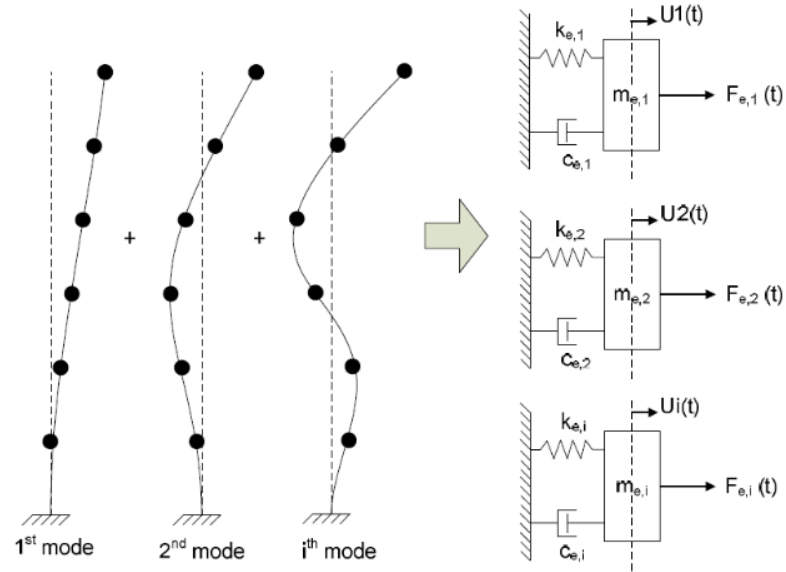
Figure 122: Modes of vibration of MDOF system and uncoupled SDOF systems per mode (Berg, 2012)

From this equation, the modal force can be derived:

$$\hat{F}_{e,i} = \sum_{p=1}^{n} \hat{x}_{i,p} \hat{F}_p = \underline{\hat{x}}_i^T \underline{\hat{F}} \tag{B.51}$$

Thus, the linear relation becomes:

$$\hat{u}_{i,q} = H_{u_q F_{e,i}}(\Omega)\, \hat{F}_{e,i} = \hat{x}_{i,q} \frac{1}{\sqrt{\left(1 - \left(\Omega/\omega_{n,i}\right)^2\right)^2 + \left(2\xi_i \Omega/\omega_{n,i}\right)^2}} \frac{1}{m_{e,i}\, \omega_{n,i}^2} \hat{F}_{e,i} \tag{B.52}$$

The modal mass, stiffness and damping are given by:

$$\begin{aligned} m_{e,i} &= \underline{\hat{x}}_i^T \boldsymbol{M}\, \underline{\hat{x}}_i \\ k_{e,i} &= \underline{\hat{x}}_i^T \boldsymbol{K}\, \underline{\hat{x}}_i \\ c_{e,i} &= \underline{\hat{x}}_i^T \boldsymbol{C}\, \underline{\hat{x}}_i \end{aligned} \tag{B.53}$$

From this derivation, the following is concluded: the maximum response in every mode of vibration can be analysed with a single-degree-of-freedom system with modal properties and a modal force.

APPENDIX C

Natural frequencies, mode shapes and modal properties of a clamped beam model

The clamped beam system is shown in Figure 123. The system parameters are assumed to be constant over the height of the beam.
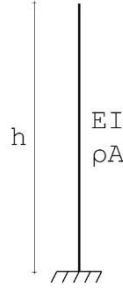
Figure 123: Clamped beam model

The equation of motion of the system is:

$$EI \frac{\partial^4}{\partial z^4} u(z,t) + \rho A \frac{\partial^2}{\partial t^2} u(z,t) = q(z,t) \tag{C.1}$$

For the free vibration, using the method of separation of variables, the eigen value problem can be obtained:

$$\frac{d^4}{dz^4} u(z) - \beta^4 u(z) = 0 \qquad\qquad \beta^4 = \frac{\rho A \omega_i^2}{EI} \tag{C.2}$$

By assuming a solution for the eigenvalue problem ($u_i(z) = e^{\lambda z}, i = 1,2$) and substitution in the characteristic equation, the solution for the free vibration is obtained. Rewriting the solution results in:

$$u(z) = D_1 \cosh(\beta z) + D_2 \sinh(\beta z) + D_3 \cos(\beta z) + D_4 \sin(\beta z) \tag{C.3}$$

To find the 4 undetermined constants, 4 equations are needed. The boundary conditions used are:

$$z = 0 \quad \begin{cases} u(0) = 0 \\ \dfrac{d}{dz} u(0) = 0 \end{cases} \qquad\qquad z = h \quad \begin{cases} EI \dfrac{d^2}{dz^2} u(h) = 0 \\ EI \dfrac{d^3}{dz^3} u(h) = 0 \end{cases} \tag{C.4}$$

The 4 equations can be written in matrix notation ($\mathbf{M} \cdot \underline{D} = \underline{0}$) resulting in $\mathbf{M}$ to be an 4x4 matrix:

$$\mathbf{M} = \begin{bmatrix} 1 & 0 & 1 & 0 \\ 0 & \beta & 0 & \beta \\ EI\cosh(\beta h)\,\beta^2 & EI\sinh(\beta h)\,\beta^2 & -EI\cos(\beta h)\,\beta^2 & -EI\sin(\beta h)\,\beta^2 \\ EI\sinh(\beta h)\,\beta^3 & EI\cosh(\beta h)\,\beta^3 & EI\sin(\beta h)\,\beta^3 & -EI\cos(\beta h)\,\beta^3 \end{bmatrix} \tag{C.5}$$

The non-trivial solution is found by setting the determinant of $\mathbf{M}$ equal to zero. By solving this equation for β, the natural frequencies of the system are found. This results in:

Mode of vibration	1	2	3	4	...
Natural frequency ω_i [rad/s]	$3.516\sqrt{\dfrac{EI}{\rho A h^4}}$	$22.034\sqrt{\dfrac{EI}{\rho A h^4}}$	$61.697\sqrt{\dfrac{EI}{\rho A h^4}}$	$120.902\sqrt{\dfrac{EI}{\rho A h^4}}$	...

Table 17: Natural frequencies of a clamped beam system with constant parameters over height

The mode shapes are found by forcing one of the constants (e.g. D_4) to be equal to 1. Solving the system and substituting in the homogeneous solution results in the mode shapes, see Figure 124.
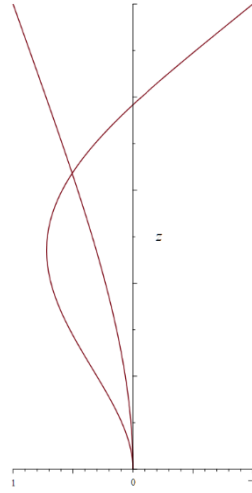
Figure 124: First and second mode shape

Modal properties

The equation of motion for a damped system is:

$$EI \frac{\partial^4}{\partial z^4} u(z,t) + \rho A \frac{\partial^2}{\partial t^2} u(z,t) + c_d \frac{\partial}{\partial t} u(z,t) = q(z,t) \tag{C.6}$$

The solution is found by making use of the method of separation of variables. The solution is assumed to be the multiplication of a coordinate and time dependent function:

$$u(z,t) = U(z)\Psi(t) \tag{C.7}$$

Substitution into the equation of motion results in:

$$EI\ U''''(z)\Psi(t) + \rho A U(z)\ddot{\Psi}(t) + c_d U(z)\dot{\Psi}(t) = q(z,t) \tag{C.8}$$

Rewriting this equation gives:

$$\left(\rho A\ddot{\Psi}(t) + c_d\dot{\Psi}(t) + \beta^4\ EI\ \Psi(t)\right) U(z) = q(z,t) \tag{C.9}$$

By making use of the orthogonality this gives for every mode:

$$\int_{z=0}^{h} \left(\rho A\ddot{\Psi}(t) + C_{d,i}\dot{\Psi}(t) + \beta_i^4\ EI\ \Psi(t)\right) U_i^2(z)\ dz = \int_{z=0}^{h} q(z,t)U_i(z)\ dz \tag{C.10}$$

Which can be written as:

$$m_{b,i}\ddot{\Psi}(t) + c_{d,i}\dot{\Psi}(t) + K_{b,i}\Psi(t) = F_{b,i} \tag{C.11}$$

The modal properties are calculated with:

$$\begin{aligned}
K_{b,i} &= \int_0^h \beta_i^4 EI\ U_i(z)^2\ dz \\
m_{b,i} &= \int_0^h \rho A\ U_i(z)^2\ dz \\
C_{d,i} &= \int_0^h c_{d,i}\ U_i(z)^2\ dz = 2\xi\sqrt{K_{b,i}m_{b,i}}
\end{aligned} \tag{C.12}$$

The modal damping ratio (ξ), is considered to be equal for both modes of vibration.

APPENDIX D

Rough mass density calculation of the Rembrandt Tower, Zalmhaven Tower and Montevideo tower

Rembrandt Tower

$h =$	135 m
top part (9 levels) =	$19.8 \times 19.8 = 392$ m^2
middle part (20 levels) =	$32.4 \times 32.4 = 1050$ m^2
bottom part (7 levels) =	$19{,}8 \times 19{,}8 = 2172$ m^2
averaged area =	1100 m^2
$b = d =$	33.2 m
# storeys =	36
storey height =	3.8 m

Concrete core

wall thickness =	0.3 m
total wall length =	100 m
total area =	30 m^2
reinf. concrete =	2500 kg/m^3
density core =	$30 \cdot 2500 = 75000$ kg/m
mass density =	$75000/1100 = 68.2$ kg/m^3

Steel columns

# columns =	32
column profile =	HD $310 \times 310 \times 143$
weight profile =	300 kg/m
density columns =	$32 \cdot 300 = 9600$ kg/m
mas density =	$9600/1100 = 8.7$ kg/m^3

Floor system

weight concrete + steel =	300 kg/m^2
weight steel beams =	17 kg/m^2
other own weight =	100 kg/m^2
total own weight =	417 kg/m^2
density floor =	$(1100 \cdot 417)/3.8 = 122320$ kg/m
mass density =	$122320/1100 = 111.2$ kg/m^3

Floor loads

live load =	300 kg/m^2
$\psi_0 =$	0.5
load =	150 kg/m^2
density loads =	$(1100 \cdot 150)/3.8 = 44000$ kg/m
mass density =	$44000/1100 = 40.0$ kg/m^3

Facade

own weight facade =	100 kg/m^2
circumference =	132.7 m
density facade =	$100 \cdot 132.7 = 13266$ kg/m
mass density =	$13266/1100 = 12.1$ kg/m^3

Total mass density =	**240 kg/m^3**

Zalmhaven Tower

h =	200 m
area =	885 m²
b =	30.0 m
d =	29.5 m
# storeys =	66
storey height =	3.0 m

Concrete shear walls

wall thickness =	0.45 m (averaged)
wall length =	27 m
wall thickness =	0.45 m
wall length =	80 m
total area =	44.2 m²
reinf. concrete =	2500 kg/m³
density core =	$44.2 \cdot 2500 = 110375$ kg/m
mass density =	$110375/885 = 124.7$ kg/m³

Floor system

floor thickness =	0.25 m
reinf. concrete =	2500 kg/m³
own weight floor =	625 kg/m²
other own weight =	100 kg/m²
total own weight =	725 kg/m²
density floor =	$(885 \cdot 725)/3.0 = 213875$ kg/m
mass density =	$213875/885 = 241.7$ kg/m³

Floor loads

live load =	175 kg/m²
ψ_0 =	0.4
load =	70 kg/m²
density loads =	$(885 \cdot 70)/3.0 = 20650$ kg/m
mass density =	$20650/885 = 23.3$ kg/m³

Facade

own weight facade =	100 kg/m²
circumference =	119 m
density facade =	$100 \cdot 119 = 11900$ kg/m
mass density =	$11900/885 = 13.4$ kg/m³

Total mass density =   403 kg/m³

Montevideo Tower

$h =$	140 m
area $=$	756 m^2
$b =$	27.0 m
$d =$	28.0 m
storeys bottom part $=$	28
storeys top part $=$	15
storey height bottom $=$	2.9 m
storey height top $=$	3.2 m

Bottom part	Top part
Concrete shear walls	**Steel**

wall thickness $=$	0.325 m	Assumption $=$	10 kg/m^3
total wall length $=$	167.2 m		
total area $=$	54.3 m^2		
reinf. concrete $=$	2400 kg/m^3		
density walls $=$	$54.3 \cdot 2400 = 130416$ kg/m		
mass density $=$	$130416/756 = 173$ kg/m^3		

Floor system		**Floor system**	
own weight $=$	528 kg/m^3	own weight $=$	528 kg/m^3
other own weight $=$	50 kg/m^3	other own weight $=$	50 kg/m^3
structural screed $=$	160 kg/m^3	structural screed $=$	160 kg/m^3
total own weight $=$	738 kg/m^3	total own weight $=$	738 kg/m^3
density floor $=$	$(738 \cdot 756)/2.9$	density floor $=$	$(738 \cdot 756)/3.2$
	$= 192389$ kg/m		$= 174353$ kg/m
mass density $=$	$192389/756 = 254$ kg/m^3	mass density $=$	$174353/756 = 231$ kg/m^3

Floor loads		**Floor loads**	
live load $=$	175 kg/m^2	live load $=$	175 kg/m^2
$\psi_0 =$	0.4	$\psi_0 =$	0.4
load $=$	70 kg/m^2	load $=$	70 kg/m^2
mas density loads $=$	$(70 \cdot 756)/2.9$	mas density loads $=$	$(70 \cdot 756)/3.2$
	$= 18248$ kg/m		$= 16538$ kg/m
mass density $=$	$18248/756 = 24$ kg/m^3	mass density $=$	$16538/756 = 22$ kg/m^3

Facade		**Facade**	
own weight $=$	100 kg/m^2	own weight $=$	100 kg/m^2
circumference $=$	110 m	circumference $=$	110 m
density facade $=$	$110 \cdot 100 \cdot 2.9$	density facade $=$	$110 \cdot 100 \cdot 3.2$
	$= 31900$ kg/m		$= 35200$ kg/m
mass density $=$	$31900/756 = 42$ kg/m^3	mass density $=$	$35200/756 = 47$ kg/m^3

Total mass density $=$	**493 kg/m^3**	**Total mass density $=$**	**309 kg/m^3**

APPENDIX E

Analytical expressions and graphs for the foundation stiffness values

The elastic horizontal stiffness at ground surface is obtained by: (National Institute of Standards and Technology, 2012)

$$K_{sur,x,Pais\ Kausel} = \frac{GB}{2-v}\left(6.8\left(\frac{L}{B}\right)^{0.65} + 0.8\left(\frac{L}{B}\right) + 1.6\right) \tag{E.1}$$

$$K_{sur,x,Gazetas} = \frac{2GL}{2-v}\left(2 + 2.5\left(\frac{B}{L}\right)^{0.85}\right) \tag{E.2}$$

$$K_{sur,y,Pais\ Kausel} = \frac{GB}{2-v}\left(6.8\left(\frac{L}{B}\right)^{0.65} + 2.4\right) \tag{E.3}$$

$$K_{sur,y,Gazetas} = K_{sur,x,Gazetas} - \frac{0.2\ GL}{0.75-v}\left(1 - \frac{B}{L}\right) \tag{E.4}$$

The elastic rotational stiffness at ground surface is obtained by: (National Institute of Standards and Technology, 2012)

$$K_{sur,r,x,Pais\ Kausel} = \frac{GB^3}{1-v}\left(3.2\left(\frac{L}{B}\right) + 0.8\right) \tag{E.5}$$

$$K_{sur,r,x,Gazetas} = \frac{G}{1-v}I_x^{0.75}\left(\frac{L}{B}\right)^{0.25}\left(2.4 + 0.5\left(\frac{B}{L}\right)\right) \tag{E.6}$$

$$K_{sur,r,y,Pais\ Kausel} = \frac{GB^3}{1-v}\left(3.73\left(\frac{L}{B}\right)^{2.4} + 0.27\right) \tag{E.7}$$

$$K_{sur,r,y,Gazetas} = \frac{G}{1-v}I_y^{0.75}\ 3.0\left(\frac{L}{B}\right)^{0.15} \tag{E.8}$$

$$I_x = \frac{(2L)(2B)^3}{12}$$

$$I_y = \frac{(2B)(2L)^3}{12}$$

The embedment modifiers for the horizontal stiffness are: (National Institute of Standards and Technology, 2012)

$$\eta_{x,Pais\ Kausel} = 1 + \left(0.33 + \frac{1.34}{1+\left(\frac{L}{B}\right)}\left(\frac{D}{B}\right)^{0.8}\right) \tag{E.9}$$

$$\eta_{x,Gazetas} = \left(1 + 0.15\sqrt{\frac{D}{B}}\right)\left(1 + 0.52\left(\frac{z_w A_{w,x}}{BL^2}\right)^{0.4}\right) \tag{E.10}$$

$$\eta_{y,Pais\ Kausel} \approx \eta_{x,Pais\ Kausel} \tag{E.11}$$

$$\eta_{y,Gazetas} = \left(1 + 0.15\sqrt{\frac{D}{B}}\right)\left(1 + 0.52\left(\frac{z_w A_{w,y}}{BL^2}\right)^{0.4}\right) \tag{E.12}$$

$$z_w = \frac{D}{2}$$

$$A_{w,x} = 4DL$$

$$A_{w,y} = 4DB$$

The embedment modifiers for the rotational stiffness are: (National Institute of Standards and Technology, 2012)

$$\eta_{r,x,Pais\ Kausel} = 1 + \left(\frac{D}{B}\right) + \left(\frac{1.6}{0.35 + \left(\frac{L}{B}\right)}\right)\left(\frac{D}{B}\right)^2 \tag{E.13}$$

$$\eta_{r,x,Gazetas} = 1 + \frac{1.26\ d_w}{B}\left(1 + \left(\frac{d_w}{B}\right)\left(\frac{d_w}{D}\right)^{-0.2}\sqrt{\frac{B}{L}}\right) \tag{E.14}$$

$$\eta_{r,y,Pais\ Kausel} = 1 + \left(\frac{D}{B}\right) + \left(\frac{1.6}{0.35 + \left(\frac{L}{B}\right)^4}\right)\left(\frac{D}{B}\right)^2 \tag{E.15}$$

$$\eta_{r,y,Gazetas} = 1 + 0.92\left(\frac{d_w}{B}\right)^{0.6}\left(1.5 + \left(\frac{d_w}{D}\right)^{1.9}\left(\frac{B}{L}\right)^{-0.6}\right) \tag{E.16}$$

$$d_w = D$$

The dynamic modifier according to Pais and Kausel for the horizontal stiffness is: (National Institute of Standards and Technology, 2012)

$$\alpha_{x,Pais\ Kausel} = 1 \tag{E.17}$$

$$\alpha_{y,Pais\ Kausel} = 1 \tag{E.18}$$

The dynamic modifiers according to Gazetas for the horizontal stiffness are: (Gazetas, 1991)

$$k_{x,Gazetas} = k_y \text{ in below graphs} \tag{E.19}$$

$$k_{y,Gazetas} \cong 1.0 \tag{E.20}$$
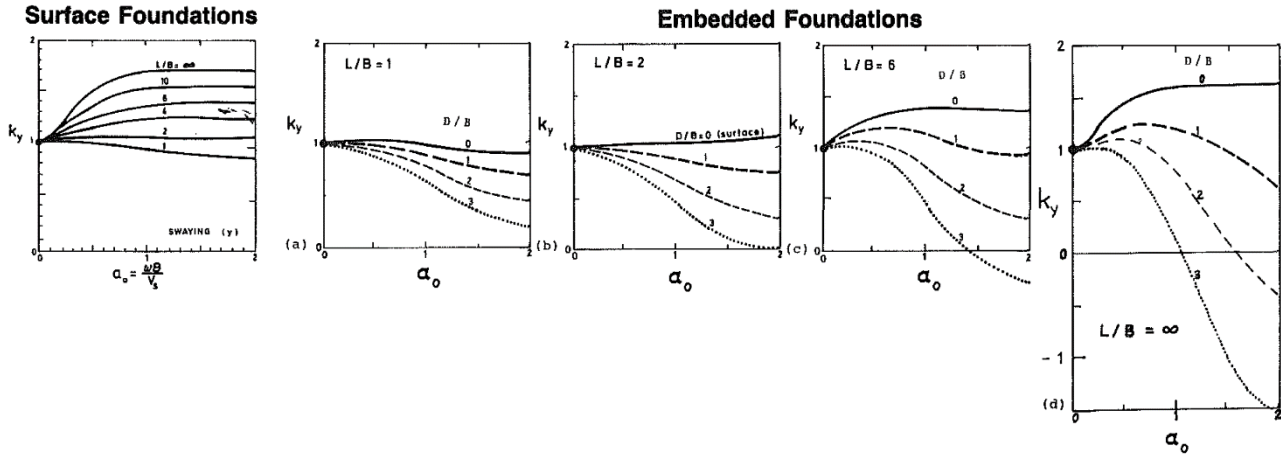
Figure 125: Dynamic modifiers according to Gazetas for the horizontal stiffness (Gazetas, 1991)

The dynamic modifiers for the rotational stiffness are: (National Institute of Standards and Technology, 2012) (Gazetas, 1991)

$$\alpha_{r,x,Pais\ Kausel} = 1 - \frac{\left(0.55 + 0.01\sqrt{\left(\frac{L}{B}\right) - 1}\right)a_0^2}{\left(2.4 - \frac{0.4}{\left(\frac{L}{B}\right)^3}\right) + a_0^2} \tag{E.21}$$

$$\alpha_{r,x,Gazetas} \cong 1 - 0.2\, a_0 \tag{E.22}$$

$$\alpha_{r,y,Pais\ Kausel} = 1 - \frac{0.55\, a_0^2}{\left(0.6 - \dfrac{1.4}{\left(\dfrac{L}{B}\right)^3}\right) + a_0^2} \tag{E.23}$$

$$\alpha_{r,y,Gazetas} \cong 1 - 0.26\, a_0 \left(\frac{L}{B}\right)^{0.3} \tag{E.24}$$

Analytical expressions and graphs for the foundation damping values

The translational damping ratio according to Pais and Kausel is obtained by: (National Institute of Standards and Technology, 2012)

$$\beta_{x,surf,Pais\ Kausel} = \left(\frac{4\left(\dfrac{L}{B}\right)}{\dfrac{K_{sur,x,Pais\ Kausel}}{GB}}\right)\left(\frac{a_0}{2\alpha_{x,Pais\ Kausel}}\right) \tag{E.25}$$

$$\beta_{y,surf,Pais\ Kausel} = \left(\frac{4\left(\dfrac{L}{B}\right)}{\dfrac{K_{sur,y,Pais\ Kausel}}{GB}}\right)\left(\frac{a_0}{2\alpha_{y,Pais\ Kausel}}\right) \tag{E.26}$$

$$\beta_{x,emb,Pais\ Kausel} = \left(\frac{4\left(\left(\dfrac{L}{B}\right) + \left(\dfrac{D}{B}\right)\left(1 + \left(\dfrac{\psi L}{B}\right)\right)\right)}{\dfrac{K_{emb,x,Pais\ Kausel}}{GB}}\right)\left(\frac{a_0}{2\alpha_{x,Pais\ Kausel}}\right) \tag{E.27}$$

$$\beta_{y,emb,Pais\ Kausel} = \left(\frac{4\left(\left(\dfrac{L}{B}\right) + \left(\dfrac{D}{B}\right)\left(\psi + \left(\dfrac{L}{B}\right)\right)\right)}{\dfrac{K_{emb,y,Pais\ Kausel}}{GB}}\right)\left(\frac{a_0}{2\alpha_{y,Pais\ Kausel}}\right) \tag{E.28}$$

$$\psi = \sqrt{\frac{2(1-v)}{1-2v}} \leq 2.5$$

The damping modifier according to Gazetas for the horizontal damping: (Gazetas, 1991)

$$\tilde{c}_{x,Gazetas} = \tilde{c}_y \text{ according to the graph below} \tag{E.29}$$

$$\tilde{c}_{y,Gazetas} = 1.0 \tag{E.30}$$
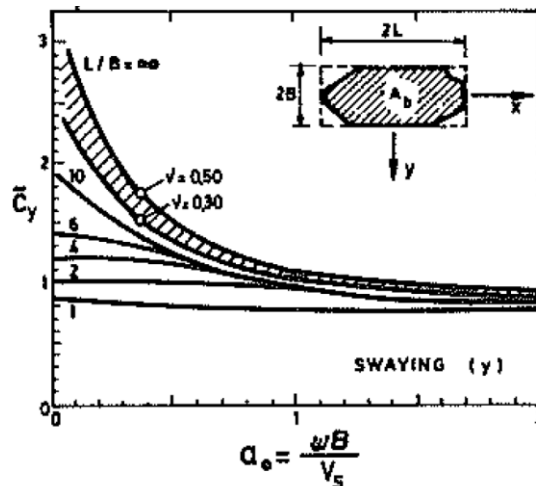
Figure 126: Damping modifier according to Gazetas for horizontal damping (Gazetas, 1991)

The rotational damping ratio according to Pais and Kausel is obtained by: (National Institute of Standards and Technology, 2012)

$$\beta_{r,x,surf,Pais\ Kausel} = \cfrac{\frac{4\psi}{3}\left(\frac{L}{B}\right)a_0^2}{\frac{K_{sur,r,x,Pais\ Kausel}}{GB^3}\left(\left(2.2 - \frac{0.4}{\left(\frac{L}{B}\right)^3}\right) + a_0^2\right)}\frac{a_0}{2\alpha_{r,x,Pais\ Kausel}} \tag{E.31}$$

$$\beta_{r,y,surf,Pais\ Kausel} = \cfrac{\frac{4\psi}{3}\left(\frac{L}{B}\right)^3 a_0^2}{\frac{K_{sur,r,y,Pais\ Kausel}}{GB^3}\left(\left(\frac{1.8}{1 + 1.75\left(\left(\frac{L}{B}\right) - 1\right)}\right) + a_0^2\right)}\frac{a_0}{2\alpha_{r,y,Pais\ Kausel}} \tag{E.32}$$

$$\beta_{r,x,emb,Pais\ Kausel} = \left(\cfrac{\frac{4}{3}\left(\left(\frac{D}{B}\right) + \left(\frac{D}{B}\right)^3 + \left(\frac{\psi L}{B}\right)\left(\frac{D}{B}\right)^3 + \left(\frac{3D}{B}\right)\left(\frac{L}{B}\right) + \left(\frac{\psi L}{B}\right)\right)a_0^2}{\frac{K_{emb,r,x,Pais\ Kausel}}{GB^3}\left(\left(\frac{1.8}{1 + 1.75\left(\left(\frac{L}{B}\right) - 1\right)}\right) + a_0^2\right)} + \frac{\frac{4}{3}\left(\left(\frac{\psi L}{B}\right) + 1\right)\left(\frac{D}{B}\right)^3}{\frac{K_{emb,r,x,Pais\ Kausel}}{GB^3}}\right)\frac{a_0}{2\alpha_{r,x,Pais\ Kausel}} \tag{E.33}$$

$$\beta_{r,y,emb,Pais\ Kausel} = \left(\cfrac{\frac{4}{3}\left(\left(\frac{L}{B}\right)^3\left(\frac{D}{B}\right) + \left(\frac{\psi L}{B}\right)\left(\frac{D}{B}\right)^3 + \left(\frac{D}{B}\right)^3 + 3.0\left(\frac{D}{B}\right)\left(\frac{L}{B}\right)^2 + \psi\left(\frac{L}{B}\right)^3\right)a_0^2}{\frac{K_{emb,r,y,Pais\ Kausel}}{GB^3}\left(\left(\frac{1.8}{1 + 1.75\left(\left(\frac{L}{B}\right) - 1\right)}\right) + a_0^2\right)} + \frac{\frac{4}{3}\left(\left(\frac{L}{B}\right) + \psi\right)\left(\frac{D}{B}\right)^3}{\frac{K_{emb,r,y,Pais\ Kausel}}{GB^3}}\right)\frac{a_0}{2\alpha_{r,y,Pais\ Kausel}} \tag{E.34}$$

The damping modifier according to Gazetas for the rotational damping: (Gazetas, 1991)

$$\tilde{c}_{r,x,Gazetas} = \tilde{c}_{ry} \text{ according to the graph below} \tag{E.35}$$

$$\tilde{c}_{r,y,Gazetas} = \tilde{c}_{rx} \text{ according to the graph below} \tag{E.36}$$
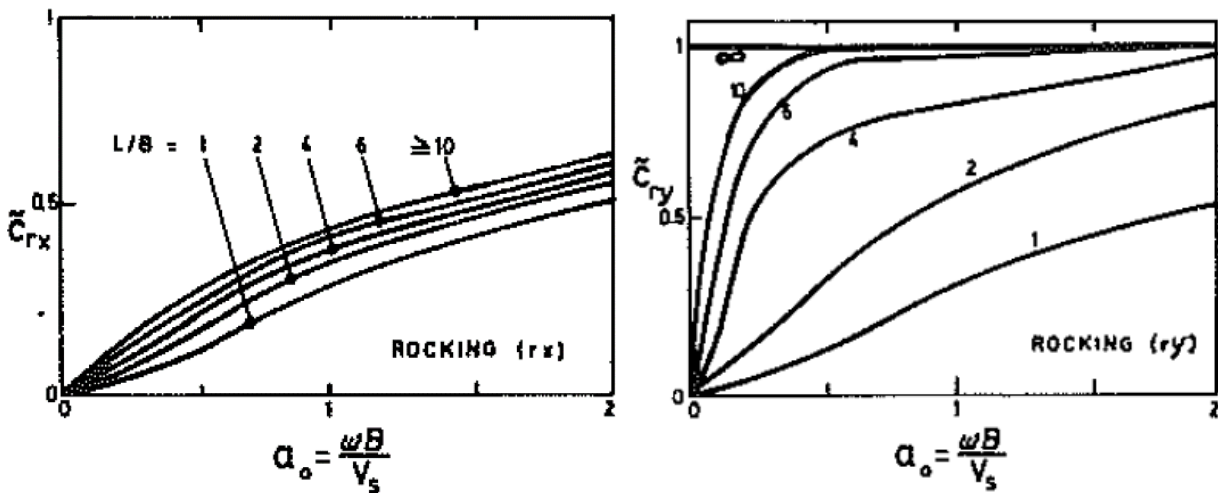

Figure 127: Damping modifier according to Gazetas for rotational damping (Gazetas, 1991)

APPENDIX F

Determination of the dynamic stiffness and damping value from displacement curves

The problem is a massless rigid foundation over a homogeneous elastic half space. The foundation is subjected to a steady-state vibration by a harmonic force, $P = P_0 \sin(\omega t)$, having amplitude P_0 and angular frequency ω. Due to radiation damping, the force is generally out of phase with the response. Therefore, the response can be divided into two components: one in phase with P and one $90°$ out of phase with P. These two components can be found from the obtained displacement curves of the analysis.

The complex notation to express the response through the dynamic force-displacement ratio is introduced: (Gazetas, et al., 1985)

$$\overline{K} + i\,\omega\,C = \frac{P}{u_0} = \frac{P_0}{u_1 + i\,u_2} \tag{F.1}$$

$\overline{K}$ is the dynamic stiffness and C is the radiation damping value. Both are a function of the frequency ω. Rewriting equation (F.1), the following is obtained:

$$\overline{K} + i\,\omega\,C = \frac{P_0}{u_1 + i\,u_2}\frac{u_1 - i\,u_2}{u_1 - i\,u_2} = P_0\left(\frac{u_1 - i\,u_2}{u_1^2 + u_2^2}\right) = P_0\left(\frac{u_1}{u_1^2 + u_2^2} - i\frac{u_2}{u_1^2 + u_2^2}\right) \tag{F.2}$$

And therefore:

$$\overline{K} = \Re\left(P_0\left(\frac{u_1}{u_1^2 + u_2^2} - i\frac{u_2}{u_1^2 + u_2^2}\right)\right) = P_0\left(\frac{u_1}{u_1^2 + u_2^2}\right)$$
$$C = \Im\left(\frac{P_0}{\omega}\left(\frac{u_1}{u_1^2 + u_2^2} - i\frac{u_2}{u_1^2 + u_2^2}\right)\right) = -\frac{P_0}{\omega}\left(\frac{u_2}{u_1^2 + u_2^2}\right) \tag{F.3}$$

The following image is provided as example.
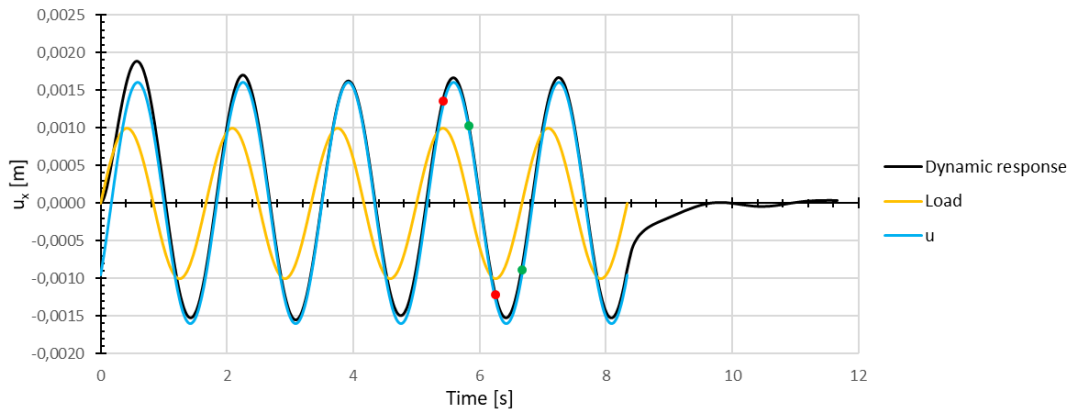
Figure 128: Dynamic response of time history analysis (black), harmonic load with arbitrary amplitude (yellow) and response function u (blue) for the horizontal foundation stiffness at a loading frequency of 0.6 Hz

The amplitude u_1 is obtained as half of the difference between the red dots. This is the component in phase with the load. The amplitude u_2 is obtained as half of the difference between the green dots. This is the component which is $90°$ out of phase with the load. The summation of both components results in the response function u which is in line with the steady state vibration of the dynamic response obtained from the time history analysis.

$$u = u_1 \sin(\omega t) + u_2 \sin\left(\omega t - \frac{\pi}{2}\right) \tag{F.4}$$

With the known amplitudes u_1 and u_2 and the loading frequency, the dynamic stiffness and damping values associated to the loading frequency, are obtained using equation (F.3).

APPENDIX G

Typical soil profiles of Rotterdam, Amsterdam and The Hague

Rotterdam

Amsterdam

The Hague

APPENDIX H

Contribution of the second run to the maximum acceleration, depending on the variables: h, b, d, D and the soil profile

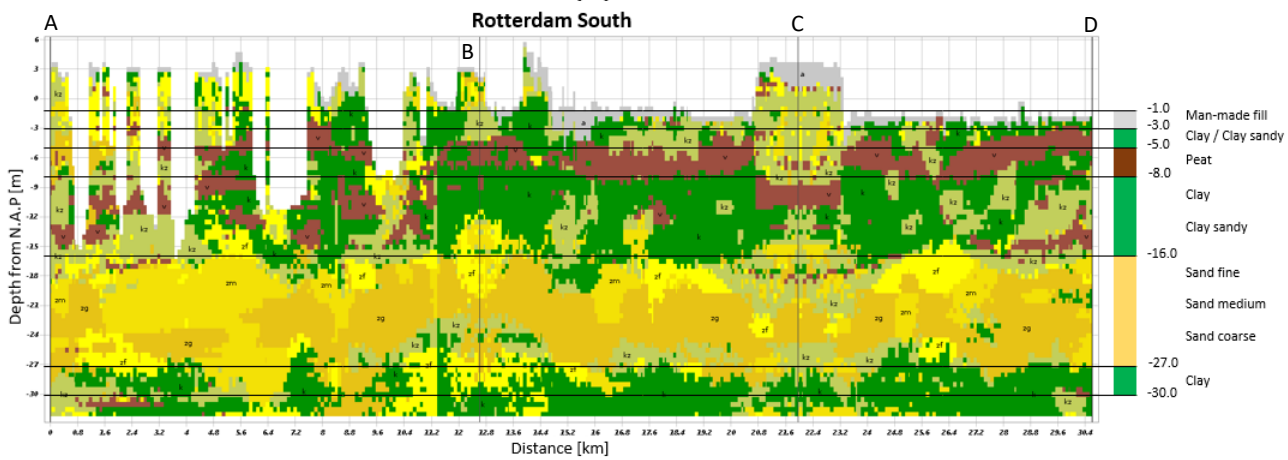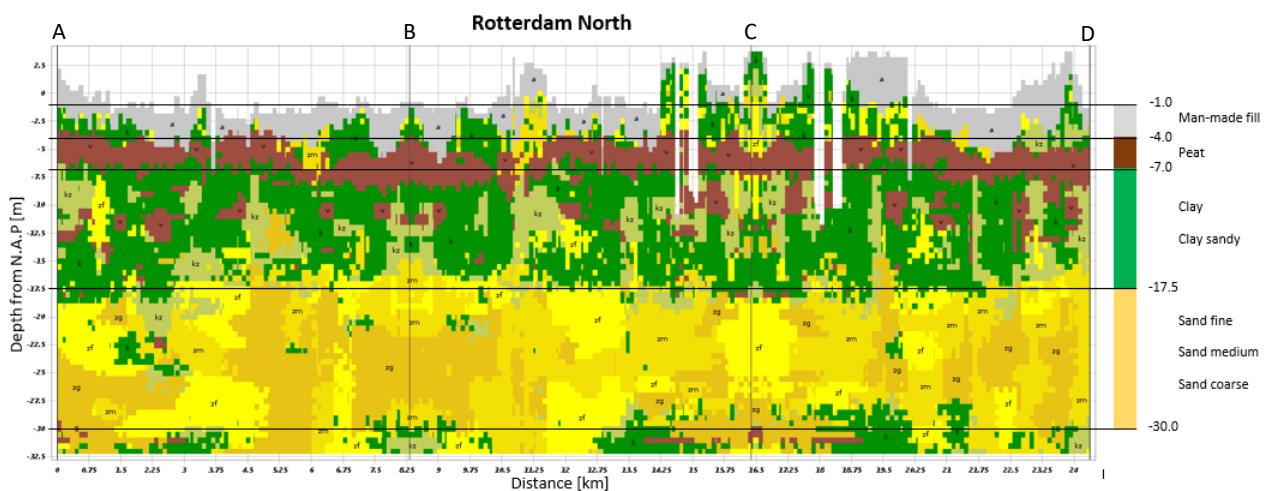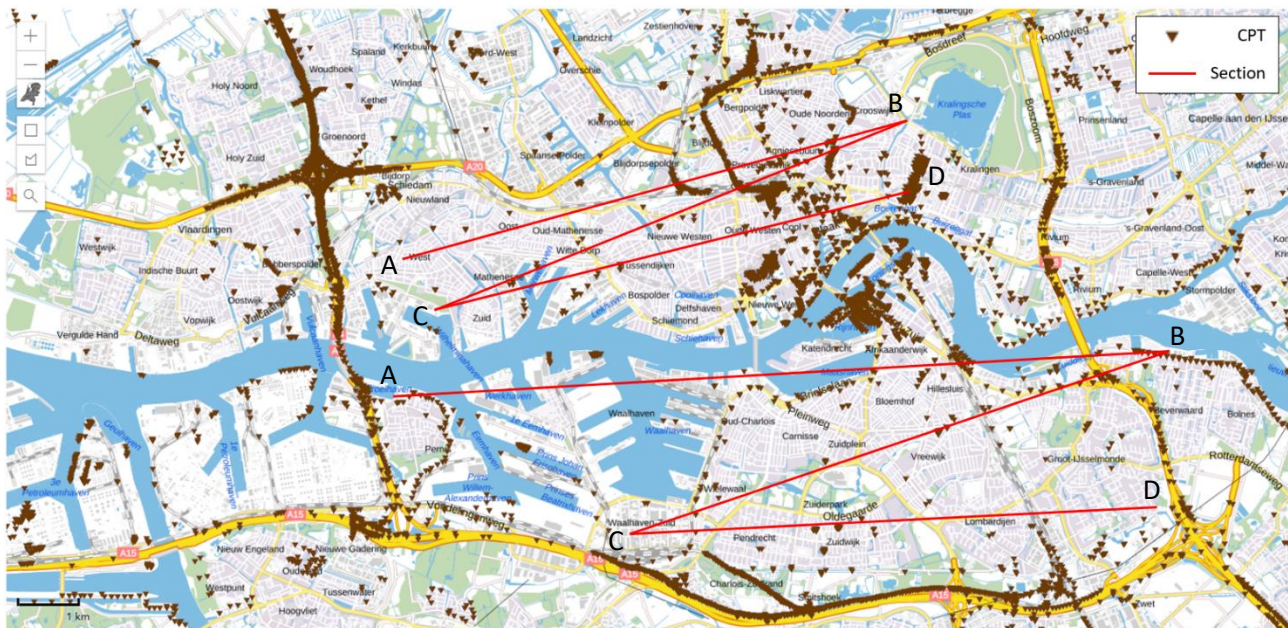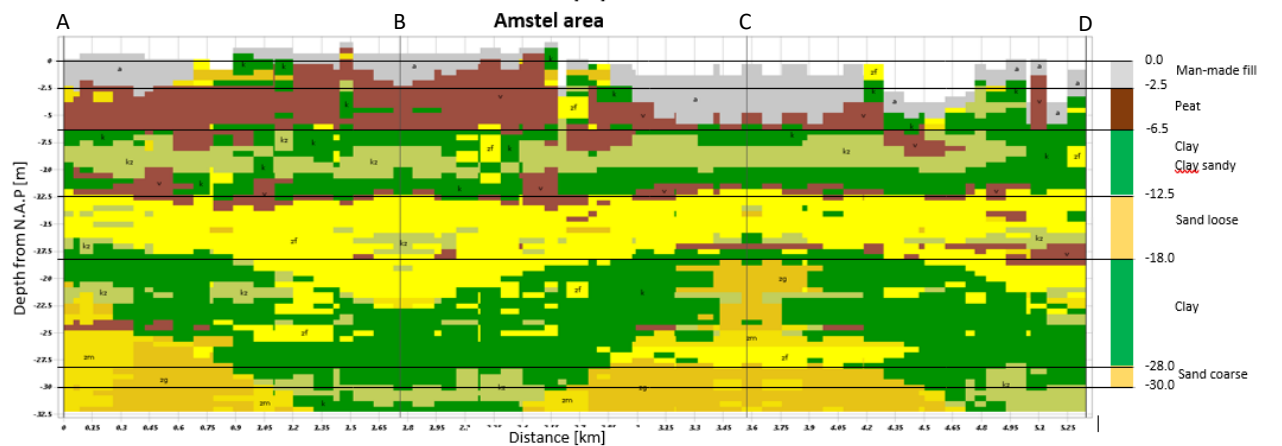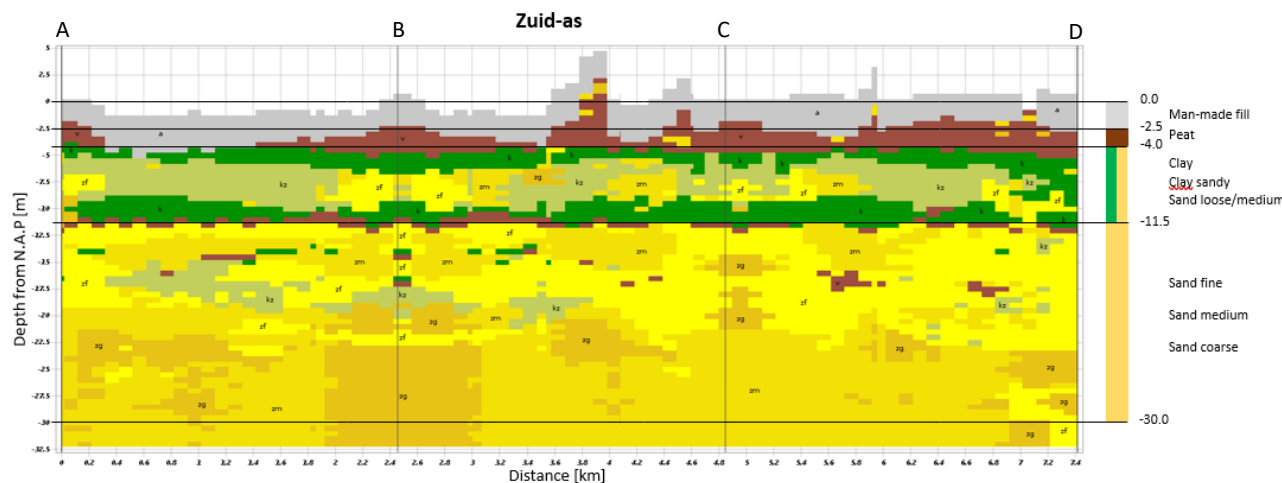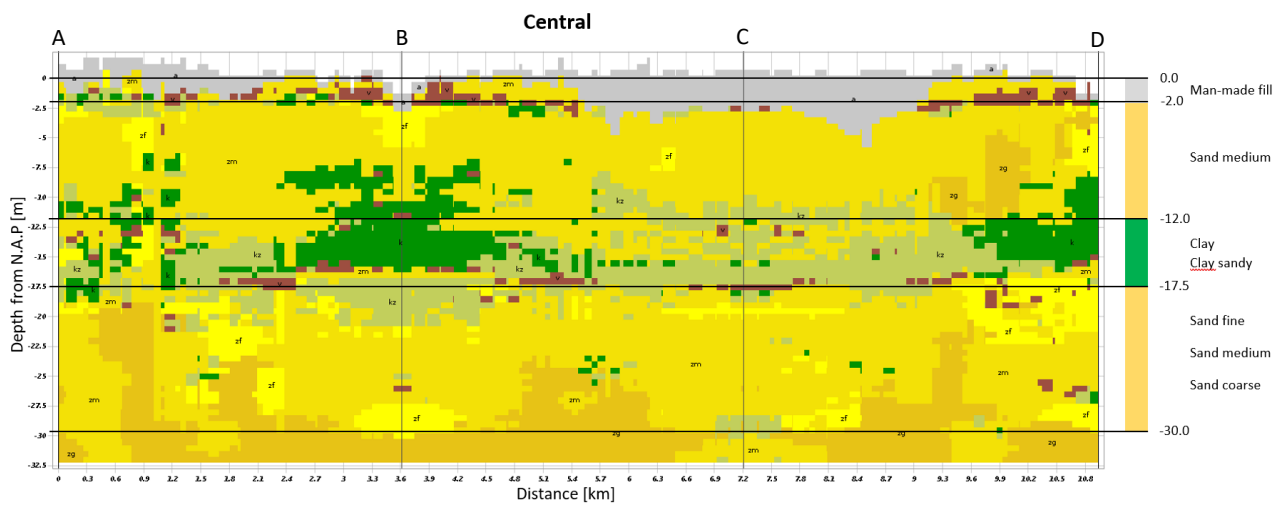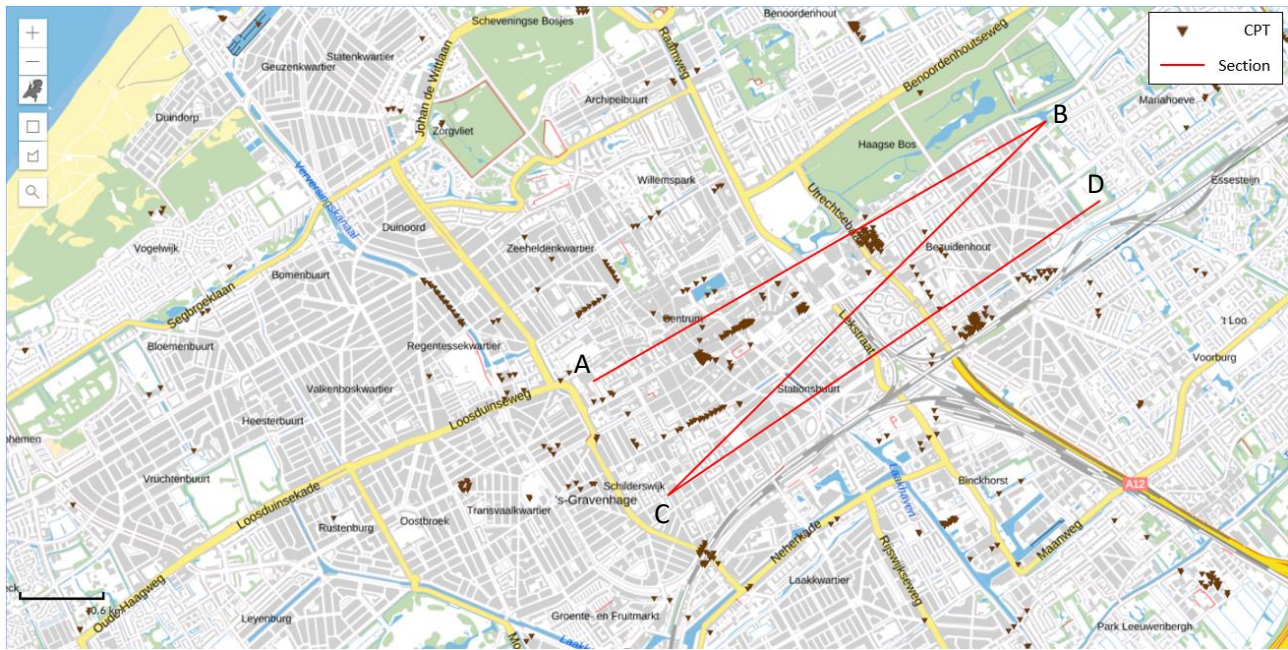| δa		d	30			40			50			70			90		
h	b	P/D	1	2	3	1	2	3	1	2	3	1	2	3	1	2	3
100	30	3,5	3%	2%	2%	2%	2%	2%	1%	2%	2%	2%	2%	2%	2%	3%	3%
		7,0	2%	2%	2%	1%	2%	2%	1%	2%	2%	2%	2%	2%	2%	3%	3%
		10,5	1%	2%	2%	1%	2%	2%	1%	2%	2%	2%	2%	2%	2%	3%	3%
		14,0	1%	1%	2%	1%	2%	2%	1%	2%	2%	2%	2%	2%	2%	3%	3%
	40	3,5	3%	2%	2%	2%	2%	2%	1%	1%	2%	1%	2%	2%	1%	2%	2%
		7,0	2%	2%	2%	1%	1%	2%	1%	1%	2%	1%	2%	2%	1%	2%	2%
		10,5	1%	1%	1%	1%	1%	1%	1%	1%	2%	1%	2%	2%	1%	2%	2%
		14,0	1%	1%	1%	1%	1%	1%	1%	1%	2%	1%	2%	2%	1%	2%	2%
	50	3,5	2%	2%	2%	1%	1%	2%	1%	1%	1%	1%	1%	2%	1%	1%	2%
		7,0	2%	1%	2%	1%	1%	1%	1%	1%	1%	1%	1%	2%	1%	1%	2%
		10,5	1%	1%	1%	1%	1%	1%	1%	1%	1%	1%	1%	2%	1%	2%	2%
		14,0	1%	1%	1%	1%	1%	1%	1%	1%	1%	1%	1%	2%	1%	2%	2%
	70	3,5	2%	2%	2%	1%	1%	1%	1%	1%	1%	1%	1%	1%	1%	1%	1%
		7,0	2%	1%	1%	1%	1%	1%	1%	1%	1%	1%	1%	1%	1%	1%	1%
		10,5	1%	1%	1%	1%	1%	1%	1%	1%	1%	1%	1%	1%	1%	1%	1%
		14,0	1%	1%	1%	1%	1%	1%	1%	1%	1%	1%	1%	1%	1%	1%	1%
	90	3,5	2%	2%	2%	1%	1%	1%	1%	1%	1%	1%	1%	1%	1%	1%	1%
		7,0	2%	1%	1%	1%	1%	1%	1%	1%	1%	1%	1%	1%	1%	1%	1%
		10,5	1%	1%	1%	1%	1%	1%	1%	1%	1%	1%	1%	1%	1%	1%	1%
		14,0	1%	1%	1%	1%	1%	1%	1%	1%	1%	0%	1%	1%	0%	1%	1%
150	30	3,5	10%	7%	6%	4%	3%	3%	3%	3%	3%	2%	3%	3%	2%	3%	3%
		7,0	6%	4%	4%	3%	3%	3%	2%	2%	3%	2%	2%	3%	2%	3%	3%
		10,5	4%	3%	3%	3%	2%	3%	2%	2%	2%	2%	2%	3%	2%	3%	3%
		14,0	3%	2%	2%	2%	2%	2%	2%	2%	2%	2%	2%	3%	2%	3%	3%
	40	3,5	10%	6%	5%	5%	4%	3%	2%	2%	2%	2%	2%	2%	2%	2%	2%
		7,0	6%	4%	4%	3%	3%	3%	2%	2%	2%	2%	2%	2%	2%	2%	2%
		10,5	4%	3%	3%	2%	2%	2%	2%	2%	2%	2%	2%	2%	2%	2%	2%
		14,0	3%	2%	2%	2%	2%	2%	2%	2%	2%	1%	2%	2%	2%	2%	2%
	50	3,5	9%	6%	5%	5%	3%	3%	3%	2%	2%	1%	2%	2%	1%	2%	2%
		7,0	6%	4%	3%	3%	2%	2%	2%	2%	2%	1%	2%	2%	1%	2%	2%
		10,5	4%	3%	2%	2%	2%	2%	2%	2%	2%	1%	2%	2%	1%	2%	2%
		14,0	3%	2%	2%	2%	2%	2%	1%	1%	2%	1%	2%	2%	1%	2%	2%
	70	3,5	8%	5%	4%	4%	3%	3%	3%	2%	2%	1%	1%	2%	1%	1%	1%
		7,0	5%	3%	3%	3%	2%	2%	2%	2%	2%	1%	1%	1%	1%	1%	1%
		10,5	4%	3%	2%	2%	2%	2%	2%	1%	1%	1%	1%	1%	1%	1%	1%
		14,0	3%	2%	2%	2%	1%	1%	1%	1%	1%	1%	1%	1%	1%	1%	1%
	90	3,5	7%	5%	4%	4%	3%	2%	2%	2%	2%	1%	1%	1%	1%	1%	1%
		7,0	5%	3%	3%	3%	2%	2%	2%	1%	1%	1%	1%	1%	1%	1%	1%
		10,5	4%	2%	2%	2%	2%	2%	1%	1%	1%	1%	1%	1%	1%	1%	1%
		14,0	3%	2%	2%	2%	1%	1%	1%	1%	1%	1%	1%	1%	1%	1%	1%
200	30	3,5	23%	16%	13%	9%	6%	5%	5%	4%	4%	3%	3%	3%	3%	3%	4%
		7,0	14%	10%	8%	7%	5%	4%	4%	4%	4%	3%	3%	3%	3%	3%	3%
		10,5	10%	7%	6%	5%	4%	4%	4%	3%	3%	3%	3%	3%	3%	3%	3%
		14,0	7%	5%	4%	4%	4%	3%	3%	3%	3%	3%	3%	3%	3%	3%	3%
	40	3,5	23%	16%	13%	12%	8%	7%	5%	4%	4%	3%	3%	3%	2%	3%	3%
		7,0	14%	10%	8%	8%	6%	5%	4%	3%	3%	2%	2%	3%	2%	2%	3%
		10,5	10%	7%	5%	6%	4%	4%	3%	3%	3%	2%	2%	3%	2%	2%	3%
		14,0	7%	5%	4%	4%	3%	3%	3%	3%	3%	2%	2%	3%	2%	2%	3%
	50	3,5	21%	14%	11%	12%	8%	6%	7%	5%	4%	2%	2%	2%	2%	2%	2%
		7,0	14%	9%	7%	8%	5%	4%	5%	4%	3%	2%	2%	2%	2%	2%	2%
		10,5	10%	6%	5%	6%	4%	3%	4%	3%	3%	2%	2%	2%	2%	2%	2%
		14,0	7%	5%	4%	5%	3%	3%	3%	2%	2%	2%	2%	2%	2%	2%	2%
	70	3,5	20%	13%	10%	10%	7%	5%	6%	4%	4%	3%	2%	2%	2%	2%	2%
		7,0	13%	8%	7%	7%	5%	4%	5%	3%	3%	2%	2%	2%	1%	2%	2%
		10,5	9%	6%	5%	6%	4%	3%	4%	3%	2%	2%	2%	2%	1%	1%	2%
		14,0	7%	4%	4%	4%	3%	3%	3%	2%	2%	2%	1%	2%	1%	1%	2%
	90	3,5	18%	12%	9%	10%	6%	5%	6%	4%	3%	3%	2%	2%	2%	2%	2%
		7,0	12%	8%	6%	7%	5%	4%	4%	3%	3%	2%	2%	2%	1%	1%	2%
		10,5	9%	6%	4%	5%	3%	3%	3%	2%	2%	2%	2%	2%	1%	1%	1%
		14,0	7%	4%	3%	4%	3%	2%	3%	2%	2%	2%	1%	1%	1%	1%	1%

NOTES: P is the soil profile: 1 (soft), 2 (medium), 3 (stiff)

h, b, d and D are in meters.

δa		d	30			40			50			70			90		
h	b	P D	1	2	3	1	2	3	1	2	3	1	2	3	1	2	3
250	30	3,5	40%	31%	25%	19%	13%	10%	10%	7%	6%	5%	4%	4%	4%	4%	4%
		7,0	26%	19%	15%	13%	9%	7%	8%	6%	5%	4%	4%	4%	3%	4%	4%
		10,5	18%	13%	10%	10%	7%	6%	6%	5%	5%	4%	4%	4%	3%	4%	4%
		14,0	13%	9%	7%	8%	6%	5%	6%	5%	4%	4%	4%	4%	3%	4%	4%
	40	3,5	39%	31%	25%	23%	16%	13%	11%	7%	6%	5%	4%	4%	3%	3%	3%
		7,0	26%	19%	15%	16%	11%	9%	8%	6%	5%	4%	3%	3%	3%	3%	3%
		10,5	18%	13%	10%	11%	8%	7%	6%	5%	4%	3%	3%	3%	3%	3%	3%
		14,0	14%	9%	7%	9%	6%	5%	5%	4%	4%	3%	3%	3%	3%	3%	3%
	50	3,5	36%	28%	23%	23%	16%	13%	14%	9%	8%	4%	4%	3%	3%	3%	3%
		7,0	25%	18%	14%	16%	11%	9%	10%	7%	6%	4%	3%	3%	2%	3%	3%
		10,5	18%	12%	10%	12%	8%	6%	7%	5%	4%	3%	3%	3%	2%	2%	3%
		14,0	13%	9%	7%	9%	6%	5%	6%	4%	4%	3%	3%	3%	2%	2%	3%
	70	3,5	34%	26%	21%	21%	14%	11%	13%	9%	7%	6%	4%	4%	2%	2%	2%
		7,0	23%	17%	13%	15%	10%	8%	10%	6%	5%	4%	3%	3%	2%	2%	2%
		10,5	17%	12%	9%	11%	7%	6%	8%	5%	4%	4%	3%	3%	2%	2%	2%
		14,0	13%	8%	7%	9%	6%	5%	6%	4%	3%	3%	2%	2%	2%	2%	2%
	90	3,5	32%	24%	19%	19%	13%	10%	12%	8%	6%	5%	4%	3%	3%	2%	2%
		7,0	22%	16%	12%	14%	9%	7%	9%	6%	5%	4%	3%	3%	2%	2%	2%
		10,5	16%	11%	9%	11%	7%	6%	7%	5%	4%	4%	3%	2%	2%	2%	2%
		14,0	13%	8%	6%	9%	5%	4%	6%	4%	3%	3%	2%	2%	2%	2%	2%
300	30	3,5	55%	49%	42%	34%	22%	17%	19%	12%	10%	8%	6%	6%	5%	5%	5%
		7,0	38%	31%	26%	23%	16%	12%	13%	9%	8%	6%	5%	5%	4%	4%	4%
		10,5	27%	21%	18%	18%	12%	10%	11%	8%	7%	6%	5%	5%	4%	4%	4%
		14,0	20%	15%	12%	14%	10%	8%	9%	7%	6%	5%	5%	5%	4%	4%	4%
	40	3,5	53%	48%	42%	37%	28%	23%	20%	13%	10%	8%	6%	5%	5%	4%	4%
		7,0	37%	31%	26%	25%	19%	15%	14%	9%	8%	6%	5%	4%	4%	4%	4%
		10,5	28%	21%	18%	19%	13%	11%	11%	8%	7%	5%	4%	4%	4%	4%	4%
		14,0	21%	15%	13%	15%	10%	8%	9%	7%	6%	5%	4%	4%	3%	4%	4%
	50	3,5	50%	45%	39%	36%	28%	23%	24%	17%	13%	8%	6%	5%	4%	4%	4%
		7,0	36%	30%	25%	25%	19%	15%	17%	12%	9%	6%	5%	4%	4%	3%	3%
		10,5	27%	21%	17%	19%	14%	11%	13%	9%	7%	5%	4%	4%	3%	3%	3%
		14,0	21%	15%	12%	15%	10%	8%	10%	7%	6%	5%	4%	4%	3%	3%	3%
	70	3,5	48%	43%	36%	33%	25%	20%	23%	16%	13%	10%	7%	6%	4%	3%	3%
		7,0	34%	28%	23%	24%	17%	14%	17%	11%	9%	8%	5%	5%	3%	3%	3%
		10,5	26%	20%	16%	18%	13%	10%	13%	9%	7%	6%	4%	4%	3%	3%	3%
		14,0	20%	14%	12%	15%	10%	8%	11%	7%	6%	5%	4%	3%	3%	2%	3%
	90	3,5	45%	39%	34%	31%	23%	19%	21%	14%	11%	10%	6%	5%	5%	4%	3%
		7,0	33%	26%	22%	23%	16%	13%	15%	10%	8%	8%	5%	4%	4%	3%	3%
		10,5	25%	19%	15%	18%	12%	10%	12%	8%	6%	6%	4%	4%	3%	3%	2%
		14,0	20%	14%	11%	14%	9%	7%	10%	7%	5%	5%	4%	3%	3%	2%	2%

NOTES: P is the soil profile: 1 (soft), 2 (medium), 3 (stiff)

h, b, d and D are in meters.

Table 18: Contribution of the second mode of vibration of the superstructure to the maximum acceleration for variation of h, b, d, D and soil profiles and constant mass density ($350\ kg/m^3$) and damping ratio (1.5%) of the superstructure